Zhegalkin Zebra Motives, Dimers, Textiles and Links in Thickened 2-Tori

Jan Stienstra

April 1, 2021

Abstract

Zhegalkin Zebra Motives are biperiodic tilings of the plane by black and white polygons given by $\mathbb{F}_2$-valued functions on $\mathbb{R}^2$ with remarkably simple defining formulas. They provide low tech methods for constructing numerous examples of planar biperiodic bipartite graphs (a.k.a. brane tilings or dimer models), textile structures, bipartite graphs embedded in a Riemann surface (a.k.a. dessins d'enfants), links and Seifert surfaces contained in a thickened 2-torus. They give accurate, nice pictures as well as manageable algorithms for computations. *Zhegalkin Zebra Motives provide simple tools for exploring connections between topics which are usually investigated with (seemingly) unrelated methods.*

Contents

1

1   Preface

The present text is somewhat fragmentary, because the work on this paper has been interrupted and redirected several times by personal circumstances. I therefore want to point out that the following sections can be read independently • Section 2.1 • Section 2.3 • Section 3.1 • Section 4.2 • Section 5.

2   Introduction

2.1   Tilings and Textiles

In 1927 **Zhegalkin** pointed out that the Boolean formalism used in set theory is equivalent to the standard addition and multiplication for functions with values in the field $\mathbb{F}_2 = \{0, 1\}$. We apply this observation to subsets of the plane, i.e. $\mathbb{F}_2$-valued functions on $\mathbb{R}^2$. The elementary building blocks for our constructions are functions which we call zebras. The **zebra with frequency** $\mathfrak{v} \in \mathbb{R}^2 \setminus \{0\}$, denoted as $\mathsf{Z}^{\mathfrak{v}}$, is defined by

$$\mathsf{Z}^{\mathfrak{v}}(\mathbf{x}) = \lfloor 2\mathbf{x} \cdot \mathfrak{v} \rfloor \bmod 2 \qquad \text{for} \quad \mathbf{x} \in \mathbb{R}^2, \tag{1}$$

where $\cdot$ is the dot product on $\mathbb{R}^2$ and for $r \in \mathbb{R}$ the integer $\lfloor r \rfloor$ is defined by $0 \le r - \lfloor r \rfloor < 1$.

Figure 1: Zebra $\mathsf{Z}^{\mathfrak{v}}$. All bands are $\perp \mathfrak{v}$ and have width $\frac{1}{2|\mathfrak{v}|}$.

The zebras with frequencies in $\mathbb{Z}^2$ generate a subring of the ring of all $\mathbb{F}_2$-valued functions on $\mathbb{R}^2$. A function $\mathcal{Z}$ in this subring gives a tiling of the plane by white (where $\mathcal{Z}$ is 0) and black (where $\mathcal{Z}$ is 1) polygons. We say that $\mathcal{Z}$ is a ***Zhegalkin Zebra Motive*** if all polygons are bounded and convex.[1]

   The tiling consists of black and white polygons, edges and vertices. We orient the edges such that the boundaries of the black (resp. white) polygons run clockwise (resp. counter-clockwise). The vertices and edges form a **quiver** (= graph with oriented edges) Γ. Combinatorially the polygons and edges form a **bipartite graph** $\Gamma^{\vee}$ dual to Γ, a.k.a. **dimer model** or **brane tiling**.

---

[1]In [22] §5.1 it is explained how one can easily draw pictures of these tilings. Boundedness and convexity of the polygons can then be checked by visual inspection.
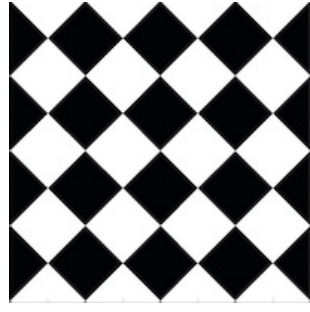
$$\mathcal{Z}_2 = \mathsf{Z}^{21} + \mathsf{Z}^{41}$$
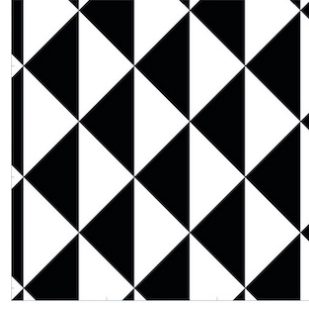
$$\mathcal{Z}_3 = \mathsf{Z}^{21} + \mathsf{Z}^{41} + \mathsf{Z}^{61}$$
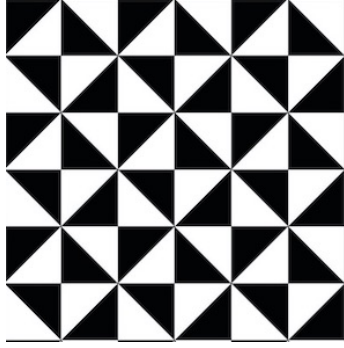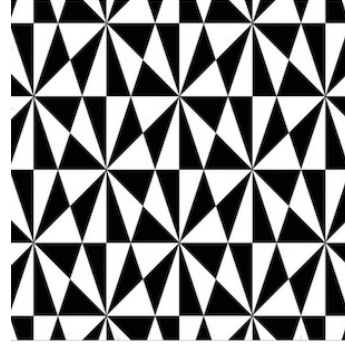
$$\mathcal{Z}_4 = \mathsf{Z}^{21} + \mathsf{Z}^{31} + \mathsf{Z}^{41} + \mathsf{Z}^{61}$$

$$\mathcal{Z}_6 = \mathsf{Z}^{11} + \mathsf{Z}^{21} + \mathsf{Z}^{31} + \mathsf{Z}^{41} + \mathsf{Z}^{51} + \mathsf{Z}^{61}$$

Figure 2: Four classical tilings realized by Zhegalkin Zebra Motives

Examples[2] are shown in Figures 2, 3, 26, 34, 35, 36, where Z^{jk} denotes the zebra with frequency $k\mathfrak{v}_j$ with $k \in \mathbb{Z}_{>0}$ and $\mathfrak{v}_j$ for $j = 1, \ldots, 6$ as in (2).
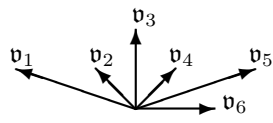
$$\mathfrak{v}_1 = \begin{pmatrix} -3 \\ 1 \end{pmatrix}, \; \mathfrak{v}_2 = \begin{pmatrix} -1 \\ 1 \end{pmatrix}, \; \mathfrak{v}_3 = \begin{pmatrix} 0 \\ 2 \end{pmatrix},$$

$$\mathfrak{v}_4 = \begin{pmatrix} 1 \\ 1 \end{pmatrix}, \; \mathfrak{v}_5 = \begin{pmatrix} 3 \\ 1 \end{pmatrix}, \; \mathfrak{v}_6 = \begin{pmatrix} 2 \\ 0 \end{pmatrix}. \tag{2}$$

A **non-negative integer weight function** on a Zhegalkin Zebra Motive $\mathcal{Z}$ is a map $\nu : \mathcal{E} \to \mathbb{Z}_{\geq 0}$ from the set $\mathcal{E}$ of edges in the planar tiling to the set $\mathbb{Z}_{\geq 0}$ of non-negative integers for which there is an integer $\deg(\nu)$, called the **degree** of ν, such that for every polygon P in the tiling

$$\sum_{e \text{ edge of } P} \nu(e) \; = \; \deg(\nu). \tag{3}$$

A non-negative integer weight function of degree 1 is called a **perfect matching** or **dimer covering**. The latter terminology refers to the following geometric structure. If ν is a non-negative integer weight function of degree 1 it follows

---

[2]announced in [22] as "to appear in a forthcoming paper"

4
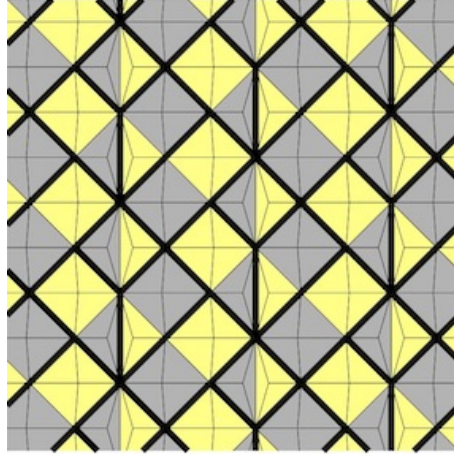
Figure 3: A dimer covering for the Zhegalkin Zebra Motive $Z^{23} + Z^{43} + Z^{61}$. The edges are oriented such that the grey polygon is on their right.

from (3) that the only possible values for $\nu(e)$ are 0 and 1 and that for every polygon P in the tiling there is exactly one edge e of P with $\nu(e) = 1$. Thus for every black polygon **b** there is exactly one white polygon **w** adjacent to **b** such that $\nu(e) = 1$ for the common edge e. It is standard practice in the literature on brane tilings to picture a perfect matching by marking on the planar bipartite graph the edges with $\nu(e) = 1$ with a special color; see e.g. [12] Figures 9, 33, 34. On a tiling of the plane by black and white polygons it is more illuminating to mark the edges with $\nu(e) = 0$ with a special color. This illustrates why one calls this a *dimer covering*; see Figure 3.[3]

A **positive integer weight function** is a non-negative integer weight function ν such that $\nu(e) > 0$ for all e. A positive integer weight function ν can be used to **mark a point** inside each polygon P by taking the convex combination specified by $\frac{1}{\deg \nu}\nu$ of the midpoints of the edges of P.

One can easily upgrade the picture of the planar polygonal black-white tiling to a tiling $\Gamma^{\square}$ of the plane by polygons colored black, yellow, green or white such that the new black polygons are scaled copies of the old black polygons, the new yellow polygons are scaled copies of the old white polygons, the new white polygons correspond with the vertices of the original tiling and each green polygon is a parallelogram which corresponds with an edge of the original tiling and has two sides parallel to that edge. The tiling $\Gamma^{\square}$ is such that the adjacency structure of the new polygons is the same as the incidence structure between edges, vertices and polygons in the original tiling. The actual drawing of $\Gamma^{\square}$ depends of the choice of certain parameters which control the visual appearance, but do not affect the adjacency structure. For examples see the $\mathcal{Z}_3$ pictures in Figures 2 and 4.

---

[3]As an instructive exercise one may search for dimer coverings in Figure 2. The brane tiling in [12] Figure 9 corresponds with the Zhegalkin Zebra Motive denoted "model 14" in Figure 35. So, it may also be an instructive exercise to recognize the perfect matchings in [12] Figure 9 as dimer coverings in this "model 14".
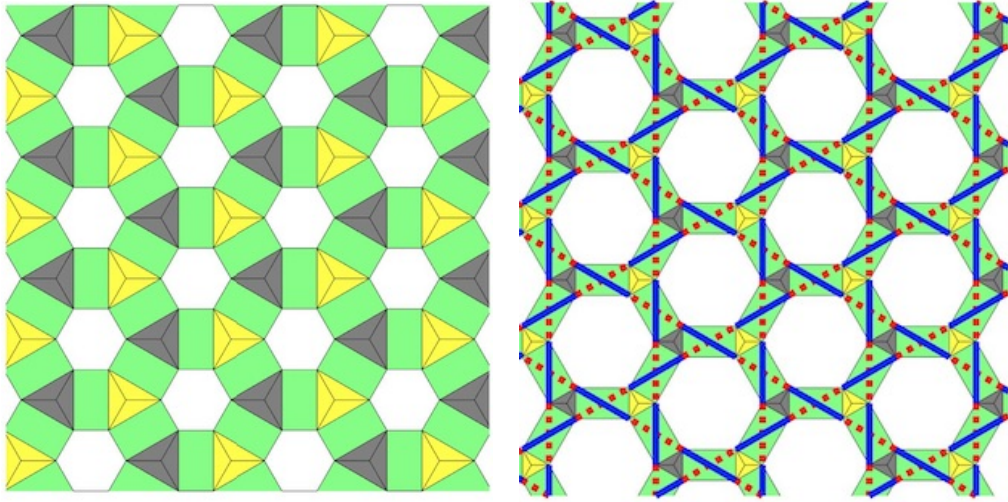
$$\mathcal{Z}_3 = \mathsf{Z}^{21} + \mathsf{Z}^{41} + \mathsf{Z}^{61}$$

Figure 4: The tiling $\Gamma^\square$ for the Zhegalkin Zebra Motive $\mathcal{Z}_3$. The new white polygons are holes in the plane and the union of the black, yellow and green polygons is a thickening of the bipartite graph $\Gamma^\vee$. For the original black-white tiling see Figure 2 top-right. The twist function for the right picture is $\eta \equiv 1$.

We define the **automorphism group** $\mathsf{Aut}(\mathcal{Z})$ of the Zhegalkin Zebra Motive $\mathcal{Z}$ to be the group of translations in the plane which leave the tiling invariant:

$$\mathsf{Aut}(\mathcal{Z}) = \{\, \tau \in \mathbb{R}^2 \,|\, \mathcal{Z}(\mathbf{x} + \tau) = \mathcal{Z}(\mathbf{x}), \ \forall \mathbf{x} \in \mathbb{R}^2 \,\}, \tag{4}$$

This is a lattice in $\mathbb{R}^2$ because by assumption the frequencies of the zebras lie in $\mathbb{Z}^2$ and the polygons in the tiling are bounded and convex[4].

Definition 1 *For a Zhegalkin Zebra Motive $\mathcal{Z}$ and a sublattice $\Lambda \subset \mathsf{Aut}(\mathcal{Z})$ we say that $(\mathcal{Z}, \Lambda)$ is* **dimer complete** *if a Λ-invariant positive weight function ν exists.* [5]

For a sublattice Λ of $\mathsf{Aut}(\mathcal{Z})$ the function $\mathcal{Z}$ induces an $\mathbb{F}_2$-valued function on the torus $\mathbb{R}^2/\Lambda$. The black-white polygonal tiling and the tiling $\Gamma^\square$ also descend to the torus $\mathbb{R}^2/\Lambda$. Taking the graphs Γ and $\Gamma^\vee$ modulo Λ one obtains the **quiver** Γ_Λ and the **bipartite graph** $\Gamma_\Lambda^\vee$, both embedded in the torus $\mathbb{R}^2/\Lambda$.

We denote the set of edges of the black-white tiling on $\mathbb{R}^2/\Lambda$ by $\mathcal{E}_\Lambda$. Identifying $\mathcal{E}_\Lambda$ with the set $\{1, \ldots, n\}$ amounts to a labeling of the edges in the black-white tiling and of the green polygons in the tiling $\Gamma^\square$. The oriented boundary of a polygon (black clockwise, white counter-clockwise) gives a cyclic permutation of elements of $\mathcal{E}_\Lambda$. Since every edge is in precisely one black polygon the cyclic permutations coming from the various black polygons are disjoint.

---

[4]In [22] §5.2.2 it is explained how one can determine (by computer) the lattice $\mathsf{Aut}(\mathcal{Z})$ from the defining formula for $\mathcal{Z}$. In practice one can see it directly in the picture of the tiling.

[5]For issues of existence of positive integer weight functions we refer to the text preceding Corollary 2.

The product of these cycles is a permutation σ_1 of the set $\mathcal{E}_\Lambda$. In the same way the white polygons lead to a permutation σ_0 of $\mathcal{E}_\Lambda$. The triple $(\mathcal{E}_\Lambda, \sigma_0, \sigma_1)$ is called the **superpotential** of $(\mathcal{Z}, \Lambda)$. Identifying $\mathcal{E}_\Lambda$ with $\{1, \ldots, n\}$ reduces the superpotential to a pair of permutations (σ_0, σ_1) of $\{1, \ldots, n\}$ [6] [7]. For examples see Figures 17, 19, 20, 32, 43. The white (resp. black) nodes of the bipartite graph $\Gamma_\Lambda^\vee$ correspond 1-1 with the cycles of the permutation σ_0 (resp. σ_1). The edges of $\Gamma_\Lambda^\vee$ between two nodes correspond with the common elements in the cycles. The abstract graph $\Gamma_\Lambda^\vee$ does not depend on the cyclic ordering within the cycles of σ_0 and σ_1. The cyclic ordering makes $\Gamma_\Lambda^\vee$ into a **ribbon graph** and provides a lot of extra structure.

According to [3] Definition 7 (also see [20]) a ***textile structure*** is an embedding of (a disjoint union of) infinitely many lines or circles into the thickened plane $\mathbb{R}^2 \times [-1, 1] \subset \mathbb{R}^3$ preserved under translations by two linearly independent vectors in $\mathbb{R}^2$. One can conveniently picture a textile structure by its **torus diagram**; see [3] Definition 7. This is the image of the configuration of lines and circles under the projection $\mathbb{R}^2 \times [-1, 1] \to \mathbb{R}^2$ plus the usual indication of over/under crossings as in knot theory. The diagram should also include a period parallelogram for the lattice Λ of translations which leave the configuration invariant.

*Taking the textile structure modulo the period lattice Λ one obtains a **link in the thickened torus** $\mathbb{R}^2/\Lambda \times [-1, 1]$.*

In the present paper we investigate textile structures which are naturally associated with a Zhegalkin Zebra Motive $\mathcal{Z}$, a sublattice $\Lambda \subset \mathsf{Aut}(\mathcal{Z})$ and a function $\eta : \mathcal{E}_\Lambda \to \{\pm 1\}$. The simplest method for constructing these textiles is to draw in the planar tiling $\Gamma^\square$ the diagonals in the green parallelograms with an indication of the over/under crossing as specified by η. For an example with $\eta(e) = 1$ for all $e \in \mathcal{E}_\Lambda$ see Figure 4 where the threads are the strings of blue and red line segments.

Putting in a period parallelogram for Λ one obtains the *torus diagram* of a textile structure; see Figures 19, 39.

2.1.1 Textiles and Seifert surfaces

In Section 4.2, we construct **real textile structures** and not just their torus diagrams for **Zhegalkin Zebra Motives** which are **dimer complete** in the sense of Definition 1. This textile structure is the boundary of a Λ-periodic oriented surface $\widetilde{\mathfrak{S}}_{\mathcal{Z}, \eta, \nu, \omega}^{\leqslant h}$ in $\mathbb{R}^2 \times [-1, 1]$. The construction of this surface involves a choice of parameters η, ν, ω, h. Figure 5 shows an example of how the projection of $\widetilde{\mathfrak{S}}_{\mathcal{Z}, \eta, \nu, \omega}^{\leqslant h}$ in the horizontal plane compares with the tiling $\Gamma^\square$ constructed with the same choice of parameters ν, ω, h.

---

[6]Once one has a picture of the planar polygonal tiling the edges can be labeled by hand.

[7]In the physics literature, e.g. [13, 14], the superpotential is usually written as a polynomial

$$\mathcal{Z}_3 = \mathsf{Z}^{21} + \mathsf{Z}^{41} + \mathsf{Z}^{61}$$
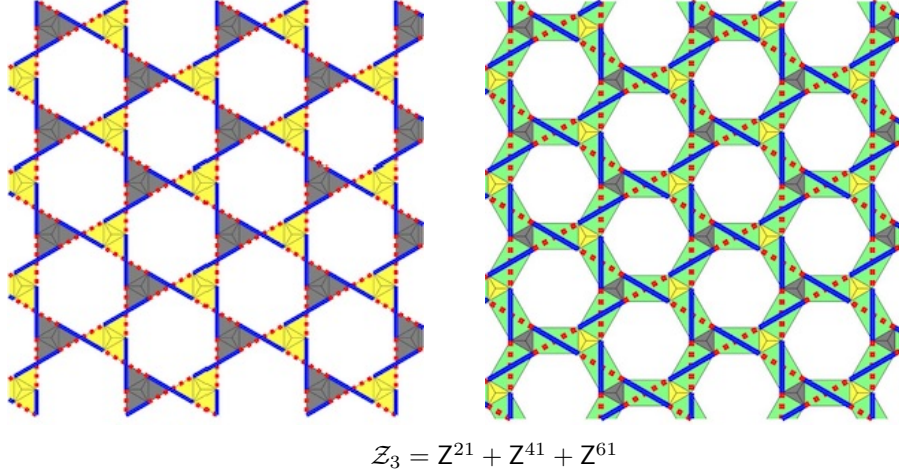
Figure 5: The tiling $\Gamma^\square$ for the Zhegalkin Zebra Motive $\mathcal{Z}_3$. The new white polygons are holes in the plane and the union of the black, yellow and green polygons is a thickening of the bipartite graph $\Gamma^\vee$. For the original black-white tiling see Figure 2 top-right. The twist function for the right picture is $\eta \equiv 1$.

Taking the surface $\widetilde{\mathfrak{S}}_{\mathcal{Z},\eta,\nu,\omega}^{\leqslant h}$ modulo Λ yields an oriented surface in the thickened torus $\mathbb{R}^2/\Lambda \times [-1,1]$, which can subsequently be embedded into $\mathbb{R}^3$. We thus obtain an explicit, accurate, real world model $\mathfrak{S}_{\mathcal{Z},\Lambda,\boxminus,r}^{\leqslant h}$ of a surface of which the boundary is the desired link in a thickened 2-torus. The surface itself is a **_Seifert surface_** for this link. For examples see Figures 15, 33, 37.

2.1.2 The kernel of the fabric

By construction the surface $\mathfrak{S}_{\mathcal{Z},\Lambda,\boxminus,r}^{\leqslant h}$ lies in a thickened torus in $\mathbb{R}^3$ which can be taken to be independent of h and r. By gluing to the thickened torus a solid torus on the outside and a solid torus on the inside one obtains a 3-sphere $\mathbb{S}^3$. Thus the boundary of $\mathfrak{S}_{\mathcal{Z},\Lambda,\boxminus,r}^{\leqslant h}$ becomes a link $\mathfrak{L}_h$ in $\mathbb{S}^3$.

Now fix h^0 close to 1 such that $0 < h^0 < 1$. Let $\mathfrak{L}$ denote the link $\mathfrak{L}_{h^0}$. The link $\mathfrak{L}$ together with the central circles X and Y of the two solid tori form the link $\mathfrak{L}^\infty = \mathsf{X} \cup \mathsf{Y} \cup \mathfrak{L}$ in $\mathbb{S}^3$. In [20] the link $\mathfrak{L}^\infty$ is called the **kernel of the fabric**.

For $0 < h < h^0$ the surface $\mathfrak{S}_{\mathcal{Z},\Lambda,\boxminus,r}^{\leqslant h}$ lies in the surface $\mathfrak{S}_{\mathcal{Z},\Lambda,\boxminus,r}^{\leqslant h^0}$ and also in the complement of an open tubular neighborhood of $\mathfrak{L}^\infty$:

$$\mathfrak{S}_{\mathcal{Z},\Lambda,\boxminus,r}^{\leqslant h} \hookrightarrow \mathbb{S}^3 \setminus \mathfrak{L}^\infty. \tag{5}$$

---

in n non-commuting variables.

2.1.3   Seifert form, Poisson structure and Monodromy

The embedding of $\mathfrak{S}_{\mathcal{Z},\Lambda,\boxminus,r}^{\leqslant h}$ into $\mathbb{S}^3$ induces on $\mathrm{H}_1(\mathfrak{S}_{\mathcal{Z},\Lambda,\boxminus,r}^{\leqslant h}, \mathbb{Z})$ a bilinear form known as the **Seifert form** [8]. By our constructions the bipartite graph $\Gamma_\Lambda^\vee$ lies as a *deformation retract* in the surface $\mathfrak{S}_{\mathcal{Z},\Lambda,\boxminus,r}^{\leqslant h}$ for all choices of the parameters h, r, $\boxminus$. Consequently

$$\mathrm{H}_1(\Gamma_\Lambda^\vee, \mathbb{Z}) \simeq \mathrm{H}_1(\mathfrak{S}_{\mathcal{Z},\Lambda,\boxminus,r}^{\leqslant h}, \mathbb{Z}) \qquad \text{for all } h, r, \boxminus. \tag{6}$$

So, the Seifert form S is actually a bilinear form on $\mathrm{H}_1(\Gamma_\Lambda^\vee, \mathbb{Z})$. *It is explicitly computed in Section 5.4.*

The surface $\mathfrak{S}_{\mathcal{Z},\Lambda,\boxminus,r}^{\leqslant h}$ depends on the *superpotential* $(\mathcal{E}_\Lambda, \sigma_0, \sigma_1)$ and all parameters h, r, $\boxminus = (\eta, \nu, \omega, \lambda_1, \lambda_2)$, but *the Seifert form S depends only on* σ_0, σ_1, $\eta, \lambda_1, \lambda_2$, while its *anti-symmetrization* $\mathsf{S} - \mathsf{S}^t$ is also independent of the choice of $\eta, \lambda_1, \lambda_2$.

The anti-symmetric bilinear form $\mathsf{S} - \mathsf{S}^t$ is used in [11] for the construction of a **Poisson structure** on the complex torus $\mathrm{H}^1(\Gamma_\Lambda^\vee, \mathbb{C}^*)$; see Theorem 6. It only depends on the superpotential $(\mathcal{E}_\Lambda, \sigma_0, \sigma_1)$.

Most interesting are the settings for $\eta, \lambda_1, \lambda_2$ for which the Seifert form S is non-degenerate. In those cases one defines the **monodromy transformation** M on $\mathrm{H}_1(\Gamma_\Lambda^\vee, \mathbb{Z})$ by

$$\mathsf{M} = \left(\mathsf{S}^t\right)^{-1}\mathsf{S} \tag{7}$$

see Definition 5. For examples see §5.4.1, §5.4.2. *The monodromy transformation induces a Poisson automorphism on the complex torus $\mathrm{H}^1(\Gamma_\Lambda^\vee, \mathbb{C}^*)$.*

The embedding (5) and the isomorphism (6) induce a linear map

$$\mathrm{H}_1(\Gamma_\Lambda^\vee, \mathbb{Z}) \longrightarrow \mathrm{H}_1(\mathbb{S}^3 \setminus \mathfrak{L}^\infty, \mathbb{Z}). \tag{8}$$

This map is explicitly computed in Section 6.2. The Seifert form and the monodromy are essential ingredients in this computation; see Formulas (209)-(213).

2.2   Hyperbolic Belyi maps

The superpotential $(\mathcal{E}_\Lambda, \sigma_0, \sigma_1)$ is equivalent to the homomorphism of groups

$$\sigma_* : \mathsf{F}_2 \longrightarrow \mathcal{S}_{\mathcal{E}_\Lambda} \,, \qquad \sigma_*(\delta_0) = \sigma_0, \quad \sigma_*(\delta_1) = \sigma_1 \tag{9}$$

from the free group F_2 on two generators δ_0 and δ_1 to the group $\mathcal{S}_{\mathcal{E}_\Lambda} = \mathcal{S}_n$ of permutations on the set $\mathcal{E}_\Lambda = \{1, \ldots, n\}$. Via σ_* the group F_2 acts transitively on $\mathcal{E}_\Lambda$. The group F_2 can be identified with the fundamental group of $\mathbb{C} \setminus \{0, 1\}$ such that δ_0 and δ_1 are the counter-clockwise oriented circles with radius $\frac{1}{2}$ around 0 and 1, respectively, starting at the point $\frac{1}{2}$. From this geometric interpretation of F_2 and σ_* one obtains with a well-known classical construction (see

---

[8]A *physical model of the surface* $\mathfrak{S}_{\mathcal{Z},\Lambda,\boxminus,r}^{\leqslant h}$ in $\mathbb{R}^3$ actually has a positive thickness and the two sides have opposite orientations. The Seifert form then gives the linking numbers of closed curves on one side with closed curves on the other side.
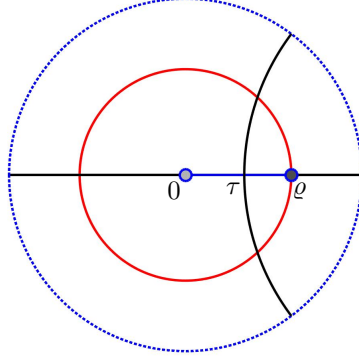
Figure 6: Closed unit disk $\overline{\mathbb{D}}$ with interval $[0, \varrho]$ and circles $\mathbb{U}(1)$, $\mathbb{U}(\varrho)$ with centre 0 and respective radii 1, ϱ; here $\varrho = \frac{3}{5}$ and $\tau = \frac{1}{3}$.

e.g. [17] 1.2.15, 1.2.17, 1.2.18) an oriented compact two-dimensional manifold $\mathbb{X}_{\sigma_0, \sigma_1}$ and a ramified covering map of degree n

$$\varphi_{\sigma_0, \sigma_1} : \mathbb{X}_{\sigma_0, \sigma_1} \longrightarrow \mathbb{CP}^1 = \mathbb{C} \cup \{\infty\} \tag{10}$$

which ramifies at most over the points 0, 1, ∞ such that the action of F_2 on the fiber $\varphi_{\sigma_0, \sigma_1}^{-1}(\frac{1}{2})$ is given by the homomorphism σ_*. The points in the fiber $\varphi_{\sigma_0, \sigma_1}^{-1}(0)$ (resp. $\varphi_{\sigma_0, \sigma_1}^{-1}(1)$, resp. $\varphi_{\sigma_0, \sigma_1}^{-1}(\infty)$) correspond 1-1 with the cycles of the permutation σ_0 (resp. σ_1, resp. $\sigma_0 \sigma_1$). The bipartite graph $\Gamma_\Lambda^\vee$ lies in $\mathbb{X}_{\sigma_0, \sigma_1}$ as the inverse image of the interval $[0, 1]$ [9].

The **Euler characteristic** of $\mathbb{X}_{\sigma_0, \sigma_1}$ is (see [17] Thm 1.3.10)

$$\chi(\mathbb{X}_{\sigma_0, \sigma_1}) = |\sigma_0| + |\sigma_1| + |\sigma_0 \sigma_1| - n, \tag{11}$$

where $|\sigma|$ denotes the number of cycles of the permutation σ.

For a real number ϱ with $0 < \varrho < 1$ we set

$$\varphi_{\sigma_0, \sigma_1, \varrho} = \varrho \cdot \varphi_{\sigma_0, \sigma_1}, \quad \mathbb{X}_{\sigma_0, \sigma_1, \varrho} = \varphi_{\sigma_0, \sigma_1, \varrho}^{-1}(\mathbb{D}), \quad \overline{\mathbb{X}}_{\sigma_0, \sigma_1, \varrho} = \varphi_{\sigma_0, \sigma_1, \varrho}^{-1}(\overline{\mathbb{D}}) \tag{12}$$

where $\mathbb{D} = \{z \in \mathbb{C} \mid |z| < 1\}$ is the open unit disc and $\overline{\mathbb{D}}$ its closure. $\mathbb{X}_{\sigma_0, \sigma_1, \varrho}$ is an open subset of the surface $\mathbb{X}_{\sigma_0, \sigma_1}$ and $\overline{\mathbb{X}}_{\sigma_0, \sigma_1, \varrho}$ is its closure.

$\mathbb{D}$ is a model for the *hyperbolic plane*. The map

$$\varphi_{\sigma_0, \sigma_1, \varrho} : \mathbb{X}_{\sigma_0, \sigma_1, \varrho} \longrightarrow \mathbb{D} \tag{13}$$

is a ramified covering map of degree n which ramifies over the points 0, ϱ. It is a **hyperbolic Belyi map** in the sense of [8] §3.

---

[9] If instead of (9) one takes the homomorphism $\delta_0 \mapsto \sigma_0$, $\delta_1 \mapsto \sigma_1^{-1}$ the constructions yield the torus $\mathbb{R}^2/\Lambda$ with the graph $\Gamma_\Lambda^\vee$ embedded in it. The appearance of σ_1^{-1} here as opposed to σ_1 in (9) is the simplest manifestation of the **twisting procedure** in [9, 11] and of the **specular duality** in [14].

Let (see Figure 6)

$$\mathbb{U}(1) \;\; = \;\; \text{circle with centre at } 0 \text{ and radius } 1 \;=\; \overline{\mathbb{D}} \setminus \mathbb{D}\,; \tag{14}$$

$$\mathbb{U}(\varrho) \;\; = \;\; \text{circle with centre at } 0 \text{ and radius } \varrho; \tag{15}$$

$$C_\tau \;\; = \;\; \overline{\mathbb{D}} \cap \{\text{circle with centre at } \varrho^{-1} \text{ and radius } \sqrt{\varrho^{-2} - 1}\,; \tag{16}$$

$$\tau \;\; = \;\; \varrho^{-1} - \sqrt{\varrho^{-2} - 1}. \tag{17}$$

Note that $\overline{\mathbb{D}}$ and $\mathbb{D}$ are invariant under the hyperbolic reflections in the line $[-1, 1]$ and the arc C_τ; see Figure 6. The first reflection leaves the points 0 and ϱ invariant. The second one interchanges 0 and ϱ.

The inverse image $\varphi_{\sigma_0,\sigma_1,\varrho}^{-1}\big(\mathbb{U}(1)\big)$ of the counter-clockwise oriented circle $\mathbb{U}(1)$ is the **boundary** of $\overline{\mathbb{X}}_{\sigma_0,\sigma_1,\varrho}$. Its connected components correspond 1-1 with the cycles of the permutation $\sigma_1\sigma_0$.

The **bipartite graph** $\Gamma_\Lambda^\vee$ lies in $\mathbb{X}_{\sigma_0,\sigma_1,\varrho}$ as the inverse image $\varphi_{\sigma_0,\sigma_1,\varrho}^{-1}\big([0,\varrho]\big)$ of the closed interval $[0, \varrho]$. It is a **deformation retract** of $\mathbb{X}_{\sigma_0,\sigma_1,\varrho}$ and $\overline{\overline{\mathbb{X}}}_{\sigma_0,\sigma_1,\varrho}$. Hence:

$$\mathrm{H}_1(\Gamma_\Lambda^\vee, \mathbb{Z}) \simeq \mathrm{H}_1(\mathbb{X}_{\sigma_0,\sigma_1,\varrho}, \mathbb{Z}) \simeq \mathrm{H}_1(\overline{\mathbb{X}}_{\sigma_0,\sigma_1,\varrho}, \mathbb{Z}). \tag{18}$$

The fiber $\varphi_{\sigma_0,\sigma_1,\varrho}^{-1}(\tau)$ can be identified with the set $\mathcal{E}_\Lambda$. Let $e^\times$ denote the point of $\varphi_{\sigma_0,\sigma_1,\varrho}^{-1}(\tau)$ which corresponds to $e \in \mathcal{E}_\Lambda$. The connected components of $\varphi_{\sigma_0,\sigma_1,\varrho}^{-1}(C_\tau)$ form a collection of disjoint, simple, **oriented curves** $\mathcal{J}_e$ in $\overline{\mathbb{X}}_{\sigma_0,\sigma_1,\varrho}$ such that $\mathcal{J}_e$ passes through the point $e^\times$. The endpoints of the closure $\overline{\mathcal{J}_e}$ of $\mathcal{J}_e$ lie on the boundary of $\overline{\mathbb{X}}_{\sigma_0,\sigma_1,\varrho}$ so that $\overline{\mathcal{J}_e}$ starts (resp. ends) at the boundary component which corresponds to the cycle of $\sigma_1\sigma_0$ which contains e (resp. contains $\sigma_0(e)$).

Remark 1 The inverse image $\varphi_{\sigma_0,\sigma_1,\varrho}^{-1}\big(\mathbb{U}(\varrho)\big)$ of the counter-clockwise oriented circle $\mathbb{U}(\varrho)$ is a quiver $\Gamma_\Lambda^\circlearrowleft$ with set of nodes $\varphi_{\sigma_0,\sigma_1,\varrho}^{-1}(\varrho)$. The arrows of $\Gamma_\Lambda^\circlearrowleft$ are the closures of the connected components of $\varphi_{\sigma_0,\sigma_1,\varrho}^{-1}\big(\mathbb{U}(\varrho)\setminus\{\varrho\}\big)$. Since $\Gamma_\Lambda^\circlearrowleft$ is embedded in the oriented surface $\mathbb{X}_{\sigma_0,\sigma_1,\varrho}$ there is at every node a specified cyclic ordering of the edges incident to that node; i.e. $\Gamma_\Lambda^\circlearrowleft$ is a **directed ribbon graph**. In Section B we give a description of the underlying **abstract quiver** $\Gamma_\Lambda^\circlearrowleft$ directly in terms of the superpotential $(\mathcal{E}_\Lambda, \sigma_0, \sigma_1)$ and discuss its relation with the bipartite graph $\Gamma_\Lambda^\vee$.

2.3   Hyperbolic Belyi maps and Seifert surfaces

In Section 4.4 Formulas (88), (98), (99) we give a construction of the surfaces $\overline{\mathbb{X}}_{\sigma_0,\sigma_1,\varrho}$ and $\mathbb{X}_{\sigma_0,\sigma_1,\varrho}$ and the hyperbolic Belyi map $\varphi_{\sigma_0,\sigma_1,\varrho}$ completely in the spirit of [8] and independent of the construction of the map (10) in [17]

More precisely in Formula (88), we construct the surface $\overline{\mathbb{X}}_{\sigma_0,\sigma_1,\varrho}$ by gluing quadrangles which are explicitly parametrized by the unit square $[0, 1] \times [0, 1]$. For every $e \in \mathcal{E}_\Lambda$ there are four quadrangles and these are glued according to the plan in Figures 14 and 21. This construction works under the condition $\varrho > \cos\big(\frac{\pi}{N}\big)$ where N is the maximal cycle length in the permutations σ_0, σ_1.

In Section 4.2 we construct surfaces $\mathfrak{S}_{\mathcal{Z},\Lambda,\boxminus,r}$ and $\mathfrak{S}_{\mathcal{Z},\Lambda,\boxminus,r}^{\leqslant h}$ in $\mathbb{R}^3$ using the permutations (σ_0, σ_1) from a dimer complete Zhegalkin Zebra Motive $\mathcal{Z}$ and a sublattice Λ of $\mathsf{Aut}(\mathcal{Z})$ as well as auxiliary parameters h, r and $\boxminus = (\eta, \nu, \omega, \lambda_1, \lambda_2)$ which are subject to certain conditions (see §4.2). We construct these surfaces by gluing charts I_e, II_e, III_e, IV_e for $e \in \mathcal{E}_\Lambda$ according to the plan in Figures 14 and 21. Each chart comes with an explicit parametrization by the unit square $[0,1] \times [0,1]$ which is given in Formulas (59), (60), (66), (69).

In Formulas (70)-(71) and (96)-(97) we use the parametrizations to define the "truncated" surfaces

$$\overline{\mathbb{X}}_{\sigma_0,\sigma_1,\varrho}^{\leqslant h}, \quad \mathbb{X}_{\sigma_0,\sigma_1,\varrho}^{<h}, \quad \mathfrak{S}_{\mathcal{Z},\Lambda,\boxminus,r}^{\leqslant h}, \quad \mathfrak{S}_{\mathcal{Z},\Lambda,\boxminus,r}^{<h}. \tag{19}$$

Since the gluing and truncation schemes in Sections 4.2 and 4.4 agree we conclude that the following theorem holds.

Theorem 1   *i. For every admissible choice of the parameters ϱ, h, r and $\boxminus = (\eta, \nu, \omega, \lambda_1, \lambda_2)$ there are orientation preserving homeomorphisms*

$$\mathbb{X}_{\sigma_0,\sigma_1,\varrho}^{<h} \simeq \mathfrak{S}_{\mathcal{Z},\Lambda,\boxminus,r}^{<h}, \qquad \overline{\mathbb{X}}_{\sigma_0,\sigma_1,\varrho}^{\leqslant h} \simeq \mathfrak{S}_{\mathcal{Z},\Lambda,\boxminus,r}^{\leqslant h}. \tag{20}$$

In the limit $h \uparrow 1$ the homeomorphisms (20) converge to a map

$$\overline{\mathbb{X}}_{\sigma_0,\sigma_1,\varrho} \longrightarrow \mathfrak{S}_{\mathcal{Z},\Lambda,\boxminus,r} \tag{21}$$

which is a homeomorphism away from $|\mathcal{E}_\Lambda|$ points on the boundary of $\overline{\mathbb{X}}_{\sigma_0,\sigma_1,\varrho}$ and $|\mathsf{P}_\Lambda^\star|$ points on the boundary of $\mathfrak{S}_{\mathcal{Z},\Lambda,\boxminus,r}$. On the exceptional boundary points the map (21) corresponds to the cycle decomposition of the permutation $\sigma_1^{-1}\sigma_0$.

ii. For every $e \in \mathcal{E}_\Lambda$ the map (21) restricts to a homeomorphism from the oriented curve $\overline{\mathcal{J}_e}$ on $\overline{\mathbb{X}}_{\sigma_0,\sigma_1,\varrho}$ onto the oriented line segment $\mathcal{I}_e$ in $\mathbb{R}^3$ defined in Formula (73). This preserves the orientation if $\eta(e) = 1$ and reverses the orientation if $\eta(e) = -1$.

$\blacksquare$

Remark 2 In Section C the topic of Theorem 1*ii* is further elaborated with algebraic combinatorial techniques using the textile code. See in particular Remark 16.

The surface $\overline{\mathbb{X}}_{\sigma_0,\sigma_1,\varrho}$ is the **conjugated surface** $\widehat{S_w}$ in [11] §1.1. The inclusion $\overline{\mathbb{X}}_{\sigma_0,\sigma_1,\varrho} \subset \mathbb{X}_{\sigma_0,\sigma_1}$ (see (12)) induces a surjective homomorphism

$$\mathrm{H}_1(\overline{\mathbb{X}}_{\sigma_0,\sigma_1,\varrho}, \mathbb{Z}) \longrightarrow \mathrm{H}_1(\mathbb{X}_{\sigma_0,\sigma_1}, \mathbb{Z}) \tag{22}$$

of which the kernel is generated by the homology classes of the connected components of the boundary of $\overline{\mathbb{X}}_{\sigma_0,\sigma_1,\varrho}$. This is the subgroup of $\mathrm{H}_1(\Gamma_\Lambda^\vee, \mathbb{Z})$ generated by the homology classes of the zigzag loops $\ell_{\mathbf{z}}$ ($\mathbf{z} \in \mathsf{P}_\Lambda^{\mathsf{z}}$); see (6), (18), (127).

The anti-symmetrization $\mathsf{S} - \mathsf{S}^t$ of the Seifert form is equal to the pull-back via (22) of the intersection form on $H_1(\mathbb{X}_{\sigma_0,\sigma_1}, \mathbb{Z})$ and is, therefore, the same as the anti-symmetric bilinear form used in [11] for the construction of a **Poisson structure** on the complex torus $H^1(\Gamma_\Lambda^\vee, \mathbb{C}^*)$; see Theorem 6.

3 Vistas and revisions

The composition of the maps in (20) and (5) gives an embedding

$$\mathbb{X}_{\sigma_0,\sigma_1,\varrho} \; \hookrightarrow \; \mathbb{S}^3 \setminus \mathfrak{L}^\infty. \tag{23}$$

One can trace through the constructions in Section 4 an explicit description of the map (23) which is, however, very complicated and not illuminating. The maps in (18) and (8) and the computations in §6.2 yield a fairly simple, explicit description of the induced map on homology

$$H_1\big(\mathbb{X}_{\sigma_0,\sigma_1,\varrho}, \mathbb{Z}\big) \; \hookrightarrow \; H_1\big(\mathbb{S}^3 \setminus \mathfrak{L}^\infty, \mathbb{Z}\big). \tag{24}$$

But that contains only secondary information about the map (23).

*For that reason we sketch in this section the beginnings of an alternative approach via an embedding of the **universal covering** of $\mathbb{X}_{\sigma_0,\sigma_1,\varrho}$ into **hyperbolic three space**.*

3.1 Schottky dance on a Zhegalkin Zebra Motive

The construction of the universal covering of $\mathbb{X}_{\sigma_0,\sigma_1,\varrho}$ is based on the **universal covering** $\widetilde{\Gamma_\Lambda^\vee}$ of the bipartite graph $\Gamma_\Lambda^\vee$, whereas in Section 4.4.2 we use a **rooted spanning tree** $\widehat{\Gamma_\Lambda^\vee}$ for $\Gamma_\Lambda^\vee$. Since the bipartite graph $\Gamma_\Lambda^\vee$ is a deformation retract of the surface $\mathbb{X}_{\sigma_0,\sigma_1,\varrho}$ the universal covering of $\Gamma_\Lambda^\vee$ is a deformation retract of the universal covering of $\mathbb{X}_{\sigma_0,\sigma_1,\varrho}$. The fundamental group $\pi_1(\Gamma_\Lambda^\vee) = \pi_1(\mathbb{X}_{\sigma_0,\sigma_1,\varrho})$ acts on these universal covering spaces and the constructions in §4.4 amount to choosing a fundamental domain for this action.

The term **Schottky dance** is taken from the title of [21] Chapter 4, because this was a great source of inspiration for our constructions which produce pictures by repeatedly applying transformations from a finite collection of Möbius transformations to a finite collection of building blocks. Both the Möbius transformations and the building blocks are directly given by the Zhegalkin Zebra Motive $\mathcal{Z}$ and one additional parameter ϱ which is the same ϱ as in $\mathbb{X}_{\sigma_0,\sigma_1,\varrho}$. It must be such that $\varrho = \cos(\beta)$ with $0 < \beta N < \pi$ where N is the maximal number of sides of the polygons in the planar tiling defined by $\mathcal{Z}$.

We start from a *dimer complete* Zhegalkin Zebra Motive $\mathcal{Z}$ and a sublattice Λ of $\mathsf{Aut}(\mathcal{Z})$. We only use the combinatorial data about the number and cyclic ordering of the sides of the black and white polygons in the planar tiling and

13

which polygons are adjacent [10]. As before the sets of edges, black polygons and white polygons of the planar tiling modulo Λ are denoted by $\mathcal{E}_\Lambda$, $\mathsf{P}_\Lambda^\bullet$ and P_Λ°, respectively. The set $\mathcal{E}_\Lambda$ is identified with $\{1, \ldots, n\}$. The combinatorial data are encoded in the two permutations σ_0 and σ_1 of $\{1, \ldots, n\}$ such that P_Λ° and $\mathsf{P}_\Lambda^\bullet$ are identified with the sets of cycles of σ_0 and σ_1, respectively. For $e \in \mathcal{E}_\Lambda$ the cycle of σ_0 (resp. σ_1) which contains e is denoted by $w(e)$ (resp. $b(e)$). In Section 2.3 the triple $(\mathcal{E}_\Lambda, \sigma_0, \sigma_1)$ is called the **superpotential** of $(\mathcal{Z}, \Lambda)$. Adjacency of the polygons is encoded in the "abstract" **bipartite graph** $\Gamma_\Lambda^\vee$: the set of white (resp. black) nodes of $\Gamma_\Lambda^\vee$ is identified with P_Λ° (resp. $\mathsf{P}_\Lambda^\bullet$) and the set of edges is identified with $\mathcal{E}_\Lambda$ such that two nodes $\mathbf{w}$ and $\mathbf{b}$ are connected by edge e if and only if the corresponding cycles of σ_0 and σ_1 both contain e. Here "abstract" means that this definition of $\Gamma_\Lambda^\vee$ does not include a cyclic ordering of the edges incident with a node.

For the purpose of correct bookkeeping we fix a perfect matching m_0 [11]. This is a map $\mathsf{m}_0 : \mathcal{E}_\Lambda \to \{0, 1\}$ such that every cycle of σ_0 and σ_1 contains exactly one $e \in \mathcal{E}_\Lambda$ with $\mathsf{m}_0(e) = 1$. This is then used to normalize the standard notation for the cycle decomposition of σ_0 and σ_1 such that in each cycle the element e with $\mathsf{m}_0(e) = 1$ appears in the leftmost position. The positions in the cycles are numbered from left to right as $0, 1, 2, \ldots$. The cycles and, hence, the nodes of $\Gamma_\Lambda^\vee$ may then be labeled as $e_\circ$ resp. $e_\bullet$ where e is the leftmost entry.

Example 1 For the Zhegalkin Zebra Motive $\mathcal{Z} = \mathsf{Z}^{21} + \mathsf{Z}^{31} + \mathsf{Z}^{41} + \mathsf{Z}^{62}$ and $\Lambda = \mathsf{Aut}(\mathcal{Z}) = \mathbb{Z}(2, 2) + \mathbb{Z}(2, -2)$ the planar tiling and the edge labels are shown in Figure 19. The permutations σ_0 and σ_1 are given in Formula (80). We take the perfect matching $\mathsf{m}_0 : \mathcal{E}_\Lambda = \{1, \ldots, 14\} \to \{0, 1\}$ such that $\mathsf{m}_0(e) = 1$ for $e = 4, 8, 9, 12$ and $\mathsf{m}_0(e) = 0$ else. Thus the normalized cycle decomposition for σ_0 and σ_1 becomes

$$
\begin{aligned}
\sigma_0 &= [4, 14, 2, 3]\,[8, 1, 6]\,[9, 10, 7]\,[12, 13, 5, 11], \\
\sigma_1 &= [4, 6, 7, 5]\,[8, 3, 11, 10]\,[9, 14, 13]\,[12, 2, 1].
\end{aligned}
\tag{25}
$$

Thus the cycles are $4_\circ, 8_\circ, 9_\circ, 12_\circ$ and $4_\bullet, 8_\bullet, 9_\bullet, 12_\bullet$, respectively. ∎

The **universal covering** $\widetilde{\Gamma_\Lambda^\vee}$ of $\Gamma_\Lambda^\vee$ can now be constructed as follows. Fix a white node $\mathbf{w}_0$ of $\Gamma_\Lambda^\vee$ and identify $\widetilde{\Gamma_\Lambda^\vee}$ with the set of **paths** on $\Gamma_\Lambda^\vee$ which start at $\mathbf{w}_0$. Such a path $\mathbf{p}$ is a finite string of elements of $\mathcal{E}_\Lambda$

$$
\mathbf{p} = (e_1, e_2, \ldots, e_{r-1}, e_r) \qquad \text{such that} \quad w(e_1) = \mathbf{w}_0, \tag{26}
$$
$$
b(e_k) = b(e_{k+1}) \quad \text{if } k \text{ is odd}, \qquad w(e_k) = w(e_{k+1}) \quad \text{if } k \text{ is even}.
$$

We emphasize that the path $\mathbf{p}$ passes alternately through white and black nodes by writing

$$
\begin{aligned}
\mathbf{p} &= e_1{}^{\circ\bullet} e_2{}^{\bullet\circ} \cdots e_{r-1}{}^{\bullet\circ} e_r{}^{\circ\bullet} & \text{if } r \text{ is odd}, \\
\mathbf{p} &= e_1{}^{\circ\bullet} e_2{}^{\bullet\circ} \cdots e_{r-1}{}^{\circ\bullet} e_r{}^{\bullet\circ} & \text{if } r \text{ is even}.
\end{aligned}
\tag{27}
$$

---

[10] Unlike Section 4.2 the present section does not make use of the lengths of the sides or the size of the angles of the polygons in the planar tiling.

[11] Perfect matchings exist because $(\mathcal{Z}, \Lambda)$ is dimer complete.

The number r will be called the *length* of the path $\mathbf{p}$. The exceptional case $r = 0$ gives the *constant path* at $\mathbf{w}_0$.

The set $\widetilde{\Gamma_\Lambda^\vee}$ has the structure of a bipartite rooted tree. The set of nodes of this tree is $\widetilde{\Gamma_\Lambda^\vee}$ (i.e. paths on $\Gamma_\Lambda^\vee$ which start $\mathbf{w}_0$) and the root is the constant path at $\mathbf{w}_0$. A node is colored white (resp. black) if the length of the corresponding path is even (resp. odd). Two nodes $\mathbf{p}$ and $\mathbf{p}'$ of the tree are connected by an edge if and only if $\mathbf{p}' = \mathbf{p} \cdot e^{\circ\bullet}$ or $\mathbf{p}' = \mathbf{p} \cdot e^{\bullet\circ}$ for some $e \in \mathcal{E}_\Lambda$. For every node $\mathbf{p}$ of the tree $\widetilde{\Gamma_\Lambda^\vee}$ there is a unique path on $\widetilde{\Gamma_\Lambda^\vee}$ which starts at $\mathbf{w}_0$ and ends at $\mathbf{p}$, which is tautologically the same as $\mathbf{p}$ viewed as a path on $\Gamma_\Lambda^\vee$.

The bipartite rooted tree $\widetilde{\Gamma_\Lambda^\vee}$ *is the **universal covering** of* $\Gamma_\Lambda^\vee$.
*The group of covering transformations is the **fundamental group** $\pi_1(\Gamma_\Lambda^\vee, \mathbf{w}_0)$*; i.e. the set of closed paths on $\Gamma_\Lambda^\vee$ which start and end at $\mathbf{w}_0$ with concatenation as group operation.

One can construct the rooted tree $\widetilde{\Gamma_\Lambda^\vee}$ as follows. The root $\mathbf{w}_0$ corresponds with a cycle of σ_0. Each edge e in this cycle is the first step on a path in the tree. For a given e one subsequently takes the cycle of σ_1 which contains e. Each edge e' in the latter cycle, except for e itself, gives the second step on a path which starts with e. Having e' one looks for the cycle of σ_0 which contains e'. One takes $e'' \neq e'$ from this cycle and thus gets the first three steps of the path $e^{\circ\bullet} \cdot e'^{\bullet\circ} \cdot e''^{\circ\bullet}$. This process continues in the obvious way and produces the desired abstract bipartite infinite tree with root $\mathbf{w}_0$; here "abstract" means that it only gives the adjacency structure but not a cyclic ordering on the set of edges incident to a given node.

Remark 3 Paths on $\Gamma_\Lambda^\vee$ can easily be drawn as *curves on the tiled plane* $\mathbb{R}^2$ which start and end in the interior of a polygon and do not pass through any vertex in the planar tiling defined by the Zhegalkin Zebra Motive $\mathcal{Z}$. Given such a drawing one simply writes the sequence of labels of the edges in the tiling which the curve intersects plus an indication of whether it passes from white-to-black or from black-to-white. This results in a path as in (27). See also Remark 9 in §5.2. ∎

We will now embed the tree $\widetilde{\Gamma_\Lambda^\vee}$ into the Poincaré disk $\mathbb{D}$ such that all edges are hyperbolic geodesics with length $\log\left(\frac{1+\varrho}{1-\varrho}\right) = -2\log\left(\tan\left(\frac{1}{2}\beta\right)\right)$. This will then also exhibit $\mathbb{D}$ as the universal covering of the surface $\mathbb{X}_{\sigma_0, \sigma_1, \varrho}$.

The construction proceeds by repeatedly applying transformations from a finite collection of Möbius transformations to a finite collection of building blocks. The building blocks are given by the cycles of σ_0 and σ_1 and consist of a collection of line segments and an ideal regular hyperbolic polygon as shown in Figure 7.
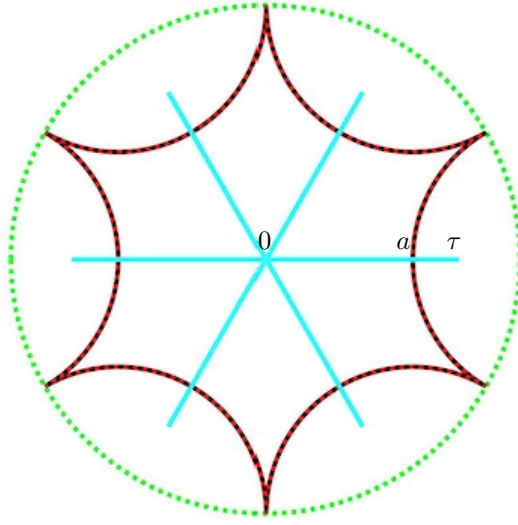
Figure 7: Basic building block corresponding with a cycle of length k of σ_0 or σ_1 and $\tau = \left(\cos(\beta)\right)^{-1} - \tan(\beta)$. In the picture $k = 6$, $\beta = \frac{\pi}{12}$. In the sequel the black-red dotted arcs will be drawn as solid red (resp. solid black) for cycles of σ_0 (resp. σ_1). Compare this with Figure 23.

Recall that the *Möbius transformation* defined by the matrix $A = \begin{pmatrix} a & b \\ c & d \end{pmatrix}$ is the map $\mathcal{A} : \mathbb{C} \cup \{\infty\} \to \mathbb{C} \cup \{\infty\}$ given by:

$$\mathcal{A}(z) = \frac{az + b}{cz + d} \qquad \text{if} \quad \det A = 1, \tag{28}$$

$$\mathcal{A}(z) = \frac{a\overline{z} + b}{c\overline{z} + d} \qquad \text{if} \quad \det A = -1. \tag{29}$$

For $e \in \mathcal{E}_\Lambda$ we define the matrices $M(e^{\circ\bullet})$ and $M(e^{\bullet\circ})$ by

$$M(e^{\circ\bullet}) = \tag{30}$$
$$\exp\left(\frac{j_{0,e}}{n_{0,e}}\pi i \begin{pmatrix} 1 & 0 \\ 0 & -1 \end{pmatrix}\right) \cdot \frac{1}{\sqrt{1 - \varrho^2}} \begin{pmatrix} 1 & -\varrho \\ \varrho & -1 \end{pmatrix} \cdot \exp\left(\frac{j_{1,e}}{n_{1,e}}\pi i \begin{pmatrix} -1 & 0 \\ 0 & 1 \end{pmatrix}\right)$$

$$M(e^{\bullet\circ}) = \overline{M(e^{\circ\bullet})}^{-1} \tag{31}$$

where $n_{0,e}$ (resp. $n_{1,e}$) is the length of the cycle of σ_0 (resp. σ_1) containing e and $j_{0,e}$ (resp. $j_{1,e}$) gives the position of e in that cycle such that the leftmost entry in the cycle is in position 0 and the rightmost entry is in position $n_{0,e} - 1$ (resp. $n_{1,e} - 1$). In (31) $\overline{M()}$ means complex conjugation. The geometric meaning and motivation for the Formulas (30)-(31) is given in the discussion around Formulas (102)-(105). Most relevant for now is that

the Möbius transformations defined by $M(e^{\circ\bullet})$ and $M(e^{\bullet\circ})$
map the unit disk $\mathbb{D}$ and the unit circle $\mathbb{U}(1)$ into themselves. $\tag{32}$

For a path $\mathbf{p} = e_1{}^{\circ\bullet}e_2{}^{\bullet\circ}\cdots e_{r-1}{}^{\bullet\circ}e_r{}^{\circ\bullet}$ with r odd as in (27) we define the 2×2-matrix $M_{\mathbf{p}}$ by

$$
\begin{aligned}
M_{\mathbf{p}} &= M(e_1{}^{\circ\bullet}) \cdot \overline{M(e_2{}^{\bullet\circ})} \cdot \ldots \cdot \overline{M(e_{r-1}{}^{\bullet\circ})} \cdot M(e_r{}^{\circ\bullet}) \\
&= M(e_1{}^{\circ\bullet}) \cdot M(e_2{}^{\circ\bullet})^{-1} \cdot \ldots \cdot M(e_{r-1}{}^{\circ\bullet})^{-1} \cdot M(e_r{}^{\circ\bullet}), \qquad (33)
\end{aligned}
$$

where $\overline{M()}$ means that in the above product the matrices in even position must be complex conjugated because the matrices in (30) have determinant -1.

Similarly, for a path $\mathbf{p} = e_1{}^{\circ\bullet}e_2{}^{\bullet\circ}\cdots e_{r-1}{}^{\circ\bullet}e_r{}^{\bullet\circ}$ with r even we define

$$
\begin{aligned}
M_{\mathbf{p}} &= M(e_1{}^{\circ\bullet}) \cdot \overline{M(e_2{}^{\bullet\circ})} \cdot \ldots \cdot M(e_{r-1}{}^{\circ\bullet}) \cdot \overline{M(e_r{}^{\bullet\circ})} \\
&= M(e_1{}^{\circ\bullet}) \cdot M(e_2{}^{\circ\bullet})^{-1} \cdot \ldots \cdot M(e_{r-1}{}^{\circ\bullet}) \cdot M(e_r{}^{\circ\bullet})^{-1}. \qquad (34)
\end{aligned}
$$

Note that $\det M_{\mathbf{p}} = (-1)^r$. So for a black node of $\widetilde{\Gamma_\Lambda^\vee}$ the matrix $M_{\mathbf{p}}$ has determinant -1 and by (29) the corresponding Möbius transformation involves complex conjugation.

Recall that P_Λ° (resp. $\mathsf{P}_\Lambda^\bullet$) denotes the set of cycles of the permutation σ_0 (resp. σ_1) as well as the set of white (resp. black) polygons in the planar tiling modulo Λ. For $\mathbf{w} \in \mathsf{P}_\Lambda^\circ$ and $\mathbf{b} \in \mathsf{P}_\Lambda^\bullet$ we define

$$
\boxplus_{\mathbf{w}} = \bigcup_{j=0}^{n_{\mathbf{w}}-1} \left[0, \tau \exp\left(\frac{2\pi i j}{n_{\mathbf{w}}}\right)\right], \qquad \boxplus_{\mathbf{b}} = \bigcup_{j=0}^{k_{\mathbf{b}}-1} \left[0, \tau \exp\left(\frac{2\pi i j}{n_{\mathbf{b}}}\right)\right], \qquad (35)
$$

where $n_{\mathbf{w}}$ and $n_{\mathbf{b}}$ denote the number of sides of the polygons $\mathbf{w}$ and $\mathbf{b}$. Thus $\boxplus_{\mathbf{w}}$ and $\boxplus_{\mathbf{b}}$ are the sets of light blue line segments in Figure 7. We denote the ideal hyperbolic polygons in Figure 7 by $\diamondsuit_{\mathbf{w}}$ and $\diamondsuit_{\mathbf{b}}$:

$$
\begin{aligned}
\text{vertices } \diamondsuit_{\mathbf{w}} : \quad & \exp(\pi i(1+2j)/n_{\mathbf{w}}), \qquad 0 \le j < n_{\mathbf{w}}, \\
\text{vertices } \diamondsuit_{\mathbf{b}} : \quad & \exp(\pi i(1+2j)/n_{\mathbf{b}}), \qquad 0 \le j < n_{\mathbf{b}}.
\end{aligned} \qquad (36)
$$

Recall that the nodes of the tree $\widetilde{\Gamma_\Lambda^\vee}$ correspond 1-1 with the paths on $\Gamma_\Lambda^\vee$ as in (27). For a black node $\mathbf{p} = e_1{}^{\circ\bullet}e_2{}^{\bullet\circ}\cdots e_{r-1}{}^{\bullet\circ}e_r{}^{\circ\bullet}$ and a white node $\mathbf{p}' = e_1{}^{\circ\bullet}e_2{}^{\bullet\circ}\cdots e_{r'-1}{}^{\circ\bullet}e_{r'}{}^{\bullet\circ}$ we set

$$
b(\mathbf{p}) = b(e_r), \qquad w(\mathbf{p}') = w(e_{r'}). \qquad (37)
$$

Finally we define

$$
\widetilde{\Gamma_{\Lambda,\varrho,M}^\vee} = \bigcup_{\mathbf{p} \text{ black node of } \widetilde{\Gamma_\Lambda^\vee}} M_{\mathbf{p}}\big(\boxplus_{b(\mathbf{p})}\big) \cup \bigcup_{\mathbf{p}' \text{ white node of } \widetilde{\Gamma_\Lambda^\vee}} M_{\mathbf{p}'}\big(\boxplus_{w(\mathbf{p}')}\big). \qquad (38)
$$
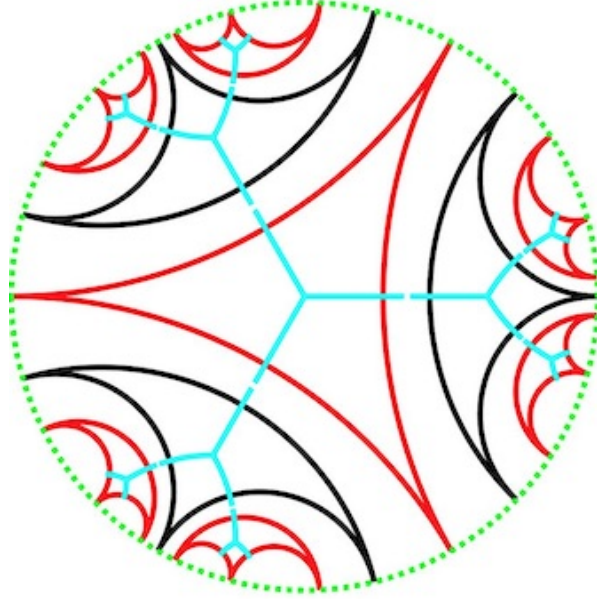
Figure 8: The rooted tree $\widetilde{\Gamma^\vee_{\Lambda,\varrho,M}}$ (light blue) up to path length 2 and the polygons $M_{\mathbf{p}}\big(\lozenge_{b(\mathbf{p})}\big)$ (black) and $M_{\mathbf{p}}\big(\lozenge_{w(\mathbf{p})}\big)$ (red) for the Zhegalkin Zebra Motive $\mathcal{Z}_3$, $\Lambda = \mathsf{Aut}(\mathcal{Z}_3)$ and $\varrho = \cos(2\pi/7)$. Compare this with Figure 24.

Theorem 2

i. $\widetilde{\Gamma^\vee_{\Lambda,\varrho,M}}$ is an embedding of the tree $\widetilde{\Gamma^\vee_\Lambda}$ into the Poincaré disk $\mathbb{D}$ such that all edges are geodesics with length $\log\left(\frac{1+\varrho}{1-\varrho}\right) = -2\log\big(\tan(\tfrac{1}{2}\beta)\big)$.

ii. The edges are labeled by the elements of $\mathcal{E}_\Lambda$. At a node $\mathbf{p}$ of $\widetilde{\Gamma^\vee_{\Lambda,\varrho,M}}$ the counter-clockwise cyclic ordering of the labels of the edges incident to $\mathbf{p}$ agrees with corresponding cycle of σ_0 if $\mathbf{p}$ is white or σ_1 if $\mathbf{p}$ is black.

iii. For every black (resp. white) node $\mathbf{p}$ of $\widetilde{\Gamma^\vee_{\Lambda,\varrho,M}}$ the polygon $M_{\mathbf{p}}\big(\lozenge_{b(\mathbf{p})}\big)$ (resp. $M_{\mathbf{p}}\big(\lozenge_{w(\mathbf{p})}\big)$) is a regular ideal hyperbolic polygon with k sides which intersect the k edges of $\widetilde{\Gamma^\vee_{\Lambda,\varrho,M}}$ incident to $\mathbf{p}$ orthogonally at hyperbolic distance $-\log\big(\tan(\tfrac{\pi}{2k})\big)$ from $\mathbf{p}$.

iv. The sides of the ideal polygons are labeled by the elements of $\mathcal{E}_\Lambda$ such that the counter-clockwise oriented boundary of a red (resp. black) polygon is a cycle of σ_0 (resp. σ_1). These polygons are pairwise disjoint and between polygons corresponding to adjacent nodes of $\Gamma^\vee_\Lambda$ lies a quadrangle with two opposite sides on the unit circle $\mathbb{U}(1)$. These quadrangles together with the ideal polygons give a tiling of the closed disk $\overline{\mathbb{D}}$.

See Figures 8 for an illustrative example.

Proof: **i+ii:** This follows from the same arguments as used in §4.4.2 for proving Proposition 3.

iii: This follows from Figure 7 because $M_{\mathbf{p}}$ is a hyperbolic isometry.

iv: Obvious from pictures like Figures 8. ∎

Recall that the bipartite graph $\Gamma_\Lambda^\vee$ lies as a deformation retract in the surface $\mathbb{X}_{\sigma_0,\sigma_1,\varrho}$. Comparing the arguments and constructions which lead to Theorem 2 with those for Proposition 3 we now arrive at the following corollary.

Corollary 1 *The disk $\mathbb{D}$ is the universal covering of the surface $\mathbb{X}_{\sigma_0,\sigma_1,\varrho}$ whereby the fundamental group $\pi_1(\mathbb{X}_{\sigma_0,\sigma_1,\varrho}, \mathbf{w}_0) = \pi_1(\Gamma_\Lambda^\vee, \mathbf{w}_0)$ acts on $\mathbb{D}$ via the Möbius transformations associated with the matrices $M_{\mathbf{p}}$ (34) for $\mathbf{p}$ a path on $\Gamma_\Lambda^\vee$ with start and finish at $\mathbf{w}_0$.* ∎

Remark 4 The action of the fundamental group in the above corollary amounts to a group homomorphism

$$M : \pi_1(\Gamma_\Lambda^\vee, \mathbf{w}_0) \longrightarrow \mathsf{Sl}_2(\mathbb{C}). \tag{39}$$

One may want to compare this with the definition of **line bundles** on $\Gamma_\Lambda^\vee$ in [11] as homomorphisms

$$\pi_1(\Gamma_\Lambda^\vee, \mathbf{w}_0) \longrightarrow \mathbb{C}^*. \tag{40}$$

As $\mathbb{C}^*$ is commutative the latter homomorphisms factorize through the homology group $\mathrm{H}_1(\Gamma_\Lambda^\vee, \mathbb{Z})$ and may therefore be identified with elements of the cohomology group $\mathrm{H}^1(\Gamma_\Lambda^\vee, \mathbb{C}^*)$. In [11] one is interested in the whole moduli space of line bundles on $\Gamma_\Lambda^\vee$ which is then identified with the complex torus $\mathrm{H}^1(\Gamma_\Lambda^\vee, \mathbb{C}^*)$. The main result of [11] is the construction of a **Poisson structure** on the complex torus $\mathrm{H}^1(\Gamma_\Lambda^\vee, \mathbb{C}^*)$. In Formula (177) and Section 5.5 of the present paper this Poisson structure is explicitly computed in terms of the permutations σ_0, σ_1 and the perfect matching m_0. *Since the permutations σ_0, σ_1 and the perfect matching m_0 are the only ingredients needed in the construction of the homomorphism (45) one may wonder if there is a deeper relation between the Poisson structure on the complex torus $\mathrm{H}^1(\Gamma_\Lambda^\vee, \mathbb{C}^*)$ and the structure of $\mathbb{D}$ as universal covering space of the surface $\mathbb{X}_{\sigma_0,\sigma_1,\varrho}$.* ∎

3.2 Schottky dance and twist

3.2.1

For the twisting construction we first embed the tree $\widetilde{\Gamma_\Lambda^\vee}$ into the Poincaré disk $\mathbb{D}$ with all edges geodesic with length $\log\left(\frac{1+\varrho}{1-\varrho}\right)$ and, more importantly, such that at a white (resp. black) node $\mathbf{p}$ the counter-clockwise (resp. clockwise) cyclic ordering of the labels of the edges incident to $\mathbf{p}$ agrees with the corresponding cycle of σ_0 (resp. σ_1). In order to construct this embedding we define for a

node $\mathbf{p}$ of $\widetilde{\Gamma_\Lambda^\vee}$ the matrix $W_\mathbf{p}$ by replacing in the Formulas (33)-(34) the matrices $M(e^{\circ\bullet})$ and $M(e^{\bullet\circ})$ from (30)-(31) by the matrices

$$W(e^{\circ\bullet}) = \tag{41}$$
$$\exp\left(\frac{j_{0,e}}{n_{0,e}}\pi i \begin{pmatrix} 1 & 0 \\ 0 & -1 \end{pmatrix}\right) \cdot \frac{1}{\sqrt{1-\varrho^2}} \begin{pmatrix} 1 & -\varrho \\ \varrho & -1 \end{pmatrix} \cdot \exp\left(\frac{j_{1,e}}{n_{1,e}}\pi i \begin{pmatrix} 1 & 0 \\ 0 & -1 \end{pmatrix}\right)$$

$$W(e^{\bullet\circ}) = \overline{W(e^{\circ\bullet})}^{-1}. \tag{42}$$

For a geometric motivation of this replacement see the discussion around Formulas (102)-(105). Next we define the embedding $\widetilde{\Gamma_{\Lambda,\varrho,W}^\vee}$ of $\widetilde{\Gamma_\Lambda^\vee}$ into $\mathbb{D}$ by replacing in Formula (38) the matrices $M_\mathbf{p}$ and $M_{\mathbf{p}'}$ by $W_\mathbf{p}$ and $W_{\mathbf{p}'}$, respectively.

In $\mathbb{D}$ one also has the ideal hyperbolic polygons $W_\mathbf{p}\big(\Diamond_{b(\mathbf{p})}\big)$ and $W_{\mathbf{p}'}\big(\Diamond_{w(\mathbf{p}')}\big)$ centered around the nodes of $\widetilde{\Gamma_{\Lambda,\varrho,W}^\vee}$. Analogous to Theorem 2$iv$ the sides of the ideal polygons are labeled by the elements of $\mathcal{E}_\Lambda$ such that the counter-clockwise (resp. clockwise) oriented boundary of a red (resp. black) polygon is a cycle of σ_0 (resp. σ_1). These polygons are pairwise disjoint and between polygons corresponding to adjacent nodes of $\Gamma_\Lambda^\vee$ lies a quadrangle with two opposite sides on the unit circle $\mathbb{U}(1)$. These quadrangles together with the ideal polygons give a tiling of $\mathbb{D}$.

For a better understanding of the twisting construction later in this section we draw the tiling in the **Beltrami-Klein model** of the hyperbolic plane. Recall that in that model the hyperbolic plane is the disk $\mathbb{D}$ and that the geodesics are Euclidean straight line intervals (i.e. connected pieces of chords) in $\mathbb{D}$. In the **Poincaré disk model** the hyperbolic plane is the disk $\mathbb{D}$ and the geodesics are connected pieces of Euclidean circles which perpendicularly intersect the boundary $\mathbb{U}(1)$ of $\mathbb{D}$.

The correspondence between the two models is best understood through the well-known classical map

$$\mathbb{C} \cup \{\infty\} \longrightarrow \mathbb{C} \times \mathbb{R} = \mathbb{R}^3, \qquad z \mapsto \left(\frac{2z}{1+|z|^2}, \frac{1-|z|^2}{1+|z|^2}\right). \tag{43}$$

It maps the horizontal plane $\mathbb{C}\cup\{\infty\}$ homeomorphically onto the unit sphere $\mathbb{S}^2$ through a projection from the point $(0,0,-1)$. It maps the closed unit disk $\overline{\mathbb{D}}$ in $\mathbb{C}$ onto the northern hemisphere and $\mathbb{C}\setminus\mathbb{D}\cup\{\infty\}$ onto the southern hemisphere. The unit circle $\mathbb{U}(1)$ is mapped onto the equator. The points 0 and ∞ are mapped to respectively the north pole and the south pole.

The map (43) maps the circle in $\mathbb{C}$ which intersects the boundary $\mathbb{U}(1)$ of $\mathbb{D}$ perpendicularly in two points a_1 and a_2 to the circle which is the intersection of $\mathbb{S}^2$ with the vertical plane in $\mathbb{R}^3$ through the points a_1 and a_2. Thus the chord between a_1 and a_2 in $\mathbb{D}$ is a diameter of that circle on $\mathbb{S}^2$.
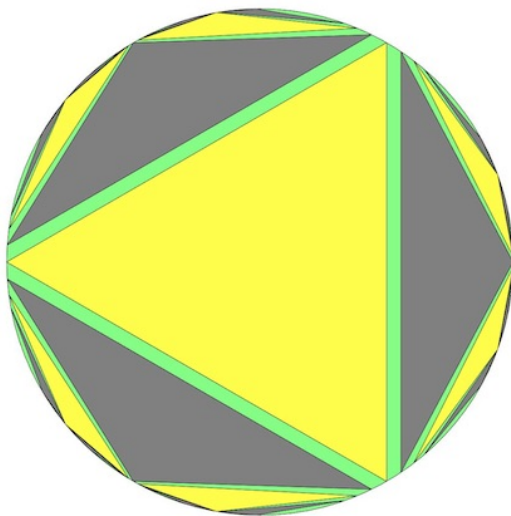
Figure 9: Tiling of $\mathbb{D}$ for $\mathcal{Z}_3$ and all paths of length ≤ 3.

In particular, in the Beltrami-Klein model the ideal hyperbolic polygons $W_{\mathbf{p}}\big(\Diamond_{b(\mathbf{p})}\big)$ and $W_{\mathbf{p}}\big(\Diamond_{w(\mathbf{p})}\big)$ are the convex Euclidean polygons with vertices

$$
\begin{aligned}
\text{vertices } W_{\mathbf{p}}\big(\Diamond_{b(\mathbf{p})}\big) &: W_{\mathbf{p}}\big(\exp\big(\pi i(1+2j)/n_{b(\mathbf{p})}\big), \quad 0 \leq j < n_{b(\mathbf{p})}\big), \\
\text{vertices } W_{\mathbf{p}}\big(\Diamond_{w(\mathbf{p})}\big) &: W_{\mathbf{p}}\big(\exp\big(\pi i(1+2j)/n_{w(\mathbf{p})}\big), \quad 0 \leq j < n_{w(\mathbf{p})}\big);
\end{aligned}
\tag{44}
$$

see Figure 7 and Formula (36). Figure 9 shows an example.

Remark 5 The above construction provides a group homomorphism

$$
W : \pi_1(\Gamma_\Lambda^\vee, \mathbf{w}_0) \longrightarrow \mathsf{Sl}_2(\mathbb{C})
\tag{45}
$$

which exhibits $\mathbb{D}$ as the universal covering of the torus $\mathbb{R}^2/\Lambda$ from which (small disks around) the vertices of the planar tiling modulo Λ have been deleted.

The tiling of $\mathbb{D}$ is the pull-back of the tiling $\Gamma^\square$; cf. Figure 4. ∎

HHHHHHHHHHH

One can now project this tiling vertically up to the upper hemisphere in $\mathbb{S}^2$ and project it vertically down to the lower hemisphere. Each ideal polygon yields a pair of polygons, one in the upper hemisphere and one in the lower hemisphere, which have their vertices on the equator and are interchanged by the reflection in the equatorial plane. Each quadrangle yields an annulus in $\mathbb{S}^2$ which is its own image under the reflection in the equatorial plane.

3.2.2

We continue in the Beltrami-Klein model of this tiling of $\overline{\mathbb{D}}$. The quadrangles correspond 1-1 with the edges of the tree $\widetilde{\Gamma_{\Lambda,\varrho,W}^\vee}$ and are accordingly labeled

by the elements of $\mathcal{E}_\Lambda$ [12]. In each quadrangle there are two diagonals which we orient such that the black side of the quadrangle lies to the right of the diagonal. Next we use the twist function $\eta : \mathcal{E}_\Lambda \to \{\pm 1\}$ to color the two diagonals red and black according to the rule shown in the diagram (46)

$$
\eta(e) = -1 \qquad\qquad \eta(e) = +1 \tag{46}
$$

red   black   black   red

....

4 Geometric constructions

In this section the Zhegalkin Zebra Motive $\mathcal{Z}$ and the lattice $\Lambda \subset \mathsf{Aut}(\mathcal{Z})$ are such that $(\mathcal{Z}, \Lambda)$ is dimer complete; cf. Definition 1.

4.1 Realizations of the superpotential

The lattice Λ acts on the sets $\mathcal{E}$, $\mathsf{P}^\star$, $\mathsf{P}^\bullet$, P° of edges, vertices, black and white polygons in the tiling of $\mathbb{R}^2$. We denote the orbit sets (i.e. the sets of edges, vertices, black and white polygons in the tiling of the torus $\mathbb{R}^2/\Lambda$) by $\mathcal{E}_\Lambda$, $\mathsf{P}_\Lambda^\star$, $\mathsf{P}_\Lambda^\bullet$ and P_Λ°. The superpotential $(\mathcal{E}_\Lambda, \sigma_0, \sigma_1)$ (see (9)) provides precise information about the number and cyclic ordering of the edges of the polygons and how the polygons must be glued together to make a biperiodic tiling of $\mathbb{R}^2$. In order to actually make the tiling one must however also supply a list of edge vectors $\omega : \mathcal{E}_\Lambda \longrightarrow \mathbb{R}^2$ which satisfies various constraints posed by the superpotential. We call such a map ω a **realization of the superpotential** $(\mathcal{E}_\Lambda, \sigma_0, \sigma_1)$ [13].

The picture of the planar tiling for the Zhegalkin Zebra Motive $\mathcal{Z}$ itself provides one realization $\omega_\mathcal{Z} : \mathcal{E}_\Lambda \longrightarrow \mathbb{R}^2 = \mathbb{C}$ of the superpotential. Since the frequencies used in the defining formula for $\mathcal{Z}$ lie in $\mathbb{Z}^2$ the edge vectors $\omega_\mathcal{Z}(e)$ lie in $\mathbb{Q}^2$. *We can therefore rescale the picture so that we obtain a realization of the superpotential with edge vectors in $\mathbb{Z}$.*

The following diagram helps in visualizing the constraints which the superpotential poses on a realization.

---

[12]Figure 9 shows an example. The labels of the quadrangles are suppressed. Therefore the picture can in this simple case not distinguish between $\widetilde{\Gamma}_{\Lambda,\varrho,W}^\vee$ and $\widetilde{\Gamma}_{\Lambda,\varrho,M}^\vee$. For $\widetilde{\Gamma}_{\Lambda,\varrho,M}^\vee$ the labels are shown in Figure 24. Labeling the edges of $\widetilde{\Gamma}_{\Lambda,\varrho,W}^\vee$ is left as an easy exercise.

[13]When it seems more convenient we will identify $\mathbb{R}^2$ with $\mathbb{C}$ in the obvious way and view the realization as a map $\omega : \mathcal{E}_\Lambda \longrightarrow \mathbb{C}$.

$$\begin{array}{c}
b(e) \\
\bullet
\end{array} \qquad \qquad \sigma_1^{-1}(e)$$

$$\sigma_1(e) \qquad\qquad\qquad e \qquad\qquad\qquad$$

$$\sigma_0(e) \qquad t(e) \qquad\qquad s(e) \qquad \sigma_0^{-1}(e)$$

$$\underset{w(e)}{\circ} \tag{47}$$
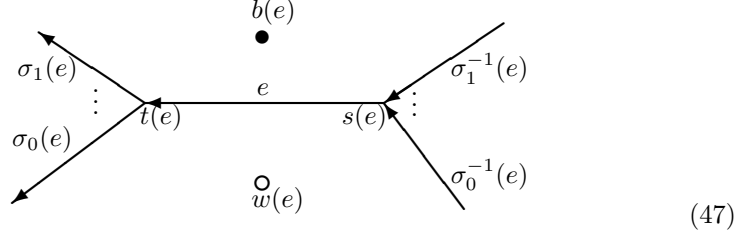
Firstly a realization $\omega : \mathcal{E}_\Lambda \longrightarrow \mathbb{C}$ of $(\mathcal{E}_\Lambda, \sigma_0, \sigma_1)$ must satisfy

$$\forall e \in \mathcal{E}_\Lambda : \qquad \omega(e) \neq 0, \tag{48}$$

$$\forall \mathbf{w} \in \mathsf{P}_\Lambda^\circ, \ \mathbf{b} \in \mathsf{P}_\Lambda^\bullet : \quad \sum_{e : w(e) = \mathbf{w}} \omega(e) = 0, \qquad \sum_{e : b(e) = \mathbf{b}} \omega(e) = 0. \tag{49}$$

Secondly, for every $\mathbf{w} \in \mathsf{P}_\Lambda^\circ$ (resp. $\mathbf{b} \in \mathsf{P}_\Lambda^\bullet$) the cyclic ordering on the unit circle of the complex numbers $\omega(e)|\omega(e)|^{-1}$ with $w(e) = \mathbf{w}$ (resp. $b(e) = \mathbf{b}$) should be the same as in the corresponding cycle of σ_0 (resp. σ_1^{-1}) and all interior angles in the polygon must be > 0 and $\leq \pi$. This condition can be restated in terms of the exterior angles and the argument function $\arg : \mathbb{C}^* \longrightarrow [0, 2\pi)$ as follows:

$$\forall e \in \mathcal{E} : \qquad \arg\big(\overline{\omega(e)}\,\omega(\sigma_0(e))\big) < \pi, \qquad \arg\big(\omega(e)\,\overline{\omega(\sigma_1(e))}\big) < \pi, \tag{50}$$

$$\forall \mathbf{w} \in \mathsf{P}_\Lambda^\circ : \qquad \sum_{e : w(e) = \mathbf{w}} \arg\big(\overline{\omega(e)}\,\omega(\sigma_0(e))\big) = 2\pi, \tag{51}$$

$$\forall \mathbf{b} \in \mathsf{P}_\Lambda^\bullet : \qquad \sum_{e : b(e) = \mathbf{b}} \arg\big(\omega(e)\,\overline{\omega(\sigma_1(e))}\big) = 2\pi. \tag{52}$$

Thirdly, at each vertex $\mathbf{v} \in \mathsf{P}_\Lambda^\star$ of the tiling the angles must add up to 2π:

$$\sum_{e : t(e) = \mathbf{v}} \Big(2\pi - \arg\big(\overline{\omega(e)}\,\omega(\sigma_0(e))\big) - \arg\big(\omega(e)\,\overline{\omega(\sigma_1(e))}\big) \Big) = 2\pi. \tag{53}$$

Moreover, if a function $\omega : \mathcal{E}_\Lambda \to \mathbb{C}$ satisfies the conditions in (48)-(53) and c is a non-zero complex number, the function $c\,\omega$ also satisfies these conditions.

Definition 2 A realization $\omega : \mathcal{E}_\Lambda \longrightarrow \mathbb{C}$ of the superpotential $(\mathcal{E}_\Lambda, \sigma_0, \sigma_1)$ is said to be a **stable realization** if all polygons are strictly convex; i.e. all exterior angles are > 0; cf. (50).

Since one can easily draw the picture of the Zhegalkin Zebra Motive $\mathcal{Z}$ stability of the realization $\omega_{\mathcal{Z}}$ can easily be checked by visual inspection. But even if $\omega_{\mathcal{Z}}$ is not stable one can often see a deformation of $\omega_{\mathcal{Z}}$ which is stable; see for example the Zhegalkin Zebra Motive $\mathsf{Z}^{22} + \mathsf{Z}^{42} + \mathsf{Z}^{31} + \mathsf{Z}^{61}\mathsf{Z}^{31}\mathsf{Z}^{22}$ in Figure 35.

Lemma 1 *Let $\omega : \mathcal{E}_\Lambda \to \mathbb{C}$ be a stable realization of the superpotential $(\mathcal{E}, \sigma_0, \sigma_1)$. Let $\varpi : \mathcal{E}_\Lambda \longrightarrow \mathbb{C}$ be a map such that $|\varpi(e)|$ is sufficiently small for all e and*

$$\forall \mathbf{w} \in \mathsf{P}_\Lambda^\circ \,,\; \forall \mathbf{b} \in \mathsf{P}_\Lambda^\bullet \; : \quad \sum_{e \in \mathcal{E}_\Lambda : w(e) = \mathbf{w}} \varpi(e) = 0 \,, \quad \sum_{e \in \mathcal{E}_\Lambda : b(e) = \mathbf{b}} \varpi(e) = 0. \qquad (54)$$

Then $\omega + \varpi$ is also a stable realization of the superpotential $(\mathcal{E}_\Lambda, \sigma_0, \sigma_1)$.

Proof: The conditions (50)-(53) and also the stability condition pertain only to the directions of the edge vectors of the realization. For stable realizations these conditions are preserved by small perturbations. ∎

Theorem 3 *The set of realizations of the superpotential $(\mathcal{E}_\Lambda, \sigma_0, \sigma_1)$ is a non-empty $\mathbb{C}^*$-invariant subset of the complex vector space $\mathrm{H}_1(\Gamma_\Lambda^\vee, \mathbb{C})$ which does not contain 0. The set of stable realizations is either empty or a non-empty $\mathbb{C}^*$-invariant open subset of $\mathrm{H}_1(\Gamma_\Lambda^\vee, \mathbb{C})$. In the latter case the tangent space to the space of realizations of $(\mathcal{E}_\Lambda, \sigma_0, \sigma_1)$ at a stable realization ω is equal to $\mathrm{H}_1(\Gamma_\Lambda^\vee, \mathbb{C})$.*

Proof: The equalities (49) mean that a realization ω is an element of the homology group $\mathrm{H}_1(\Gamma_\Lambda^\vee, \mathbb{C})$; also see (116). Thus the conditions (48)-(53) imply that the set of realizations of the superpotential $(\mathcal{E}_\Lambda, \sigma_0, \sigma_1)$ is a subset of $\mathrm{H}_1(\Gamma_\Lambda^\vee, \mathbb{C})$ which does not contain 0. It is not empty because it contains $\omega_{\mathcal{Z}}$. The statements about stable realizations follow from Lemma 1. ∎

We want to view $\omega + \varpi$ in Lemma 1 as a **deformation** of ω. A special kind of deformations is obtained by slightly moving the vertices in the tiling. We call them **vertex deformations**. A vertex deformation comes from a map $\alpha : \mathsf{P}_\Lambda^\star \longrightarrow \mathbb{C}$ by setting

$$\forall e \in \mathcal{E}_\Lambda : \quad \varpi(e) \,=\, \alpha(t(e)) - \alpha(s(e))\,. \qquad (55)$$

This can be rewritten as[14]

$$\varpi \,=\, -\sum_{\mathbf{v} \in \mathsf{P}_\Lambda^\star} \alpha(\mathbf{v}) \ell_\mathbf{v} \qquad (56)$$

where $\ell_\mathbf{v}$ denotes the function $\mathcal{E}_\Lambda \to \mathbb{Z}$ defined by

$$\ell_\mathbf{v}(e) = 1 \text{ if } s(e) = \mathbf{v}, \qquad \ell_\mathbf{v}(e) = -1 \text{ if } t(e) = \mathbf{v}, \qquad \ell_\mathbf{v}(e) = 0 \text{ else}. \qquad (57)$$

There is only one linear relation between the latter functions, namely their sum is 0. The vertex deformations therefore form a $(|\mathsf{P}_\Lambda^\star| - 1)$-dimensional subspace of the $(|\mathsf{P}_\Lambda^\star| + 1)$-dimensional complex vector space $\mathrm{H}_1(\Gamma_\Lambda^\vee, \mathbb{C})$; see Proposition 4 Formula (119).

---

[14]The $-$-sign in (56) is needed because we want (57) to define the same function $\ell_\mathbf{v}$ as (123).
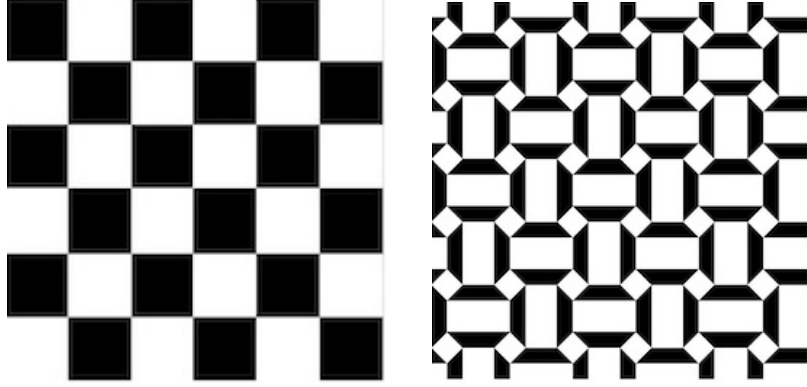
Figure 10: The realizations ω_L (left) and ω_R (right) in Example 2.

Definition 3 The tiling of $\mathbb{R}^2$ given by a realization ω of the superpotential $(\mathcal{E}_\Lambda, \sigma_0, \sigma_1)$ is biperiodic. We denote the **period lattice** by Λ_ω.

For the realization $\omega_{\mathcal{Z}}$ provided by the picture of the Zhegalkin Zebra Motive $\mathcal{Z}$ the lattice $\Lambda_{\omega_{\mathcal{Z}}}$ is by definition equal to Λ. *Vertex deformations do preserve the period lattice Λ_ω, but more general deformations do not.*

Example 2 The two tilings in Figure 10 are realizations of the superpotential

$$\begin{aligned}
\sigma_0 &= (1,4,8,5)(2,6,7,3)(9,12,16,13)(10,14,15,11)\,, \\
\sigma_1 &= (1,13,14,2)(3,15,16,4)(5,6,10,9)(7,8,12,11)\,.
\end{aligned}$$

The following table lists the edge labels, the labels of the sources and targets and the complex numbers $\omega_L(e)$ and $\omega_R(e)$ of the two realizations (where $\eta = \frac{1+i}{2}$)

e	1	2	3	4	5	6	7	8	9	10	11	12	13	14	15	16
s	7	1	8	2	1	4	2	3	3	5	4	6	5	8	6	7
t	1	8	2	7	3	1	4	2	5	4	6	3	7	5	8	6
ω_L	1	i	1	i	$-i$	-1	$-i$	-1	1	i	1	i	$-i$	-1	$-i$	-1
ω_R	η	i	2	$-\overline{\eta}$	$\overline{\eta}$	-2	$-i$	$-\eta$	1	η	$\overline{\eta}$	$2i$	$-2i$	$-\overline{\eta}$	$-\eta$	-1

It is an instructive exercise to put edge labels in the pictures in Figure 10 which match with the data σ_0, σ_1, ω_L, ω_R. The table shows that

$$\omega_R - \omega_L = \tfrac{1}{2}(-\mathbf{v}_1 + \mathbf{v}_2 + i\mathbf{v}_3 + \mathbf{v}_4 + i\mathbf{v}_5 - i\mathbf{v}_6 - i\mathbf{v}_7 - \mathbf{v}_8)\,,$$

where $\mathbf{v}_1, \ldots, \mathbf{v}_8 \in \mathbb{Z}^{\mathcal{E}_\Lambda}$ are the functions associated in (57) with the eight vertices. So the two realizations are related by a vertex deformation. It is an amusing exercise to see the vertex deformation in Figure 10.

A $\mathbb{Z}$-basis for the period lattice of the realization ω_R is given by the vectors

$$\begin{aligned}
\omega_R(3) + \omega_R(2) + \omega_R(1) + \omega_R(4) &= 2 + 2i, \\
\omega_R(10) + \omega_R(14) + \omega_R(2) + \omega_R(6) &= -2 + 2i.
\end{aligned}$$
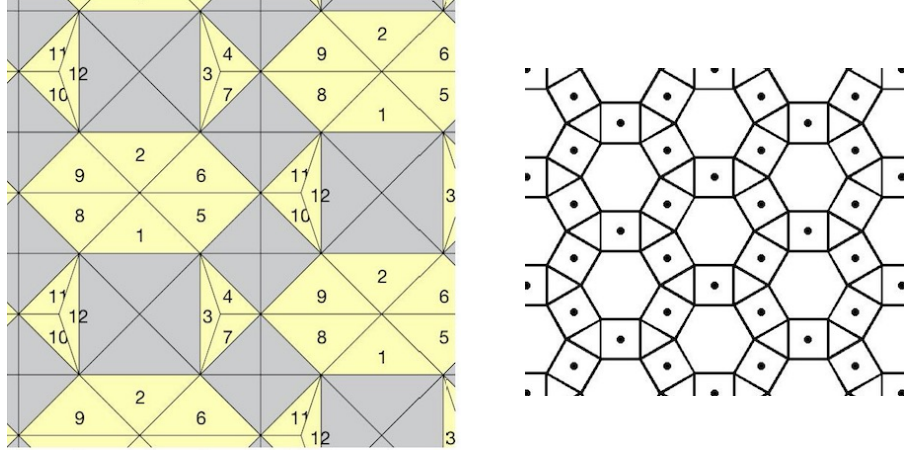
Figure 11: The realizations $\omega_{\mathcal{Z}}$ (left) and ω (right) in Example 3.

A $\mathbb{Z}$-basis for the period lattice of the realization ω_L is given by the vectors

$$
\begin{aligned}
\omega_L(3) + \omega_L(2) + \omega_L(1) + \omega_L(4) &= 2 + 2i, \\
\omega_L(10) + \omega_L(14) + \omega_L(2) + \omega_L(6) &= -2 + 2i.
\end{aligned}
$$

This illustrates the fact that vertex deformations preserve the period lattice.

■

Example 3 The tiling for $\mathcal{Z} = (1 + \mathsf{Z}^{62})(\mathsf{Z}^{32} + \mathsf{Z}^{61}) + \mathsf{Z}^{62}(\mathsf{Z}^{24} + \mathsf{Z}^{44})$ is shown in Figure 36. The left picture in Figure 11 shows a close-up of this tiling with edge labels. We see that $\mathsf{Aut}(\mathcal{Z}) = \mathbb{Z}(0,4) \oplus \mathbb{Z}(4,2)$ and that for $\Lambda = \mathsf{Aut}(\mathcal{Z})$ the superpotential $(\mathcal{E}_\Lambda, \sigma_0, \sigma_1)$ is given by $\mathcal{E}_\Lambda = \{1, \ldots, 12\}$,

$$
\sigma_0 = (1, 5, 6, 2, 9, 8)(4, 3, 7)(11, 10, 12), \quad \sigma_1 = (1, 3, 2, 12)(4, 5, 10, 9)(11, 6, 7, 8).
$$

The right picture in Figure 11 shows another realization of the superpotential. The edge vectors for these realizations are given in the following table, with $\varepsilon = e^{\pi i/6} = \frac{1}{2}(\sqrt{3} + i)$.

e	1	2	3	4	5	6	7	8	9	10	11	12
$\omega_{\mathcal{Z}}$	2	-2	$-2i$	$-1+i$	$1+i$	$-1+i$	$1+i$	$1-i$	$-1-i$	$1-i$	$-1-i$	$2i$
ω	1	ε^6	ε^9	ε^5	ε^2	ε^4	ε	ε^{10}	ε^8	ε^{11}	ε^7	ε^3

The period lattice for the realization $\omega_{\mathcal{Z}}$ is Λ. A $\mathbb{Z}$-basis for Λ is

$$
\begin{aligned}
\omega_{\mathcal{Z}}(5) + \omega_{\mathcal{Z}}(6) - \omega_{\mathcal{Z}}(3) &= 4i, \\
\omega_{\mathcal{Z}}(1) + \omega_{\mathcal{Z}}(5) - \omega_{\mathcal{Z}}(11) &= 4 + 2i.
\end{aligned}
$$

A $\mathbb{Z}$-basis for the period lattice Λ_ω of the realization ω is

$$
\begin{aligned}
\omega(5) + \omega(6) - \omega(3) &= \varepsilon^2 + \varepsilon^4 - \varepsilon^9 = (1 + \sqrt{3})\, i, \\
\omega(1) + \omega(5) - \omega(11) &= 1 + \varepsilon^2 - \varepsilon^7 = \tfrac{1}{2}(1 + \sqrt{3})\,(\sqrt{3} + i).
\end{aligned}
$$

A computer check reveals that $\omega_{\mathcal{Z}}$, ω and $\mathbf{v}$ for $\mathbf{v} \in \mathsf{P}_\Lambda^\star$ (cf. (57)) span a subspace of dimension $|\mathsf{P}_\Lambda^\star| + 1$ in $\mathbb{C}^{\mathcal{E}_\Lambda}$. This implies that no (complex) multiple of ω is related to $\omega_{\mathcal{Z}}$ by a vertex deformation.

Note that in this example one can easily see a positive integer weight function ν, namely $\nu(e) = 1$ if e is an edge of a white hexagon and $\nu(e) = 2$ if e is an edge of a white triangle. In the realization ω all black and white polygons are regular and the marked points given by ν are the centres of the circumcircles.

∎

4.2   Surfaces in $\mathbb{R}^3$

In this section we construct from input data $\big(\mathcal{Z}, \Lambda, \boxminus, h, r\big)$ a connected oriented surface $\mathfrak{S}_{\mathcal{Z},\Lambda,\boxminus,r}^{\leqslant h}$ in $\mathbb{R}^3$ which contains the bipartite graph $\Gamma_\Lambda^\vee$ as a deformation retract. Here $\mathcal{Z}$ is a Zhegalkin Zebra Motive and Λ is a sublattice of $\mathsf{Aut}(\mathcal{Z})$ such that $(\mathcal{Z}, \Lambda)$ is dimer complete and such that the superpotential $(\mathcal{E}_\Lambda, \sigma_0, \sigma_1)$ admits a stable realization; see Definitions 1 and 2. The other input data consist of a 5-tuple

$$\boxminus = (\eta, \nu, \omega, \lambda_1, \lambda_2) \tag{58}$$

where η is a Λ-invariant function $\eta : \mathcal{E} \to \{\pm 1\}$ (called **twist function**), ν is a Λ-invariant positive integer weight function, ω is a stable realization of the superpotential and $\{\lambda_1, \lambda_2\}$ is an ordered basis of the period lattice Λ_ω; h and r are real numbers such that $0 < h < 1$ and $0 < r < 3^{-h}$.

The stable realization ω gives a tiling of $\mathbb{R}^2$ by convex black and white polygons. We mark a point inside each polygon P by taking the convex combination specified by $\frac{1}{\deg \nu} \nu$ of the midpoints of the edges of P. The corresponding **barycentric subdivision** of the polygonal tiling is constructed by connecting for every polygon P the marked point to the vertices and the midpoints of the edges of P. The barycentric subdivision is a triangulation of $\mathbb{R}^2$. By connecting for every polygon P the marked point to the vertices of P one obtains a tiling of $\mathbb{R}^2$ by quadrangles in which each quadrangle is the union of four triangles from the barycentric subdivison; see Figure 12.

Using the barycentric subdivision and elementary surface charts described by the parametrization in Equations (59) and (60) we first construct an oriented surface $\widetilde{\mathfrak{S}}_{\mathcal{Z},\eta,\nu,\omega}$ in the thickened horizontal plane $\mathbb{R}^2 \times [-\log 3, \log 3]$ [15] in $\mathbb{R}^3$.

For four not co-planar points A, B, C, D in $\mathbb{R}^3$ we take the surface V_{ABCD} in $\mathbb{R}^3$ given by the parametrization

$$x(1-y)A + (1-x)yB + (1-x)(1-y)C + xyD \tag{59}$$

with $0 \leq x \leq 1$, $0 \leq y \leq 1$. This surface lies in the tetrahedron $\mathsf{conv}(A, B, C, D)$; see Figure 13. The edges $x = 0$ resp. $y = 0$ resp. $x = 1$ resp. $y = 1$ of the unit square $[0,1] \times [0,1]$ are mapped to the edges $[CB]$ resp. $[CA]$ resp. $[AD]$ resp. $[BD]$ of the tetrahedron.

---

[15]Here and it what follows we use 3 as a notationally convenient number which is a bit larger than $e = \exp(1)$.

$$\mathcal{Z}_2 = \mathsf{Z}^{21} + \mathsf{Z}^{41}$$

$$\mathcal{Z}_3 = \mathsf{Z}^{21} + \mathsf{Z}^{41} + \mathsf{Z}^{61}$$

$$\mathcal{Z}_4 = \mathsf{Z}^{21} + \mathsf{Z}^{31} + \mathsf{Z}^{41} + \mathsf{Z}^{61}$$

$$\mathcal{Z}_6 = \mathsf{Z}^{11} + \mathsf{Z}^{21} + \mathsf{Z}^{31} + \mathsf{Z}^{41} + \mathsf{Z}^{51} + \mathsf{Z}^{61}$$
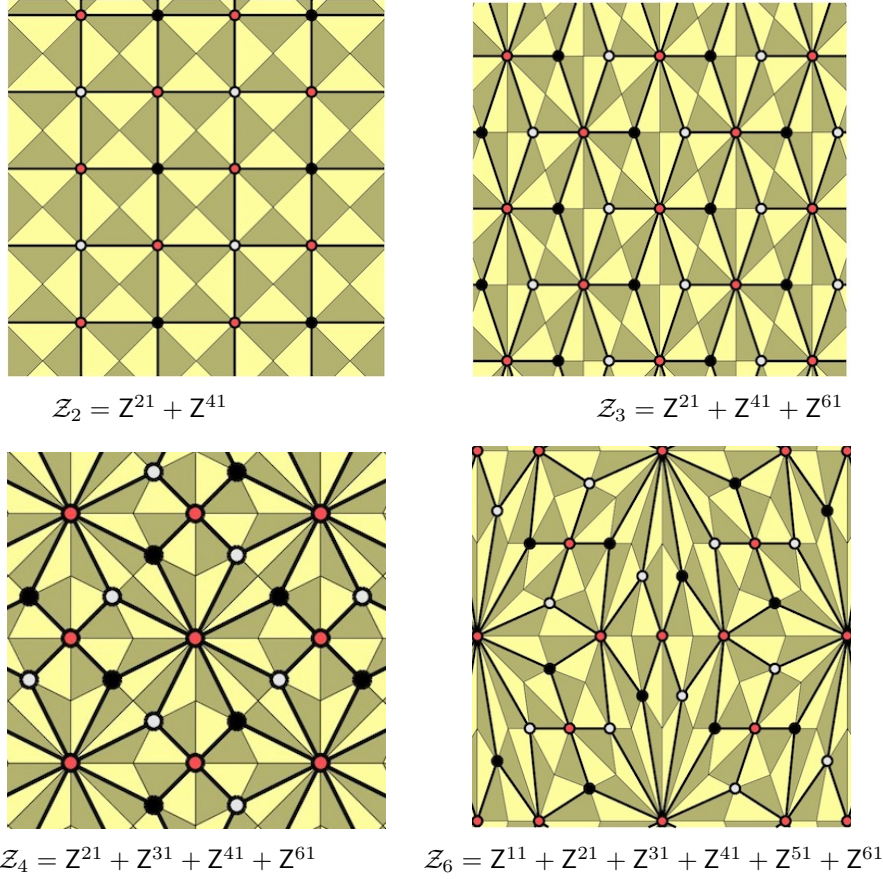
Figure 12: Barycentric subdivision (with $\nu(e) = 1$ for all e) of the tilings in Figure 2. Highlighted is the tiling by the quadrangles formed by the four triangles with a common vertex at the midpoint of an edge in the black-white tiling. The quiver Γ and the bipartite graph $\Gamma^\vee$ appear as the diagonals in these quadrangles.
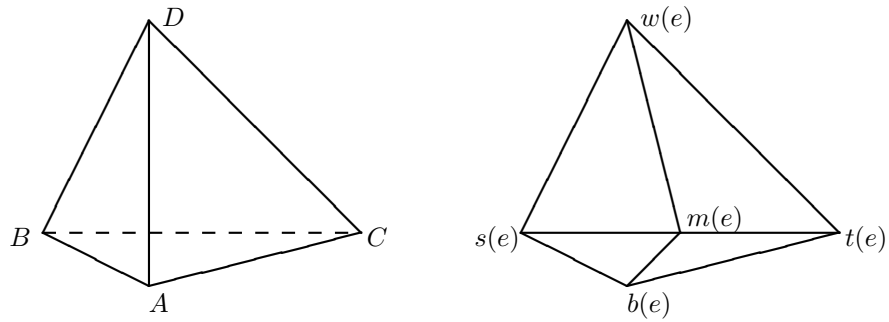
Figure 13: Left: tetrahedron $\mathsf{conv}(A, B, C, D)$. Right: the four triangles adjacent to the edge e in the barycentric subdivision. Here $w(e)$, $b(e)$, $s(e)$, $t(e)$ and $m(e)$ denote the white and black marked points adjacent to e and the source, target and midpoint of e, respectively.

28
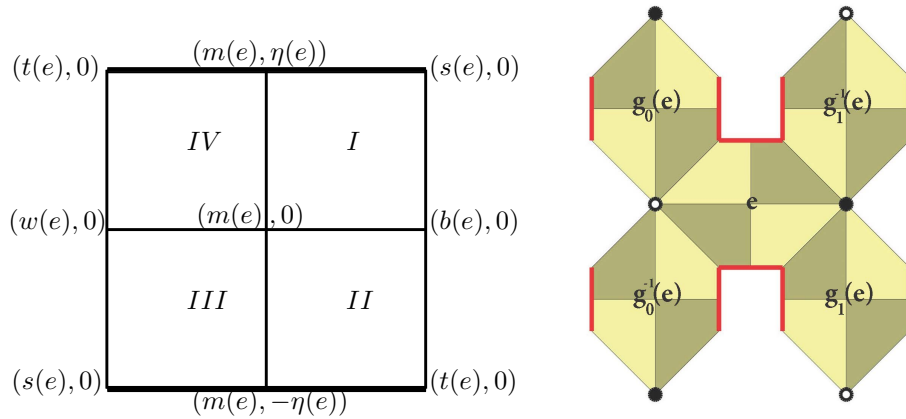
Figure 14: Left: surface chart for $\widetilde{\mathfrak{S}}_{\mathcal{Z},\eta,\nu}$ corresponding to one edge e built from four surfaces V_{ABCD}; cf. (60). Right: surface charts for $\widetilde{\mathfrak{S}}_{\mathcal{Z},\eta,\nu}$ corresponding to the edges e, $\sigma_0(e)$, $\sigma_0^{-1}(e)$, $\sigma_1(e)$, $\sigma_1^{-1}(e)$. Note: here $\mathbf{g} = \sigma$.

For an edge e in the tiling consider the four triangles in the barycentric subdivision which are adjacent to e; see Figures 12 and 13. Edge e contributes to the surface $\widetilde{\mathfrak{S}}_{\mathcal{Z},\eta,\nu,\omega}$ the four charts V_{ABCD} as in (59) with

$$
\begin{array}{llllll}
I: & A = (m(e), 0), & B = (s(e), 0), & C = (b(e), 0), & D = (m(e), \eta(e)), \\
II: & A = (m(e), 0), & B = (t(e), 0), & C = (b(e), 0), & D = (m(e), -\eta(e)), \\
III: & A = (m(e), 0), & B = (s(e), 0), & C = (w(e), 0), & D = (m(e), -\eta(e)), \\
IV: & A = (m(e), 0), & B = (t(e), 0), & C = (w(e), 0), & D = (m(e), \eta(e)).
\end{array}
\tag{60}
$$

These four charts fit together to one chart corresponding to the edge e as shown in Figure 14. The surface $\widetilde{\mathfrak{S}}_{\mathcal{Z},\eta,\nu,\omega}$ is obtained by glueing the charts for the various edges exactly as in the barycentric subdivision of the original black-white tiling given by $\mathcal{Z}$; see Figure 14. It is an oriented surface; i.e. as a surface in $\mathbb{R}^3$ it has two sides which can be colored with two different colors (but Figure 14 shows just one side; the light-dark shading indicates the barycentric subdivision).

The coordinate function y on the parametrized chart (59)-(60) defines a continuous map

$$
\Xi : \widetilde{\mathfrak{S}}_{\mathcal{Z},\eta,\nu,\omega} \longrightarrow [0,1].
\tag{61}
$$

For $0 < h < 1$ we define the surfaces $\widetilde{\mathfrak{S}}^{\leqslant h}_{\mathcal{Z},\eta,\nu,\omega}$ and $\widetilde{\mathfrak{S}}^{<h}_{\mathcal{Z},\eta,\nu,\omega}$ by

$$
\widetilde{\mathfrak{S}}^{\leqslant h}_{\mathcal{Z},\eta,\nu,\omega} := \Xi^{-1}([0,h]), \qquad \widetilde{\mathfrak{S}}^{<h}_{\mathcal{Z},\eta,\nu,\omega} := \Xi^{-1}([0,h)).
\tag{62}
$$

The surfaces $\widetilde{\mathfrak{S}}^{<h}_{\mathcal{Z},\eta,\nu,\omega}$ and $\widetilde{\mathfrak{S}}^{\leqslant h}_{\mathcal{Z},\eta,\nu,\omega}$ are contained in the thickened horizontal plane $\mathbb{R}^2 \times [-h \log 3, h \log 3]$ and contain the bipartite graph $\Gamma^{\vee} = \Xi^{-1}(0)$ as a **deformation retract**.

Vertical projection onto the horizontal plane defines a continuous map

$$
\mathsf{q} : \widetilde{\mathfrak{S}}^{\leqslant h}_{\mathcal{Z},\eta,\nu,\omega} \longrightarrow \mathbb{R}^2.
\tag{63}
$$

If $\mathbf{x}$ is not the midpoint of an edge of Γ then the inverse image $\mathsf{q}^{-1}(\mathbf{x})$ is either empty or consists of one point. If $\mathbf{x}$ is the midpoint of an edge of Γ then $\mathsf{q}^{-1}(\mathbf{x})$ is the vertical line segment

$$\mathsf{q}^{-1}(\mathbf{x}) = \left\{ t(\mathbf{x}, -h) + (1-t)(\mathbf{x}, h) \mid 0 \le t \le 1 \right\} \tag{64}$$

in $\mathbb{R}^3$; cf. (60). For illustrative examples showing the projected image of $\widetilde{\mathfrak{S}}^{\leqslant h}_{\mathcal{Z}, \eta, \nu, \omega}$ we refer to Figure **??**. The shading in Figure **??** reflects the barycentric subdivision in Figure 12 and indicates the covering of $\widetilde{\mathfrak{S}}^{\leqslant h}_{\mathcal{Z}, \eta, \nu, \omega}$ by charts as defined in Figure 14 and Formulas (59)-(60).

Remark 6 The boundary of $\widetilde{\mathfrak{S}}^{\leqslant h}_{\mathcal{Z}, \eta, \nu, \omega}$ is a configuration of non-intersecting curves in the thickened plane $\mathbb{R}^2 \times [-1, 1] \subset \mathbb{R}^3$. This configuration is invariant under the action of Λ_ω by horizontal translations. The pattern of over/under crossings is determined by the twist function η. Examples of the projection diagram of this configuration on the horizontal plane are shown in Figure **??**. In this diagram the curves are oriented such that the black points are on their right hand side and the white points are on their left hand side. The shown diagrams are for the twist function $\eta(e) = 1$ for all $e \in \mathcal{E}_\Lambda$. For a general twist function the crossing corresponding to an e where $\eta(e) = -1$ must be switched.

The orientation of the curves in the projection diagram is induced by the orientation we have chosen on the boundaries of the polygons in the planar tiling, i.e. black clockwise, white counter-clockwise. The over/under crossings in the diagram are given by the twist function η and Formula (60). Comparing our projection diagram with the standard conventions (see (65)) for assigning a ± 1 sign to a crossing of oriented curves we see that in the standard conventions the sign for the crossing at e is $-\eta(e)$.
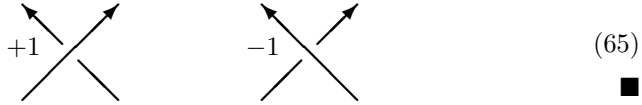
$$\tag{65}$$

$$\blacksquare$$

We let Λ_ω act on $\mathbb{R}^3$ by translations parallel to the horizontal plane and consider the previous constructions modulo Λ_ω. In order to concretely realize the "mod Λ_ω-objects" in $\mathbb{R}^3$ we use the basis λ_1, λ_2 for the lattice Λ_ω and the positive real number $r < 3^{-h}$ to define the Λ_ω-periodic map

$$\mathbb{R}^2 \times [-h \log 3, h \log 3] \longrightarrow \mathbb{R}^3, \qquad (\xi, z) \mapsto (X, Y, Z),$$

$$\tag{66}$$

$$X = \left(1 + r \exp(z) \cos\left(2\pi \frac{\det(\xi, \lambda_1)}{\det(\lambda_2, \lambda_1)} \right) \right) \sin\left(2\pi \frac{\det(\xi, \lambda_2)}{\det(\lambda_1, \lambda_2)} \right)$$

$$Y = \left(1 + r \exp(z) \cos\left(2\pi \frac{\det(\xi, \lambda_1)}{\det(\lambda_2, \lambda_1)} \right) \right) \cos\left(2\pi \frac{\det(\xi, \lambda_2)}{\det(\lambda_1, \lambda_2)} \right)$$

$$Z = r \exp(z) \sin\left(2\pi \frac{\det(\xi, \lambda_1)}{\det(\lambda_2, \lambda_1)} \right)$$

The image of the thickened horizontal plane $\mathbb{R}^2 \times [-h\log 3, h\log 3]$ is the thickened torus obtained by rotating the annulus in the plane $X = 0$ with centre $(0, 1, 0)$ and radii $r3^{-h}$ and $r3^h$ around the vertical axis $X = Y = 0$. The condition $r < 3^{-h}$ ensures that the thickened torus does not intersect the vertical axis and is contained in the 3-ball (with radius 2)

$$\mathbb{D}^3 = \left\{ (X, Y, Z) \in \mathbb{R}^3 \mid X^2 + Y^2 + Z^2 \le 4 \right\} \tag{67}$$

which is the $(W \ge 0)$-half of the 3-sphere (with radius 2)

$$\mathbb{S}^3 = \left\{ (X, Y, Z, W) \in \mathbb{R}^4 \mid X^2 + Y^2 + Z^2 + W^2 = 4 \right\}. \tag{68}$$

Definition 4 (cf. (62)) *For $0 < h < 1$ and $0 < r < 3^{-h}$ we define*

$$\begin{aligned}
\mathfrak{S}_{\mathcal{Z},\Lambda,\boxminus,r} &= \text{ image under the map (66) of } & \widetilde{\mathfrak{S}}_{\mathcal{Z},\eta,\nu,\omega}, & \tag{69} \\
\mathfrak{S}^{<h}_{\mathcal{Z},\Lambda,\boxminus,r} &= \text{ image under the map (66) of } & \widetilde{\mathfrak{S}}^{<h}_{\mathcal{Z},\eta,\nu,\omega}, & \tag{70} \\
\mathfrak{S}^{\le h}_{\mathcal{Z},\Lambda,\boxminus,r} &= \text{ image under the map (66) of } & \widetilde{\mathfrak{S}}^{\le h}_{\mathcal{Z},\eta,\nu,\omega}. & \tag{71}
\end{aligned}$$

Proposition 1 *This construction/definition has the following properties:*

*i. The maps $\widetilde{\mathfrak{S}}^{\le h}_{\mathcal{Z},\eta,\nu,\omega} \longrightarrow \mathfrak{S}^{\le h}_{\mathcal{Z},\Lambda,\boxminus,r}$ and $\widetilde{\mathfrak{S}}^{<h}_{\mathcal{Z},\eta,\nu,\omega} \longrightarrow \mathfrak{S}^{<h}_{\mathcal{Z},\Lambda,\boxminus,r}$ are **unramified covering maps** with **covering group** Λ.*

*ii. The surfaces $\mathfrak{S}^{<h}_{\mathcal{Z},\Lambda,\boxminus,r}$ and $\mathfrak{S}^{\le h}_{\mathcal{Z},\Lambda,\boxminus,r}$ contain the graph $\Gamma^\vee_\Lambda$ as a **deformation retract**. This implies that*

$$\mathrm{H}_1(\Gamma^\vee_\Lambda, \mathbb{Z}) = \mathrm{H}_1(\mathfrak{S}^{<h}_{\mathcal{Z},\Lambda,\boxminus,r}, \mathbb{Z}) = \mathrm{H}_1(\mathfrak{S}^{\le h}_{\mathcal{Z},\Lambda,\boxminus,r}, \mathbb{Z}). \tag{72}$$

*iii. The boundary $\partial\mathfrak{S}^{\le h}_{\mathcal{Z},\Lambda,\boxminus,r}$ of the surface $\mathfrak{S}^{\le h}_{\mathcal{Z},\Lambda,\boxminus,r}$ is a **link in the 3-sphere** $\mathbb{S}^3$ and $\mathfrak{S}^{\le h}_{\mathcal{Z},\Lambda,\boxminus,r}$ is a **Seifert surface** for this link; i.e. an oriented surface in $\mathbb{S}^3$ with boundary equal to the link; see Figure 15.*

*iv. The embedding $\mathfrak{S}^{\le h}_{\mathcal{Z},\Lambda,\boxminus,r} \subset \mathbb{S}^3$ induces on its homology a bilinear form known as the **Seifert form**; for the definition and explicit computation of the Seifert form see §5.4.*

v. For every $e \in \mathcal{E}_\Lambda$ the surface $\mathfrak{S}^{\le h}_{\mathcal{Z},\Lambda,\boxminus,r}$ contains the oriented line segment in $\mathbb{R}^3$

$$\mathcal{I}_e = \left\{ \Sigma_1 + \left(t\,r\exp(h) + (1-t)\,r\exp(-h) \right)\Sigma_2 \mid 0 \le t \le 1 \right\} \tag{73}$$

$$\mathcal{Z}_2 = \mathsf{Z}^{21} + \mathsf{Z}^{41}$$

$$\mathcal{Z}_3 = \mathsf{Z}^{21} + \mathsf{Z}^{41} + \mathsf{Z}^{61}$$

$$\mathcal{Z}_4 = \mathsf{Z}^{21} + \mathsf{Z}^{31} + \mathsf{Z}^{41} + \mathsf{Z}^{61}$$

$$\mathcal{Z}_6 = \mathsf{Z}^{11} + \mathsf{Z}^{21} + \mathsf{Z}^{31} + \mathsf{Z}^{41} + \mathsf{Z}^{51} + \mathsf{Z}^{61}$$
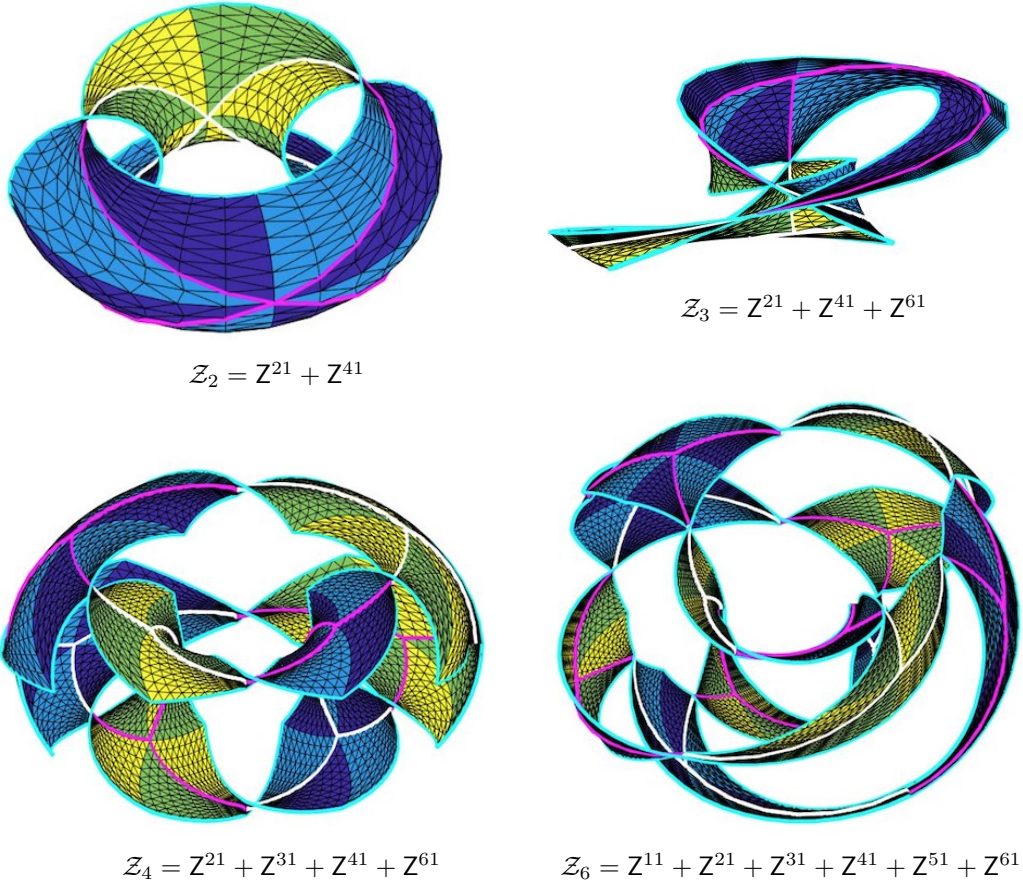
Figure 15: Some Seifert surfaces $\mathfrak{S}^{\leqslant h}_{\mathcal{Z},\Lambda,\boxminus,r}$ with embedded bipartite graphs for $\Lambda = \mathsf{Aut}(\mathcal{Z})$, all $\nu(e) = \eta(e) = 1$ and $h \approx 0.4$. The half edges of the bipartite graph have the color of the adjacent node of the graph. What looks like triangles are actually quadrangles on $\mathfrak{S}^{\leqslant h}_{\mathcal{Z},\Lambda,\boxminus,r}$. The light/dark shading of these quadrangles reflects the barycentric subdivision in Figure 12. The light-dark blue quadrangles show one side of the oriented surface; the yellow-green quadrangles show the other side.

where (see (64), (66))

$$\Sigma_1 = \begin{pmatrix} \sin\left(2\pi \frac{\det(\mathbf{x},\lambda_2)}{\det(\lambda_1,\lambda_2)}\right) \\ \cos\left(2\pi \frac{\det(\mathbf{x},\lambda_2)}{\det(\lambda_1,\lambda_2)}\right) \\ 0 \end{pmatrix}, \quad \Sigma_2 = \begin{pmatrix} \cos\left(2\pi \frac{\det(\mathbf{x},\lambda_1)}{\det(\lambda_2,\lambda_1)}\right) \\ \cos\left(2\pi \frac{\det(\mathbf{x},\lambda_1)}{\det(\lambda_2,\lambda_1)}\right) \\ \sin\left(2\pi \frac{\det(\mathbf{x},\lambda_1)}{\det(\lambda_2,\lambda_1)}\right) \end{pmatrix}, \quad (74)$$

$\mathbf{x}$ *is the midpoint of any edge in the planar tiling which modulo Λ is e.*

The endpoints of $\mathcal{I}_e$ lie on the boundary of $\mathfrak{S}_{\mathcal{Z},\Lambda,\boxminus,r}^{\leqslant h}$. It depends on $\eta(e)$ which endpoint lies on which boundary component. More precisely, the boundary components correspond bijectively with the cycles of the permutation $\sigma_1\sigma_0$. If $\eta(e) = 1$ then the endpoint $\Sigma_1 + r\exp(-h)\Sigma_2$ lies on the boundary component given by the cycle of $\sigma_1\sigma_0$ which contains $\sigma_1(e)$ and the endpoint $\Sigma_1 + r\exp(h)\Sigma_2$ lies on the boundary component given by the cycle which contains e. If $\eta(e) = -1$ it is precisely the other way round.

vi. *The surface $\mathfrak{S}_{\mathcal{Z},\Lambda,\boxminus,r}^{\leqslant h}$ lies in the thickened torus which is obtained by rotating the annulus in the plane $X = 0$ with centre $(0,1,0)$ and radii $r\exp(-h)$ and $r\exp(h)$ around the vertical axis $X = Y = 0$.*

■

Since the quantities $\frac{\det(\xi,\lambda_2)}{\det(\lambda_1,\lambda_2)}$ and $\frac{\det(\xi,\lambda_1)}{\det(\lambda_2,\lambda_1)}$ are the coordinates of ξ w.r.t. the basis λ_1, λ_2 of $\mathbb{R}^2$ the map

$$\mathbb{R}^3 \longrightarrow \mathbb{U}(1) \times \mathbb{U}(1) \times \mathbb{R}_{>0}, \quad (75)$$

$$(\xi, z) \mapsto \left(\exp\left(2\pi i \frac{\det(\xi,\lambda_2)}{\det(\lambda_1,\lambda_2)}\right), \exp\left(2\pi i \frac{\det(\xi,\lambda_1)}{\det(\lambda_2,\lambda_1)}\right), \exp(z)\right),$$

with $\mathbb{U}(1) = \{z \in \mathbb{C} \mid |z| = 1\}$, induces an isomorphism

$$\mathbb{R}^3/\Lambda_\omega \xrightarrow{\simeq} \mathbb{U}(1) \times \mathbb{U}(1) \times \mathbb{R}_{>0}. \quad (76)$$

Proposition 2 *The maps (66) and (75) induce embeddings of the surfaces $\mathfrak{S}_{\mathcal{Z},\Lambda,\boxminus,r}^{\leqslant h}$ and $\mathfrak{S}_{\mathcal{Z},\Lambda,\boxminus,r}^{<h}$ into the thickened torus $\mathbb{U}(1) \times \mathbb{U}(1) \times [3^{-h}, 3^h]$.*

Proof: See Definition 4 and note that the equalities

$$\exp\left(2\pi i \frac{\det(\xi,\lambda_2)}{\det(\lambda_1,\lambda_2)}\right) = \frac{iX + Y}{|iX + Y|}$$

$$\exp\left(2\pi i \frac{\det(\xi,\lambda_1)}{\det(\lambda_2,\lambda_1)}\right) = \frac{|iX + Y| - 1 + iZ}{||iX + Y| - 1 + iZ|} \quad (77)$$

$$\exp(z) = \frac{1}{r}||iX + Y| - 1 + iZ|$$

33

$$\mathcal{Z}_2 = \mathsf{Z}^{21} + \mathsf{Z}^{41} \qquad\qquad \mathcal{Z}_3 = \mathsf{Z}^{21} + \mathsf{Z}^{41} + \mathsf{Z}^{61}$$
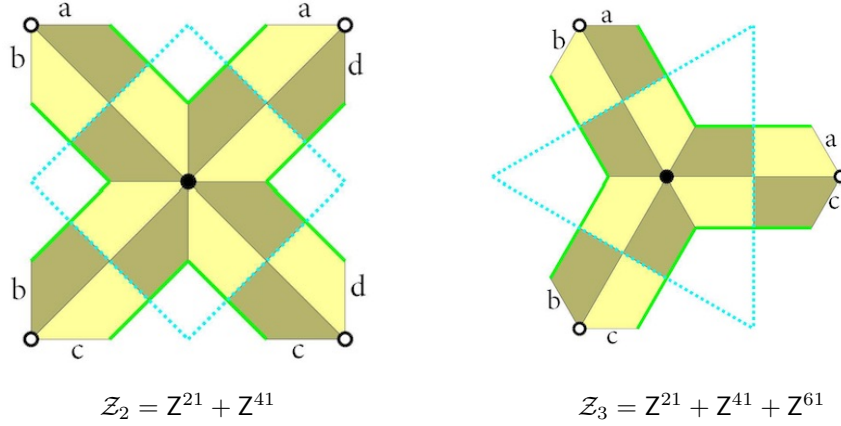
Figure 16: Unfolded charts for $\mathcal{Z}_2$ (left) and $\mathcal{Z}_3$ (right) both with $\Lambda = \mathsf{Aut}(\mathcal{Z})$.

are equivalent to (66). ∎

4.3 Examples

4.3.1 Examples: $\mathcal{Z}_2$ and $\mathcal{Z}_3$.

Consider the Zhegalkin Zebra Motives $\mathcal{Z}_2$ and $\mathcal{Z}_3$ with their automorphism lattices. For $\mathcal{Z}_2$ there are four charts and for $\mathcal{Z}_3$ three. Figure 16 shows how these charts fit together. The letters a,b,c,d indicate which sides should be identified. This identification can be achieved by folding along the dotted lines. From this we see that the surface $\mathfrak{S}_{\mathcal{Z}_2,\Lambda,\boxminus,r}^{\leqslant h}$ (resp. $\mathfrak{S}_{\mathcal{Z}_3,\Lambda,\boxminus,r}^{\leqslant h}$) is homeomorphic to a 2-sphere $\mathbb{S}^2$ from which four (resp. three) disjoint open discs have been removed. Embeddings of $\mathfrak{S}_{\mathcal{Z}_2,\Lambda,\boxminus,r}^{\leqslant h}$ and $\mathfrak{S}_{\mathcal{Z}_3,\Lambda,\boxminus,r}^{\leqslant h}$ into $\mathbb{R}^3$ are shown in Figure 15.
The superpotentials are (cf. Figure 2)

$$\text{for} \quad \big(\mathcal{Z}_2, \mathsf{Aut}(\mathcal{Z}_2)\big): \quad \sigma_0 = (1,2,3,4),\ \sigma_1 = (4,3,2,1)\,, \tag{78}$$

$$\text{for} \quad \big(\mathcal{Z}_3, \mathsf{Aut}(\mathcal{Z}_3)\big): \quad \sigma_0 = (1,2,3),\ \sigma_1 = (3,2,1)\,. \tag{79}$$

Since in both cases $\sigma_1\sigma_0$ is the identity permutation it follows from (11) that $\chi(\mathbb{X}_{\sigma_0,\sigma_1}) = 2$ and that $\mathbb{X}_{\sigma_0,\sigma_1}$ is indeed a 2-sphere. ∎

4.3.2 Examples: $\mathcal{Z}_4$ and $\mathcal{Z}_6$.

Consider the Zhegalkin Zebra Motives $\mathcal{Z}_4$ and $\mathcal{Z}_6$ with their automorphism lattices. The fundamental domains and edge labels are shown in Figure 17.
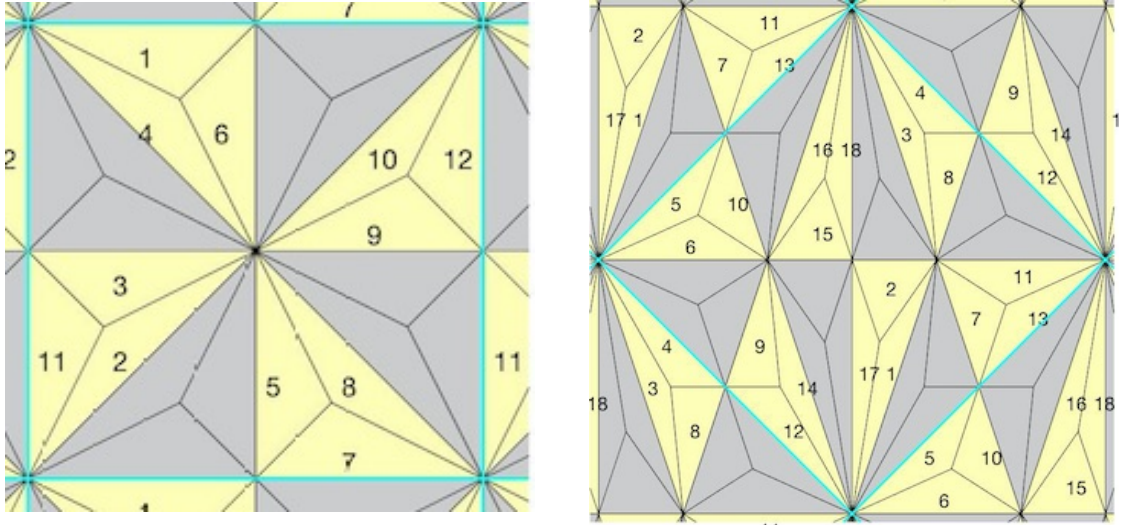
$$\mathcal{Z}_4 = Z^{21} + Z^{31} + Z^{41} + Z^{61} \qquad\qquad \mathcal{Z}_6 = Z^{11} + Z^{21} + Z^{31} + Z^{41} + Z^{51} + Z^{61}$$

Figure 17: Fundamental domain in tiling with labeled edges for $\mathcal{Z}_4$ (left) and $\mathcal{Z}_6$ (right) both with $\Lambda = \mathsf{Aut}(\mathcal{Z})$.

From this we find the permutations σ_0, σ_1, $\sigma_1\sigma_0$:

$$\sigma_0 = (1,4,6)(2,3,11)(5,7,8)(9,12,10)$$
$$\text{for } \mathcal{Z}_4: \qquad \sigma_1 = (1,2,5)(3,12,4)(6,7,10)(8,9,11)$$
$$\sigma_1\sigma_0 = (1,3,8)(2,12,6)(4,7,9)(5,10,11)$$

$$\sigma_0 = (1,2,17)(3,8,4)(5,6,10)(7,13,11)(9,12,14)(15,18,16)$$
$$\text{for } \mathcal{Z}_6: \qquad \sigma_1 = (1,7,5)(2,18,3)(4,6,9)(8,12,11)(10,13,16)(14,15,17)$$
$$\sigma_1\sigma_0 = (1,18,10)(2,14,4)(3,12,15)(5,9,11)(6,13,8)(7,16,17)$$

The surface $\mathfrak{S}^{\leqslant h}_{\mathcal{Z}_4,\Lambda,\boxminus,r}$ (resp. $\mathfrak{S}^{\leqslant h}_{\mathcal{Z}_6,\Lambda,\boxminus,r}$) is covered by 12 (resp. 18) charts which are glued as shown in Figure 18. Thus we see that these surfaces are homeomorphic to a 2-torus from which four (resp. six) disjoint open discs have been removed. This agrees with the fact that according to (11) the surface $\mathbb{X}_{\sigma_0,\sigma_1}$ has Euler characteristic 0 and, hence, is a 2-torus. Embeddings of the surfaces $\mathfrak{S}^{\leqslant h}_{\mathcal{Z}_4,\Lambda,\boxminus,r}$ and $\mathfrak{S}^{\leqslant h}_{\mathcal{Z}_6,\Lambda,\boxminus,r}$ into $\mathbb{R}^3$ are shown in Figure 15.

The atlases in Figure 18 show that the 2-torus $\mathbb{X}_{\sigma_0,\sigma_1}$ comes with a triangulation which is precisely the triangulated torus given by the Zhegalkin Zebra Motive $\mathcal{Z}_3$ and the sublattice $\Lambda_4 = \mathbb{Z}(3,1)+\mathbb{Z}(2,-2)$ (resp. $\Lambda_6 = \mathbb{Z}(3,3)+\mathbb{Z}(2,-2)$) of $\mathsf{Aut}(\mathcal{Z}_3) = \mathbb{Z}(1,1) + \mathbb{Z}(1,-1)$.

The pair $(\mathcal{Z}_4, \mathsf{Aut}(\mathcal{Z}_4))$ corresponds to model 15b in [13, 14], while the pair $(\mathcal{Z}_3, \Lambda_4)$ corresponds to model 13 in op.cit.. Similarly, the pair $(\mathcal{Z}_6, \mathsf{Aut}(\mathcal{Z}_6))$ corresponds to model 10d, while the pair $(\mathcal{Z}_3, \Lambda_6)$ corresponds to model 7. These
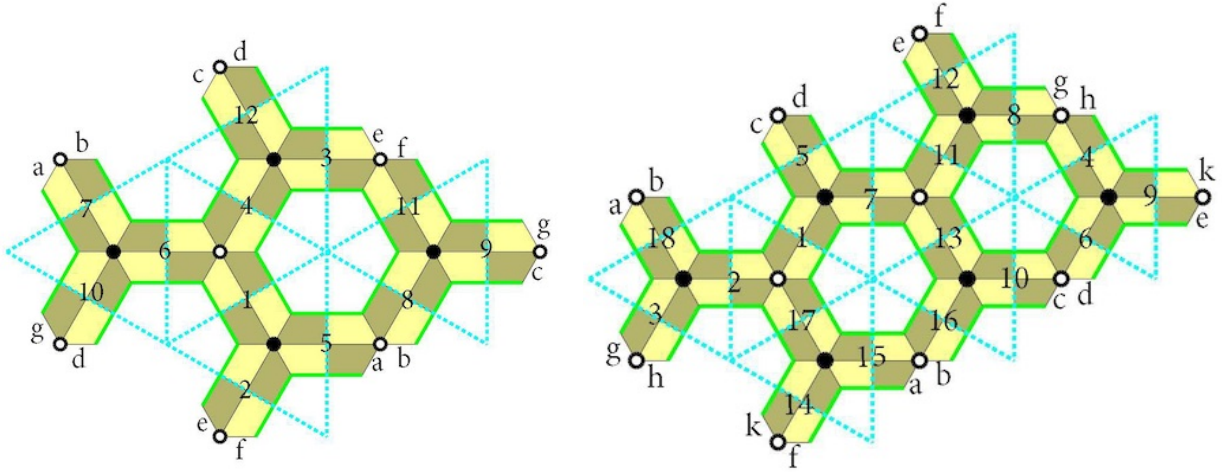
$$\mathcal{Z}_4 = \mathsf{Z}^{21} + \mathsf{Z}^{31} + \mathsf{Z}^{41} + \mathsf{Z}^{61} \qquad\qquad \mathcal{Z}_6 = \mathsf{Z}^{11} + \mathsf{Z}^{21} + \mathsf{Z}^{31} + \mathsf{Z}^{41} + \mathsf{Z}^{51} + \mathsf{Z}^{61}$$

Figure 18: Atlas with unfolded charts for $\mathcal{Z}_4$ and $\mathcal{Z}_6$ both with $\Lambda = \mathsf{Aut}(\mathcal{Z})$. The $\mathcal{Z}_4$ picture is in fact isomorphic to picture b) in [9] Figure 10.

correspondences are an expression of the phenomenon called **specular duality** in [14]; see in particular op.cit. Figure 1. ∎

4.3.3 Example: $\mathcal{Z} = \mathsf{Z}^{21} + \mathsf{Z}^{31} + \mathsf{Z}^{41} + \mathsf{Z}^{62}$.

The planar tiling for the Zhegalkin Zebra Motive $\mathcal{Z} = \mathsf{Z}^{21} + \mathsf{Z}^{31} + \mathsf{Z}^{41} + \mathsf{Z}^{62}$ is shown in Figure 34. A close up with edge labelings and period parallelogram for the lattice $\Lambda = \mathsf{Aut}(\mathcal{Z}) = \mathbb{Z}\,(2,2) + \mathbb{Z}\,(2,-2)$ are shown in Figure 19. From this one sees that the superpotential is:

$$\begin{aligned}
\sigma_0 &= (1,6,8)(2,3,4,14)(5,11,12,13)(7,9,10), \\
\sigma_1 &= (1,12,2)(3,11,10,8)(4,6,7,5)(9,14,13).
\end{aligned} \tag{80}$$

The cycle decompositions of the permutations $\sigma_1^{-1}\sigma_0$ and $\sigma_1\sigma_0$ are

$$\sigma_1^{-1}\sigma_0 = (3,5)(2,8)(6,10)(1,4,9,11)(7,13)(12,14), \tag{81}$$

$$\sigma_1\sigma_0 = (3,6)(5,10)(2,11)(8,12,9)(4,13)(1,7,14). \tag{82}$$

Thus by (11) the surface $\mathbb{X}_{\sigma_0,\sigma_1}$ is a torus.

One immediately checks that the superpotential for the Zhegalkin Zebra Motive $\mathcal{Z}'$ and the lattice Λ' shown on the left in Figure 20 is given by the pair of permutations $(\sigma_0, \sigma_1^{-1})$. It follows that the surface $\mathbb{X}_{\sigma_0,\sigma_1}$ for the Zhegalkin Zebra Motive $\mathcal{Z}$ and lattice Λ with the embedded bipartite graph $\Gamma_\Lambda^\vee$ is the same as the torus with black-white polygonal tiling for the Zhegalkin Zebra Motive $\mathcal{Z}'$ and lattice Λ'. The right-hand picture in Figure 20 shows, in the style of Figures 16-17, how the charts for the surface $\mathfrak{S}_{\mathcal{Z},\Lambda,\boxminus,r}^{\leqslant h}$ fit together. It is obtained
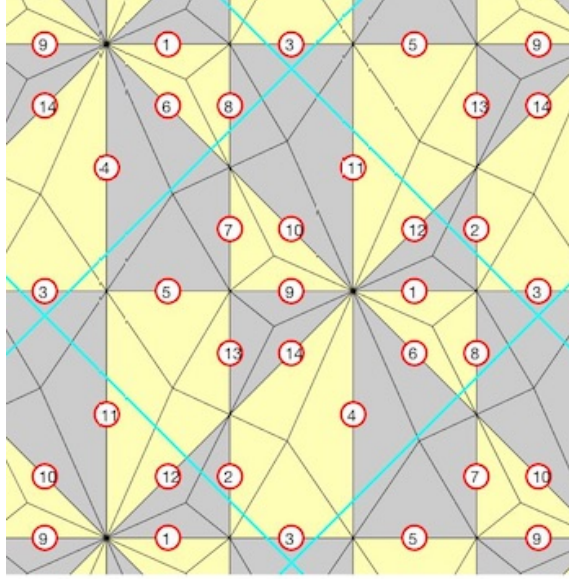
Figure 19: Planar tiling and period parallelogram for the Zhegalkin Zebra Motive $\mathcal{Z} = \mathsf{Z}^{21} + \mathsf{Z}^{31} + \mathsf{Z}^{41} + \mathsf{Z}^{62}$ and $\Lambda = \mathsf{Aut}(\mathcal{Z}) = \mathbb{Z}(2,2) + \mathbb{Z}(2,-2)$.

by removing small (open) discs around the vertices of the tiling in the left-hand picture. For an embedding as a surface $\mathfrak{S}_{\mathcal{Z},\Lambda,\boxminus,r}^{\leqslant h}$ in $\mathbb{R}^3$ see Figure 33.

The Zhegalkin Zebra Motive $\mathcal{Z}$ and lattice Λ correspond to [13] model 10c. The Zhegalkin Zebra Motive $\mathcal{Z}'$ and the lattice Λ' correspond to [13] model 8a. The observed equality of the surface $\mathbb{X}_{\sigma_0,\sigma_1}$ for $(\mathcal{Z},\Lambda)$ and the tiled torus for $(\mathcal{Z}',\Lambda')$ is another example of **specular duality**; cf. [14] Figure 1. ∎

4.4 Cartography and hyperbolic Belyi maps

4.4.1

In this section we give a construction of the surface $\mathbb{X}_{\sigma_0,\sigma_1,\varrho}$ completely in the spirit of the constructions in [8]. We set $\tau = \varrho^{-1} - \sqrt{\varrho^{-2} - 1}$. Then $0 < \tau < \varrho$ and

$$\tfrac{1}{2}(\tau^{-1} + \tau) = \varrho^{-1}, \qquad \tfrac{1}{2}(\tau^{-1} - \tau) = \sqrt{\varrho^{-2} - 1}. \tag{83}$$

On the closed disk $\overline{\mathbb{D}}$ we distinguish the following landmarks (see Figure 6):

- *The points $0 < \tau < \varrho < 1$ and the closed interval $[0,\varrho]$.*
  The hyperbolic distances between the points 0 and τ (resp. 0 and ϱ) are:

$$d_H(0,\tau) = \log\left(\frac{1+\tau}{1-\tau}\right) = \tfrac{1}{2}\log\left(\frac{1+\varrho}{1-\varrho}\right) = \tfrac{1}{2}d_H(0,\varrho). \tag{84}$$

- *The circles $\mathbb{U}(1)$, $\mathbb{U}(\varrho)$ and the arc C_τ.*
  These were defined in (14), (15) and (16) and are oriented counter-clockwise.
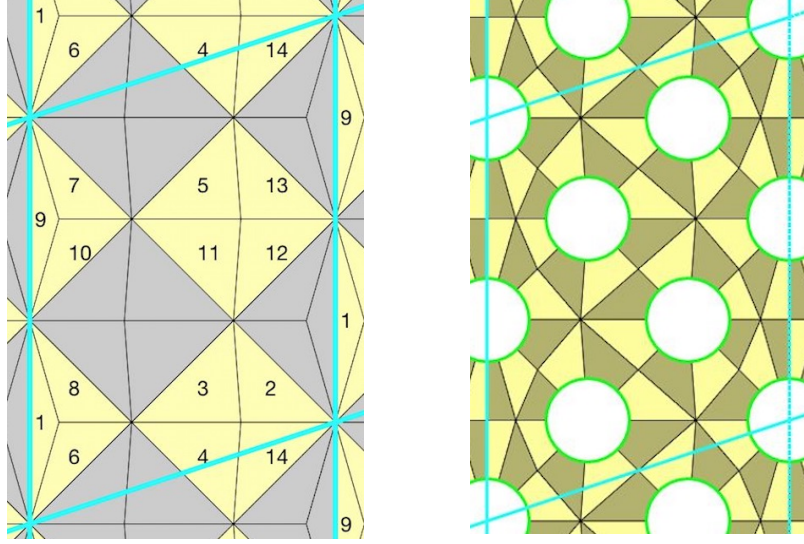
$$\mathcal{Z}' = \mathsf{Z}^{23} + \mathsf{Z}^{43} + \mathsf{Z}^{61}, \quad \Lambda' = \mathbb{Z}(3,1) + \mathbb{Z}(0,4) \subset \mathsf{Aut}(\mathcal{Z}') = \mathbb{Z}(3,1) + \mathbb{Z}(0,2)$$

Figure 20: Left: Period parallelogram with edge labelings for the Zhegalkin Zebra Motive $\mathcal{Z}' = \mathsf{Z}^{23} + \mathsf{Z}^{43} + \mathsf{Z}^{61}$ and lattice Λ'. For the biperiodic planar tiling given by $\mathcal{Z}'$ see Figure 34. Right: atlas with unfolded charts for the surface $\mathfrak{S}_{\mathcal{Z},\Lambda,\boxminus,r}^{\leqslant h}$.

The arc C_τ intersects the interval $[0, \varrho]$ perpendicularly at the point τ and its closure intersects the circle $\mathbb{U}(1)$ perpendicularly at the points $\varrho \pm i\sqrt{1 - \varrho^2}$.

- *The quadrangles*

$$
\begin{array}{llll}
I & : & \text{corners} & \tau,\, \varrho,\, 1,\, \varrho + i\sqrt{1 - \varrho^2}, \\
II & : & \text{corners} & \tau,\, \varrho,\, 1,\, \varrho - i\sqrt{1 - \varrho^2}, \\
III & : & \text{corners} & \tau,\, 0,\, -1,\, \varrho - i\sqrt{1 - \varrho^2}, \\
IV & : & \text{corners} & \tau,\, 0,\, -1,\, \varrho + i\sqrt{1 - \varrho^2}.
\end{array}
\tag{85}
$$

The sides of these quadrangles are subintervals of $[-1, 1]$ or subarcs of C_τ or of $\mathbb{U}(1)$. Thus we have

$$\overline{\mathbb{D}} = I \cup II \cup III \cup IV. \tag{86}$$

These special structures on $\overline{\mathbb{D}}$ lift via $\varphi_{\sigma_0,\sigma_1,\varrho}^{-1}$ to special structures on $\overline{\mathbb{X}}_{\sigma_0,\sigma_1,\varrho}$:

- $\varphi_{\sigma_0,\sigma_1,\varrho}^{-1}\big(\mathbb{U}(1)\big)$ is the boundary of $\overline{\mathbb{X}}_{\sigma_0,\sigma_1,\varrho}$. Its connected components correspond 1-1 with the cycles of the permutation $\sigma_1\sigma_0$.

- $\varphi_{\sigma_0,\sigma_1,\varrho}^{-1}\big(\mathbb{U}(\varrho)\big)$ is a quiver $\Gamma_\Lambda^{\circlearrowleft}$ with set of nodes $\varphi_{\sigma_0,\sigma_1,\varrho}^{-1}(\varrho)$. The arrows of $\Gamma_\Lambda^{\circlearrowleft}$ are the closures of the connected components of $\varphi_{\sigma_0,\sigma_1,\varrho}^{-1}\big(\mathbb{U}(\varrho)\setminus\{\varrho\}\big)$.
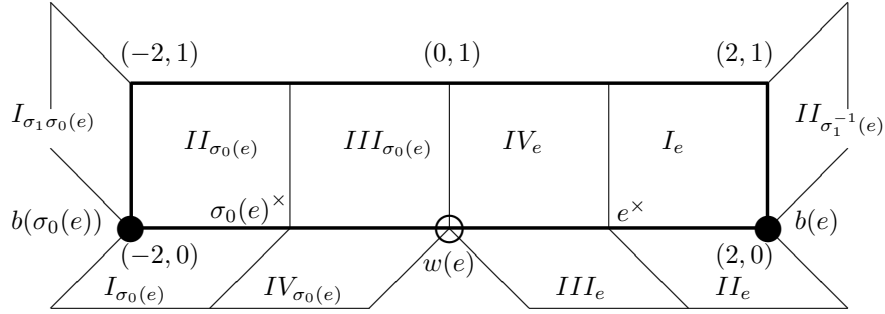
Figure 21: Adjacency in the tilings of $\overline{\mathbb{X}}_{\sigma_0,\sigma_1,\varrho}$ by quadrangles; see (87)-(88).

- The bipartite graph $\Gamma_\Lambda^\vee$ lies in $\mathbb{X}_{\sigma_0,\sigma_1,\varrho}$ as the inverse image $\varphi_{\sigma_0,\sigma_1,\varrho}^{-1}\big([0,\varrho]\big)$. The set of white nodes is $\varphi_{\sigma_0,\sigma_1,\varrho}^{-1}(0)$. The set of black nodes is $\varphi_{\sigma_0,\sigma_1,\varrho}^{-1}(\varrho)$. The white nodes correspond 1-1 with the cycles of the permutation σ_0. The black nodes correspond 1-1 with the cycles of the permutation σ_1.

- There is a bijection $\mathcal{E}_\Lambda \leftrightarrow \varphi_{\sigma_0,\sigma_1,\varrho}^{-1}(\tau)$. We denote the point on $\mathbb{X}_{\sigma_0,\sigma_1,\varrho}$ which corresponds to $e \in \mathcal{E}_\Lambda$ by $e^\times$.

- The connected components of $\varphi_{\sigma_0,\sigma_1,\varrho}^{-1}(C_\tau)$ form a collection of *disjoint, simple, oriented curves* $\mathcal{J}_e$ ($e \in \mathcal{E}_\Lambda$) in $\overline{X}_{\sigma_0,\sigma_1,\varrho}$ such that $\mathcal{J}_e$ passes through the point $e^\times$. The endpoints of the closure $\overline{\mathcal{J}_e}$ of $\mathcal{J}_e$ lie on the boundary of $\overline{\mathbb{X}}_{\sigma_0,\sigma_1,\varrho}$ so that $\overline{\mathcal{J}_e}$ starts (resp. ends) at the boundary component which corresponds to the cycle of $\sigma_1\sigma_0$ which contains e (resp. contains $\sigma_0(e)$).

- For every $e \in \mathcal{E}_\Lambda$ we have the four quadrangles I_e, II_e, III_e, IV_e:

$$
\begin{array}{llll}
I_e & : & \text{component of } \varphi_{\sigma_0,\sigma_1,\varrho}^{-1}(I) & \text{with a corner at } e^\times \\
II_e & : & \text{component of } \varphi_{\sigma_0,\sigma_1,\varrho}^{-1}(II) & \text{with a corner at } e^\times \\
III_e & : & \text{component of } \varphi_{\sigma_0,\sigma_1,\varrho}^{-1}(III) & \text{with a corner at } e^\times \\
IV_e & : & \text{component of } \varphi_{\sigma_0,\sigma_1,\varrho}^{-1}(IV) & \text{with a corner at } e^\times
\end{array}
\tag{87}
$$

Then (cf. (86))

$$
\overline{\mathbb{X}}_{\sigma_0,\sigma_1,\varrho} = \bigcup_{e\in\mathcal{E}_\Lambda} \big(I_e \cup II_e \cup III_e \cup IV_e\big).
\tag{88}
$$

In (88) the quadrangles are glued as indicated in Figure 21. For examples of how the gluing rules work out globally see Figures 16, 18, 20.

For $0 < \beta < \alpha < \frac{1}{2}\pi$ we set

$$
\varrho = \cos(\beta), \qquad \tau = \frac{1 - \sin(\beta)}{\cos(\beta)}.
\tag{89}
$$

39
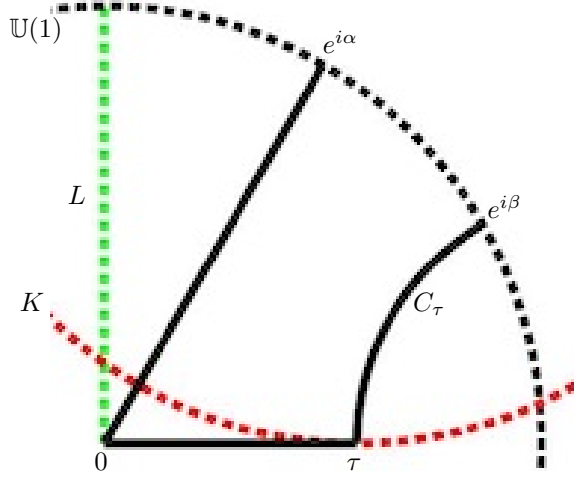
Figure 22: Parametrization of quadrangle $Q_{\alpha,\beta}$ for $\alpha = \frac{\pi}{3}$, $\beta = \frac{\pi}{6}$ and, hence, $\varrho = \frac{1}{2}\sqrt{3}$, $\tau = \frac{1}{\sqrt{3}}$.

Let $Q_{\alpha,\beta}$ denote the quadrangle enclosed by the line segments $[e^{i\alpha}, 0]$, $[0, \tau]$, the upper half of the arc C_τ and the arc between $e^{i\alpha}$ and $e^{i\beta}$ along $\mathbb{U}(1)$; see Figure 22. Formula (84) now reads

$$d_H(0, \tau) = -\log\big(\tan(\tfrac{1}{2}\beta)\big). \tag{90}$$

With these notations we have (see Figures 14 and 21)

$$\begin{aligned}
I_e &= II_e &= Q_{\alpha,\beta} \quad &\text{with} \quad \alpha = \tfrac{\pi}{k_e}, \\
III_e &= IV_e &= Q_{\alpha,\beta} \quad &\text{with} \quad \alpha = \tfrac{\pi}{n_e},
\end{aligned} \tag{91}$$

where n_e (resp. k_e) is the length of the cycle of the permutation σ_0 (resp. σ_1) which contains e and $\beta = \arccos(\varrho)$. In order to glue such a quadrangular chart Q' to another one Q such that side S' of Q' gets identified with side S of Q one first puts Q' and Q in the disk $\overline{\mathbb{D}}$ so that S' coincides with S and subsequently identifies the side S of Q with the side S' of the image of Q' under the hyperbolic reflection in S'.

In order to give a parametrization of the quadrangles $Q_{\alpha,\beta}$ we take the circle $\mathbb{U}(1)$ as in (14), the arc C_τ as in (16) and let (see Figure 22)

$$\begin{aligned}
L &= \text{line through } 0 \text{ and } i, \tag{92} \\
K &= \text{circle with centre at } \tau + i\tau\tan(\alpha) \text{ and radius } \tau\tan(\alpha). \tag{93}
\end{aligned}$$

40

Then the parametrization is

$$[0,1] \times [0,1] \longrightarrow Q_{\alpha,\beta}, \qquad (x,y) \mapsto \text{point of intersection of} \qquad (94)$$
$$\text{the circle through } x\tau \text{ perpendicular to } \mathbb{U}(1) \text{ and } K$$
$$\text{with the circle through } ye^{i\alpha} \text{ perpendicular to } C_\tau \text{ and } L.$$

The parametrization (94) applies to all quadrangles I_e, II_e, III_e, IV_e in (91) provided

$$\frac{\pi}{\beta} > \text{length of every cycle of the permutations } \sigma_0 \text{ and } \sigma_1. \qquad (95)$$

For $0 < h \leq 1$ we define $Q_{\alpha,\beta}^{\leqslant h}$ (resp. $Q_{\alpha,\beta}^{<h}$) to be the image under the parametrization (94) of the rectangle $[0,1] \times [0,h]$ (resp. $[0,1] \times [0,h[$). In this way Formula (91) yields $I_e^{\leqslant h}, \ldots, IV_e^{<h}$. In combination with (88) this yields the surfaces $\overline{\mathbb{X}}_{\sigma_0,\sigma_1,\varrho}^{\leqslant h}$ and $\mathbb{X}_{\sigma_0,\sigma_1,\varrho}^{<h}$ such that for $0 < h' < h \leq 1$

$$\mathbb{X}_{\sigma_0,\sigma_1,\varrho}^{<h'} \subset \overline{\mathbb{X}}_{\sigma_0,\sigma_1,\varrho}^{\leqslant h'} \subset \mathbb{X}_{\sigma_0,\sigma_1,\varrho}^{<h} \subset \overline{\mathbb{X}}_{\sigma_0,\sigma_1,\varrho}^{\leqslant h}, \qquad (96)$$

$$\mathbb{X}_{\sigma_0,\sigma_1,\varrho} = \mathbb{X}_{\sigma_0,\sigma_1,\varrho}^{<1}, \qquad \overline{\mathbb{X}}_{\sigma_0,\sigma_1,\varrho} = \overline{\mathbb{X}}_{\sigma_0,\sigma_1,\varrho}^{\leqslant 1} \qquad (97)$$

The hyperbolic Belyi map (cf. (13))

$$\varphi_{\sigma_0,\sigma_1,\varrho} : \overline{\mathbb{X}}_{\sigma_0,\sigma_1,\varrho} \longrightarrow \overline{\mathbb{D}} \qquad (98)$$

is defined, as follows, so that it maps the quadrangles I_e, II_e, III_e, IV_e homeomorphically onto the respective quadrangles I, II, III, IV; see (85)-(88). The homeomorphism which maps the quadrangle $IV_e = Q_{\alpha,\beta}$ in Figure 22 onto the quadrangle IV in Figure 6 and Formula (85) is the identity map on the triangle with vertices 0, τ, $e^{i\beta}$ and is an obvious homeomorphism from the triangle with vertices 0, $e^{i\beta}$, $e^{i\alpha}$ onto the triangle with vertices 0, $e^{i\beta}$, -1. For the quadrangles I_e (resp. III_e, resp. II_e one must subsequently compose this map with the hyperbolic reflection in the arc C_τ (resp. the reflection in the interval $[0,\tau]$, resp. the composite of these two reflections). The hyperbolic Belyi map

$$\varphi_{\sigma_0,\sigma_1,\varrho} : \mathbb{X}_{\sigma_0,\sigma_1,\varrho} \longrightarrow \mathbb{D} \qquad (99)$$

is just the restriction of (98).

4.4.2

In this section we give a construction of $\mathbb{X}_{\sigma_0,\sigma_1,\varrho}$ based on the embedding of the bipartite graph $\Gamma_\Lambda^\vee$ into $\mathbb{X}_{\sigma_0,\sigma_1,\varrho}$. For this construction we must fix a *rooted spanning tree* $\widehat{\Gamma_\Lambda^\vee}$ for $\Gamma_\Lambda^\vee$; i.e. a simply connected subgraph $\widehat{\Gamma_\Lambda^\vee}$ of $\Gamma_\Lambda^\vee$ with the same set of nodes as $\Gamma_\Lambda^\vee$ and one marked white node $\mathbf{w}_0$ (the root).

For efficient bookkeeping we also fix a perfect matching m_0, i.e. a map $\mathsf{m}_0 :$ $\mathcal{E}_\Lambda \to \{0, 1\}$ such that in every cycle of the permutation σ_0 and in every cycle of the permutation σ_1 there is precisely one element e for which $\mathsf{m}_0(e) = 1$.

For $\mathbf{w} \in \mathsf{P}_\Lambda^\circ$ and all $e \in \mathcal{E}_\Lambda$ such that $w(e) = \mathbf{w}$ - i.e. for a white polygon $\mathbf{w}$ in the planar tiling associated with the Zhegalkin Zebra Motive $\mathcal{Z}$ and all of its sides - the quadrangles III_e and IV_e have one angle equal to $\frac{\pi}{n_\mathbf{w}}$, three angles $\frac{\pi}{2}$ and one side of finite hyperbolic length $-\log\left(\tan(\frac{1}{2}\beta)\right)$ (cf. (90)); here $n_\mathbf{w}$ is the number of sides of the polygon $\mathbf{w}$. In $\overline{\mathbb{X}}_{\sigma_0,\sigma_1,\varrho}$ these $2n_\mathbf{w}$ quadrangles form a polygon

$$\mathfrak{H}_\mathbf{w} = \bigcup_{e \in \mathcal{E}_\Lambda,\, w(e) = \mathbf{w}} \left(III_e \cup IV_e\right) \tag{100}$$

with $n_\mathbf{w}$ sides which are arcs of length $\frac{2\pi}{n_\mathbf{w}} - 2\beta$ along the circle $\mathbb{U}(1)$ and $n_\mathbf{w}$ sides which are circular arcs perpendicular to $\mathbb{U}(1)$. The arcs of the second kind span an angle $\pi - 2\beta$ on a circle with radius $\tan(\beta)$. The centers of these circles are the points $\varrho^{-1}\exp(2\pi i j/n_\mathbf{w})$ for $j = 0, \ldots, n_\mathbf{w} - 1$ and the midpoint of the arc is $\tau\exp(2\pi i j/n_\mathbf{w})$; see (83), (89).

The arcs of the first kind on the boundary of $\mathfrak{H}_\mathbf{w}$ correspond 1-1 with the corners of the polygon $\mathbf{w}$ in the planar tiling. The arcs of the second kind correspond 1-1 with the sides of the planar polygon $\mathbf{w}$. These are counterclockwise cyclically labeled as the elements of $\mathcal{E}_\Lambda$ in the cycle of σ_0 corresponding to $\mathbf{w}$ such that the label of the arc with center ϱ^{-1} and midpoint τ is e with $\mathsf{m}_0(e) = 1$. See the left picture in Figure 23 where we also have drawn the line segments from the center 0 of the polygon $\mathfrak{H}_\mathbf{w}$ to the midpoints of its sides.

Similarly, for every $\mathbf{b} \in \mathsf{P}_\Lambda^\bullet$ - i.e. a black polygon $\mathbf{b}$ in the planar tiling - the quadrangles I_e and II_e with $b(e) = \mathbf{b}$ have one angle equal to $\frac{\pi}{k_\mathbf{b}}$, three angles $\frac{\pi}{2}$ and one side of finite hyperbolic length $-\log\left(\tan(\frac{1}{2}\beta)\right)$ (cf. (90)); here $k_\mathbf{b}$ is the number of sides of the polygon $\mathbf{b}$. Together these form the polygon

$$\mathfrak{H}_\mathbf{b} = \bigcup_{e \in \mathcal{E}_\Lambda,\, b(e) = \mathbf{b}} \left(I_e \cup II_e\right) \tag{101}$$

in $\overline{\mathbb{X}}_{\sigma_0,\sigma_1,\varrho}$ with $k_\mathbf{b}$ sides which are arcs of length $\frac{2\pi}{k_\mathbf{b}} - 2\beta$ along the circle $\mathbb{U}(1)$ and $k_\mathbf{b}$ sides which are circular arcs perpendicular to the circle $\mathbb{U}(1)$. The arcs of the second kind all span an angle $\pi - 2\beta$ on a circle with radius $\tan(\beta)$. The centers of these circles are at the points $\varrho^{-1}\exp(2\pi i j/k_\mathbf{b})$ for $j = 0, \ldots, k_\mathbf{b} - 1$ and the midpoint of the arc is $\tau\exp(2\pi i j/k_\mathbf{b})$. The arcs of the first kind on the boundary of $\mathfrak{H}_\mathbf{b}$ correspond 1-1 with the corners of the polygon $\mathbf{b}$ in the planar tiling. The arcs of the second kind correspond 1-1 with the sides of the planar polygon $\mathbf{b}$. They are clockwise cyclically labeled as the elements of $\mathcal{E}_\Lambda$ in the cycle of σ_1 corresponding to $\mathbf{b}$ such that the label of the arc with center ϱ^{-1} and midpoint τ is e with $\mathsf{m}_0(e) = 1$.

If the polygons $\mathbf{w}$ and $\mathbf{b}$ in the planar tiling have a common side e one can glue the polygon $\mathfrak{H}_\mathbf{b}$ to the polygon $\mathfrak{H}_\mathbf{w}$ as follows. Take the image of $\mathfrak{H}_\mathbf{b}$ under the reflection in its side which is the circular arc with label e and fit this image
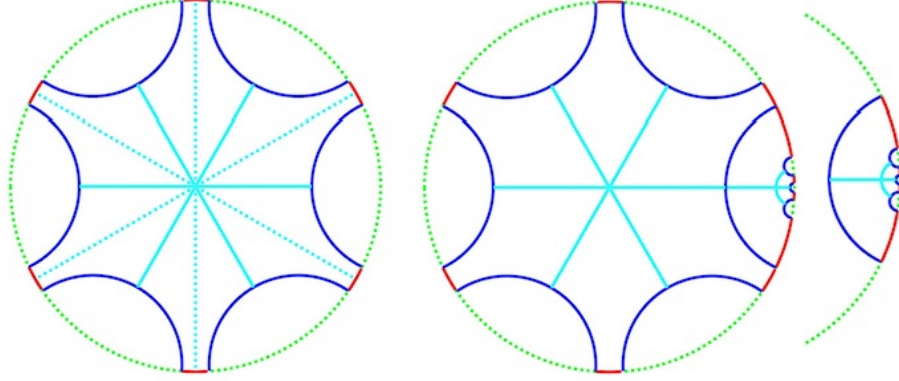
Figure 23: Left: polygon $\mathfrak{H}_\mathbf{w}$ for $n_\mathbf{w} = 6$. Right: image of polygon $\mathfrak{H}_\mathbf{b}$ for $k_\mathbf{b} = 4$ under reflection in one of its boundary arcs of the second kind. Middle: right polygon glued into an arc of the second kind of the left polygon.

by a rotation with center 0 into the side of $\mathfrak{H}_\mathbf{w}$ which is the circular arc with label e. Note that the reflection reverses the cyclic ordering of the arcs on the boundary of $\mathfrak{H}_\mathbf{b}$ from clockwise to counter-clockwise. In the same way one can glue the polygon $\mathfrak{H}_\mathbf{w}$ to the polygon $\mathfrak{H}_\mathbf{b}$ along the arc e. See Figure 23.

Recall that the circle with center $\mathbf{c} \in \mathbb{C}$ which intersects the unit circle perpendicularly has radius $\sqrt{\mathbf{c}\overline{\mathbf{c}} - 1}$ and that the reflection $R_\mathbf{c}$ in this circle is given by

$$R_\mathbf{c}(z) = \frac{\mathbf{c}\overline{z} - 1}{\overline{z} - \overline{\mathbf{c}}} \qquad \text{for} \quad z \in \mathbb{C}. \tag{102}$$

If e is the jth element in the cycle of σ_1 corresponding to $\mathbf{b}$ ($0 \leq j < k_\mathbf{b}$), then $\mathbf{c} = \varrho^{-1} \exp(-2\pi i j / k_\mathbf{b})$ and (102) is the Möbius transformation with matrix

$$\exp\left(\frac{\pi i j}{k_\mathbf{b}} \begin{pmatrix} -1 & 0 \\ 0 & 1 \end{pmatrix}\right) \cdot \frac{1}{\sqrt{1 - \varrho^2}} \begin{pmatrix} 1 & -\varrho \\ \varrho & -1 \end{pmatrix} \cdot \exp\left(\frac{\pi i j}{k_\mathbf{b}} \begin{pmatrix} -1 & 0 \\ 0 & 1 \end{pmatrix}\right). \tag{103}$$

The fact that the determinant of the matrix in (103) is -1 accounts for the appearance of $\overline{z}$ in (102).

The image of $\mathfrak{H}_\mathbf{b}$ under the transformation (102) lies in the disc with center $\varrho^{-1} \exp(-2\pi i j / k_\mathbf{b})$. If e is the hth element in the cycle of σ_0 corresponding to $\mathbf{w}$ ($0 \leq h < n_\mathbf{w}$) the image of $\mathfrak{H}_\mathbf{b}$ must subsequently be mapped by a rotation into the disc with center $\varrho^{-1} \exp(2\pi i h / n_\mathbf{w})$. The required rotation amounts to multiplication by $\exp\big(2\pi i (h/n_\mathbf{w} + j/k_\mathbf{b})\big)$ and is the Möbius transformation defined by the diagonal matrix with entries $\exp\big(\pm\pi i (h/n_\mathbf{w} + j/k_\mathbf{b})\big)$. Thus we find that the Möbius transformation which puts $\mathfrak{H}_\mathbf{b}$ in the correct arc of $\mathfrak{H}_\mathbf{w}$ is given by the matrix

$$M(e^{\circ\bullet}) = \exp\left(\frac{\pi i h}{n_\mathbf{w}} \begin{pmatrix} 1 & 0 \\ 0 & -1 \end{pmatrix}\right) \cdot \frac{1}{\sqrt{1 - \varrho^2}} \begin{pmatrix} 1 & -\varrho \\ \varrho & -1 \end{pmatrix} \cdot \exp\left(\frac{\pi i j}{k_\mathbf{b}} \begin{pmatrix} -1 & 0 \\ 0 & 1 \end{pmatrix}\right). \tag{104}$$

Similarly, the Möbius transformation which puts $\mathfrak{H}_{\mathbf{w}}$ in the correct arc of $\mathfrak{H}_{\mathbf{b}}$ is given by the matrix

$$
\begin{aligned}
M(e^{\bullet\circ}) &= \exp\left(\frac{\pi i j}{k_{\mathbf{b}}}\begin{pmatrix} -1 & 0 \\ 0 & 1 \end{pmatrix}\right) \cdot \frac{1}{\sqrt{1-\varrho^2}}\begin{pmatrix} 1 & -\varrho \\ \varrho & -1 \end{pmatrix} \cdot \exp\left(\frac{\pi i h}{n_{\mathbf{w}}}\begin{pmatrix} 1 & 0 \\ 0 & -1 \end{pmatrix}\right) \\
&= \overline{M(e^{\circ\bullet})}^{-1}. \tag{105}
\end{aligned}
$$

Using the tree $\widehat{\Gamma_\Lambda^{\vee}}$ with root $\mathbf{w}_0$ we now construct a surface $\breve{\mathbb{X}}_{\sigma_0,\sigma_1,\varrho}$ as follows. A black node $\mathbf{b}$ of $\widehat{\Gamma_\Lambda^{\vee}}$ is connected to the root $\mathbf{w}_0$ by a unique path $e_1{}^{\circ\bullet} \cdot e_2{}^{\bullet\circ} \cdots e_{2r+1}{}^{\circ\bullet}$ in $\widehat{\Gamma_\Lambda^{\vee}}$ with $r \geq 0$, $w(e_1) = \mathbf{w}_0$, $b(e_{2r+1}) = \mathbf{b}$ (notation as in (122)). Using the matrices in (104)-(105) we define the 2×2-matrix $M_{\mathbf{b}}$ by

$$
\begin{aligned}
M_{\mathbf{b}} &= M(e_1{}^{\circ\bullet}) \cdot \overline{M(e_2{}^{\bullet\circ})} \cdot \ldots \cdot \overline{M(e_{2r}{}^{\bullet\circ})} \cdot M(e_{2r+1}{}^{\circ\bullet}) \tag{106} \\
&= M(e_1{}^{\circ\bullet}) \cdot M(e_2{}^{\circ\bullet})^{-1} \cdot \ldots \cdot M(e_{2r}{}^{\circ\bullet})^{-1} \cdot M(e_{2r+1}{}^{\circ\bullet}), \tag{107}
\end{aligned}
$$

where $\overline{M()}$ means that in the above product the matrices in even position must be complex conjugated because the matrices have determinant -1. The equality (107) follows from (106) and (105).

Similarly, a white node $\mathbf{w} \neq \mathbf{w}_0$ of $\widehat{\Gamma_\Lambda^{\vee}}$ is connected to the root $\mathbf{w}_0$ by a unique path $e_1{}^{\circ\bullet} \cdot e_2{}^{\bullet\circ} \cdots e_{2r}{}^{\bullet\circ}$ in $\widehat{\Gamma_\Lambda^{\vee}}$ with $r \geq 1$, $w(e_1) = \mathbf{w}_0$, $w(e_{2r}) = \mathbf{w}$. We define the 2×2-matrix $M_{\mathbf{w}}$ by

$$
M_{\mathbf{w}} = M(e_1{}^{\circ\bullet}) \cdot M(e_2{}^{\circ\bullet})^{-1} \cdot \ldots \cdot M(e_{2r-1}{}^{\circ\bullet}) \cdot M(e_{2r}{}^{\circ\bullet})^{-1}. \tag{108}
$$

We define $M_{\mathbf{w}_0}$ to be the 2×2 identity matrix. Writing $M_{\mathbf{w}}$ and $M_{\mathbf{b}}$ also for the Möbius transformations defined by (106)-(108) we can finally construct the surface $\breve{\mathbb{X}}_{\sigma_0,\sigma_1,\varrho}$ as a subset of $\overline{\mathbb{D}}$:

$$
\breve{\mathbb{X}}_{\sigma_0,\sigma_1,\varrho} = \bigcup_{\mathbf{w}\in\mathsf{P}_\Lambda^{\circ}} M_{\mathbf{w}}(\mathfrak{H}_{\mathbf{w}}) \cup \bigcup_{\mathbf{b}\in\mathsf{P}_\Lambda^{\bullet}} M_{\mathbf{b}}(\mathfrak{H}_{\mathbf{b}}). \tag{109}
$$

Note that for $\mathbf{w}' \neq \mathbf{w}$ and $\mathbf{b}' \neq \mathbf{b}$ and for $\mathbf{w}$ and $\mathbf{b}$ which are not connected by an edge in the tree $\widehat{\Gamma_\Lambda^{\vee}}$

$$
\begin{aligned}
M_{\mathbf{w}}(\mathfrak{H}_{\mathbf{w}}) \cap M_{\mathbf{w}'}(\mathfrak{H}_{\mathbf{w}'}) = \emptyset, \quad M_{\mathbf{b}}(\mathfrak{H}_{\mathbf{b}}) \cap M_{\mathbf{b}'}(\mathfrak{H}_{\mathbf{b}'}) = \emptyset, \\
M_{\mathbf{w}}(\mathfrak{H}_{\mathbf{w}}) \cap M_{\mathbf{b}}(\mathfrak{H}_{\mathbf{b}}) = \emptyset,
\end{aligned} \tag{110}
$$

while for nodes $\mathbf{w}$ and $\mathbf{b}$ which are connected by an edge in the tree $\widehat{\Gamma_\Lambda^{\vee}}$:

$$
M_{\mathbf{w}}(\mathfrak{H}_{\mathbf{w}}) \cap M_{\mathbf{b}}(\mathfrak{H}_{\mathbf{b}}) = \overline{\mathbb{D}} \cap \{ \text{ circle perpendicular to } \mathbb{U}(1)\}. \tag{111}
$$

In $\breve{\mathbb{X}}_{\sigma_0,\sigma_1,\varrho}$ lies the set

$$
\widehat{\widehat{\Gamma_\Lambda^{\vee}}} = \bigcup_{\mathbf{w}\in\mathsf{P}_\Lambda^{\circ}} M_{\mathbf{w}}(\boxplus_{\mathbf{w}}) \cup \bigcup_{\mathbf{b}\in\mathsf{P}_\Lambda^{\bullet}} M_{\mathbf{b}}(\boxplus_{\mathbf{b}}), \tag{112}
$$

where $\boxplus_\mathbf{w}$ (resp. $\boxplus_\mathbf{b}$) denotes the union of the line segments $[0, \tau \exp(2\pi i j/m)]$ for $j = 0, \ldots, m-1$ and $m = n_\mathbf{w}$ (resp. $m = k_\mathbf{b}$) connecting the center of $\mathfrak{H}_\mathbf{w}$ (resp. $\mathfrak{H}_\mathbf{b}$) to the midpoints of its boundary arcs of the second kind.

The image of such a line segment is a hyperbolic geodesic arc in $\widehat{\widehat{\Gamma_\Lambda^\vee}}$ (i.e. a piece of a circle which is perpendicular to the unit circle $\mathbb{U}(1)$). There are $2|\mathcal{E}_\Lambda|$ such arcs. They all have length $d_H(0, \tau)$ (see (90)). Their interiors are pairwise disjoint and if two arcs γ and γ' have a common endpoint ξ then either $\xi = M_\mathbf{w}(0)$ for some $\mathbf{w} \in \mathsf{P}_\Lambda^\circ$ or $\xi = M_\mathbf{b}(0)$ for some $\mathbf{b} \in \mathsf{P}_\Lambda^\bullet$ or the endpoints of γ and γ' are $\{\xi, M_\mathbf{w}(0)\}$ and $\{\xi, M_\mathbf{b}(0)\}$, respectively, such that the nodes $\mathbf{w}$ and $\mathbf{b}$ in the tree $\widehat{\Gamma_\Lambda^\vee}$ are connected by an edge e, in which case $\gamma \cup \gamma'$ equals the edge e of $\widehat{\Gamma_\Lambda^\vee}$ and ξ is the midpoint of the arc (111).

A white node $\mathbf{w}$ corresponds to a cycle of the permutation σ_0. The line segments in $\boxplus_\mathbf{w}$ are labeled counter-clockwise cyclically with the elements of $\mathcal{E}_\Lambda$ in that cycle. As $\det(M_\mathbf{w}) = 1$ the arcs in $\widehat{\widehat{\Gamma_\Lambda^\vee}}$ with one endpoint equal to $M_\mathbf{w}(0)$ are also counter-clockwise cyclically labeled with the elements of $\mathcal{E}_\Lambda$ in that cycle.

A black node $\mathbf{b}$ corresponds to a cycle of the permutation σ_1. The line segments in $\boxplus_\mathbf{b}$ are labeled clockwise cyclically with the elements of $\mathcal{E}_\Lambda$ in that cycle. As $\det(M_\mathbf{b}) = -1$ the arcs in $\widehat{\widehat{\Gamma_\Lambda^\vee}}$ with one endpoint equal to $M_\mathbf{b}(0)$ are counter-clockwise cyclically labeled with the elements of $\mathcal{E}_\Lambda$ in that cycle.

The following proposition summarizes the above results.

Proposition 3

i. $\widehat{\widehat{\Gamma_\Lambda^\vee}}$ *is a tree with leaves, i.e. a connected graph without loops in which the edges are incident to one or two nodes. The nodes of the tree $\widehat{\Gamma_\Lambda^\vee}$ are the same as those of $\widehat{\widehat{\Gamma_\Lambda^\vee}}$. The edges of $\widehat{\Gamma_\Lambda^\vee}$ are $\gamma \cup \gamma'$ where γ, γ' are arcs in $\widehat{\widehat{\Gamma_\Lambda^\vee}}$ with one common endpoint ξ which is not a node of $\widehat{\Gamma_\Lambda^\vee}$.*

   The leaves of $\widehat{\widehat{\Gamma_\Lambda^\vee}}$ (i.e. edges incident to only one node) come in pairs which correspond 1-1 with the elements of $\mathcal{E}_\Lambda$ which are not an edge of $\widehat{\Gamma_\Lambda^\vee}$.

ii. *A node $M_\mathbf{w}(0)$ for $\mathbf{w} \in \mathsf{P}_\Lambda^\circ$ (resp. $M_\mathbf{b}(0)$ for $\mathbf{b} \in \mathsf{P}_\Lambda^\bullet$) corresponds to a cycle of the permutation σ_0 (resp. σ_1) and the arcs of $\widehat{\widehat{\Gamma_\Lambda^\vee}}$ incident to $M_\mathbf{w}(0)$ (resp. $M_\mathbf{b}(0)$) are counter-clockwise cyclically ordered as the elements in that cycle.*

iii. *The boundary of $\breve{\mathbb{X}}_{\sigma_0, \sigma_1, \varrho}$ consists of arcs along the circle $\mathbb{U}(1)$ and circular arcs perpendicular to $\mathbb{U}(1)$. The arcs of the latter type correspond 1-1 with the leaves of the tree $\widehat{\widehat{\Gamma_\Lambda^\vee}}$. They come in pairs and when they are pairwise identified we obtain the surface $\overline{\mathbb{X}}_{\sigma_0, \sigma_1, \varrho}$.*

45
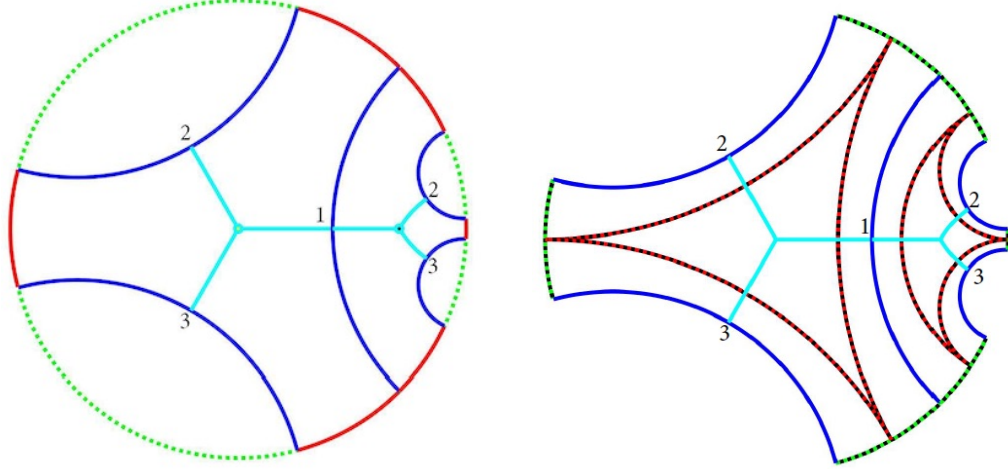
Figure 24: Polygon $\check{\mathbb{X}}_{\sigma_0,\sigma_1,\varrho}$ (red arcs and blue arcs 2 and 3) for Zhegalkin Zebra Motive $\mathcal{Z}_3$, $\Lambda = \mathsf{Aut}(\mathcal{Z}_3)$ and $\varrho = \frac{1}{2}\sqrt{2}$, $\beta = \frac{\pi}{4}$.

> *There is no identification between arcs on $\mathbb{U}(1) \cap \check{\mathbb{X}}_{\sigma_0,\sigma_1,\varrho}$. Thus the union of these arcs is the boundary of $\overline{\mathbb{X}}_{\sigma_0,\sigma_1,\varrho}$.*

iv. *The surface $\mathbb{X}_{\sigma_0,\sigma_1,\varrho}$ is $\overline{\mathbb{X}}_{\sigma_0,\sigma_1,\varrho}$ without its boundary.* ∎

4.4.3   Examples: $\mathcal{Z}_3$, $\mathcal{Z}_4$, $\mathcal{Z}_6$.

In the planar tilings for the Zhegalkin Zebra Motives $\mathcal{Z}_3$, $\mathcal{Z}_4$, $\mathcal{Z}_6$ in Figure 2 all polygons are triangles. Therefore, the hyperbolic quadrangles used in the above construction of $\overline{\mathbb{X}}_{\sigma_0,\sigma_1,\varrho}$ all have angles $\frac{1}{3}\pi$, $\frac{1}{2}\pi$, $\frac{1}{2}\pi$, $\frac{1}{2}\pi$. For $\mathcal{Z}_3$ and $\Lambda = \mathsf{Aut}(\mathcal{Z}_3)$ there is one white and one black polygon and the permutations are $\sigma_0 = (1,2,3)$, $\sigma_1 = (3,2,1)$; see (79). Figure 24 shows the polygon $\check{\mathbb{X}}_{\sigma_0,\sigma_1,\varrho}$ and the tree with leaves $\widehat{\widecheck{\Gamma_\Lambda^\vee}}$; see also Figure 16. Identification of the arcs with equal labels yields the surface $\overline{\mathbb{X}}_{\sigma_0,\sigma_1,\varrho}$. Topologically this surface is a 2-sphere from which three disjoint open disks have been removed.

We leave it as an instructive exercise to convert the pictures for $(\mathcal{Z}_4, \mathsf{Aut}(\mathcal{Z}_4))$ and $(\mathcal{Z}_6, \mathsf{Aut}(\mathcal{Z}_6))$ from Figure 18 into the format of Figure 24. ∎

5   Algebraic structures

5.1   Tabulating the structure

For the investigation of the algebraic structures associated with a Zhegalkin Zebra Motive $\mathcal{Z}$, a sublattice Λ of $\mathsf{Aut}(\mathcal{Z})$ and a Λ-invariant positive integer weight function $\nu : \mathcal{E} \to \mathbb{Z}_{>0}$ we restrict the pictures of the polygonal tiling given by $\mathcal{Z}$ to a period parallelogram for the lattice Λ; cf. Figure 19.

The lattice Λ acts on the sets $\mathcal{E}$, $\mathsf{P}^\star$, $\mathsf{P}^\bullet$, P° of edges, vertices, black and white polygons in the tiling of $\mathbb{R}^2$. We denote the orbit sets (i.e. the sets of edges, vertices, black and white polygons in the tiling of the torus $\mathbb{R}^2/\Lambda$) by $\mathcal{E}_\Lambda$, $\mathsf{P}^\star_\Lambda$, $\mathsf{P}^\bullet_\Lambda$ and P°_Λ. These are finite sets with cardinalities satisfying the relation

$$|\mathsf{P}^\star_\Lambda| + |\mathsf{P}^\bullet_\Lambda| + |\mathsf{P}^\circ_\Lambda| = |\mathcal{E}_\Lambda|. \tag{113}$$

We label the vertices with the numbers $1,\ldots,|\mathsf{P}^\star_\Lambda|$, the black polygons with the numbers $1,\ldots,|\mathsf{P}^\bullet_\Lambda|$, the white polygons with the numbers $1,\ldots,|\mathsf{P}^\circ_\Lambda|$ and the edges with the numbers $1,\ldots,|\mathcal{E}_\Lambda|$. It suffices to only include the edge labels in the picture; cf. Figure 19.

The structure maps for the quiver Γ_Λ and the bipartite graph $\Gamma^\vee_\Lambda$ are

$$s,t : \mathcal{E}_\Lambda \to \mathsf{P}^\star_\Lambda, \qquad b : \mathcal{E}_\Lambda \to \mathsf{P}^\bullet_\Lambda, \qquad w : \mathcal{E}_\Lambda \to \mathsf{P}^\circ_\Lambda. \tag{114}$$

These maps can be given in a table as in Figure 25. We also include in the table two columns for the edge vectors $\big(\omega_1(e), \omega_2(e)\big)$, one column for the positive weight function ν and two columns encoding the period parallelogram. The latter two are constructed as follows. First shift the period parallelogram such that its sides do not pass through a vertex in the tiling and its corners lie in the interior of black polygons. Choose a corner of the period parallelogram and look at how the two sides of the polygon incident to this corner intersect the edges of the tiling. This yields two maps

$$\mathfrak{l}_1, \mathfrak{l}_2 : \mathcal{E}_\Lambda \to \{-1, 0, +1\} \tag{115}$$

such that $\mathfrak{l}_j(e) = 0$ if side j does not intersect edge e, $\mathfrak{l}_j(e) = -1$ if side j intersects edge e from black to white, $\mathfrak{l}_j(e) = +1$ if side j intersects edge e from white to black. Finally we also include in the table a column for a twist function η.

Remark 7 Note that the picture in Figure 19 and the table in Figure 25 (except for the η-column) are equivalent, in the sense that one can easily be (re)constructed from the other. Actually there is some redundancy in the table.

For instance, using the columns e, $s(e)$, $t(e)$, $\omega_1(e)$, $\omega_2(e)$ one can draw the quiver Γ with periodically labeled edges in $\mathbb{R}^2$. The (closures of the) connected components of the complement $\mathbb{R}^2 \setminus \Gamma$ are the polygons of the tiling. The boundaries of these polygons are oriented and the polygons can be colored black (resp. white) if the orientation is clockwise (resp. counter-clockwise). Choosing labels for the polygons one thus finds the columns $b(e)$ and $w(e)$.

Alternatively, one may use the columns e, $b(e)$, $w(e)$, $\omega_1(e)$, $\omega_2(e)$ and the requirement that the polygons must be convex to draw the individual polygons. If the polygons are strictly convex, the labels on the edges are uniquely determined and thus provide unambiguous instructions for building the planar tiling by glueing the polygons. Choosing labels for the vertices in the tiling one thus finds the columns $s(e)$ and $t(e)$. ■

e	$s(e)$	$t(e)$	$b(e)$	$w(e)$	$\omega_1(e)$	$\omega_2(e)$	$\nu(e)$	$\mathsf{l}_1(e)$	$\mathsf{l}_2(e)$	$\eta(e)$
1	2	4	1	1	-1	0	2	0	0	1
2	6	2	1	2	0	-1	1	0	-1	1
3	2	1	2	2	1	0	1	-1	1	1
4	1	4	3	2	0	2	1	1	0	-1
5	5	1	3	3	-1	0	1	0	0	1
6	4	3	3	1	1	-1	1	-1	0	1
7	3	5	3	4	0	-1	1	0	0	1
8	3	2	2	1	0	1	1	1	0	-1
9	5	4	4	4	1	0	2	0	0	-1
10	4	3	2	4	-1	1	1	0	0	1
11	1	4	2	3	0	-2	1	0	-1	1
12	4	6	1	3	1	1	1	0	1	-1
13	6	5	4	3	0	1	1	0	0	1
14	4	6	4	2	-1	-1	1	0	0	1

Figure 25: Tabulated version of the data in Figure 19.

Remark 8 The data in the columns e, $s(e)$, $t(e)$, $b(e)$, $w(e)$ are equivalent to the data of the superpotential $(\mathcal{E}_\Lambda, \sigma_0, \sigma_1)$. Indeed the cycle decompositions of σ_0 and σ_1 immediately give the columns $b(e)$ and $w(e)$. The vertices in the tiling correspond with the cycles of the permutation $\sigma_1^{-1}\sigma_0$. The edges in a cycle are the incoming edges at the vertex corresponding to that cycle. The outgoing edges at a vertex are found by applying σ_0 to the incoming edges. In this way, the superpotential $(\mathcal{E}_\Lambda, \sigma_0, \sigma_1)$ yields columns e through $w(e)$ in the table.

Conversely, column $b(e)$ (resp. $w(e)$) shows which edges e belong to which cycle of σ_1 (resp. σ_0). If edges e and e' belong to the same cycle, e' is the immediate successor of e in the cyclic ordering if and only if $t(e) = s(e')$.

For an illustration of this remark one may compare the table in Figure 25 and Formulas (80)-(81). ∎

5.2 The (co)homology of $\Gamma_\Lambda^\vee$

The **homology group** $\mathrm{H}_1(\Gamma_\Lambda^\vee, \mathbb{Z})$ is by definition a subgroup of the free abelian group on the set of edges $\mathcal{E}_\Lambda$. The latter group can be canonically identified with the group $\mathbb{Z}^{\mathcal{E}_\Lambda}$ of maps from $\mathcal{E}_\Lambda$ to $\mathbb{Z}$. The homology group $\mathrm{H}_1(\Gamma_\Lambda^\vee, \mathbb{Z})$ then consists of those maps $\theta : \mathcal{E}_\Lambda \to \mathbb{Z}$ which satisfy

$$\forall \mathbf{b} \in \mathsf{P}_\Lambda^\bullet, \ \forall \mathbf{w} \in \mathsf{P}_\Lambda^\circ : \quad \sum_{e \in \mathcal{E}_\Lambda, b(e) = \mathbf{b}} \theta(e) = 0, \qquad \sum_{e \in \mathcal{E}_\Lambda, w(e) = \mathbf{w}} \theta(e) = 0. \quad (116)$$

The **cohomology group** $\mathrm{H}^1(\Gamma_\Lambda^\vee, \mathbb{C}^*) = \mathrm{Hom}_{\mathrm{groups}}\big(\mathrm{H}_1(\Gamma_\Lambda^\vee, \mathbb{Z}), \mathbb{C}^*\big)$ is a quotient of the group $\mathbb{C}^{*\mathcal{E}_\Lambda}$ of maps from $\mathcal{E}_\Lambda$ to $\mathbb{C}^*$ whereby a map $\alpha : \mathcal{E}_\Lambda \to \mathbb{C}^*$ induces the homomorphism

$$\mathrm{H}_1(\Gamma_\Lambda^\vee, \mathbb{Z}) \longrightarrow \mathbb{C}^*, \qquad \theta \mapsto \prod_{e \in \mathcal{E}_\Lambda} \alpha(e)^{\theta(e)}. \quad (117)$$

Two maps $\alpha_1, \alpha_2 : \mathcal{E}_\Lambda \to \mathbb{C}^*$ yield the same element of $\mathrm{H}^1(\Gamma_\Lambda^\vee, \mathbb{C}^*)$ if and only if α_1/α_2 lies in the subgroup of $\mathbb{C}^{*\mathcal{E}_\Lambda}$ defined by the equations

$$\prod_{e \in \mathcal{E}_\Lambda} \alpha(e)^{\theta(e)} = 1 \tag{118}$$

for all maps $\theta : \mathcal{E}_\Lambda \to \mathbb{Z}$ which satisfy (116). Of course, it suffices to take (118) only for a set of θ's which form a basis for $\mathrm{H}_1(\Gamma_\Lambda^\vee, \mathbb{Z})$.

Example 4

i. Equation (49) means that a realization $\omega : \mathcal{E}_\Lambda \to \mathbb{C}$ of the superpotential is an element of the homology group $\mathrm{H}_1(\Gamma_\Lambda^\vee, \mathbb{C})$. If the components of all edge vectors $(\omega_1(e), \omega_2(e))$ are integers ω_1 and ω_2 are elements of the homology group $\mathrm{H}_1(\Gamma_\Lambda^\vee, \mathbb{Z})$.

ii. Equation (48) means that a realization of the superpotential can also be viewed as a map $\omega : \mathcal{E}_\Lambda \to \mathbb{C}^*$ which then through (117) defines an element of the cohomology group $\mathrm{H}^1(\Gamma_\Lambda^\vee, \mathbb{C}^*)$.

iii. A twist function $\eta : \mathcal{E}_\Lambda \to \{\pm 1\}$ yields an element in the cohomology group $\mathrm{H}^1(\Gamma_\Lambda^\vee, \mathbb{C}^*)$. ∎

Proposition 4 *The rank of the homology group* $\mathrm{H}_1(\Gamma_\Lambda^\vee, \mathbb{Z})$ *is*

$$\mathrm{rank}\, \mathrm{H}_1(\Gamma_\Lambda^\vee, \mathbb{Z}) = |\mathcal{E}_\Lambda| + 1 - |\mathsf{P}_\Lambda^\bullet| - |\mathsf{P}_\Lambda^\circ| = 1 + |\mathsf{P}_\Lambda^\star|. \tag{119}$$

If $(\mathcal{Z}, \Lambda)$ *is dimer complete (i.e. positive integer weight functions exist) the group* $\mathrm{H}_1(\Gamma_\Lambda^\vee, \mathbb{Z})$ *is the subgroup of* $\mathbb{Z}^{\mathcal{E}_\Lambda}$ *generated by the differences* $\mathsf{m} - \mathsf{m}'$ *of perfect matchings* m, m'.

Proof: The first equality in (119) follows from the fact that (116) is a system of $|\mathsf{P}_\Lambda^\bullet| + |\mathsf{P}_\Lambda^\circ|$ linear equations for $|\mathcal{E}_\Lambda|$ unknows with exactly one linear relation between the equations. The second equality in (119) follows from (113).

In [11] §3.4 the **matching polytope** for $\Gamma_\Lambda^\vee$ is defined as the set

$$\left\{ \begin{array}{c} \text{maps } \vartheta : \mathcal{E}_\Lambda \to \mathbb{R}_{\geq 0} \text{ such that for all } \mathbf{w} \in \mathsf{P}_\Lambda^\circ \text{ and all } \mathbf{b} \in \mathsf{P}_\Lambda^\bullet: \\ \displaystyle\sum_{e \in \mathcal{E}_\Lambda,\, w(e) = \mathbf{w}} \vartheta(e) = 1 \quad \text{and} \quad \sum_{e \in \mathcal{E}_\Lambda,\, b(e) = \mathbf{b}} \vartheta(e) = 1 \end{array} \right\}. \tag{120}$$

Assume that a positive integer weight function ν exists. Then for every map $\alpha : \mathcal{E}_\Lambda \to \mathbb{Z}$ representing an element of $\mathrm{H}_1(\Gamma_\Lambda^\vee, \mathbb{Z})$ and every sufficiently large integer k the map $\frac{1}{k \deg \nu}(k\nu + \alpha)$ is a point in the matching polytope. Thus (119) implies that the matching polytope is a convex polyhedron of dimension $1 + |\mathsf{P}_\Lambda^\star|$. By [11] Lemma 3.10 the vertices of the matching polytope are precisely the perfect matchings.

Now consider an element of $H_1(\Gamma_\Lambda^\vee, \mathbb{Z})$ and represent it by a map $\alpha : \mathcal{E}_\Lambda \to \mathbb{Z}$. Take a positive integer k such that all values of the map $k\nu + \alpha : \mathcal{E}_\Lambda \to \mathbb{Z}$ are ≥ 0. Then $k\nu + \alpha$ is a non-negative integer weight function of degree $k \deg \nu$. So there are real numbers $r_\mathsf{m} \geq 0$ such that

$$k\nu + \alpha = \sum_{\mathsf{m}\,\text{perfect matching}} r_\mathsf{m}\,\mathsf{m}. \tag{121}$$

Then $k\nu(e) + \alpha(e) \geq r_\mathsf{m}\mathsf{m}(e)$ for all m and e. Now take m such that $r_\mathsf{m} > 0$. Then $k\nu + \alpha - \mathsf{m}$ is a non-negative integer weight function of degree $k \deg \nu - 1$. If $k\nu + \alpha - \mathsf{m} \neq 0$ we repeat this procedure with $k\nu + \alpha - \mathsf{m}$ in place of $k\nu + \alpha$. After finitely many steps we arrive at the situation that

$$k\nu + \alpha - \sum_\mathsf{m} n_\mathsf{m}\mathsf{m} = 0$$

with all $n_\mathsf{m} \in \mathbb{Z}$ and $\sum_\mathsf{m} n_\mathsf{m} = k \deg \nu$. In the same way one shows that $k\nu - \sum_\mathsf{m} n'_\mathsf{m}\mathsf{m} = 0$ with all $n'_\mathsf{m} \in \mathbb{Z}$ and $\sum_\mathsf{m} n'_\mathsf{m} = k \deg \nu$. It follows that

$$\alpha = \sum_\mathsf{m} n''_\mathsf{m}\mathsf{m}$$

with all $n''_\mathsf{m} \in \mathbb{Z}$ and $\sum_\mathsf{m} n''_\mathsf{m} = 0$. This completes the proof of Proposition 4. ∎

It is an amusing challenge to find positive integer weight functions by just looking at the picture of the planar tiling, but one may fail. Here is a method for proving or disproving the existence of positive integer weight functions which works in general. From (3) one sees that the simplest necessary (but not sufficient) condition for existence of non-negative integer weight functions of degree ≥ 1 is that in the cycle decompositions of the permutations σ_0 and σ_1 there must be as many cycles for σ_0 as for σ_1. If that condition is satisfied one can easily find (by computer) from the cycle decompositions of σ_0 and σ_1 all perfect matchings. If one finds nothing there are no perfect matchings and therefore according to the Proposition 4 there are no positive integer weight functions either. So let us now assume that there are perfect matchings. Then the sum of all perfect matchings is a positive integer weight function if and only if for every $e \in \mathcal{E}_\Lambda$ there is a perfect matching m such that $\mathsf{m}(e) = 1$. As said in the proof of Proposition 4, by [11] Lemma 3.10 the perfect matchings are the vertices of the matching polytope (120). So every positive integer weight function ν must be a linear combination of perfect matchings with non-negative real coefficients. Thus if a positive integer weight function exists there must be for every $e \in \mathcal{E}_\Lambda$ at least one perfect matching m such that $\mathsf{m}(e) = 1$. We conclude:

Corollary 2 *Positive integer weight functions exist if and only if the sum of all perfect matchings is a positive integer weight function.* ∎

This shows that the definitions of **dimer completeness** – Definition 1 in the present paper and Definition 1.5. in [22] – agree.

$$\mathsf{Z}^{21} + \mathsf{Z}^{41} + \mathsf{Z}^{61} + \mathsf{Z}^{62} \qquad\qquad \mathsf{Z}^{21} + \mathsf{Z}^{41} + \mathsf{Z}^{62}$$
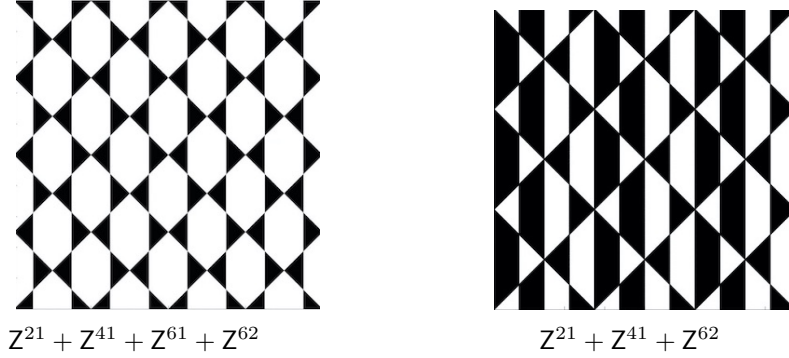
Figure 26: Zhegalkin Zebra Motives which do not admit positive integer weight functions.

Example 5 The Zhegalkin Zebra Motives shown in Figure 26 do not admit positive integer weight functions. For $\mathsf{Z}^{21} + \mathsf{Z}^{41} + \mathsf{Z}^{61} + \mathsf{Z}^{62}$ this is because there are twice as many black polygons as white polygons. For $\mathcal{Z} = \mathsf{Z}^{21} + \mathsf{Z}^{41} + \mathsf{Z}^{62}$ and $\Lambda = \mathsf{Aut}(\mathcal{Z})$ it turns out that there are 14 edges and 25 perfect matchings. The sum of the perfect matchings as a function $\mathcal{E}_\Lambda = \{1, \ldots, 14\} \to \mathbb{Z}$ is

$$10,\ 10,\ 5,\ 5,\ 10,\ 10,\ 0,\ 10,\ 10,\ 5,\ 5,\ 10,\ 10,\ 0.$$

This shows that for this $(\mathcal{Z}, \Lambda)$ there are no positive integer weight functions. ∎

For $e \in \mathcal{E}_\Lambda$ we denote by $e^{\bullet\circ}$ (resp. $e^{\circ\bullet}$) the directed edge of the bipartite graph $\Gamma_\Lambda^\vee$ from $b(e)$ to $w(e)$ (resp. from $w(e)$ to $b(e)$). Every closed loop ℓ on $\Gamma_\Lambda^\vee$ can then be written as a string

$$\ell = e_1{}^{\bullet\circ} \cdot e_2{}^{\circ\bullet} \cdot e_3{}^{\bullet\circ} \cdot e_4{}^{\circ\bullet} \cdots e_{2m-1}{}^{\bullet\circ} \cdot e_{2m}{}^{\circ\bullet} \qquad \text{with} \qquad (122)$$
$$w(e_k) = w(e_{k+1}) \text{ if } k \text{ odd}, \quad b(e_k) = b(e_{k+1}) \text{ if } k \text{ even}, \ b(e_{2m}) = b(e_1).$$

The homology class of the loop ℓ (122) in $\mathrm{H}_1(\Gamma_\Lambda^\vee, \mathbb{Z}) \subset \mathbb{Z}^{\mathcal{E}_\Lambda}$ is given by the function

$$\ell : \mathcal{E}_\Lambda \to \mathbb{Z}, \qquad \ell(e) = \sharp\{k \,|\, e = e_k,\ k \text{ even }\} - \sharp\{k \,|\, e = e_k,\ k \text{ odd }\}. \quad (123)$$

Remark 9 Loops on $\Gamma_\Lambda^\vee$ in the format (122) can immediately be seen in the picture of the planar tiling as paths in $\mathbb{R}^2$ which start in the interior of some black polygon $\mathbf{b}$, end in the interior of some Λ-translate of $\mathbf{b}$, do not pass through any vertex of the tiling and transversely intersect the edges of the tiling. Thus, in Figure 19 one can see, for instance, the loop $1^{\bullet\circ}8^{\circ\bullet}11^{\bullet\circ}5^{\circ\bullet}7^{\bullet\circ}9^{\circ\bullet}14^{\bullet\circ}2^{\circ\bullet}$. ∎

In Section 2 we defined the superpotential $(\mathcal{E}_\Lambda, \sigma_0, \sigma_1)$ for the Zhegalkin Zebra Motive $\mathcal{Z}$ and lattice Λ. **Vertices** in the tiling modulo Λ correspond to the orbits of the permutation $\sigma_1^{-1}\sigma_0$ as follows. For a vertex $\mathbf{v}$ fix an edge e_1 with $\mathbf{v} = t(e_1)$. Let $(e_1, e_3, e_5, \ldots, e_{2m-1})$ be the orbit of $\sigma_1^{-1}\sigma_0$ which contains the edge e_1; i.e. $e_{2j+1} = \sigma_1^{-1}\sigma_0(e_{2j-1})$ for $j = 1, \ldots, m-1$ and $\sigma_1^{-1}\sigma_0(e_{2m-1}) = e_1$. Then the incoming arrows at the vertex $\mathbf{v}$ are $e_1, e_3, \ldots, e_{2m-1}$ and the outgoing arrows at $\mathbf{v}$ are $\sigma_0(e_1), \sigma_0(e_3), \ldots, \sigma_0(e_{2m-1})$. Setting $e_{2j} = \sigma_0(e_{2j-1})$ for $j = 1, \ldots m$ we may combine this to one string of edges

$$\mathbf{v} = (e_1, e_2, e_3, \ldots, e_{2m-1}, e_{2m}),$$
$$e_{k+1} = \sigma_0(e_k) \text{ if } k \text{ odd}, \quad e_{k+1} = \sigma_1^{-1}(e_k) \text{ if } k \text{ even}, \quad e_1 = \sigma_1^{-1}(e_{2m}), \quad (124)$$
$$\mathbf{v} = t(e_k) \text{ if } k \text{ odd}, \quad \mathbf{v} = s(e_k) \text{ if } k \text{ even}.$$

This string of edges directly gives the following loop on $\Gamma_\Lambda^\vee$ in the format (122)

$$\ell_\mathbf{v} = e_1{}^{\bullet\circ} \cdot e_2{}^{\circ\bullet} \cdot e_3{}^{\bullet\circ} \cdot \ldots \cdot e_{2m-1}{}^{\bullet\circ} \cdot e_{2m}{}^{\circ\bullet}. \quad (125)$$

Remark 10 The right-hand side of $\mathbf{v} = (e_1, e_2, e_3, \ldots, e_{2m-1}, e_{2m})$ in (124) gives precisely the cyclic ordering of the arrows in the quiver Γ_Λ incident (incoming as well as outgoing) to the vertex $\mathbf{v}$. This cyclic ordering at all vertices of Γ_Λ is precisely what **makes Γ_Λ a ribbon graph**. It is obvious from (124) that one can read the superpotential (σ_0, σ_1) directly from this ribbon graph structure on Γ_Λ, and vice versa.

Passing from $\mathbf{v} = (e_1, e_2, e_3, \ldots, e_{2m-1}, e_{2m})$ in (124) to $\ell_\mathbf{v} = e_1{}^{\bullet\circ} \cdot e_2{}^{\circ\bullet} \cdot e_3{}^{\bullet\circ} \cdot \ldots \cdot e_{2m-1}{}^{\bullet\circ} \cdot e_{2m}{}^{\circ\bullet}$ in (125) is just a notational make-up which preserves the information on the cyclic ordering. There is however a clash between the notation $\ell_\mathbf{v}$ in (125) and the notation $\ell_\mathbf{v}$ in (57): the latter gives only the incoming and outgoing arrows at the vertex $\mathbf{v}$, but contains no information about the cyclic ordering. Or rather, (125) describes a closed loop on the graph $\Gamma_\Lambda^\vee$ and (57) only gives the homology class of that loop in $H_1(\Gamma_\Lambda^\vee, \mathbb{Z})$. ∎

In the same way the orbits of the permutation $\sigma_1\sigma_0$ define strings of edges known as **zigzags**:

$$\mathbf{z} = (e_1, e_2, e_3, \ldots, e_{2m-1}, e_{2m}),$$
$$e_{k+1} = \sigma_0(e_k) \text{ if } k \text{ odd}, \quad e_{k+1} = \sigma_1(e_k) \text{ if } k \text{ even}, \quad e_1 = \sigma_1(e_{2m}). \quad (126)$$

This string of edges directly gives the following loop on $\Gamma_\Lambda^\vee$ in the format (122)

$$\ell_\mathbf{z} = e_1{}^{\bullet\circ} \cdot e_2{}^{\circ\bullet} \cdot e_3{}^{\bullet\circ} \cdot \ldots \cdot e_{2m-1}{}^{\bullet\circ} \cdot e_{2m}{}^{\circ\bullet}. \quad (127)$$

The string of edges for the zigzag $\mathbf{z}$ in (126) also is a path along the edges of the tiling (i.e. a path on the quiver Γ_Λ) which alternately turns sharp left and sharp right. That is why it is called a **zigzag**. We denote the set of zigzags by $\mathsf{P}_\Lambda^\mathsf{z}$.

Remark 11 Note that one can immediately recover the permutations σ_0 and σ_1 from the strings of edges $\mathbf{v}$ in (124) for all vertices $\mathbf{v} \in \mathsf{P}_\Lambda^\star$.
Similarly one can immediately recover the permutations σ_0 and σ_1 from the strings of edges $\mathbf{z}$ in (126) for all zigzags $\mathbf{z} \in \mathsf{P}_\Lambda^\mathsf{z}$. ∎

Proposition 5 *The homology classes of the loops $\ell_{\mathbf{v}}$ ($\mathbf{v} \in \mathsf{P}_\Lambda^\star$) generate a sublattice of rank $|\mathsf{P}_\Lambda^\star| - 1$ in $\mathrm{H}_1(\Gamma_\Lambda^\vee, \mathbb{Z})$. The homology classes of the loops $\ell_{\mathbf{z}}$ ($\mathbf{z} \in \mathsf{P}_\Lambda^\mathsf{z}$) generate a sublattice of rank $|\mathsf{P}_\Lambda^\mathsf{z}| - 1$ in $\mathrm{H}_1(\Gamma_\Lambda^\vee, \mathbb{Z})$.* ∎

The string of edges $\mathbf{z}$ in (126) is a closed loop on the quiver Γ_Λ, while the string $\ell_{\mathbf{z}}$ in (127) is a closed loop on the bipartite graph $\Gamma_\Lambda^\vee$. The correspondence (126)-(127) is exceptionally simple. In general the correspondence between closed loops on Γ_Λ and closed loops on $\Gamma_\Lambda^\vee$ is more complicated. Here is a (canonical) way to convert a closed loop ℓ on $\Gamma_\Lambda^\vee$ given in the format (122) to a closed loop on Γ_Λ. A pair $e_{2j-1}{}^{\bullet\circ}e_{2j}{}^{\circ\bullet}$ on ℓ corresponds to a white polygon $\mathbf{w}_j$ which ℓ enters through the edge e_{2j-1} and leaves through the edge e_{2j}. Let $e_{j,1}, \ldots, e_{j,n_j}$ be the edges between e_{2j-1} and e_{2j} on the counter-clockwise oriented boundary of $\mathbf{w}_j$. A pair $e_{2j}{}^{\circ\bullet}e_{2j+1}{}^{\bullet\circ}$ on ℓ corresponds to a black polygon $\mathbf{b}_j$ which ℓ enters through the edge e_{2j} and leaves through the edge e_{2j+1}. Let $e'_{j,1}, \ldots, e'_{j,n'_j}$ be the edges between e_{2j} and e_{2j+1} on the clockwise oriented boundary of $\mathbf{b}_j$. Here j runs from 1 to m and $e_{2m+1} = e_1$ by convention. Then the closed loop on Γ_Λ which corresponds to ℓ is

$$
(e_1, e_{1,1}, \ldots, e_{1,n_1}, e_2, e'_{1,1}, \ldots, e'_{1,n'_1}, e_3, \ldots\ldots\ldots\ldots \\
\ldots\ldots, e_{2m-1}, e_{m,1}, \ldots, e_{m,n_m}, e_{2m}, e'_{m,1}, \ldots, e'_{m,n'_m}). \tag{128}
$$

Note that this reproduces for the zigzag loop $\ell_{\mathbf{z}}$ in (127) the loop $\mathbf{z}$ in (126). For the vertex loop $\ell_{\mathbf{v}}$ in (125) Formula (128)produces a loop on Γ_Λ which is the string of edges $\mathbf{v}$ in (124) with extra edges inserted between e_{2j-1} and e_{2j} for $j = 1, \ldots, m$. The resulting closed path on Γ_Λ is in fact the concatenation of the boundaries of the white polygons incident to $\mathbf{v}$.

Using Formula (128) one can associate with a closed loop ℓ on $\Gamma_\Lambda^\vee$ and a realization ω of the superpotential the vector

$$
\omega(e_1) + \omega(e_{1,1}) + \ldots + \omega(e_{1,n_1}) + \omega(e_2) + \omega(e'_{1,1}) + \ldots + \omega(e'_{1,n'_1}) + \omega(e_3) + \ldots \\
\ldots + \omega(e_{2m-1}) + \omega(e_{m,1}) + \ldots + \omega(e_{m,n_m}) + \omega(e_{2m}) + \omega(e'_{m,1}) + \ldots + \omega(e'_{m,n'_m}). \tag{129}
$$

This is an element of the lattice Λ_ω (see Definition 3) and can be seen in the picture of the planar tiling as a shift of the polygon $b(e_1)$. For a vertex loop $\ell_{\mathbf{v}}$ Formula (129) yields 0.

5.2.1   Example: $\mathcal{Z} = \mathsf{Z}^{21} + \mathsf{Z}^{31} + \mathsf{Z}^{41} + \mathsf{Z}^{62}$.

Consider the Zhegalkin Zebra Motive $\mathcal{Z} = \mathsf{Z}^{21} + \mathsf{Z}^{31} + \mathsf{Z}^{41} + \mathsf{Z}^{62}$ and the lattice $\Lambda = \mathsf{Aut}(\mathcal{Z}) = \mathbb{Z}(2,2) + \mathbb{Z}(2,-2)$; see Figures 19 and 25. From the cycle decompositions of the permutations $\sigma_1^{-1}\sigma_0$ and $\sigma_1\sigma_0$ in (81)-(82) we see that there are six vertices and six zigzags. Written in the form of strings of edges as in (124) and (126) the vertices are

$$
\begin{array}{l}
(3,4,5,11),\ (2,3,8,1),\ (6,8,10,7),\ (1,6,4,14,9,10,11,12), \\
(7,9,13,5),\ (12,13,14,2)
\end{array} \tag{130}
$$

and the zigzags are

$$(3,4,6,8),\ (5,11,10,7),\ (2,3,11,12),\ (8,1,12,13,9,10),$$
$$(4,14,13,5),\ (1,6,7,9,14,2). \tag{131}$$

Using (124)-(125) and (126)-(127) one can see these as paths in Figure 19.

We take $\ell_{\mathbf{v}}$ ($\mathbf{v} = 2,\ldots,6$) together with $\mathfrak{l}_1 = 3^{\bullet\circ}4^{\circ\bullet}6^{\bullet\circ}8^{\circ\bullet}$ and $\mathfrak{l}_2 = 11^{\bullet\circ}12^{\circ\bullet}2^{\bullet\circ}3^{\circ\bullet}$ (see Figure 19). The corresponding functions $\mathcal{E}_\Lambda \to \mathbb{Z}$ are the rows of the matrix

$$\mathbb{B} = \begin{pmatrix}
1 & -1 & 1 & 0 & 0 & 0 & 0 & -1 & 0 & 0 & 0 & 0 & 0 & 0 \\
0 & 0 & 0 & 0 & 0 & -1 & 1 & 1 & 0 & -1 & 0 & 0 & 0 & 0 \\
-1 & 0 & 0 & -1 & 0 & 1 & 0 & 0 & -1 & 1 & -1 & 1 & 0 & 1 \\
0 & 0 & 0 & 0 & 1 & 0 & -1 & 0 & 1 & 0 & 0 & 0 & -1 & 0 \\
0 & 1 & 0 & 0 & 0 & 0 & 0 & 0 & 0 & 0 & 0 & -1 & 1 & -1 \\
0 & 0 & -1 & 1 & 0 & -1 & 0 & 1 & 0 & 0 & 0 & 0 & 0 & 0 \\
0 & -1 & 1 & 0 & 0 & 0 & 0 & 0 & 0 & 0 & -1 & 1 & 0 & 0
\end{pmatrix}. \tag{132}$$

Note that these $\mathfrak{l}_1$ and $\mathfrak{l}_2$ are the same as in the table in Figure 25. Note also that the top five rows of matrix $\mathbb{B}$ are just another way of displaying the information in the columns $s(e)$ and $t(e)$ in the table in Figure 25.

Here is the list of perfect matchings for $(\mathcal{Z}, \Lambda)$ (also see (80)):

$$\{4,8,9,12\},\quad \{1,4,9,11\},\quad \{1,3,5,9\},\quad \{2,5,8,9\},\quad \{3,6,9,12\},$$
$$\{2,6,9,11\},\quad \{1,4,10,13\},\quad \{2,6,10,13\},\quad \{1,3,7,13\},\quad \{2,7,8,13\}, \tag{133}$$
$$\{1,5,10,14\},\quad \{6,10,12,14\},\quad \{7,8,12,14\},\quad \{1,7,11,14\}.$$

Take $\mathsf{m}_0 = \{4,8,9,12\}$. Writing the elements $\mathsf{m} - \mathsf{m}_0$ in coordinates w.r.t. the basis $\mathbb{B}$ (132) gives the columns of the following matrix

$$\begin{pmatrix}
0 & 1 & 2 & 1 & 0 & 0 & 2 & 1 & 2 & 1 & 3 & 1 & 1 & 2 \\
0 & 0 & 1 & 1 & 0 & 0 & 0 & 0 & 1 & 1 & 1 & 0 & 1 & 1 \\
0 & 0 & 1 & 1 & 0 & 0 & 1 & 1 & 1 & 1 & 2 & 1 & 1 & 1 \\
0 & 0 & 1 & 1 & 0 & 0 & 0 & 0 & 0 & 0 & 1 & 0 & 0 & 0 \\
0 & 0 & 1 & 1 & 0 & 0 & 1 & 1 & 1 & 1 & 1 & 0 & 0 & 0 \\
0 & 0 & 0 & 0 & -1 & -1 & 1 & 0 & 0 & 0 & 1 & 0 & 0 & 0 \\
0 & -1 & -1 & -1 & 0 & -1 & -1 & -1 & -1 & -1 & -2 & -1 & -1 & -2
\end{pmatrix}. \tag{134}$$

The fact that all entries in (134) are integers together with Proposition 4 proves that the rows of $\mathbb{B}$ indeed form a $\mathbb{Z}$-basis for $\mathrm{H}_1(\Gamma_\Lambda^\vee, \mathbb{Z})$.

The loops $\mathfrak{l}_1 = 3^{\bullet\circ}4^{\circ\bullet}6^{\bullet\circ}8^{\circ\bullet}$ and $\mathfrak{l}_2 = 11^{\bullet\circ}12^{\circ\bullet}2^{\bullet\circ}3^{\circ\bullet}$ correspond to the zigzags $(3,4,6,8)$ and $(2,3,11,12)$ in (131). These zigzags are paths on the quiver Γ_Λ. The sums of the edge vectors along these paths in the realization ω given in Figure 25 are

$$\omega(3) + \omega(4) + \omega(6) + \omega(8) = (1,0) + (0,2) + (1,-1) + (0,1) = (2,2),$$
$$\omega(2) + \omega(3) + \omega(11) + \omega(12) = (0,-1) + (1,0) + (0,-2) + (1,1) = (2,-2).$$

This is the basis for Λ corresponding to the period parallelogram in Figure 19.

54

Now consider the loops $\mathfrak{l}_1' = 11^{\bullet\circ}13^{\circ\bullet}9^{\bullet\circ}10^{\circ\bullet}$ and $\mathfrak{l}_2' = 11^{\bullet\circ}12^{\circ\bullet}1^{\bullet\circ}8^{\circ\bullet}$; see Figure 19. One can easily write $\mathfrak{l}_1'$ and $\mathfrak{l}_2'$ as linear combinations of the rows of the matrix $\mathbb{B}$ and check that $\mathfrak{l}_1'$ and $\mathfrak{l}_2'$ together with $\ell_{\mathbf{v}}$ ($\mathbf{v} = 2, \ldots, 6$) also form a basis of $\mathrm{H}_1(\Gamma_\Lambda^\vee, \mathbb{Z})$. From Figure 19 one sees that Formula (128) converts

$$\mathfrak{l}_1' \text{ to} : (11, 12, 13, 9, 10, 8, 3), \qquad \mathfrak{l}_2' \text{ to } (11, 12, 2, 1, 6, 8, 3).$$

Formula (129) now yields the vectors

$$\begin{aligned}
\omega(11) + \omega(12) + \omega(13) + \omega(9) + \omega(10) + \omega(8) + \omega(3) &= (2, 2), \\
\omega(11) + \omega(12) + \omega(2) + \omega(1) + \omega(6) + \omega(8) + \omega(3) &= (2, -2),
\end{aligned}$$

which is the same basis of Λ as before. $\blacksquare$

5.3 The Newton polygon

According to Proposition 4 the group $\mathrm{H}_1(\Gamma_\Lambda^\vee, \mathbb{Z})$ is generated by the differences $\mathsf{m} - \mathsf{m}_0$ with m_0 a fixed perfect matching and m varying through the set of perfect matchings $\mathcal{M}_{\mathcal{Z},\Lambda}$. By Proposition 5 we can take a basis $\mathbb{B}$ of $\mathrm{H}_1(\Gamma_\Lambda^\vee, \mathbb{Z})$ consisting of the loops $\ell_{\mathbf{v}}$ (see (125)) for all but one of the vertices and two more maps $\mathfrak{l}_1, \mathfrak{l}_2 : \mathcal{E}_\Lambda \to \mathbb{Z}$. We write the elements $\mathsf{m} - \mathsf{m}_0$ for $\mathsf{m} \in \mathcal{M}_{\mathcal{Z},\Lambda}$ in coordinates w.r.t. the basis $\mathbb{B}$. Taking the coordinates corresponding to $\mathfrak{l}_1, \mathfrak{l}_2$ defines a map

$$\mathfrak{n}_{\mathsf{m}_0, \mathfrak{l}_1, \mathfrak{l}_2} : \mathcal{M}_{\mathcal{Z},\Lambda} \longrightarrow \mathbb{Z}^2. \tag{135}$$

The image is a finite collection of points in $\mathbb{Z}^2$. We define

$$\begin{aligned}
\mathcal{N}_{\mathcal{Z},\Lambda,\mathsf{m}_0,\mathfrak{l}_1,\mathfrak{l}_2} &= \mathfrak{n}_{\mathsf{m}_0,\mathfrak{l}_1,\mathfrak{l}_2}\big(\mathcal{M}_{\mathcal{Z},\Lambda}\big) && (136) \\
\mathsf{Newt}_{\mathcal{Z},\Lambda,\mathsf{m}_0,\mathfrak{l}_1,\mathfrak{l}_2} &= \text{convex hull of } \mathcal{N}_{\mathcal{Z},\Lambda,\mathsf{m}_0,\mathfrak{l}_1,\mathfrak{l}_2} \text{ in } \mathbb{R}^2 && (137)
\end{aligned}$$

The polygon $\mathsf{Newt}_{\mathcal{Z},\Lambda,\mathsf{m}_0,\mathfrak{l}_1,\mathfrak{l}_2}$ is called the **Newton polygon** of $\mathcal{Z}$, Λ; cf. [11] §3.5. It follows from Propositions 4 and 5 that $\mathsf{Newt}_{\mathcal{Z},\Lambda,\mathsf{m}_0,\mathfrak{l}_1,\mathfrak{l}_2}$ is a 2-dimensional polygon.

Changing the choices of $\mathsf{m}_0, \mathfrak{l}_1, \mathfrak{l}_2$ changes $\mathcal{N}_{\mathcal{Z},\Lambda,\mathsf{m}_0,\mathfrak{l}_1,\mathfrak{l}_2}$ and $\mathsf{Newt}_{\mathcal{Z},\Lambda,\mathsf{m}_0,\mathfrak{l}_1,\mathfrak{l}_2}$ at most by an affine transformation (i.e. the composite of a translation and an invertible linear map). So, we can define an equivalence relation $\sim$ on $\mathcal{M}_{\mathcal{Z},\Lambda}$ which is independent of the choices of $\mathsf{m}_0, \mathfrak{l}_1, \mathfrak{l}_2$ by setting

$$\mathsf{m} \sim \mathsf{m}' \qquad \Leftrightarrow \qquad \mathfrak{n}_{\mathsf{m}_0,\mathfrak{l}_1,\mathfrak{l}_2}(\mathsf{m}) = \mathfrak{n}_{\mathsf{m}_0,\mathfrak{l}_1,\mathfrak{l}_2}(\mathsf{m}') \quad \text{for some } \mathsf{m}_0, \mathfrak{l}_1, \mathfrak{l}_2. \tag{138}$$

Then

$$\mathsf{m} \sim \mathsf{m}' \qquad \Leftrightarrow \qquad \mathsf{m} - \mathsf{m}' = \sum_{\mathbf{v} \in \mathsf{P}_\Lambda^\star} n_{\mathbf{v}} \ell_{\mathbf{v}} \text{ with all } n_{\mathbf{v}} \in \mathbb{Z}. \tag{139}$$

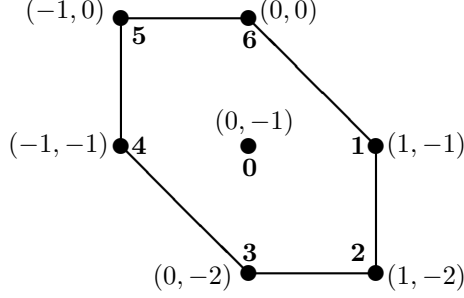We denote the set of equivalence classes by $\mathcal{N}_{\mathcal{Z},\Lambda}$.

Figure 27: The set $\mathcal{N}_{\mathcal{Z},\Lambda,\mathsf{m}_0,\mathfrak{l}_1,\mathfrak{l}_2}$ and polygon $\mathsf{Newt}_{\mathcal{Z},\Lambda,\mathsf{m}_0,\mathfrak{l}_1,\mathfrak{l}_2}$ for Example 5.2.1.

5.4 The Seifert form

In Section 4 we constructed from the data $\big(\mathcal{Z},\Lambda,\boxminus,h,r\big)$, $\boxminus = (\eta,\nu,\omega,\lambda_1,\lambda_2)$ a connected oriented surface $\mathfrak{S}^{<h}_{\mathcal{Z},\Lambda,\boxminus,r}$ in $\mathbb{S}^3$. It contains the bipartite graph $\Gamma^\vee_\Lambda$ as a deformation retract and we have the equalities of homology groups in (72). The **Seifert form** is the bilinear form $\mathcal{S}_{\eta,\lambda_1,\lambda_2}$ on $\mathrm{H}_1(\mathfrak{S}^{<h}_{\mathcal{Z},\Lambda,\boxminus,r},\mathbb{Z})$ such that for two oriented loops ℓ_1 and ℓ_2 on $\mathfrak{S}^{<h}_{\mathcal{Z},\Lambda,\boxminus,r}$

$$\mathcal{S}_{\eta,\lambda_1,\lambda_2}(\ell_1,\ell_2) \;=\; \mathsf{link}(\ell_1^+,\ell_2)\,. \tag{140}$$

Here $\mathsf{link}(\ell_1^+,\ell_2)$ is the **linking number** of loops in $\mathbb{S}^3$ and the loop ℓ_1^+ is obtained by pushing ℓ_1 a little bit off the surface $\mathfrak{S}^{<h}_{\mathcal{Z},\Lambda,\boxminus,r}$ in the positive normal direction; see [18] Definition 6.4.

The graph $\Gamma^\vee_\Lambda$ is also contained in the torus $\mathbb{T}_{\lambda_1,\lambda_2}$ which is the image of the horizontal plane $\mathbb{R}^2 \times \{0\}$ under the map (66). For a loop ℓ on $\Gamma^\vee_\Lambda$ we denote by $\ell^\dagger$ the loop in $\mathbb{S}^3$ obtained by pushing ℓ a little bit off the torus $\mathbb{T}_{\lambda_1,\lambda_2}$ in the outward normal direction. For pictures comparing ℓ, ℓ^+ and $\ell^\dagger$ see Figure 28. *Our strategy for computing the Seifert form will be to split* (140) *as*

$$\mathcal{S}_{\eta,\lambda_1,\lambda_2}(\ell_1,\ell_2) \;=\; \mathsf{link}(\ell_1^+ - \ell_1^\dagger,\ell_2) + \mathsf{link}(\ell_1^\dagger,\ell_2) \tag{141}$$

and to compute matrices w.r.t. a suitable basis of $\mathrm{H}_1(\Gamma^\vee_\Lambda,\mathbb{Z})$ *for the two pieces separately.*

A pair of perfect matchings m,m_0 determines a set of oriented edges of the bipartite graph $\Gamma^\vee_\Lambda$:

$$\{e^{\bullet\circ}, e'^{\circ\bullet} \mid e,e' \in \mathcal{E}_\Lambda,\; \mathsf{m}_0(e) = 1,\; \mathsf{m}(e) = 0,\; \mathsf{m}_0(e') = 0,\; \mathsf{m}(e') = 1\}\,. \tag{142}$$

The elements of this set fit together to a collection of disjoint simple loops on $\Gamma^\vee_\Lambda$ such that the sum the functions (123) for these simple loops is precisely $\mathsf{m} - \mathsf{m}_0$. The functions $\mathsf{m} - \mathsf{m}_0$ with m_0 fixed and m varying through the set of perfect matchings $\mathcal{M}_{\mathcal{Z},\Lambda}$ generate the homology group $\mathrm{H}_1(\Gamma^\vee_\Lambda,\mathbb{Z})$; see Proposition 4.
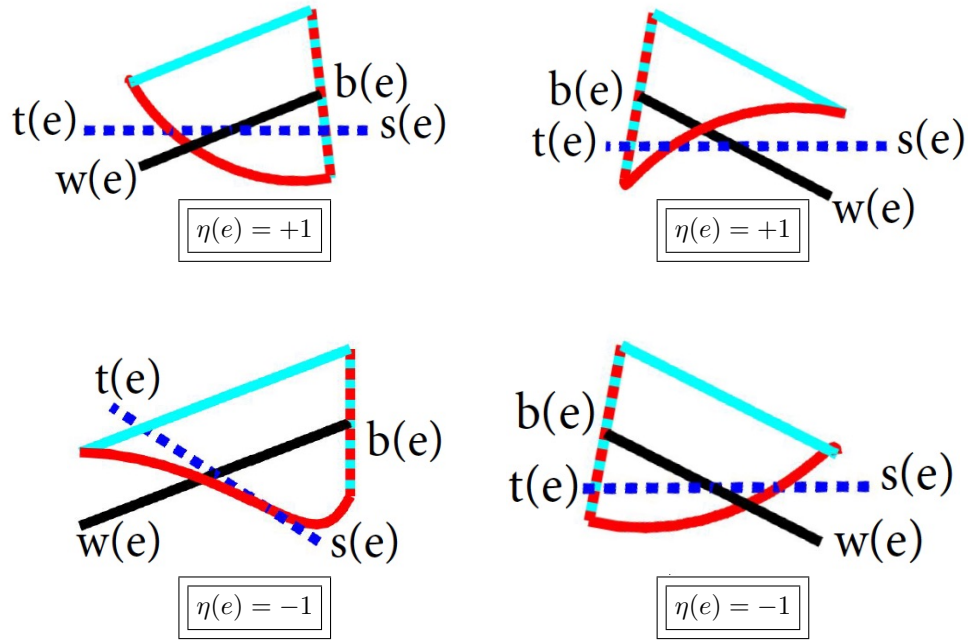
Figure 28: $e^{\circ\bullet}$, $e^{\circ\bullet+}$, $e^{\circ\bullet\dagger}$ (left), $e^{\bullet\circ}$, $e^{\bullet\circ+}$, $e^{\bullet\circ\dagger}$ (right); $e^{\circ\bullet}$, $e^{\bullet\circ}$ (black), $e^{\circ\bullet+}$, $e^{\bullet\circ+}$ (red), $e^{\circ\bullet\dagger}$, $e^{\bullet\circ\dagger}$ (blue), e (dotted blue); all directed from right to left.

The first step in computing the Seifert form is to derive Formula (149) for the linking numbers

$$\mathsf{link}\big((\mathsf{m}_1 - \mathsf{m}_0)^+ - (\mathsf{m}_1 - \mathsf{m}_0)^\dagger, (\mathsf{m}_2 - \mathsf{m}_0)\big) \qquad (143)$$

for all pairs of perfect matchings m_1, m_2 (keeping m_0 fixed). The number in (143) is a sum with one term for every black node of $\Gamma_\Lambda^\vee$. The contribution from node $\mathbf{b}$ is 0, -1, $+1$ and depends only on the edges e_0, e_1, e_2 satisfying $\mathbf{b} = b(e_0) = b(e_1) = b(e_2)$, $\mathsf{m}_0(e_0) = \mathsf{m}_1(e_1) = \mathsf{m}_2(e_2) = 1$. Using the pictures in Figure 28 one can easily see that only the four configurations in Figure 29 make non-zero contributions.
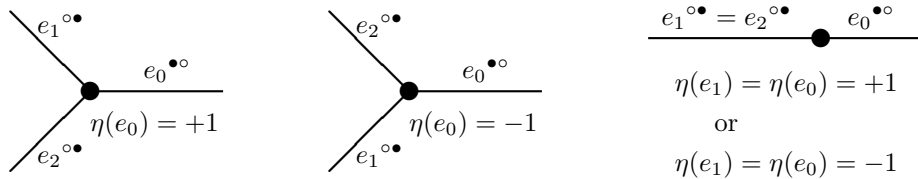
Figure 29: The only configurations which make local contributions; the local contribution is $-\eta(e_0)$.

The bookkeeping for these local contributions is most easily done by means of matrices with rows and columns indexed by the elements of $\mathcal{E}_\Lambda$. We start

from the permutation matrix for σ_1: it has in column e only one non-zero entry, namely 1 in row $\sigma_1(e)$. Using the perfect matching m_0 we define the matrix

$$\rho_{1,\mathsf{m}_0} = \big(\mathbb{I} - \varsigma_{1,\mathsf{m}_0}\big)^{-1} \tag{144}$$

where the matrix $\varsigma_{1,\mathsf{m}_0}$ is obtained by multiplying the e-th row of the permutation matrix σ_1 by $1 - \mathsf{m}_0(e)$. Denoting the identity matrix by $\mathbb{I}$ and the diagonal matrix with (e,e)-entry equal to $\eta(e)$ by $\mathsf{diag}(\eta)$ we form the matrices

$$
\begin{aligned}
R_{\eta,\mathsf{m}_0} &:= \mathsf{diag}(\eta) + \rho_{1,\mathsf{m}_0} - \rho_{1,\mathsf{m}_0}^t , &(145) \\
|R_{\eta,\mathsf{m}_0}| &:= -\mathbb{I} + \rho_{1,\mathsf{m}_0} + \rho_{1,\mathsf{m}_0}^t . &(146)
\end{aligned}
$$

The matrices R_{η,m_0} and $|R_{\eta,\mathsf{m}_0}|$ have the following interpretation. Write the cycle decomposition of the permutation σ_1 such that the elements e with $\mathsf{m}_0(e) = 1$ are in the first position in their cycle. Then the entry of R_{η,m_0} in row e_1 and column e_2 for $e_1 \neq e_2$ is -1 (resp. $+1$) if e_1 and e_2 lie in the same cycle of σ_1 with e_1 to the left (resp. right) of e_2. So, the (e_1, e_2)-entry is $+1$ for the left picture in Figure 29 and -1 for the middle one. All other off-diagonal entries of R_{η,m_0} are 0.

The matrix $|R_{\eta,\mathsf{m}_0}|$ is obtained from R_{η,m_0} by replacing all entries by their absolute value. Thus the entry of $|R_{\eta,\mathsf{m}_0}|$ in row e_1 and column e_2 is 1 if e_1 and e_2 lie in the same cycle of σ_1 and is 0 otherwise. View the function $\eta\mathsf{m}_0$ given by $\eta\mathsf{m}_0(e) = \eta(e)\mathsf{m}_0(e)$ for all e as a row vector and use it to define the row vector $\eta\mathsf{m}_0 \cdot |R_{\eta,\mathsf{m}_0}|$ by matrix multiplication. Let $\mathsf{diag}\big(\eta\mathsf{m}_0 \cdot |R_{\eta,\mathsf{m}_0}|\big)$ denote the corresponding diagonal matrix. The non-zero entries of the matrix $|R_{\eta,\mathsf{m}_0}| \cdot \mathsf{diag}\big(\eta\mathsf{m}_0 \cdot |R_{\eta,\mathsf{m}_0}|\big)$ are then $\eta(e_0)$ in row e_1 and column e_2 if e_1 and e_2 lie in the same cycle of σ_1 and e_0 is the first element in that cycle.

Proposition 6 *The matrix*

$$\Omega_{\eta,\mathsf{m}_0} := -\tfrac{1}{2}\,\mathsf{diag}(1-\mathsf{m}_0)\cdot\big(R_{\eta,\mathsf{m}_0} + |R_{\eta,\mathsf{m}_0}|\cdot\mathsf{diag}\big(\eta\mathsf{m}_0\cdot|R_{\eta,\mathsf{m}_0}|\big)\big)\cdot\mathsf{diag}(1-\mathsf{m}_0) \tag{147}$$

satisfies:

$$
\begin{aligned}
\Omega_{\eta,\mathsf{m}_0} - \Omega_{\eta,\mathsf{m}_0}^t &= \mathsf{diag}(1-\mathsf{m}_0)\cdot\big(\rho_{1,\mathsf{m}_0}^t - \rho_{1,\mathsf{m}_0}\big)\cdot\mathsf{diag}(1-\mathsf{m}_0) &(148) \\
\ell_1 \cdot \Omega_{\eta,\mathsf{m}_0} \cdot \ell_2^t &= \mathsf{link}(\ell_1^+ - \ell_1^\dagger, \ell_2) &(149)
\end{aligned}
$$

for all simple loops ℓ_1, ℓ_2 on $\Gamma_\Lambda^\vee$. On the left-hand side of Formula (149) ℓ_1, ℓ_2 are viewed as row vectors with entries $\ell_1(e)$ resp. $\ell_2(e)$ ($e \in \mathcal{E}_\Lambda$).
Note: The right-hand side of Formula (148) - hence also the left-hand side - is independent of the choice of the twist function η. The right-hand side of Formula (149) - hence also the left-hand side - is independent of the choice of the perfect matching m_0.

Proof: Formula (148) follows immediately from (145)-(146) and the fact that the matrices $|R_{\eta,\mathsf{m}_0}|$ and $\mathsf{diag}\big(\eta\mathsf{m}_0 \cdot |R_{\eta,\mathsf{m}_0}|\big)$ commute.

By construction the non-zero entries of the matrix $\Omega_{\eta,\mathsf{m}_0}$ give exactly the local contributions described in Figure 29. So, Formula (149) holds if $\ell_1 = \mathsf{m}_1 - \mathsf{m}_0$ and $\ell_2 = \mathsf{m}_2 - \mathsf{m}_0$ for two perfect matchings m_1, m_2. Since the functions $\mathsf{m} - \mathsf{m}_0$ with $\mathsf{m} \in \mathcal{M}_{\mathcal{Z},\Lambda}$ generate the homology group $\mathrm{H}_1(\Gamma_\Lambda^\vee, \mathbb{Z})$ it now follows that Formula (149) holds for all simple loops ℓ_1, ℓ_2. ∎

The subgroup of $\mathrm{H}_1(\Gamma_\Lambda^\vee, \mathbb{Z})$ generated by the homology classes $[\ell_{\mathbf{v}}]$ ($\mathbf{v} \in \mathsf{P}_\Lambda^\star$) has rank $|\mathsf{P}_\Lambda^\star| - 1$ (see Proposition 5). It is the kernel of the homomorphism $\mathrm{H}_1(\Gamma_\Lambda^\vee, \mathbb{Z}) \longrightarrow \mathrm{H}_1(\mathbb{T}_{\lambda_1,\lambda_2}, \mathbb{Z}) = \Lambda$ induced by the inclusion $\Gamma_\Lambda^\vee \hookrightarrow \mathbb{T}_{\lambda_1,\lambda_2}$. Thus as a $\mathbb{Z}$-basis of $\mathrm{H}_1(\Gamma_\Lambda^\vee, \mathbb{Z})$ we can take all but one of the classes $[\ell_{\mathbf{v}}]$ ($\mathbf{v} \in \mathsf{P}_\Lambda^\star$) together with the homology classes of two loops $\mathfrak{l}_1$ and $\mathfrak{l}_2$ on $\Gamma_\Lambda^\vee \subset \mathbb{T}_{\lambda_1,\lambda_2}$ of which the homology classes in $\mathrm{H}_1(\mathbb{T}_{\lambda_1,\lambda_2}, \mathbb{Z}) = \Lambda_\omega$ are λ_1 and λ_2, respectively.

More precisely, for $\mathfrak{l}_1$ we take the image under the map (66) of the line segment $\{(t\lambda_1, 0) \,|\, 0 \le t < 1\}$ and for $\mathfrak{l}_2$ we take the image of the line segment $\{(t\lambda_2, 0) \,|\, 0 \le t < 1\}$. Thus $\mathfrak{l}_1$ is the circle with centre $(0,0,0)$ and radius $1 + r$ in the plane $Z = 0$ and $\mathfrak{l}_2$ is the circle with centre $(0,1,0)$ and radius r in the plane $X = 0$. We denote by $\mathfrak{l}_1^\dagger$ (resp. $\mathfrak{l}_2^\dagger$) the circles obtained by pushing $\mathfrak{l}_1$ (resp. $\mathfrak{l}_2$) a little off the torus $\mathbb{T}_{\lambda_1,\lambda_2}$ in the positive normal direction. So, $\mathfrak{l}_1^\dagger$ is the circle in the plane $Z = 0$ with centre $(0,0,0)$ and radius $1 + r + \epsilon$ and $\mathfrak{l}_2^\dagger$ is the circle in the plane $X = 0$ with centre $(0,1,0)$ and radius $r + \epsilon$ for some small positive real number ϵ. Figure 30 shows that:

$$\mathsf{link}(\mathfrak{l}_2^\dagger, \mathfrak{l}_1) = 1\,, \qquad \mathsf{link}(\mathfrak{l}_1^\dagger, \mathfrak{l}_2) = \mathsf{link}(\mathfrak{l}_1^\dagger, \mathfrak{l}_1) = \mathsf{link}(\mathfrak{l}_2^\dagger, \mathfrak{l}_2) = 0\,. \tag{150}$$

Such loops $\mathfrak{l}_1$ and $\mathfrak{l}_2$ written as in (122) can easily be seen in pictures which display the edge labels (see Figure 19). In order to see which of the two loops should be $\mathfrak{l}_1$ and which $\mathfrak{l}_2$ one must then bear in mind that (150) implies that

$$\det(\lambda_1, \lambda_2) = \mathsf{link}(\mathfrak{l}_1^\dagger, \mathfrak{l}_2) - \mathsf{link}(\mathfrak{l}_2^\dagger, \mathfrak{l}_1) = -1\,. \tag{151}$$
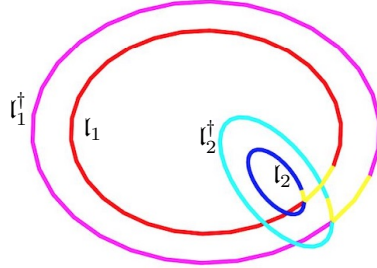
Figure 30: The loops $\mathfrak{l}_1$, $\mathfrak{l}_2$, $\mathfrak{l}_1^\dagger$, $\mathfrak{l}_2^\dagger$ for the torus $\mathbb{T}_{\lambda_1,\lambda_2}$. The loops are oriented and start with the yellow arcs.

Once the basis has been fixed the Seifert form can be given by its matrix with respect to this basis: the **Seifert matrix**. We fix here our notational conventions by taking for two loops ℓ_1, ℓ_2 in the chosen basis the entry of the Seifert matrix in row ℓ_1 and column ℓ_2 to be $\mathcal{S}_{\eta,\lambda_1,\lambda_2}(\ell_1, \ell_2)$.

Theorem 4

i. *View the functions* $\ell_{\mathbf{v}}$, $\mathfrak{l}_1$, $\mathfrak{l}_2 : \mathcal{E}_\Lambda \to \{-1, 0, 1\}$ *as row vectors. Let* $\mathbb{B}$ *denote the matrix of which the rows constitute the chosen basis of* $\mathrm{H}_1(\Gamma_\Lambda^\vee, \mathbb{Z})$. *Then the Seifert matrix w.r.t. this basis is*

$$\mathsf{S}_{\eta, \mathfrak{l}_1, \mathfrak{l}_2} = \mathbb{B} \cdot \Omega_{\eta, \mathsf{m}_0} \cdot \mathbb{B}^t + E_{\mathfrak{l}_2, \mathfrak{l}_1} \tag{152}$$

where in the matrix $E_{\mathfrak{l}_2, \mathfrak{l}_1}$ *the entry in row* $\mathfrak{l}_2$, *column* $\mathfrak{l}_1$ *is* 1 *and all other entries are* 0.

ii. *The Seifert form* $\mathcal{S}_{\eta, \lambda_1, \lambda_2}$ *on* $\mathrm{H}_1(\Gamma_\Lambda^\vee, \mathbb{Z}) = \mathrm{H}_1(\mathfrak{S}_{\mathcal{Z}, \Lambda, \boxminus, r}^{<h}, \mathbb{Z})$ *does not depend on the data* ν, ω, h, r *used in the construction of the surface* $\mathfrak{S}_{\mathcal{Z}, \Lambda, \boxminus, r}^{<h}$.
It also does not depend on the choice of the perfect matching m_0 *and the lifts* $\mathfrak{l}_1$, $\mathfrak{l}_2$ *of the basis* λ_1, λ_2 *of* Λ_ω.
It does, however, crucially depend on the choice of the twist function η and the ordered basis $\{\lambda_1, \lambda_2\}$ for Λ_ω.

iii. *The Seifert forms* $\mathcal{S}_{\eta, \lambda_1, \lambda_2}$ *and* $\mathcal{S}_{-\eta, -\lambda_2, \lambda_1}$ *satisfy*

$$\mathcal{S}_{-\eta, -\lambda_2, \lambda_1} = -\mathcal{S}_{\eta, \lambda_1, \lambda_2}^t. \tag{153}$$

Proof: **i.** The first term on the right in (152) is an immediate consequence of Formula (149). For the second term on the right in (152) we use the result in (150) and the fact that the homology class of a loop $\ell_{\mathbf{v}}$ on the torus $\mathbb{T}_{\lambda_1, \lambda_2}$ is $\mathsf{0}$.
ii. The data ν, ω, R, r, h did not appear in the preceding calculations of the Seifert matrix (152). The perfect matching m_0 does not appear in the defining formula (140) for the Seifert form.
iii. Write $p = 1 + |\mathsf{P}_\Lambda^\star| = \dim \mathrm{H}_1(\Gamma_\Lambda^\vee, \mathbb{Z})$. The matrix for the Seifert form $\mathcal{S}_{\eta, \lambda_1, \lambda_2}$ w.r.t. the basis $\mathbb{B}$ is given by Formula (152) i.e.

$$\mathsf{S}_{\eta, \mathfrak{l}_1, \mathfrak{l}_2} = \mathbb{B} \cdot \Omega_{\eta, \mathsf{m}_0} \cdot \mathbb{B}^t + E \tag{154}$$

where E denotes the $p \times p$-matrix with $(p, p-1)$-entry 1 and all other entries 0. Similarly, the matrix for the Seifert form $\mathcal{S}_{-\eta, -\lambda_2, \lambda_1}$ w.r.t. the basis $\mathbb{B}'$ is given by

$$\mathsf{S}_{-\eta, -\mathfrak{l}_2, \mathfrak{l}_1} = \mathbb{B}' \cdot \Omega_{-\eta, \mathsf{m}_0} \cdot \mathbb{B}'^t + E. \tag{155}$$

The bases $\mathbb{B}$ and $\mathbb{B}'$ are related by

$$\mathbb{B}' = J \cdot \mathbb{B} \qquad \text{with} \quad J = \begin{pmatrix} 1 & 0 \\ 0 & 0 \end{pmatrix} + E - E^t \tag{156}$$

where 1 denotes the identity matrix of size $p - 1$ and 0 denotes the appropriate zero matrices. Note that $J^t = J^{-1}$. The matrix for the Seifert form $\mathcal{S}_{\eta, \lambda_1, \lambda_2}$ w.r.t. the basis $\mathbb{B}'$ is therefore

$$J \cdot \mathsf{S}_{\eta, \mathfrak{l}_1, \mathfrak{l}_2} \cdot J^t = \mathbb{B}' \cdot \Omega_{\eta, \mathsf{m}_0} \cdot \mathbb{B}'^t - E^t. \tag{157}$$

60

Formulas (145) and (147) imply

$$\Omega_{-\eta,\mathsf{m}_0} = -\Omega^t_{\eta,\mathsf{m}_0}. \tag{158}$$

The result (153) now follows from (155), (157) and (158). ∎

Theorem 5

i. *Let* $\ell_0 = \sum_{\mathbf{z} \in \mathsf{P}^{\mathsf{z}}_\Lambda} n_{\mathbf{z}} \ell_{\mathbf{z}}$ *be an element in the sublattice of* $\mathrm{H}_1(\Gamma^\vee_\Lambda, \mathbb{Z})$ *which is spanned by the zigzag loops. Then one has for every* $\ell \in \mathrm{H}_1(\Gamma^\vee_\Lambda, \mathbb{Z})$

$$\mathcal{S}_{\eta,\lambda_1,\lambda_2}(\ell, \ell_0) = \mathcal{S}_{\eta,\lambda_1,\lambda_2}(\ell_0, \ell). \tag{159}$$

ii. *There is a 1-1 correspondence* $\ell_{\mathbf{z}} \leftrightarrow \widetilde{\ell}_{\mathbf{z}}$ *between zigzag loops* $\ell_{\mathbf{z}}$ *on the bipartite graph* $\Gamma^\vee_\Lambda$ *and connected components* $\widetilde{\ell}_{\mathbf{z}}$ *of the boundary of the surface* $\mathfrak{S}^{\leqslant h}_{\mathcal{Z},\Lambda,\boxminus,r}$ *such that*

$$\mathcal{S}_{\eta,\lambda_1,\lambda_2}(\ell_{\mathbf{z}_1}, \ell_{\mathbf{z}_2}) = \mathsf{link}(\widetilde{\ell_{\mathbf{z}_1}}, \widetilde{\ell_{\mathbf{z}_2}}). \tag{160}$$

In particular, the Seifert form $\mathcal{S}_{\eta,\lambda_1,\lambda_2}$ *restricts to a* symmetric *bilinear form on the sublattice which is spanned by the loops* $\ell_{\mathbf{z}}$ *(* $\mathbf{z} \in \mathsf{P}^{\mathsf{z}}_\Lambda$ *).*

iii. *Let the twist function be such that either* $\eta(e) = 1$ *for all* $e \in \mathcal{E}_\Lambda$ *or* $\eta = (-1)^{\mathsf{m}}$ *for some perfect matching* m. *Let* $\ell_1, \ell_2 \in \mathrm{H}_1(\Gamma^\vee_\Lambda, \mathbb{Z})$ *be such that* ℓ_1 *or* ℓ_2 *lies in the sublattice spanned by the loops* $\ell_{\mathbf{v}}$ *(* $\mathbf{v} \in \mathsf{P}^\star_\Lambda$ *). Then:*

$$\mathcal{S}_{\eta,\lambda_1,\lambda_2}(\ell_1, \ell_2) = -\tfrac{1}{2}\ell_1 \cdot \mathsf{diag}(1-\mathsf{m}) \cdot \left(\rho_{1,\mathsf{m}} - \rho^t_{1,\mathsf{m}}\right) \cdot \mathsf{diag}(1-\mathsf{m}) \cdot \ell^t_2 \tag{161}$$

$$- \tfrac{1}{2}\ell_1 \cdot \mathsf{diag}(\eta) \cdot \ell^t_2.$$

Here ℓ_1, ℓ_2 *on the right are functions* $\mathcal{E}_\Lambda \to \mathbb{Z}$ *viewed as row vectors.*

Proof: **i+ii**. A zigzag $\mathbf{z}$ written as in (126) gives a loop $\ell_{\mathbf{z}}$ as in (122) on the bipartite graph $\Gamma^\vee_\Lambda$ which on the surface $\mathfrak{S}^{\leqslant h}_{\mathcal{Z},\Lambda,\boxminus,r}$ is homologous to a connected component $\widetilde{\ell}_{\mathbf{z}}$ of the boundary $\partial \mathfrak{S}^{\leqslant h}_{\mathcal{Z},\Lambda,\boxminus,r}$. This $\widetilde{\ell}_{\mathbf{z}}$ is disjoint from every loop ℓ supported on $\Gamma^\vee_\Lambda$. Therefore when computing values of the Seifert form there is no need to push loops off the surface (cf. (140)):

$$\mathcal{S}_{\eta,\lambda_1,\lambda_2}(\ell, \ell_{\mathbf{z}}) = \mathsf{link}(\ell, \widetilde{\ell}_{\mathbf{z}}) = \mathsf{link}(\widetilde{\ell}_{\mathbf{z}}, \ell) = \mathcal{S}_{\eta,\lambda_1,\lambda_2}(\ell_{\mathbf{z}}, \ell). \tag{162}$$

iii. The Seifert form (140) is independent of the choice of the reference perfect matching m_0 used in the calculations which led to (152). So, if the twist function is $\eta = (-1)^{\mathsf{m}}$ we can take $\mathsf{m}_0 = \mathsf{m}$. If $\eta(e) = 1$ for all e we can take any reference perfect matching and for uniformity in the formulas denote it as m.

For ℓ_1, ℓ_2 as in **iii** Formula (152) reduces to

$$\mathcal{S}_{\eta,\lambda_1,\lambda_2}(\ell_1, \ell_2) = \ell_1 \cdot \Omega_{\eta,\mathsf{m}} \cdot \ell^t_2. \tag{163}$$

61

From Formulas (145), (146), (147) we see that

$$\Omega_{\eta,\mathsf{m}} = -\tfrac{1}{2}\mathsf{diag}(1-\mathsf{m}) \cdot \left(\rho_{1,\mathsf{m}} - \rho_{1,\mathsf{m}}^t\right) \cdot \mathsf{diag}(1-\mathsf{m})$$
$$-\tfrac{1}{2}\mathsf{diag}(1-\mathsf{m}) \cdot \left(\mathsf{diag}(\eta) + |R_{\eta,\mathsf{m}}| \cdot \mathsf{diag}\left(\eta\mathsf{m}\cdot|R_{\eta,\mathsf{m}}|\right)\right) \cdot \mathsf{diag}(1-\mathsf{m}) \tag{164}$$

Recall that the entry of the matrix $|R_{\eta,\mathsf{m}}|$ in row e_1 and column e_2 is 1 if e_1 and e_2 lie in the same cycle of σ_1 and is 0 otherwise. In particular $|R_{\eta,\mathsf{m}}|$ is a symmetric matrix with diagonal equal to $\mathbb{I}$. The diagonal matrix $\mathsf{diag}(\eta) \cdot \mathsf{diag}(1-\mathsf{m})$ is equal to $\mathsf{diag}(1-\mathsf{m})$.

If $\eta = (-1)^{\mathsf{m}}$, the diagonal matrix $\mathsf{diag}\left(\eta\mathsf{m}\cdot|R_{\eta,\mathsf{m}}|\right)$ is equal to $-\mathbb{I}$ and the second term on the right in (164) is equal to

$$-\tfrac{1}{2}\,\mathsf{diag}(1-\mathsf{m}) \cdot \left(\mathbb{I} - |R_{\eta,\mathsf{m}}|\right) \cdot \mathsf{diag}(1-\mathsf{m}) \tag{165}$$

If $\eta(e) = 1$ for all e, the diagonal matrix $\mathsf{diag}\left(\eta\mathsf{m}\cdot|R_{\eta,\mathsf{m}}|\right)$ is equal to $\mathbb{I}$ and the second term on the right in (164) is equal to

$$-\tfrac{1}{2}\,\mathsf{diag}(1-\mathsf{m}) \cdot \left(\mathbb{I} + |R_{\eta,\mathsf{m}}|\right) \cdot \mathsf{diag}(1-\mathsf{m}) \tag{166}$$

Note that all entries of the matrix $\mathsf{diag}(1-\mathsf{m})\cdot|R_{\eta,\mathsf{m}}|\cdot\mathsf{diag}(1-\mathsf{m})$ are 0 or 1 and that the entry in row e_1 and column e_2 is 1 if and only if $\mathsf{m}(e_1) = \mathsf{m}(e_2) = 0$ and $b(e_1) = b(e_2)$. From this one sees that

$$\ell_1 \cdot \mathsf{diag}(1-\mathsf{m}) \cdot |R_{\eta,\mathsf{m}}| \cdot \mathsf{diag}(1-\mathsf{m}) \cdot \ell_2^t = \sum_{e_1,e_2\in\mathcal{P}_{\mathsf{m}}} \ell_1(e_1)\ell_2(e_2) \tag{167}$$

$$\text{with}\quad \mathcal{P}_{\mathsf{m}} = \left\{e_1, e_2 \in \mathcal{E}_\Lambda \mid \mathsf{m}(e_1) = \mathsf{m}(e_2) = 0,\; b(e_1) = b(e_2)\right\}$$

Next note that ℓ_1 and ℓ_2 represent elements of $H_1(\Gamma_\Lambda^\vee, \mathbb{Z})$ and therefore satisfy

$$\sum_{b(e)=\mathbf{b}} \ell_1(e) = \sum_{b(e)=\mathbf{b}} \ell_2(e) = 0$$

for every black polygon $\mathbf{b}$. The contribution of the terms with $b(e_1) = b(e_2) = \mathbf{b}$ to the right hand side of (167) is therefore

$$\left(\sum_{b(e_1)=\mathbf{b},\,\mathsf{m}(e_1)=0} \ell_1(e_1)\right)\left(\sum_{b(e_2)=\mathbf{b},\,\mathsf{m}(e_2)=0} \ell_2(e_2)\right) = \sum_{b(e)=\mathbf{b},\,\mathsf{m}(e)=1} \ell_1(e)\ell_2(e).$$

Thus (167) becomes

$$\ell_1\cdot\mathsf{diag}(1-\mathsf{m})\cdot|R_{\eta,\mathsf{m}}|\cdot\mathsf{diag}(1-\mathsf{m})\cdot\ell_2^t = \sum_{\mathsf{m}(e)=1} \ell_1(e)\ell_2(e) = \ell_1\cdot\mathsf{diag}(\mathsf{m})\cdot\ell_2^t. \tag{168}$$

On the other hand,

$$\ell_1 \cdot \mathsf{diag}(1-\mathsf{m}) \cdot \mathbb{I} \cdot \mathsf{diag}(1-\mathsf{m}) \cdot \ell_2^t = \ell_1 \cdot \mathsf{diag}(1-\mathsf{m}) \cdot \ell_2^t. \tag{169}$$

By combining Formulas (164), (165), (166), (168) and (169) we see that

$$\Omega_{\eta,\mathsf{m}} \;=\; -\tfrac{1}{2}\left(\mathsf{diag}(1-\mathsf{m})\cdot\left(\rho_{1,\mathsf{m}}-\rho_{1,\mathsf{m}}^{t}\right)\cdot\mathsf{diag}(1-\mathsf{m}) \,+\, \mathsf{diag}(\eta)\right) \qquad (170)$$

The result **iii** now follows from (163) and (170). ∎

Definition 5

i. The **intersection form** on $H_1(\Gamma_\Lambda^\vee,\mathbb{Z}) = H_1(\mathfrak{S}_{\mathcal{Z},\Lambda,\boxminus,r}^{\leq h},\mathbb{Z})$ associated with the Seifert form $\mathcal{S}_{\eta,\lambda_1,\lambda_2}$ is the bilinear form $\langle\ ,\ \rangle_{\eta,\lambda_1,\lambda_2}$ given by

$$\langle \ell_1,\ell_2\rangle_{\eta,\lambda_1,\lambda_2} \;=\; \mathcal{S}_{\eta,\lambda_1,\lambda_2}(\ell_1,\ell_2) - \mathcal{S}_{\eta,\lambda_1,\lambda_2}(\ell_2,\ell_1). \qquad (171)$$

Its matrix w.r.t. the basis $\mathbb{B}$ is $\mathsf{S}_{\eta,\mathsf{l}_1,\mathsf{l}_2} - \mathsf{S}_{\eta,\mathsf{l}_1,\mathsf{l}_2}^{t}$; see (152).

ii. If the Seifert form $\mathcal{S}_{\eta,\lambda_1,\lambda_2}$ is non-degenerate (i.e. $\det(\mathsf{S}_{\eta,\mathsf{l}_1,\mathsf{l}_2})\neq 0$) then there is a unique linear automorphism $\mathbb{M}_{\eta,\lambda_1,\lambda_2}$ of $H_1(\Gamma_\Lambda^\vee,\mathbb{Q})$ such that for all $\ell_1,\ell_2 \in H_1(\Gamma_\Lambda^\vee,\mathbb{Z})$

$$\mathcal{S}_{\eta,\lambda_1,\lambda_2}\big(\mathbb{M}_{\eta,\lambda_1,\lambda_2}\ell_1,\ell_2\big) \;=\; \mathcal{S}_{\eta,\lambda_1,\lambda_2}\big(\ell_2,\ell_1\big). \qquad (172)$$

The matrix of $\mathbb{M}_{\eta,\lambda_1,\lambda_2}$ w.r.t. the basis $\mathbb{B}$ is $\mathsf{M}_{\eta,\mathsf{l}_1,\mathsf{l}_2} = (\mathsf{S}_{\eta,\mathsf{l}_1,\mathsf{l}_2}^{t})^{-1}\mathsf{S}_{\eta,\mathsf{l}_1,\mathsf{l}_2}$. If all entries of this matrix are integers one calls $\mathbb{M}_{\eta,\lambda_1,\lambda_2}$ the **monodromy transformation** associated with the Seifert form $\mathcal{S}_{\eta,\lambda_1,\lambda_2}$.

Theorem 6

i. For all choices of the twist function η and the basis $\lambda_1,\ \lambda_2$ for Λ_ω the intersection form $\langle\ ,\ \rangle_{\eta,\lambda_1,\lambda_2}$ is equal to the intersection form $\varepsilon_{\widehat{S}_w}$ on $H_1(\Gamma_\Lambda^\vee,\mathbb{Z})$ used in [11].

Notation: We henceforth denote the intersection form on $H_1(\Gamma_\Lambda^\vee,\mathbb{Z})$ as $\langle .,.\rangle$.

ii. When defined for η,λ_1,λ_2 the monodromy transformation $\mathbb{M}_{\eta,\lambda_1,\lambda_2}$ preserves the Seifert form $\mathcal{S}_{\eta,\lambda_1,\lambda_2}$ and the intersection form $\langle\ ,\ \rangle$. Moreover for every zigzag $\mathbf{z}$ the homology class of the zigzag loop $\ell_{\mathbf{z}}$ in $H_1(\Gamma_\Lambda^\vee,\mathbb{Z})$ is an eigenvector of $\mathbb{M}_{\eta,\lambda_1,\lambda_2}$ with eigenvalue 1.

Proof: **i.**: Formulas (152) and (148) imply

$$\mathsf{S}_{\eta,\mathsf{l}_1,\mathsf{l}_2}-\mathsf{S}_{\eta,\mathsf{l}_1,\mathsf{l}_2}^{t} \;=\; \mathbb{B}\cdot\mathsf{diag}(1-\mathsf{m}_0)\cdot\big(\rho_{1,\mathsf{m}_0}^{t}-\rho_{1,\mathsf{m}_0}\big)\cdot\mathsf{diag}(1-\mathsf{m}_0)\cdot\mathbb{B}^{t} + E_{\mathsf{l}_2,\mathsf{l}_1}-E_{\mathsf{l}_2,\mathsf{l}_1}^{t}. \qquad (173)$$

Next note the following analogue of Formulas (140)-(141)

$$\mathcal{S}_{\eta,\lambda_1,\lambda_2}(\ell_1,\ell_2) \;=\; \mathsf{link}(\ell_1,\ell_2^{-}) \;=\; \mathsf{link}(\ell_1,\ell_2^{-}-\ell_2^{\dagger}) + \mathsf{link}(\ell_1,\ell_2^{\dagger}) \qquad (174)$$

where the loop ℓ_2^- is obtained by pushing ℓ_2 a little off the surface $\mathfrak{S}_{\mathcal{Z},\Lambda,\boxminus}^{\leq h}$ in the negative normal direction and $\ell_2^\dagger$ is the loop in $\mathbb{S}^3$ obtained by pushing ℓ_2 a little off the torus $\mathbb{T}_{\lambda_1,\lambda_2}$ in the outward normal direction. In order to compute $\mathsf{link}(\ell_1,\ell_2^- - \ell_2^\dagger)$ we look for an analogue of Formula (149) based on an analysis of local contributions. The local contributions now come from the white nodes of $\Gamma_\Lambda^\vee$. The local situations require the following modifications in Figure 28: $b(e) \leftrightarrow w(e)$, $s(e) \leftrightarrow t(e)$, $[\eta(e) = +1] \leftrightarrow [\eta(e) = -1]$. The only configurations with non-trivial local contributions are shown in Figure 31.
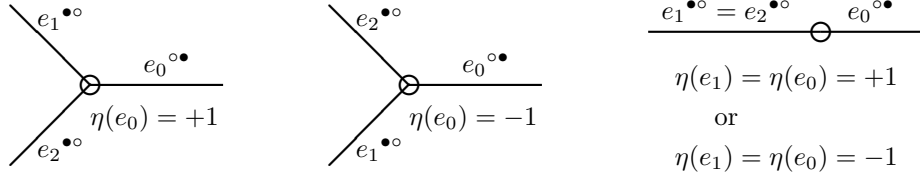

Figure 31: The only configurations which make local contributions; the local contribution is $\eta(e_0)$.

For bookkeeping of the local contributions we can use the same matrix formalism as in Formulas (144), (145) and (146) but now based on the permutation σ_0 instead of σ_1, i.e.

$$\rho_{0,\mathsf{m}_0} = \bigl(\mathbb{I} - \varsigma_{0,\mathsf{m}_0}\bigr)^{-1}. \tag{175}$$

where the matrix $\varsigma_{0,\mathsf{m}_0}$ is obtained by multiplying the e-th row of the permutation matrix σ_0 by $1 - \mathsf{m}_0(e)$. Write the cycle decomposition of the permutation σ_0 such that the elements e with $\mathsf{m}_0(e) = 1$ are in the first position in their cycle. Then the entry of the matrix $\rho_{0,\mathsf{m}_0} - \rho_{0,\mathsf{m}_0}^t$ in row e_1 and column e_2 is -1 (resp. $+1$) if e_1 and e_2 lie in the same cycle of σ_0 with e_1 to the left (resp. right) of e_2. So, the (e_1, e_2)-entry is -1 for the left picture in Figure 31 and $+1$ for the middle one. The other entries of $\rho_{0,\mathsf{m}_0} - \rho_{0,\mathsf{m}_0}^t$ are 0. Proceeding as before we now find the following analogue of Formula (173)

$$\mathsf{S}_{\eta,\mathfrak{l}_1,\mathfrak{l}_2} - \mathsf{S}_{\eta,\mathfrak{l}_1,\mathfrak{l}_2}^t = \mathbb{B}\cdot\mathsf{diag}(1-\mathsf{m}_0)\cdot\bigl(\rho_{0,\mathsf{m}_0}^t - \rho_{0,\mathsf{m}_0}\bigr)\cdot\mathsf{diag}(1-\mathsf{m}_0)\cdot\mathbb{B}^t + E_{\mathfrak{l}_1,\mathfrak{l}_2} - E_{\mathfrak{l}_1,\mathfrak{l}_2}^t, \tag{176}$$

where $E_{\mathfrak{l}_1,\mathfrak{l}_2}$ is the matrix with entry 1 in row $\mathfrak{l}_1$, column $\mathfrak{l}_2$ and all other entries 0; i.e. $E_{\mathfrak{l}_1,\mathfrak{l}_2} = E_{\mathfrak{l}_2,\mathfrak{l}_1}^t$. Taking the sum of (173) and (176) yields

$$\mathsf{S}_{\eta,\mathfrak{l}_1,\mathfrak{l}_2} - \mathsf{S}_{\eta,\mathfrak{l}_1,\mathfrak{l}_2}^t = \tfrac{1}{2}\mathbb{B}\cdot\mathsf{diag}(1-\mathsf{m}_0)\cdot\bigl(\rho_{1,\mathsf{m}_0}^t - \rho_{1,\mathsf{m}_0} + \rho_{0,\mathsf{m}_0}^t - \rho_{0,\mathsf{m}_0}\bigr)\cdot\mathsf{diag}(1-\mathsf{m}_0)\cdot\mathbb{B}^t. \tag{177}$$

This formula shows how the intersection form is built up from local contributions. The local contributions correspond to the left and middle pictures in Figures 29 and 31. The local contribution is $-\tfrac{1}{2}$ for Fig.29left and Fig.31middle; it is $+\tfrac{1}{2}$ for Fig.29middle and Fig.31left. By comparing these local contributions with [[11] Figure 38, Lemma 8.1, Definition 8.2] we see that the intersection form $\mathsf{S}_{\eta,\mathfrak{l}_1,\mathfrak{l}_2} - \mathsf{S}_{\eta,\mathfrak{l}_1,\mathfrak{l}_2}^t$ is indeed the same as the form ε in [11] Definition 8.2.

ii follows from (162) and (172). ∎

Corollary 3 *The restriction of the intersection form $\langle \,,\, \rangle$ to the lattice generated by the homology classes of the loops $\ell_{\mathbf{v}}$ ($\mathbf{v} \in \mathsf{P}_\Lambda^\star$) satisfies:*

$$\langle \ell_{\mathbf{v}}, \ell_{\mathbf{v}'} \rangle \;=\; \sharp\{e \in \mathcal{E}_\Lambda \mid s(e) = \mathbf{v}, \, t(e) = \mathbf{v}'\} \;-\; \sharp\{e \in \mathcal{E}_\Lambda \mid t(e) = \mathbf{v}, \, s(e) = \mathbf{v}'\} \tag{178}$$

for all $\mathbf{v}$, $\mathbf{v}' \in \mathsf{P}_\Lambda^\star$. So, it only depends on the abstract quiver Γ_Λ.

Proof: It follows from Formula (161) that

$$\langle \ell_{\mathbf{v}}, \ell_{\mathbf{v}'} \rangle \;=\; -\ell_{\mathbf{v}} \cdot \mathsf{diag}(1 - \mathsf{m}) \cdot \big(\rho_{1,\mathsf{m}} - \rho_{1,\mathsf{m}}^t\big) \cdot \mathsf{diag}(1 - \mathsf{m}) \cdot \ell_{\mathbf{v}'}^t \,. \tag{179}$$

Recall from the elucidation to Formula (145), that when we write the cycle decomposition of the permutation σ_1 such that the elements e with $\mathsf{m}(e) = 1$ are in the first position in their cycle, the entry of $\rho_{1,\mathsf{m}} - \rho_{1,\mathsf{m}}^t$ in row e_1 and column e_2 is -1 (resp. $+1$) if e_1 and e_2 lie in the same cycle of σ_1 with e_1 to the left (resp. right) of e_2 and is 0 otherwise. It follows that the right-hand side of (179) is a sum with one term for every black polygon $\mathbf{b}$ of which both $\mathbf{v}$ and $\mathbf{v}'$ are vertices.

Let us first consider the situation in which $\mathbf{v} = s(e)$, $\mathbf{v}' = t(e)$ and $\mathbf{b} = b(e)$ for some edge $e \in \mathcal{E}_\Lambda$. Then there are unique sides e_1 and e_4 of $\mathbf{b}$ such that $\mathbf{v} = t(e_1)$ and $\mathbf{v}' = s(e_4)$. It follows from (57) that $\ell_{\mathbf{v}}(e_1) = -1$, $\ell_{\mathbf{v}}(e) = +1$, $\ell_{\mathbf{v}'}(e) = -1$, $\ell_{\mathbf{v}'}(e_4) = +1$. There is also a unique side e_0 of $\mathbf{b}$ such that $\mathsf{m}(e_0) = 1$. The three edges e_1, e, e_4 are distinct. For e_0 one must distinguish four cases depending on whether it does or does not coincide with one of e_1, e, e_4. It follows from the above description of $\rho_{1,\mathsf{m}} - \rho_{1,\mathsf{m}}^t$ that in each case the contribution from $\mathbf{b}$ to (179) is $+1$ (where the extra $-$-sign on the right in (179) has been taken into account).

In the same way one checks that in case $\mathbf{v} = t(e)$, $\mathbf{v}' = s(e)$ and $\mathbf{b} = b(e)$ for some edge $e \in \mathcal{E}_\Lambda$ the contribution to (179) is -1.

If $\mathbf{v}$ and $\mathbf{v}'$ are vertices of the black polygon $\mathbf{b}$, but not the two endpoints of a side of $\mathbf{b}$, then there are four distinct sides e_1, e_2, e_3, e_4 of $\mathbf{b}$ such that $t(e_1) = s(e_2) = \mathbf{v}$ and $t(e_3) = s(e_4) = \mathbf{v}'$. Then $\ell_{\mathbf{v}}(e_1) = -1$, $\ell_{\mathbf{v}}(e_2) = +1$, $\ell_{\mathbf{v}'}(e_3) = -1$, $\ell_{\mathbf{v}'}(e_4) = +1$. It follows from the above description of $\rho_{1,\mathsf{m}} - \rho_{1,\mathsf{m}}^t$ that in this case the contribution to (179) is 0. ∎

The following corollary summarizes some results of this section in terms of the surfaces $\mathbb{X}_{\sigma_0,\sigma_1}$ and $\overline{\mathbb{X}}_{\sigma_0,\sigma_1,\varrho}$; see (10) and (12).

Corollary 4 *The inclusion $\overline{\mathbb{X}}_{\sigma_0,\sigma_1,\varrho} \subset \mathbb{X}_{\sigma_0,\sigma_1}$ induces a surjective homomorphism*

$$\mathrm{H}_1(\overline{\mathbb{X}}_{\sigma_0,\sigma_1,\varrho}, \mathbb{Z}) \longrightarrow \mathrm{H}_1(\mathbb{X}_{\sigma_0,\sigma_1}, \mathbb{Z}) \tag{180}$$

of which the kernel is generated by the homology classes of the connected components of the boundary of $\overline{\mathbb{X}}_{\sigma_0,\sigma_1,\varrho}$. The homology classes of the boundary components are precisely the homology classes of the zigzag loops $\ell_{\mathbf{z}}$ on $\Gamma_\Lambda^\vee$.

Thus, Theorems 5 and 6 imply that the intersection form $\langle .,. \rangle$ induces an intersection form $\langle .,. \rangle$ on $\mathsf{H}_1(\mathbb{X}_{\sigma_0,\sigma_1}, \mathbb{Z})$. When defined, the monodromy transformation $\mathbb{M}_{\eta,\mathfrak{l}_1,\mathfrak{l}_2}$ is the identity on the kernel of the homomorphism (180) *and induces, therefore, an automorphism*

$$\mathbb{M}_{\eta,\mathfrak{l}_1,\mathfrak{l}_2} : \mathsf{H}_1(\mathbb{X}_{\sigma_0,\sigma_1}, \mathbb{Z}) \longrightarrow \mathsf{H}_1(\mathbb{X}_{\sigma_0,\sigma_1}, \mathbb{Z}) \tag{181}$$

which preserves the intersection form $\langle .,. \rangle$. ∎

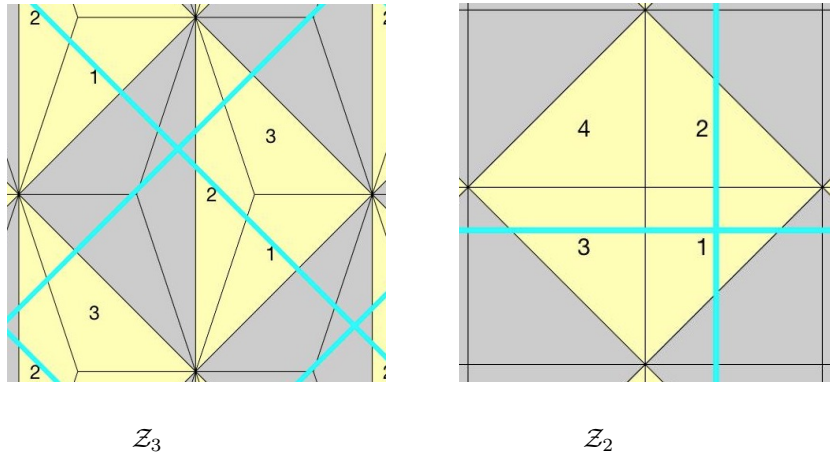$$\mathcal{Z}_3 \qquad\qquad\qquad\qquad \mathcal{Z}_2$$

Figure 32: Display of the information needed in Example 5.4.1.

5.4.1 Example: $\mathcal{Z}_3$ and $\mathcal{Z}_2$

There are $2^{|\mathcal{E}_\Lambda|}$ twist functions. So, only in very simple cases one can list all twist functions and inspect them for the existence of the monodromy matrix. The simplest cases are $\mathcal{Z} = \mathcal{Z}_3$ or $\mathcal{Z}_2$ with $\Lambda = \mathsf{Aut}(\mathcal{Z})$.

For $\mathcal{Z}_3$ there are three edges labeled $1, 2, 3$. We take $\mathfrak{l}_1 = 2^{\bullet\circ}3^{\circ\bullet}$, $\mathfrak{l}_2 = 2^{\bullet\circ}1^{\circ\bullet}$ (see Figure 32). The twist functions η with invertible Seifert matrix $\mathsf{S}_{\eta,\mathfrak{l}_1,\mathfrak{l}_2}$ are given by the following lists of values on the three edges $(1, 1, 1)$, $(1, -1, 1)$, $(1, -1, -1)$, $(-1, -1, 1)$. But, if we take $\mathfrak{l}_1 = 1^{\bullet\circ}2^{\circ\bullet}$, $\mathfrak{l}_2 = 2^{\bullet\circ}3^{\circ\bullet}$ (see Figure 32) then the Seifert matrix $\mathsf{S}_{\eta,\mathfrak{l}_1,\mathfrak{l}_2}$ is invertible for $\eta = (-1, -1, -1)$, $(-1, 1, -1)$, $(-1, 1, 1)$ or $(1, 1, -1)$. See also Formula (153).

For $\mathcal{Z}_2$ there are four edges labeled $1, 2, 3, 4$. We take $\mathfrak{l}_1 = 3^{\bullet\circ}4^{\circ\bullet}$, $\mathfrak{l}_2 = 3^{\bullet\circ}1^{\circ\bullet}$ (see Figure 32). The twist functions η with invertible Seifert matrix $\mathsf{S}_{\eta,\mathfrak{l}_1,\mathfrak{l}_2}$ are given by the following lists of values on the four edges $(-1, -1, -1, 1)$, $(1, -1, -1, -1)$, $(1, -1, 1, 1)$, $(1, 1, -1, 1)$. On the other hand, for $\mathfrak{l}_1 = 1^{\bullet\circ}3^{\circ\bullet}$, $\mathfrak{l}_2 = 3^{\bullet\circ}4^{\circ\bullet}$ the twist functions η with invertible Seifert matrix $\mathsf{S}_{\eta,\mathfrak{l}_1,\mathfrak{l}_2}$ are $\eta = (1, 1, 1, -1)$, $(-1, 1, 1, 1)$, $(-1, 1, -1, -1)$, $(-1, -1, 1, -1)$; cf. Formula (153).

For both $\mathcal{Z}_2$ and $\mathcal{Z}_3$ we have $|\mathsf{P}_\Lambda^z| - 1 = |\mathsf{P}_\Lambda^\star| + 1$. So, according to Corollary 4 when the monodromy transformation is defined it is the identity transformation.

5.4.2 Example: $\mathcal{Z} = \mathsf{Z}^{21} + \mathsf{Z}^{31} + \mathsf{Z}^{41} + \mathsf{Z}^{62}$.

We look at Seifert forms for the example in Figures 19 and 25 and §4.3.3, §5.2.1.

The intersection form can be computed using the twist function with $\eta(e) = 1$ for all e. The matrix of the intersection form w.r.t. the basis $\mathbb{B}$ (132) is

$$
\text{intersection form on } H_1(\Gamma_\Lambda^\vee, \mathbb{Z}) : \quad
\begin{pmatrix}
0 & -1 & 1 & 0 & -1 & 0 & 0 \\
1 & 0 & -2 & 1 & 0 & 0 & 0 \\
-1 & 2 & 0 & -1 & 2 & 0 & 0 \\
0 & -1 & 1 & 0 & -1 & 0 & 0 \\
1 & 0 & -2 & 1 & 0 & 0 & 0 \\
0 & 0 & 0 & 0 & 0 & 0 & 0 \\
0 & 0 & 0 & 0 & 0 & 0 & 0
\end{pmatrix} . \tag{182}
$$

With the labels for the vertices as in the table in Figure 25 the intersection numbers $\langle \ell_\mathbf{v}, \ell_{\mathbf{v}'} \rangle$ for $\mathbf{v}, \mathbf{v}' \neq 1$ are given in the upper-left 5×5-block of the matrix (182). The remaining intersection numbers $\langle \ell_\mathbf{v}, \ell_{\mathbf{v}'} \rangle$ can be derived from this and the relation $\sum_{\mathbf{v} \in \mathsf{P}_\Lambda^\star} \ell_\mathbf{v} = 0$. This agrees with Formula (178) and the table in Figure 25.

There are six zigzags; see §5.2.1.. The coordinates of the homology classes of the zigzag loops $\ell_\mathbf{z}$ w.r.t. to the basis $\mathbb{B}$ are given in the columns of the matrix

$$
\begin{pmatrix}
0 & -1 & 0 & 2 & 1 & -2 \\
0 & 0 & 0 & 0 & 1 & -1 \\
0 & -1 & 0 & 1 & 1 & -1 \\
0 & -1 & 0 & 0 & 1 & 0 \\
0 & -1 & 0 & 1 & 0 & 0 \\
1 & -1 & 0 & 1 & 0 & -1 \\
0 & 0 & 1 & -1 & -1 & 1
\end{pmatrix} . \tag{183}
$$

The columns of this matrix are indeed in the kernel of the intersection matrix.

Since there are 2^{14} twist functions η it would be a time consuming task to compute the Seifert matrix $\mathsf{S}_{\eta, \mathsf{l}_1, \mathsf{l}_2}$ and its determinant for all η, even for a fixed choice of $\mathsf{l}_1, \mathsf{l}_2$. We therefore restrict to the 28 twist functions $\eta = \tau(-1)^\mathsf{m}$ with m a perfect matching and $\tau = \pm 1$. The following table shows all cases with $\mathsf{l}_1 = 3^{\bullet\circ} 4^{\circ\bullet} 6^{\bullet\circ} 8^{\circ\bullet}$ and $\mathsf{l}_2 = 11^{\bullet\circ} 12^{\circ\bullet} 2^{\bullet\circ} 3^{\circ\bullet}$ in which the Seifert matrix $\mathsf{S}_{\eta, \mathsf{l}_1, \mathsf{l}_2}$ is invertible

m				τ	$\det(\mathsf{S}_{\eta, \mathsf{l}_1, \mathsf{l}_2})$
4	8	9	12	1	1
3	6	9	12	-1	-1
2	6	9	11	1	1
1	4	10	13	1	1
1	5	10	14	-1	-1
1	7	11	14	1	1

(184)

The result of checking for Seifert matrices with non-zero determinant in case $\mathfrak{l}_1 = 3^{\bullet\circ}4^{\circ\bullet}6^{\bullet\circ}8^{\circ\bullet}$ and $\mathfrak{l}_2 = 7^{\bullet\circ}10^{\circ\bullet}11^{\bullet\circ}12^{\circ\bullet}2^{\bullet\circ}4^{\circ\bullet}$ is given in the following table.

m				τ	$\det\left(\mathsf{S}_{\eta,\mathfrak{l}_1,\mathfrak{l}_2}\right)$
4	8	9	12	1	1
3	6	9	12	-1	-1
2	6	9	11	1	2
2	6	9	11	-1	1
1	4	10	13	1	2
1	4	10	13	-1	1
1	5	10	14	-1	-1
1	7	11	14	1	1

(185)

A subsequent check reveals that in all cases in (184) and (185) the monodromy matrix $\mathbb{M} = \mathbb{M}_{\eta,\mathfrak{l}_1,\mathfrak{l}_2}$ has entries in $\mathbb{Z}$ (not obvious if the determinant of the Seifert matrix is 2) and that the ranks of the matrices $\mathbb{M} - \mathbb{I}$, $(\mathbb{M} - \mathbb{I})(\mathbb{M} + \mathbb{I})$ and $(\mathbb{M} - \mathbb{I})(\mathbb{M} + \mathbb{I})^2$ are 2, 1 and 0, respectively. This means that in all cases the eigenspace for the eigenvalue $+1$ has rank 5 and that there is a Jordan block of size 2 for the eigenvalue -1. The eigenspace for the eigenvalue $+1$ is spanned by the homology classes of the zigzag loops $\ell_{\mathbf{z}}$ and is independent of $\eta, \mathfrak{l}_1, \mathfrak{l}_2$.

For instance, the monodromy matrix for the top line in (184) is

$$\mathbb{M} = \begin{pmatrix} 1 & 0 & 0 & 0 & 0 & 0 & 0 \\ 1 & -1 & 0 & 1 & -2 & 0 & 0 \\ 1 & -1 & 0 & 1 & -1 & 0 & 0 \\ 0 & -1 & 1 & 1 & -1 & 0 & 0 \\ 0 & -1 & 1 & 0 & 0 & 0 & 0 \\ 0 & 0 & 0 & 0 & 0 & 1 & 0 \\ 0 & 0 & 0 & 0 & 0 & 0 & 1 \end{pmatrix}$$

(186)

It satisfies

$$\mathbb{T}^{-1}\mathbb{M}\mathbb{T} = \begin{pmatrix} 1 & 0 & 0 & 0 & 0 & 1 & 0 \\ 0 & 1 & 0 & 0 & 0 & 2 & -1 \\ 0 & 0 & 1 & 0 & 0 & 1 & -1 \\ 0 & 0 & 0 & 1 & 0 & 1 & -1 \\ 0 & 0 & 0 & 0 & 1 & 0 & -1 \\ 0 & 0 & 0 & 0 & 0 & -1 & 1 \\ 0 & 0 & 0 & 0 & 0 & 0 & -1 \end{pmatrix}$$

(187)

where $\mathbb{T}$ is the matrix

$$\mathbb{T} = \begin{pmatrix} -1 & 0 & 2 & 1 & -2 & 1 & 0 \\ 0 & 0 & 0 & 1 & -1 & 0 & 1 \\ -1 & 0 & 1 & 1 & -1 & 0 & 0 \\ -1 & 0 & 0 & 1 & 0 & 0 & 0 \\ -1 & 0 & 1 & 0 & 0 & 0 & 0 \\ -1 & 0 & 1 & 0 & -1 & 0 & 0 \\ 0 & 1 & -1 & -1 & 1 & 0 & 0 \end{pmatrix}$$

(188)

The first five columns of $\mathbb{T}$ are the last five columns of the matrix (183). The last two columns of $\mathbb{T}$ correspond to the loops $\alpha = 1^{\bullet\circ}8^{\circ\bullet}3^{\bullet\circ}2^{\circ\bullet}$ and $\beta = 6^{\bullet\circ}8^{\circ\bullet}10^{\bullet\circ}7^{\circ\bullet}$ on $\Gamma_\Lambda^\vee$. The homology classes of α and β in $\mathrm{H}_1(\Gamma_\Lambda^\vee, \mathbb{Z})$ are the first and second line of the matrix $\mathbb{B}$ in (132). The loops α and β can be seen in Figure 19 and Figure 20. In Figure 20 they are the sides of the period parallelogram.

Remark 12 One can check that the twist functions in (184) and (185) are precisely the twist functions of the form $\eta = \pm(-1)^{\mathsf{m}}$ with the property

$$\forall \mathbf{v} \in \mathsf{P}_\Lambda^\star : \qquad \prod_{e \in \mathcal{E}_\Lambda, s(e) = \mathbf{v}} \eta(e) \times \prod_{e \in \mathcal{E}_\Lambda, t(e) = \mathbf{v}} \eta(e) \; = \; (-1)^{1 + \sharp\{e \in \mathcal{E}_\Lambda \mid s(e) = \mathbf{v}\}}. \qquad (189)$$

Twist functions η which satisfy (189) are called **Kasteleyn orientations** or **Kasteleyn line bundles with connection**; see [11] §1.4.1. $\qquad\blacksquare$

5.4.3   Example 5.4.2 continued

We computed for the cases in Table (184) the restriction of the Seifert form $\mathsf{S}_{\eta, \mathfrak{l}_1, \mathfrak{l}_2}$ to the lattice spanned by the homology classes of the zigzag loops $\ell_{\mathbf{z}}$ and found in all these cases that the restriction of $\tau \mathsf{S}_{\eta, \mathfrak{l}_1, \mathfrak{l}_2}$ is a symmetric form with signature $(+1, -4)$.

For example for the first line in table (184) we found that the Seifert form on the six zigzags is given by the matrix

$$\begin{pmatrix} 0 & 0 & 1 & -1 & -1 & 1 \\ 0 & -2 & 0 & 1 & 1 & 0 \\ 1 & 0 & -1 & 0 & 0 & 0 \\ -1 & 1 & 0 & -1 & 0 & 1 \\ -1 & 1 & 0 & 0 & -1 & 1 \\ 1 & 0 & 0 & 1 & 1 & -3 \end{pmatrix}. \qquad (190)$$

Figure 33 shows for the first line in table (184) (and some choice of parameters ν, r, h which for now is irrelevant) the surface $\mathfrak{S}_{\mathcal{Z}, \Lambda, \boxminus}^{\leqslant h}$ and its boundary link in $\mathbb{R}^3$. One can check that the off-diagonal part of (190) is precisely the matrix of linking numbers of the link components. The diagonal entries follow from the fact that the row sums must be 0 and are not the self-linking numbers of the link components! $\qquad\blacksquare$

5.5   The Poisson structure

In this section $\mathcal{Z}$ is a Zhegalkin Zebra Motive and Λ is a sublattice of $\mathsf{Aut}(\mathcal{Z})$ such that $(\mathcal{Z}, \Lambda)$ is dimer complete; cf. Definition 1.
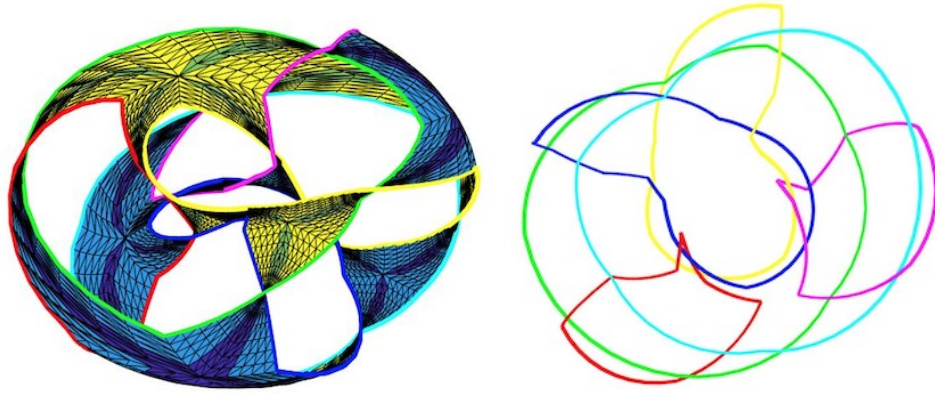
Figure 33: Surface $\mathfrak{S}_{\mathcal{Z},\Lambda,\boxminus,r}^{\leqslant h}$ and its boundary link for the first line in table (184). Colors and zigzag labels: 1:magenta, 2:red, 3:cyan, 4:blue, 5:green, 6:yellow.

Take a basis $\mathbb{B}$ for $\mathrm{H}_1(\Gamma_\Lambda^\vee, \mathbb{Z})$ consisting of the homology classes of all but one of the loops $\ell_{\mathbf{v}}$ ($\mathbf{v} \in \mathsf{P}_\Lambda^\star$) and two more elements $\mathfrak{l}_1, \mathfrak{l}_2 \in \mathrm{H}_1(\Gamma_\Lambda^\vee, \mathbb{Z})$. By means of the basis $\mathbb{B}$ one can identify the group algebra $\mathbb{Z}[\mathrm{H}_1(\Gamma_\Lambda^\vee, \mathbb{Z})]$ with the ring of Laurent polynomials $\mathbb{Z}[X_1^{\pm 1}, \ldots, X_k^{\pm 1}]$ in $k = |\mathsf{P}_\Lambda^\star| + 1$ variables. It carries a Poisson structure given by [11] Formula (5):

$$\{X_i, X_j\} = \varepsilon_{ij} X_i X_j, \tag{191}$$

where $\varepsilon = (\varepsilon_{ij})$ is the matrix of the intersection form $\langle .,. \rangle$ w.r.t. the basis $\mathbb{B}$; see also Theorem 6.

Proposition 7 *The elements of $\mathbb{Z}[\mathrm{H}_1(\Gamma_\Lambda^\vee, \mathbb{Z})]$ which correspond to (homology classes of) zigzag loops $\ell_{\mathbf{z}}$ ($\mathbf{z} \in \mathsf{P}_\Lambda^z$) lie in the center of this Poisson structure, i.e. they Poisson commute with all elements in $\mathbb{Z}[\mathrm{H}_1(\Gamma_\Lambda^\vee, \mathbb{Z})]$.*

Proof: This follows from (159). ∎

We now choose the reference perfect matching m_0 such that it lies over a corner of the Newton polygon (see §5.3). For a perfect matching m the element $X^{\mathsf{m}-\mathsf{m}_0}$ in the group algebra which corresponds to $\mathsf{m} - \mathsf{m}_0 \in \mathrm{H}_1(\Gamma_\Lambda^\vee, \mathbb{Z})$ is then a monomial in the variables $X_1, \ldots, X_k$ where the exponents are the coordinates of $\mathsf{m} - \mathsf{m}_0$ w.r.t. the basis $\mathbb{B}$; in particular, $X^{\mathsf{m}_0-\mathsf{m}_0} = 1$.

For every $\mathfrak{a} \in \mathcal{N}_{\mathcal{Z},\Lambda,\mathsf{m}_0,\mathfrak{l}_1,\mathfrak{l}_2}$ (see (136)) one then has an element $A_\mathfrak{a}$ in the group algebra:

$$A_\mathfrak{a} = \sum_{\mathsf{m} \in \mathcal{M}_{\mathcal{Z},\Lambda} : \, \mathfrak{n}_{\mathsf{m}_0,\mathfrak{l}_1,\mathfrak{l}_2}(\mathsf{m}) = \mathfrak{a}} X^{\mathsf{m}-\mathsf{m}_0}. \tag{192}$$

In [11] Goncharov and Kenyon prove that under the special condition of **"minimality"** these elements Poisson commute with each other, i.e.

$$\{A_\mathfrak{a}, A_{\mathfrak{a}'}\} = 0 \qquad \text{for all} \quad \mathfrak{a}, \mathfrak{a}' \in \mathcal{N}_{\mathcal{Z},\Lambda,\mathsf{m}_0,\mathfrak{l}_1,\mathfrak{l}_2}. \tag{193}$$

They also prove that for perfect matchings m, m' for which $\mathfrak{n}_{\mathsf{m}_0,\mathfrak{l}_1,\mathfrak{l}_2}(\mathsf{m})$ and $\mathfrak{n}_{\mathsf{m}_0,\mathfrak{l}_1,\mathfrak{l}_2}(\mathsf{m}')$ are neighboring points on the boundary of the Newton polygon the

difference $\mathsf{m} - \mathsf{m}'$ is a zigzag loop and, hence, $\{A_\mathfrak{a}, X_j\} = 0$ for all $\mathfrak{a}$ on the boundary of the Newton polygon and for $j = 1, \ldots, n$.

However, not all Zhegalkin Zebra Motives satisfy the minimality condition and when discussing examples we must check what remains true of these statements; see §5.5.1 and §E.

Let $\eta, \lambda_1, \lambda_2$ be such that the monodromy transformation $\mathbb{M}_{\eta,\lambda_1,\lambda_2}$ is defined (see Definition 5). Then, by Theorem 6, $\mathbb{M}_{\eta,\lambda_1,\lambda_2}$ preserves the intersection form $\langle\,,\,\rangle$ and, therefore, induces an automorphism of the Poisson structure on the torus $\mathrm{H}^1(\Gamma_\Lambda^\vee, \mathbb{C}^*)$.

5.5.1 Example: $\mathcal{Z} = \mathsf{Z}^{21} + \mathsf{Z}^{31} + \mathsf{Z}^{41} + \mathsf{Z}^{62}$.

We look at the Poisson structure for the example in Figures 19 and 25 and §4.3.3, §5.2.1. The basis $\mathbb{B}$ (132) of $\mathrm{H}_1(\Gamma_\Lambda^\vee, \mathbb{Z})$ provides an isomorphism of rings $\mathbb{Z}[\mathrm{H}_1(\Gamma_\Lambda^\vee, \mathbb{Z})] \simeq \mathbb{Z}[X_1^{\pm 1}, \ldots, X_7^{\pm 1}]$ and coordinates $X_1, \ldots, X_7$ on the torus $\mathrm{H}^1(\Gamma_\Lambda^\vee, \mathbb{C}^*)$. From the matrix (134) one sees that the polynomials $A_0, \ldots, A_6$ defined by (192) and the labels on the lattice points in the Newton diagram as in Figure 27 are:

$$A_1 = X_1^2 X_3 X_5 X_6 X_7^{-1}, \quad A_2 = X_1^3 X_2 X_3^2 X_4 X_5 X_6 X_7^{-2},$$

$$A_3 = X_1^2 X_2 X_3 X_7^{-2}, \quad A_4 = X_6^{-1} X_7^{-1}, \quad A_5 = X_6^{-1}, \quad A_6 = 1,$$

$$A_0 = \left(X_1 + X_1^2 X_2 X_3 X_4 X_5 + X_1 X_2 X_3 X_4 X_5 + X_1 X_3 X_5 + \right. $$
$$\left. + X_1^2 X_2 X_3 X_5 + X_1 X_2 X_3 X_5 + X_1 X_3 + X_1 X_2 X_3\right) X_7^{-1}$$

$$(194)$$

By multiplying the matrices (182) and (134) one checks that

$$\{A_i, X_j\} = 0 \quad \text{for } i = 1, \ldots, 6, \ j = 1, \ldots, 7. \tag{195}$$

It follows in particular, that the sequence of functions $\mathbf{A} := (A_0, \ldots, A_5)$ is **involutive**, i.e.

$$\{A_i, A_j\} = 0 \quad \text{for } i, j = 0, \ldots, 6. \tag{196}$$

The 7-dimensional manifold $\mathrm{H}^1(\Gamma_\Lambda^\vee, \mathbb{C}^*)$ equipped with Poisson bracket $\{.,.\}$ as in (191), (182) and the sequence of functions $\mathbf{A} := (A_0, \ldots, A_5)$ is a **completely integrable system** (see e.g. [1] Definition 4.13.). The **momentum map** is

$$\mathbf{A} : \ \mathrm{H}^1(\Gamma_\Lambda^\vee, \mathbb{C}^*) \ \longrightarrow \ \mathbb{C}^6. \tag{197}$$

The monomials $A_1, \ldots, A_5$ in (194) generate the ring of the **Casimirs**, i.e. the elements C in $\mathbb{Z}[X_1^{\pm 1}, \ldots, X_7^{\pm 1}]$ with $\{C, F\} = 0$ for every $F \in \mathbb{Z}[X_1^{\pm 1}, \ldots, X_7^{\pm 1}]$. The symplectic leaves for the Poisson structure on the torus $\mathrm{H}^1(\Gamma_\Lambda^\vee, \mathbb{C}^*)$ are therefore given by the system of equations with $c_1, \ldots, c_5 \in \mathbb{C}$

$$A_i = c_i \qquad \text{for} \quad i = 1, \ldots, 5. \tag{198}$$

We now illustrate the effect of the monodromy transformation for the first line in table (184), i.e. $\mathfrak{l}_1 = 3^{\bullet\circ}4^{\circ\bullet}6^{\bullet\circ}8^{\circ\bullet}$, $\mathfrak{l}_2 = 11^{\bullet\circ}12^{\circ\bullet}2^{\bullet\circ}3^{\circ\bullet}$, $\mathsf{m} = \{4,8,9,12\}$ and $\eta = (-1)^{\mathsf{m}}$. The matrix of the monodromy transformation $\mathbb{M}_{\eta,\lambda_1,\lambda_2}$ w.r.t. the basis $\mathbb{B}$ is given in (186). The monodromy transformation acts on the torus $\mathrm{H}^1(\Gamma_\Lambda^\vee, \mathbb{C}^*)$. It sends, for $j = 1,\ldots,7$, the coordinate function X_j to the monomial with exponents given by the j-th row of the matrix (186). Thus to see the effect of the monodromy transformation on the functions $A_0,\ldots,A_6$ one must simply multiply the matrices (186) and (134). The result is

$$
\begin{pmatrix}
0 & 1 & 2 & 1 & 0 & 0 & 2 & 1 & 2 & 1 & 3 & 1 & 1 & 2 \\
0 & 1 & 0 & -1 & 0 & 0 & 0 & -1 & -1 & -2 & 1 & 1 & 0 & 1 \\
0 & 1 & 1 & 0 & 0 & 0 & 1 & 0 & 0 & -1 & 2 & 1 & 0 & 1 \\
0 & 0 & 0 & 0 & 0 & 0 & 0 & 0 & -1 & -1 & 1 & 1 & 0 & 0 \\
0 & 0 & 0 & 0 & 0 & 0 & 1 & 1 & 0 & 0 & 1 & 1 & 0 & 0 \\
0 & 0 & 0 & 0 & -1 & -1 & 1 & 0 & 0 & 0 & 1 & 0 & 0 & 0 \\
0 & -1 & -1 & -1 & 0 & -1 & -1 & -1 & -1 & -2 & -1 & -1 & -2
\end{pmatrix}. \tag{199}
$$

The columns of (199) in which the last two entries are not $(0,-1)$ are equal to the corresponding columns of (134). This confirms that the functions $A_1,\ldots,A_6$ are invariant under the monodromy transformation. Comparing (199) and (134) one sees that A_0 is not invariant under the monodromy transformation. ∎

6 Textile structures

6.1 The kernel of the fabric

By gluing to the thickened torus a solid torus on the inside and a solid torus on the outside one obtains a 3-sphere $\mathbb{S}^3$. The central circles of the two solid tori together with the link in the thickened torus form a link in $\mathbb{S}^3$ which in [20] is called a **kernel for the fabric**. In the context of the present paper it can be constructed as follows.

Realize the textile structure as the boundary of the surface $\widetilde{\mathfrak{S}}_{\mathcal{Z},\eta,\nu,\omega}^{\leqslant h}$ constructed in §4.2 for some $0 < h < 1$, some positive integer weight function ν and list of edge vectors $\omega = \omega_{\mathcal{Z}}$ (see §4.1). It lies in the thickened plane $\mathbb{R}^2 \times [-h, +h]$. Fixing a point $\mathbf{p}$ in $\mathbb{R}^2$ and a basis λ_1, λ_2 for the lattice Λ in $\mathbb{R}^2$ such that $\det(\lambda_1, \lambda_2) = -1$ (cf. (151) and Figure 30) we obtain a period parallelogram for Λ with corners $\mathbf{p}$, $\mathbf{p} + \lambda_1$, $\mathbf{p} + \lambda_2$, $\mathbf{p} + \lambda_1 + \lambda_2$. The sides (oriented line segments) of the parallelogram are H, V, $H + \lambda_1$ and $V + \lambda_2$ with

$$
H = \{\mathbf{p} + t\lambda_2 \mid 0 \le t \le 1\}, \qquad V = \{\mathbf{p} + t\lambda_1 \mid 0 \le t \le 1\}. \tag{200}
$$

We choose $\mathbf{p}$ such that none of the four sides contains a vertex in the black/white tiling defined by $\mathcal{Z}$. Then $(H + \Lambda, 1) \subset \mathbb{R}^3$ is a Λ-invariant collection of parallel lines in the horizontal plane at height 1 and $(V + \Lambda, -1) \subset \mathbb{R}^3$ is a Λ-invariant collection of parallel lines in the horizontal plane at height -1. Take the union of the textile structure with these two sets of parallel lines modulo Λ, i.e.

$$
\left((\text{boundary of } \widetilde{\mathfrak{S}}_{\mathcal{Z},\eta,\nu,\omega}^{\leqslant h}) \cup (H + \Lambda, 1) \cup (V + \Lambda, -1)\right)/_\Lambda, \tag{201}
$$

and embed it into $\mathbb{R}^3$ by means of Formula (66) (with $r = \frac{1}{3}$). The resulting link in $\mathbb{R}^3$ is then a **kernel for the fabric**. We denote it by $\mathfrak{L}^\infty$. It is the union,

$$\mathfrak{L}^\infty = \mathfrak{L} \cup \mathsf{X} \cup \mathsf{Y}, \tag{202}$$

of the link $\mathfrak{L}$ which is the boundary of the Seifert surface $\mathfrak{S}^{\leqslant h}_{\mathcal{Z}, \Lambda, \boxminus, r}$ with the central circle X of the outer solid torus coming from H and the central circle Y of the inner solid torus coming from V; see Figure 30.

For practical purposes one may sometimes want to think of (201) as

$$\left[\begin{array}{c} \text{boundary of } \widetilde{\mathfrak{S}}^{\leqslant h}_{\mathcal{Z}, \eta, \nu, \omega} \\ \cup \begin{pmatrix} H + \Lambda \\ 1 \end{pmatrix} \cup \begin{pmatrix} V + \Lambda \\ -1 \end{pmatrix} \end{array} \right] \bigcap \left[\begin{array}{c} \text{box with corners} \\ \begin{pmatrix} \mathbf{p} \\ \pm 1 \end{pmatrix}, \begin{pmatrix} \mathbf{p} + \lambda_1 \\ \pm 1 \end{pmatrix}, \begin{pmatrix} \mathbf{p} + \lambda_2 \\ \pm 1 \end{pmatrix}, \begin{pmatrix} \mathbf{p} + \lambda_1 + \lambda_2 \\ \pm 1 \end{pmatrix} \end{array} \right]$$
$$\tag{203}$$

with opposite vertical faces identified.

6.2 The linear map $\mathrm{H}_1(\Gamma_\Lambda^\vee, \mathbb{Z}) \longrightarrow \mathrm{H}_1(\mathbb{S}^3 \setminus \mathfrak{L}^\infty, \mathbb{Z})$

Recall from §6.1 that $\mathfrak{L}^\infty$ denotes the *kernel of the fabric.* By the construction of the Seifert surface $\mathfrak{S}^{\leqslant h}_{\mathcal{Z}, \Lambda, \boxminus, r}$ the bipartite graph $\Gamma_\Lambda^\vee$ lies in the complement of $\mathfrak{L}^\infty$ in $\mathbb{S}^3$. We are going to explicitly describe the induced linear map

$$\mathrm{H}_1(\Gamma_\Lambda^\vee, \mathbb{Z}) \longrightarrow \mathrm{H}_1(\mathbb{S}^3 \setminus \mathfrak{L}^\infty, \mathbb{Z}) \tag{204}$$

w.r.t. natural bases of the two homology groups.

For $\mathrm{H}_1(\Gamma_\Lambda^\vee, \mathbb{Z})$ we take the basis $\mathbb{B}$ as in Theorem 4; this basis consists of the homology classes of the loops $\ell_{\mathbf{v}}$ for all but one $\mathbf{v} \in \mathsf{P}_\Lambda^\star$ (say $\mathbf{v} \neq \mathbf{v}_0$) and two loops $\mathfrak{l}_1$ and $\mathfrak{l}_2$ which lift the chosen basis λ_1, λ_2 of Λ.

Since $\mathfrak{L}^\infty = \mathfrak{L} \cup \mathsf{X} \cup \mathsf{Y}$ (see (202)) a natural basis for $\mathrm{H}_1(\mathbb{S}^3 \setminus \mathfrak{L}^\infty, \mathbb{Z})$ is given by the homology classes $\delta_{\mathsf{X}}, \delta_{\mathsf{Y}}, \delta_{\mathbf{z}}$ ($\mathbf{z} \in \mathsf{P}_\Lambda^{\mathsf{z}}$) of the boundaries of little discs transversal to the components of the link $\mathfrak{L}^\infty$. These classes are characterized by their linking numbers with the components of $\mathfrak{L}^\infty$:

$$\mathsf{link}(\delta_{\mathbf{c}}, \mathbf{c}) = 1, \qquad \mathsf{link}(\delta_{\mathbf{c}}, \mathbf{c}') = 0 \tag{205}$$

for all components $\mathbf{c}$, $\mathbf{c}'$ of $\mathfrak{L}^\infty$ with $\mathbf{c}' \neq \mathbf{c}$. A loop $\mathbf{p}$ on $\Gamma_\Lambda^\vee$ lies in $\mathbb{S}^3 \setminus \mathfrak{L}^\infty$. Its homology class in $\mathrm{H}_1(\mathbb{S}^3 \setminus \mathfrak{L}^\infty, \mathbb{Z})$ is

$$[\mathbf{p}] = \mathsf{link}(\mathbf{p}, \mathsf{X}) \, \delta_{\mathsf{X}} + \mathsf{link}(\mathbf{p}, \mathsf{Y}) \, \delta_{\mathsf{Y}} + \sum_{\mathbf{z} \in \mathsf{P}_\Lambda^{\mathsf{z}}} \mathsf{link}(\mathbf{p}, \widetilde{\ell_{\mathbf{z}}}) \, \delta_{\mathbf{z}}, \tag{206}$$

where, as in Theorem 5 $\widetilde{\ell_{\mathbf{z}}}$ denotes the component of $\mathfrak{L}^\infty$ which corresponds to the zigzag $\mathbf{z}$. For the loops $\mathfrak{l}_1, \mathfrak{l}_2, \ell_{\mathbf{v}}$ ($\mathbf{v} \in \mathsf{P}_\Lambda^\star$) whose homology classes in $\mathrm{H}_1(\Gamma_\Lambda^\vee, \mathbb{Z})$ constitute the basis $\mathbb{B}$ we have (see Figure 30)

$$\begin{aligned} \mathsf{link}(\mathfrak{l}_1, \mathsf{X}) = 1, &\quad \mathsf{link}(\mathfrak{l}_2, \mathsf{X}) = \mathsf{link}(\ell_{\mathbf{v}}, \mathsf{X}) = 0, \forall \mathbf{v} \in \mathsf{P}_\Lambda^\star, \\ \mathsf{link}(\mathfrak{l}_2, \mathsf{Y}) = 1, &\quad \mathsf{link}(\mathfrak{l}_1, \mathsf{Y}) = \mathsf{link}(\ell_{\mathbf{v}}, \mathsf{Y}) = 0, \forall \mathbf{v} \in \mathsf{P}_\Lambda^\star. \end{aligned} \tag{207}$$

According to Formula (162) the other linking numbers in (206) are given by the Seifert form:

$$\mathsf{link}(\mathbf{p}, \widetilde{\ell_{\mathbf{z}}}) \,=\, \mathcal{S}_{\eta,\lambda_1,\lambda_2}(\mathbf{p}, \ell_{\mathbf{z}}), \tag{208}$$

where on the right $\ell_{\mathbf{z}}$ is the homology class of the zigzag $\mathbf{z}$ in $\mathrm{H}_1(\Gamma_\Lambda^\vee, \mathbb{Z})$.

The above arguments prove

Proposition 8 *The matrix of the linear map* (204) *w.r.t. the basis* $\ell_{\mathbf{v}}$ ($\mathbf{v} \in \mathsf{P}_\Lambda^\star$, $\mathbf{v} \neq \mathbf{v}_0$), $\mathfrak{l}_1$, $\mathfrak{l}_2$ *of* $\mathrm{H}_1(\Gamma_\Lambda^\vee, \mathbb{Z})$ *and the basis* $\delta_{\mathbf{z}}$ ($\mathbf{z} \in \mathsf{P}_\Lambda^\mathsf{z}$), δ_X, δ_Y *of* $\mathrm{H}_1(\mathbb{S}^3 \setminus \mathfrak{L}^\infty, \mathbb{Z})$ *is the* $(|\mathsf{P}_\Lambda^\mathsf{z}| + 2) \times (|\mathsf{P}_\Lambda^\star| + 1)$*-matrix*

$$\left(\begin{array}{|c|c|} \hline L^t \cdot \mathsf{S}_{\eta,\mathfrak{l}_1,\mathfrak{l}_2}^t \\ \hline 0 & 1 \\ \hline \end{array} \right) \tag{209}$$

where 0 *denotes the* $2 \times (|\mathsf{P}_\Lambda^\star| - 1)$ *zero matrix,* 1 *is the* 2×2 *identity matrix,* $\mathsf{S}_{\eta,\mathfrak{l}_1,\mathfrak{l}_2}$ *is the* $(|\mathsf{P}_\Lambda^\star| + 1) \times (|\mathsf{P}_\Lambda^\star| + 1)$*-matrix giving the Seifert form (see Formula* (152)*),* L *is the* $(|\mathsf{P}_\Lambda^\star| + 1) \times |\mathsf{P}_\Lambda^\mathsf{z}|$*-matrix of which the columns give the coordinates of the homology classes of the zigzag loops w.r.t. the basis* $\mathbb{B}$ *of* $\mathrm{H}_1(\Gamma_\Lambda^\vee, \mathbb{Z})$. *Note that Formula* (159) *implies*

$$L^t \cdot \mathsf{S}_{\eta,\mathfrak{l}_1,\mathfrak{l}_2}^t = L^t \cdot \mathsf{S}_{\eta,\mathfrak{l}_1,\mathfrak{l}_2}. \tag{210}$$

∎

Implicit in the above computation is the computation of the linear map

$$\mathrm{H}_1(\mathfrak{S}_{\mathcal{Z},\Lambda,\boxminus,r}^{<h}) \longrightarrow \mathrm{H}_1(\mathbb{S}^3 \setminus \mathfrak{L}, \mathbb{Z}); \tag{211}$$

cf. (**??**). This turns out to be an immediate illustration of the general theory in [18] Chapter 6. So we may conclude from [18] Definition 6.6.:

The (one variable) **Alexander polynomial** *of the link* $\mathfrak{L}$ *is:*

$$\Delta_\mathfrak{L}(u) \,=\, \det\!\big(u\,\mathsf{S}_{\eta,\mathfrak{l}_1,\mathfrak{l}_2} - \mathsf{S}_{\eta,\mathfrak{l}_1,\mathfrak{l}_2}^t\big) \,=\, \det\!\big(u\,\mathsf{S}_{\eta,\mathfrak{l}_1,\mathfrak{l}_2}^t - \mathsf{S}_{\eta,\mathfrak{l}_1,\mathfrak{l}_2}\big). \tag{212}$$

where $\mathsf{S}_{\eta,\mathfrak{l}_1,\mathfrak{l}_2}$ is the Seifert matrix (154). If $\det \mathsf{S}_{\eta,\mathfrak{l}_1,\mathfrak{l}_2} = \pm 1$, the (one variable) Alexander polynomial is the **characteristic polynomial** of the monodromy matrix $\mathsf{M}_{\eta,\lambda_1,\lambda_2} = (\mathsf{S}_{\eta,\mathfrak{l}_1,\mathfrak{l}_2}^t)^{-1}\mathsf{S}_{\eta,\mathfrak{l}_1,\mathfrak{l}_2}$ (see (172)):

$$\Delta_\mathfrak{L}(u) \,=\, \pm \det\!\big(u\,\mathbb{I} - \mathsf{M}_{\eta,\lambda_1,\lambda_2}\big). \tag{213}$$

Assume that $\mathfrak{l}_1$, $\mathfrak{l}_2$ *lie in the kernel of the matrix* $\mathsf{S}_{\eta,\mathfrak{l}_1,\mathfrak{l}_2} - \mathsf{S}_{\eta,\mathfrak{l}_1,\mathfrak{l}_2}^t$. *Assume also that* $\det(\mathsf{S}_{\eta,\mathfrak{l}_1,\mathfrak{l}_2}) \neq 0$ *and that the monodromy matrix* $\mathsf{M} = \mathsf{M}_{\eta,\lambda_1,\lambda_2} = (\mathsf{S}_{\eta,\mathfrak{l}_1,\mathfrak{l}_2}^t)^{-1}\mathsf{S}_{\eta,\mathfrak{l}_1,\mathfrak{l}_2}$ *has all its entries in* $\mathbb{Z}$.

Formula (210) implies

$$\mathsf{image}\big(\mathsf{M} - \mathbb{I}\big) \subset \mathsf{kernel}\big(\mathrm{H}_1(\mathbb{X}_{\sigma_0,\sigma_1,\varrho}, \mathbb{Z}) \longrightarrow \mathrm{H}_1(\mathbb{S}^3 \setminus \mathfrak{L}^\infty, \mathbb{Z})\big). \tag{214}$$

On the other hand, according to Corollary 4 the kernel of the surjective linear map

$$H_1(\Gamma_\Lambda^\vee, \mathbb{Z}) = H_1(\mathbb{X}_{\sigma_0,\sigma_1,\varrho}, \mathbb{Z}) = H_1(\overline{\mathbb{X}}_{\sigma_0,\sigma_1,\varrho}, \mathbb{Z}) \twoheadrightarrow H_1(\mathbb{X}_{\sigma_0,\sigma_1}, \mathbb{Z}) \qquad (215)$$

is generated by the homology classes of the zigzag loops $\ell_\mathbf{z}$ ($\mathbf{z} \in \mathsf{P}_\Lambda^\mathsf{z}$) and is equal to the kernel of the matrix $\mathsf{M} - \mathbb{I}$. So the matrix $\mathsf{M} - \mathbb{I}$ induces an isomorphism

$$H_1(\mathbb{X}_{\sigma_0,\sigma_1}, \mathbb{Z}) \xrightarrow{\simeq} \mathsf{image}(\mathsf{M} - \mathbb{I}). \qquad (216)$$

Restricting the map (204) to $\ker(\mathsf{M} - \mathbb{I})$ amounts to multiplying the matrix in (209) from the right by the matrix L. The result is a $(|\mathsf{P}_\Lambda^\mathsf{z}| + 2) \times |\mathsf{P}_\Lambda^\mathsf{z}|$-matrix of which the top $|\mathsf{P}_\Lambda^\mathsf{z}|$ rows form the symmetric $|\mathsf{P}_\Lambda^\mathsf{z}| \times |\mathsf{P}_\Lambda^\mathsf{z}|$-matrix

$$L^t \cdot \mathsf{S}_{\eta,\mathfrak{l}_1,\mathfrak{l}_2} \cdot L. \qquad (217)$$

This matrix gives the restriction of the Seifert form $\mathsf{S}_{\eta,\mathfrak{l}_1,\mathfrak{l}_2}$ to $\ker(\mathsf{M} - \mathbb{I})$. The restriction of the Seifert form to $\ker(\mathsf{M} - \mathbb{I})$ is non-degenerate. Therefore the matrix in (217) has rank $|\mathsf{P}_\Lambda^\mathsf{z}| - 1$ and its kernel is generated by $\sum_{\mathbf{z} \in \mathsf{P}_\Lambda^\mathsf{z}} \ell_\mathbf{z}$.

It follows that the restriction of the map (204) to $\ker(\mathsf{M} - \mathbb{I})$ induces an injective linear map

$$\ker(\mathsf{M} - \mathbb{I}) \hookrightarrow \mathsf{image}\big(H_1(\mathbb{X}_{\sigma_0,\sigma_1,\varrho}, \mathbb{Z}) \longrightarrow H_1(\mathbb{S}^3 \setminus \mathfrak{L}^\infty, \mathbb{Z})\big) \qquad (218)$$

with finite cokernel. From the known ranks of the homology groups we now see that

$$
\begin{aligned}
\mathsf{rank}\big(\mathsf{image}\big(H_1(\mathbb{X}_{\sigma_0,\sigma_1,\varrho}, \mathbb{Z}) \longrightarrow H_1(\mathbb{S}^3 \setminus \mathfrak{L}^\infty, \mathbb{Z})\big) &= |\mathsf{P}_\Lambda^\mathsf{z}| - 1, \\
\mathsf{rank}\big(\mathsf{cokernel}\big(H_1(\mathbb{X}_{\sigma_0,\sigma_1,\varrho}, \mathbb{Z}) \longrightarrow H_1(\mathbb{S}^3 \setminus \mathfrak{L}^\infty, \mathbb{Z})\big) &= 3.
\end{aligned}
\qquad (219)
$$

Representatives in $H_1(\mathbb{S}^3 \setminus \mathfrak{L}^\infty, \mathbb{Z})$ for three independent generators of the $\mathsf{cokernel}$ in (219) are the homology classes δ_X, δ_Y, δ_Z where

$$\delta_\mathsf{Z} = \sum_{\mathbf{z} \in \mathsf{P}_\Lambda^\mathsf{z}} \delta_\mathbf{z}. \qquad (220)$$

6.2.1   Example 5.4.3 continued

For this example the matrix L was already given in Formula (183). The matrix $\mathsf{S}_{\eta,\mathfrak{l}_1,\mathfrak{l}_2}$ can be computed and turns out to be

$$
\mathsf{S}_{\eta,\mathfrak{l}_1,\mathfrak{l}_2} =
\begin{pmatrix}
-1 & -1 & 1 & 0 & 0 & 0 & -1 \\
0 & -1 & 0 & 1 & 0 & 0 & 0 \\
0 & 2 & -1 & -1 & 1 & 0 & 0 \\
0 & 0 & 0 & -1 & 0 & 0 & 0 \\
1 & 0 & -1 & 1 & -1 & 0 & 0 \\
0 & 0 & 0 & 0 & 0 & 0 & 1 \\
-1 & 0 & 0 & 0 & 0 & 1 & -1
\end{pmatrix}
\qquad (221)
$$

This agrees with the matrices (182) and (186) for the intersection form and the monodromy, respectively. Substituting the matrices for $\mathsf{S}_{\eta,\mathfrak{l}_1,\mathfrak{l}_2}$ and L into Formula (209) gives the matrix for the linear map $\mathrm{H}_1(\Gamma_\Lambda^\vee, \mathbb{Z}) \to \mathrm{H}_1(\mathbb{S}^3 \setminus \mathfrak{L}^\infty, \mathbb{Z})$:

$$
\begin{pmatrix}
0 & 0 & 0 & 0 & 0 & 0 & 1 \\
0 & -1 & 1 & 1 & 0 & 0 & 0 \\
-1 & 0 & 0 & 0 & 0 & 1 & -1 \\
0 & 0 & 0 & 0 & 0 & -1 & 0 \\
0 & 0 & 0 & -1 & 1 & -1 & 0 \\
1 & 1 & -1 & 0 & -1 & 1 & 0 \\
0 & 0 & 0 & 0 & 0 & 1 & 0 \\
0 & 0 & 0 & 0 & 0 & 0 & 1
\end{pmatrix}.
\tag{222}
$$

Since $\det(\mathsf{S}_{\eta,\mathfrak{l}_1,\mathfrak{l}_2}) = 1$ it follows from (213) that the (one variable) Alexander polynomial of the link $\mathfrak{L}$ is

$$
\Delta_\mathfrak{L}(u) = \det(u\,\mathbb{I} - \mathsf{M}_{\eta,\mathfrak{l}_1,\mathfrak{l}_2}) = (u-1)^5(u+1)^2.
\tag{223}
$$

The eigenspace for the eigenvalue 1 (i.e. $\ker(\mathsf{M} - \mathbb{I})$) has rank 5 and is spanned by the homology classes of the zigzag loops. The eigenspace for the eigenvalue -1 has rank 1 and is spanned by the vector $(0,1,1,0,0,0,0)^t$. The generalized eigenspace for the eigenvalue -1 has rank 2 and is spanned by the vectors $(0,1,1,0,0,0,0)^t$ and $(0,0,1,-1,-1,0,0)^t$.

The matrix $L^t \cdot \mathsf{S}_{\eta,\mathfrak{l}_1,\mathfrak{l}_2}^t \cdot L$ which gives the restriction of the Seifert form to $\ker(\mathsf{M} - \mathbb{I})$ is the 6×6-matrix in Formula (190). Let

$$
\Xi =
\begin{pmatrix}
0 & -3 & -20 & -5 & -5 & -6 \\
9 & 0 & -11 & -14 & -14 & -9 \\
-4 & -7 & 0 & -9 & -9 & -10 \\
11 & -10 & -9 & 0 & -24 & -7 \\
11 & -10 & -9 & -24 & 0 & -7 \\
6 & -9 & -14 & -11 & -11 & 0
\end{pmatrix}.
\tag{224}
$$

Then

$$
L^t \cdot \mathsf{S}_{\eta,\mathfrak{l}_1,\mathfrak{l}_2}^t \cdot L \cdot \Xi =
\begin{pmatrix}
-20 & 4 & 4 & 4 & 4 & 4 \\
4 & -20 & 4 & 4 & 4 & 4 \\
4 & 4 & -20 & 4 & 4 & 4 \\
4 & 4 & 4 & -20 & 4 & 4 \\
4 & 4 & 4 & 4 & -20 & 4 \\
4 & 4 & 4 & 4 & 4 & -20
\end{pmatrix}.
\tag{225}
$$

Using that is this example L is the matrix (183) one easily checks that the last two rows of the matrix $L \cdot \Xi^t$ are

$$
\begin{pmatrix}
4 & 4 & 4 & 28 & 4 & 4 \\
-16 & 8 & 8 & 8 & 8 & 8
\end{pmatrix}.
\tag{226}
$$

One now easily finds $24\delta_\mathbf{z}$ for every $\mathbf{z} \in \mathsf{P}_\Lambda^z$ as an explicit linear combination of δ_X, δ_Y, δ_Z and the homology classes of the zigzag loops $\ell_{\mathbf{z}'}$ ($\mathbf{z}' \in \mathsf{P}_\Lambda^z$). In these linear combinations the coefficients of δ_X and δ_Y are given by (226) , the coefficient of δ_Z is 4 (see (225)) and the other coefficients are given by (224). ∎

A   More examples of Zhegalkin Zebra Motives

In this section we show the tilings of the plane $\mathbb{R}^2$ by black and white polygons for some more Zhegalkin Zebra Motives. In the pictures one can easily recognize the dual bipartite graphs: the black (resp. white) polygons correspond to the black (resp. white) nodes; two polygons with a common edge give an edge between the corresponding nodes of the bipartite graph. For the planar bipartite graphs which also appear in [13, 14] we will indicate which model it is in op. cit..

From the planar bipartite graph associated with a Zhegalkin Zebra Motive $\mathcal{Z}$ one then obtains a bipartite graph on the torus $\mathbb{R}^2/\Lambda$ for every sublattice $\Lambda \subset \mathsf{Aut}(\mathcal{Z})$. The actual models (brane tilings) in [13, 14] live on a torus. So, in addition to the Zhegalkin Zebra Motive $\mathcal{Z}$ we must also specify the lattice Λ.

The functions in Figure 2 appear in [13, 14] as

- $\mathcal{Z}_2 = \mathsf{Z}^{21} + \mathsf{Z}^{41}$: $\mathsf{Aut}(\mathcal{Z}_2) = \mathbb{Z}(1,0) + \mathbb{Z}(0,1)$.

    - model 4a: $\Lambda = \mathbb{Z}(2,0) + \mathbb{Z}(0,2)$.
    - model 15a: $\Lambda = \mathbb{Z}(1,1) + \mathbb{Z}(1,-1)$.

- $\mathcal{Z}_3 = \mathsf{Z}^{21} + \mathsf{Z}^{41} + \mathsf{Z}^{61}$: $\mathsf{Aut}(\mathcal{Z}_3) = \mathbb{Z}(1,1) + \mathbb{Z}(1,-1)$.

    - model 1: $\Lambda = \mathbb{Z}(3,3) + \mathbb{Z}(3,-3)$.
    - model 2: $\Lambda = \mathbb{Z}(4,4) + \mathbb{Z}(2,-2)$.
    - model 7: $\Lambda = \mathbb{Z}(3,3) + \mathbb{Z}(2,-2)$.
    - model 13: $\Lambda = \mathbb{Z}(3,1) + \mathbb{Z}(2,-2)$.
    - model 16: $\Lambda = \mathbb{Z}(3,3) + \mathbb{Z}(1,-1)$.

- $\mathcal{Z}_4 = \mathsf{Z}^{21} + \mathsf{Z}^{31} + \mathsf{Z}^{41} + \mathsf{Z}^{61}$: $\mathsf{Aut}(\mathcal{Z}_4) = \mathbb{Z}(1,0) + \mathbb{Z}(0,1)$.

    - model 4d: $\Lambda = \mathbb{Z}(1,1) + \mathbb{Z}(1,-1)$.
    - model 15b: $\Lambda = \mathbb{Z}(1,0) + \mathbb{Z}(0,1)$.

- $\mathcal{Z}_6 = \mathsf{Z}^{11} + \mathsf{Z}^{21} + \mathsf{Z}^{31} + \mathsf{Z}^{41} + \mathsf{Z}^{51} + \mathsf{Z}^{61}$: $\mathsf{Aut}(\mathcal{Z}_6) = \mathbb{Z}(1,1) + \mathbb{Z}(1,-1)$

    - model 10d: $\Lambda = \mathbb{Z}(1,1) + \mathbb{Z}(1,-1)$.

Figures 34 - 36 include Zhegalkin Zebra Motives for the models 3a, 4b, 4c, 6a, 6b, 6c, 8a, 8b, 9a, 9b, 10a, 10b, 10c, 12b, 14 in [13, 14]. The pictures show the planar tilings. For the models 4c, 6a, 6b, 6c, 8b, 9a, 9b, 10a, 10b, 10c, 12b, 14 the lattice Λ is equal to $\mathsf{Aut}(\mathcal{Z})$. For the models 3a, 4b, 8a, the lattice Λ has index 2 in $\mathsf{Aut}(\mathcal{Z})$ (i.e. $\mathsf{Aut}(\mathcal{Z})/\Lambda = \mathbb{Z}/2\mathbb{Z}$); more precisely (see Figure 34):

- model 3a: $\mathsf{Aut}(\mathcal{Z}) = \mathbb{Z}(2,2) + \mathbb{Z}(0,1)$, $\Lambda = \mathbb{Z}(2,2) + \mathbb{Z}(0,2)$.

- model 4b: $\mathsf{Aut}(\mathcal{Z}) = \mathbb{Z}(2,2) + \mathbb{Z}(0,1)$, $\Lambda = \mathbb{Z}(2,2) + \mathbb{Z}(0,2)$.

- model 8a: $\mathsf{Aut}(\mathcal{Z}) = \mathbb{Z}(3,3) + \mathbb{Z}(0,2)$, $\Lambda = \mathbb{Z}(3,3) + \mathbb{Z}(0,4)$.

The models 3b, 5, 9c, 11, 12a in [13, 14] can also be described by Zhegalkin Zebra Motives, but these we have not included in our figures.
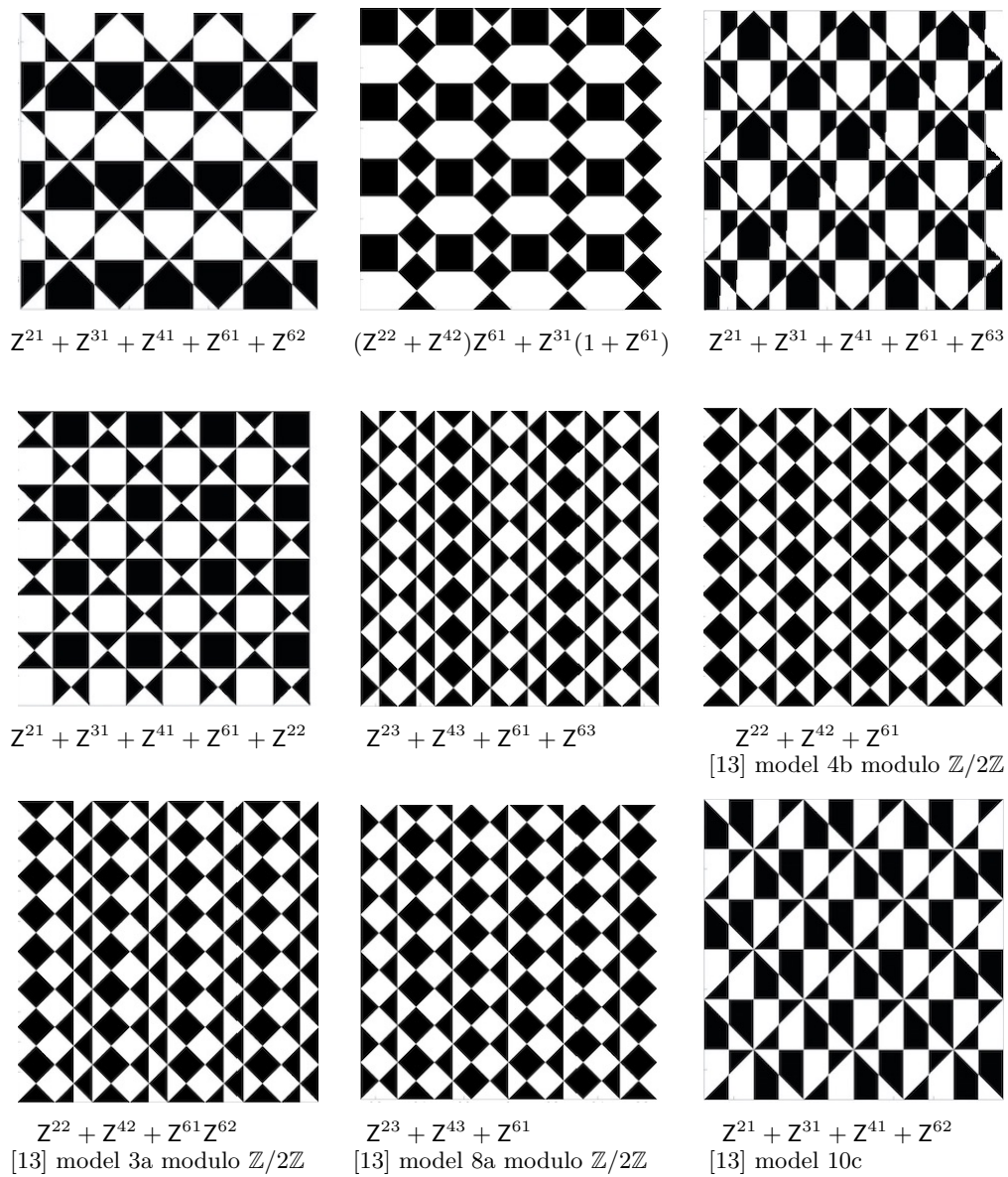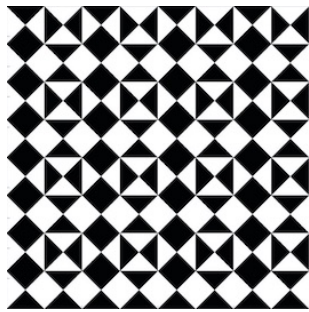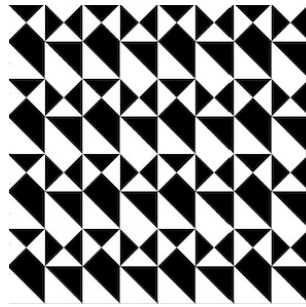
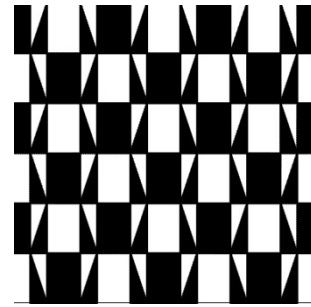$\mathsf{Z}^{21} + \mathsf{Z}^{31} + \mathsf{Z}^{41} + \mathsf{Z}^{61} + \mathsf{Z}^{62}$

$(\mathsf{Z}^{22} + \mathsf{Z}^{42})\mathsf{Z}^{61} + \mathsf{Z}^{31}(1 + \mathsf{Z}^{61})$

$\mathsf{Z}^{21} + \mathsf{Z}^{31} + \mathsf{Z}^{41} + \mathsf{Z}^{61} + \mathsf{Z}^{63}$

$\mathsf{Z}^{21} + \mathsf{Z}^{31} + \mathsf{Z}^{41} + \mathsf{Z}^{61} + \mathsf{Z}^{22}$

$\mathsf{Z}^{23} + \mathsf{Z}^{43} + \mathsf{Z}^{61} + \mathsf{Z}^{63}$

$\mathsf{Z}^{22} + \mathsf{Z}^{42} + \mathsf{Z}^{61}$
[13] model 4b modulo $\mathbb{Z}/2\mathbb{Z}$

$\mathsf{Z}^{22} + \mathsf{Z}^{42} + \mathsf{Z}^{61}\mathsf{Z}^{62}$
[13] model 3a modulo $\mathbb{Z}/2\mathbb{Z}$

$\mathsf{Z}^{23} + \mathsf{Z}^{43} + \mathsf{Z}^{61}$
[13] model 8a modulo $\mathbb{Z}/2\mathbb{Z}$

$\mathsf{Z}^{21} + \mathsf{Z}^{31} + \mathsf{Z}^{41} + \mathsf{Z}^{62}$
[13] model 10c

Figure 34:

$Z^{22} + Z^{42} + Z^{31}Z^{61}$
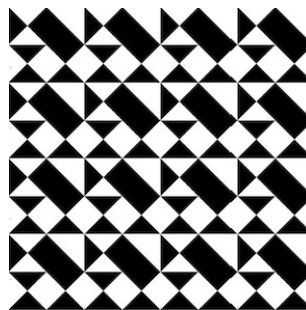[13] model 4c

$Z^{42} + Z^{61} + Z^{31}Z^{22}$
[13] model 8b

$(Z^{11} + Z^{51} + Z^{62})(Z^{63} + Z^{61})+$
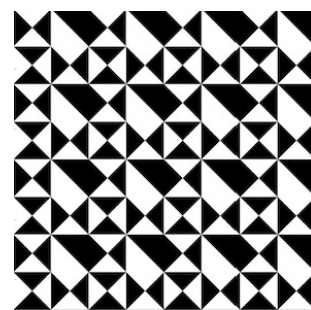$+Z^{61}Z^{63} + Z^{62} + Z^{31}$
[13] model 14
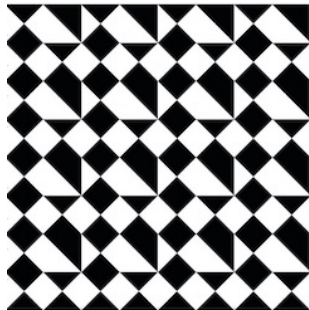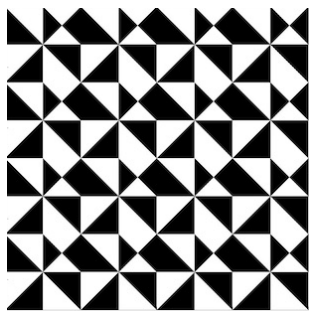
$Z^{22} + Z^{42} + Z^{61}Z^{31}Z^{22}$
[13] model 6a

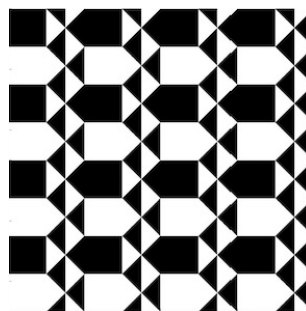$Z^{22} + Z^{42} + Z^{31} + Z^{61}Z^{31}Z^{22}$
[13] model 6b

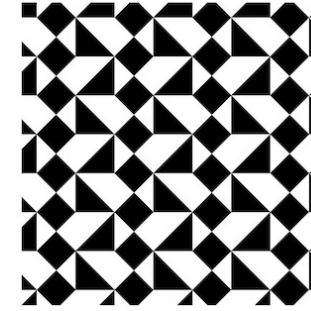$Z^{22} + Z^{42} + Z^{31} + Z^{61} + Z^{61}Z^{31}Z^{22}$
[13] model 6c

$Z^{21} + Z^{31} + Z^{41} + Z^{61}+$
$+Z^{61}Z^{31}Z^{42}$

[13] model 12b

$(Z^{22} + Z^{42} + Z^{62})Z^{61}+$
$+Z^{31}(1 + Z^{61})$

[13] model 9a

$Z^{22} + Z^{42}+$
$+(Z^{22} + Z^{31}Z^{22} + Z^{31}Z^{42})Z^{61}$
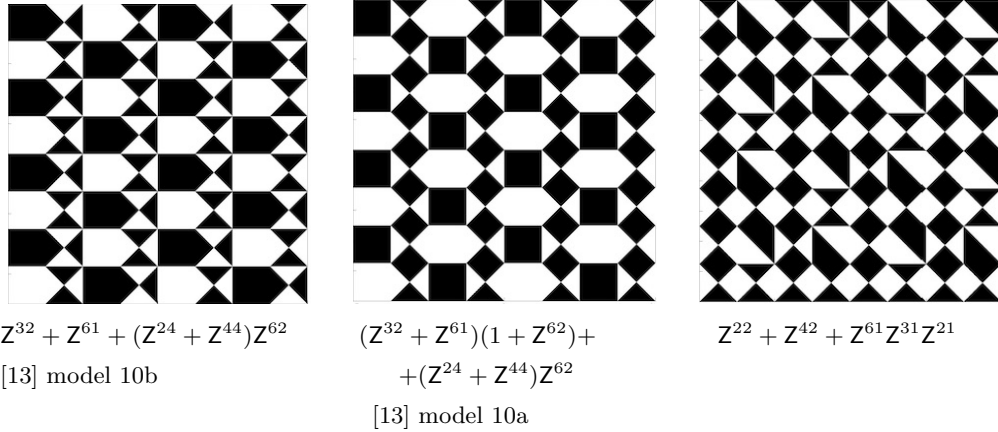
[13] model 9b

Figure 35:

$Z^{32} + Z^{61} + (Z^{24} + Z^{44})Z^{62}$

[13] model 10b

$(Z^{32} + Z^{61})(1 + Z^{62}) +$

$+ (Z^{24} + Z^{44})Z^{62}$

[13] model 10a

$Z^{22} + Z^{42} + Z^{61}Z^{31}Z^{21}$

Figure 36:

B   The quiver $\Gamma_\Lambda^{\circlearrowleft}$

B.1 $\Gamma_\Lambda^{\circlearrowleft}$ on Seifert surface

The quiver $\Gamma_\Lambda^{\circlearrowleft}$ appears very naturally in the construction of hyperbolic Belyi map (13)

$$\varphi_{\sigma_0,\sigma_1,\varrho} : \mathbb{X}_{\sigma_0,\sigma_1,\varrho} \longrightarrow \mathbb{D}$$

as the inverse image $\varphi_{\sigma_0,\sigma_1,\varrho}^{-1}\big(\mathbb{U}(\varrho)\big)$ of the counter-clockwise oriented circle $\mathbb{U}(\varrho)$; see Section 2.3 and Figure 6. For $\varrho < h < 1$ the connected components of $\varphi_{\sigma_0,\sigma_1,\varrho}^{-1}\big\{ z \in \mathbb{C} \,\big|\, |z| < \varrho \,\big\}$ and those of $\varphi_{\sigma_0,\sigma_1,\varrho}^{-1}\big\{ z \in \mathbb{C} \,\big|\, \varrho < |z| \leq h \,\big\}$ give a bipartite tiling of $\mathbb{X}_{\sigma_0,\sigma_1\varrho}^{\leqslant h} \setminus \Gamma_\Lambda^{\circlearrowleft}$. Via the homeomorphism (20) this induces a bipartite tiling on $\mathfrak{S}_{\mathcal{Z},\Lambda,\boxminus,r}^{\leqslant h}$ as illustrated in Figure 37.

B.2 $\Gamma_\Lambda^{\circlearrowleft}$ and the superpotential $(\mathcal{E}_\Lambda, \sigma_0, \sigma_1)$

Recall that the set of nodes of the quiver $\Gamma_\Lambda^{\circlearrowleft}$ is identified with the set $\mathsf{P}_\Lambda^{\bullet}$ and that the set of arrows of $\Gamma_\Lambda^{\circlearrowleft}$ is identified with the set $\mathcal{E}_\Lambda$. The arrow corresponding to $e \in \mathcal{E}_\Lambda$ is denoted as $e^{\blacktriangleleft}$. It runs from the node $b(e)$ to the node $b(\sigma_0(e))$ and can be identified with the path $e^{\bullet\circ}\sigma_0(e)^{\circ\bullet}$ on the bipartite graph $\Gamma_\Lambda^{\vee}$.

The embedding of $\Gamma_\Lambda^{\circlearrowleft}$ into the oriented surface $\mathbb{X}_{\sigma_0,\sigma_1,\varrho}$ provides the quiver $\Gamma_\Lambda^{\circlearrowleft}$ with the additional structure of a **ribbon graph**; i.e. at each node a cyclic ordering of the edges incident to that node. For the cyclic structure at a node $\mathbf{b} \in \mathsf{P}_\Lambda^{\bullet}$ we note that the outgoing arrows at $\mathbf{b}$ are those $e^{\blacktriangleleft}$ for which $b(e) = \mathbf{b}$ and the incoming arrows are those $e'^{\blacktriangleleft}$ for which $b(\sigma_0(e')) = \mathbf{b}$. The outgoing arrows are cyclically ordered as in the cycle of σ_1 which corresponds to $\mathbf{b}$. Between the outgoing arrows $e^{\blacktriangleleft}$ and $\sigma_1(e)^{\blacktriangleleft}$ lies the incoming arrow $\sigma_0^{-1}(e)^{\blacktriangleleft}$.

By writing for every $\mathbf{b} \in \mathsf{P}_\Lambda^{\bullet}$ the cyclically ordered set of arrows incident to $\mathbf{b}$ as linear strings with an outgoing arrow in first position, the permutations σ_1 and σ_0 can immediately be read from the list of these strings. Thus we see that
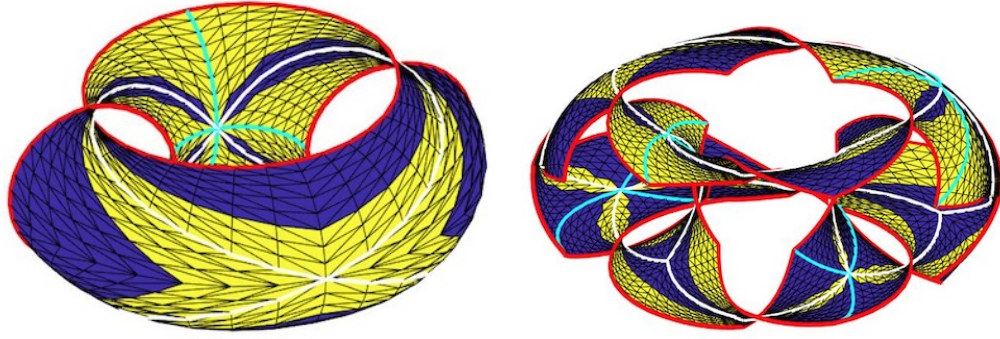
$$\mathcal{Z}_2 = \mathsf{Z}^{21} + \mathsf{Z}^{41} \qquad\qquad \mathcal{Z}_4 = \mathsf{Z}^{21} + \mathsf{Z}^{31} + \mathsf{Z}^{41} + \mathsf{Z}^{61}$$

Figure 37: Examples of the bipartite tiling on $\mathfrak{S}_{\mathcal{Z},\Lambda,\boxminus,r}^{\leqslant h}$ given by $\Gamma_\Lambda^{\circlearrowleft}$. Other landmarks: the boundary of $\mathfrak{S}_{\mathcal{Z},\Lambda,\boxminus,r}^{\leqslant h}$ (red) and the bipartite graph $\Gamma_\Lambda^{\vee}$ (white).

Proposition 9 *The data of the ribbon graph $\Gamma_\Lambda^{\circlearrowleft}$ are equivalent to the data of the superpotential $(\mathcal{E}_\Lambda, \sigma_0, \sigma_1)$.* ∎

Ignoring the cyclic ordering of the edges at the nodes leaves $\Gamma_\Lambda^{\circlearrowleft}$ only as an abstract quiver as described in the first paragraph of this section. *The data for this abstract quiver are no longer equivalent to the superpotential $(\mathcal{E}_\Lambda, \sigma_0, \sigma_1)$.*

The data for this abstract quiver can be given as a table listing the edges $e^{\blacktriangleleft}$ ($e \in \mathcal{E}_\Lambda$) with their source $b(e)$ and target $b(\sigma_0(e))$ or as a matrix

$$\mathsf{Mat}_{\Gamma_\Lambda^{\circlearrowleft}} = \sum_{e \in \mathcal{E}_\Lambda} \mathsf{Mat}_{\Gamma_\Lambda^{\circlearrowleft}}(e) \tag{227}$$

with rows and columns indexed by the nodes of $\Gamma_\Lambda^{\circlearrowleft}$, i.e. indexed by the elements of the set $\mathsf{P}_\Lambda^\bullet$, and

$$\mathsf{Mat}_{\Gamma_\Lambda^{\circlearrowleft}}(e)_{\mathbf{b},\mathbf{b}'} = \begin{cases} e^{\blacktriangleleft} & \text{if} \quad \mathbf{b} = b(e), \ \mathbf{b}' = b(\sigma_0(e)) \\ 0 & \text{else} \end{cases} \tag{228}$$

B.2.1 Example: $\mathcal{Z} = \mathsf{Z}^{21} + \mathsf{Z}^{31} + \mathsf{Z}^{41} + \mathsf{Z}^{62}$.

The superpotential for Example 4.3.3 as given in (80) is

$$\begin{aligned} \sigma_0 &= (1,6,8)(2,3,4,14)(5,11,12,13)(7,9,10), \\ \sigma_1 &= (1,12,2)(3,11,10,8)(4,6,7,5)(9,14,13). \end{aligned}$$

The nodes of $\Gamma_\Lambda^{\circlearrowleft}$ correspond with the cycles of σ_1 and are labeled from left to right as $1, 2, 3, 4$. This is the same labeling as in Figure 25. So, the arrows of the quiver $\Gamma_\Lambda^{\circlearrowleft}$ are

arrow	$1^{\blacktriangleleft}$	$2^{\blacktriangleleft}$	$3^{\blacktriangleleft}$	$4^{\blacktriangleleft}$	$5^{\blacktriangleleft}$	$6^{\blacktriangleleft}$	$7^{\blacktriangleleft}$	$8^{\blacktriangleleft}$	$9^{\blacktriangleleft}$	$10^{\blacktriangleleft}$	$11^{\blacktriangleleft}$	$12^{\blacktriangleleft}$	$13^{\blacktriangleleft}$	$14^{\blacktriangleleft}$
from	1	1	2	3	3	3	3	2	4	2	2	1	4	4
to	3	2	3	4	2	2	4	1	2	3	1	4	3	1

In matrix form this table becomes

0	$2^{\blacktriangleleft}$	$1^{\blacktriangleleft}$	$12^{\blacktriangleleft}$
$8^{\blacktriangleleft} + 11^{\blacktriangleleft}$	0	$3^{\blacktriangleleft} + 10^{\blacktriangleleft}$	0
0	$5^{\blacktriangleleft} + 6^{\blacktriangleleft}$	0	$4^{\blacktriangleleft} + 7^{\blacktriangleleft}$
$14^{\blacktriangleleft}$	$9^{\blacktriangleleft}$	$13^{\blacktriangleleft}$	0

The cyclic orderings of the arrows incident to the four vertices of $\Gamma_\Lambda^{\circlearrowleft}$ are

$$
\begin{aligned}
\text{vertex } 1 &: \quad (1^{\blacktriangleleft}, \quad 8^{\blacktriangleleft}, \quad 12^{\blacktriangleleft}, \quad 11^{\blacktriangleleft}, \quad 2^{\blacktriangleleft}, \quad 14^{\blacktriangleleft}); \\
\text{vertex } 2 &: \quad (3^{\blacktriangleleft}, \quad 2^{\blacktriangleleft}, \quad 11^{\blacktriangleleft}, \quad 5^{\blacktriangleleft}, \quad 10^{\blacktriangleleft}, \quad 9^{\blacktriangleleft}, \quad 8^{\blacktriangleleft}, \quad 6^{\blacktriangleleft}); \\
\text{vertex } 3 &: \quad (4^{\blacktriangleleft}, \quad 3^{\blacktriangleleft}, \quad 6^{\blacktriangleleft}, \quad 1^{\blacktriangleleft}, \quad 7^{\blacktriangleleft}, \quad 10^{\blacktriangleleft}, \quad 5^{\blacktriangleleft}, \quad 13^{\blacktriangleleft}); \\
\text{vertex } 4 &: \quad (9^{\blacktriangleleft}, \quad 7^{\blacktriangleleft}, \quad 14^{\blacktriangleleft}, \quad 4^{\blacktriangleleft}, \quad 13^{\blacktriangleleft}, \quad 12^{\blacktriangleleft}).
\end{aligned}
$$

∎

A **path** on the quiver $\Gamma_\Lambda^{\circlearrowleft}$ is a string of composable arrows:

$$
\mathbf{p} = e_1{}^{\blacktriangleleft} e_2{}^{\blacktriangleleft} e_3{}^{\blacktriangleleft} \cdots e_k{}^{\blacktriangleleft} \qquad \text{with} \quad b(\sigma_0(e_j)) = b(e_{j+1}), \quad 1 \le j < k. \tag{229}
$$

The source $s(\mathbf{p})$ and target $t(\mathbf{p})$ of the path $\mathbf{p}$ in (229) are

$$
s(\mathbf{p}) = b(e_1), \quad t(\mathbf{p}) = b(\sigma_0(e_k)). \tag{230}
$$

The path $\mathbf{p}$ is closed if $t(\mathbf{p}) = s(\mathbf{p})$.

The **path algebra** $\mathbb{Z}[\mathsf{Path}(\Gamma_\Lambda^{\circlearrowleft})]$ is the free $\mathbb{Z}$-module on the set of paths on $\Gamma_\Lambda^{\circlearrowleft}$ equipped with the product $*$ such that $\mathbf{p} * \mathbf{p}'$ is the concatenation of the strings $\mathbf{p}$ and $\mathbf{p}'$ if $t(\mathbf{p}) = s(\mathbf{p}')$, while $\mathbf{p} * \mathbf{p}' = 0$ if $t(\mathbf{p}) \ne s(\mathbf{p}')$. The constant paths $\{1_\mathbf{b}\}_{\mathbf{b} \in \mathsf{P}_\Lambda^\bullet}$ form a collection of orthogonal idempotents and $1 = \sum_{\mathbf{b} \in \mathsf{P}_\Lambda^\bullet} 1_\mathbf{b}$ is the unit element of $\mathbb{Z}[\mathsf{Path}(\Gamma_\Lambda^{\circlearrowleft})]$.

B.2.2 Example: some closed paths on $\Gamma_\Lambda^{\circlearrowleft}$.

Here are three examples of closed paths in $\Gamma_\Lambda^{\circlearrowleft}$.

- Take $e \in \mathcal{E}_\Lambda$. Let $k > 0$ be such that $\sigma_0^k(e) = e$ and $\sigma_0^j(e) \ne e$ for $j < k$. Then

$$
W_e = e^{\blacktriangleleft} \cdot (\sigma_0(e))^{\blacktriangleleft} \cdot \ldots \cdot (\sigma_0^{k-1}(e))^{\blacktriangleleft} \tag{231}
$$

is a closed path in $\Gamma_\Lambda^{\circlearrowleft}$ which starts and ends at the node $\mathbf{b} = b(e)$.

- For $\mathbf{v} \in \mathsf{P}_\Lambda^\star$ the loop on $\Gamma_\Lambda^\vee$ given in (124)-(125),

$$
\ell_\mathbf{v} = e_1{}^{\bullet\circ} \cdot e_2{}^{\circ\bullet} \cdot e_3{}^{\bullet\circ} \cdot \ldots \cdot e_{2m-1}{}^{\bullet\circ} \cdot e_{2m}{}^{\circ\bullet}, \tag{232}
$$

becomes on $\Gamma_\Lambda^{\circlearrowleft}$ the closed path which starts and ends at node $\mathbf{b} = b(e_1)$:

$$
\ell_\mathbf{v} = e_1{}^{\blacktriangleleft} \cdot e_3{}^{\blacktriangleleft} \cdot \ldots \cdot e_{2m-1}{}^{\blacktriangleleft} \tag{233}
$$

with $e_1 = \sigma_1^{-1}\sigma_0(e_{2m-1})$, $e_{2k+1} = \sigma_1^{-1}\sigma_0(e_{2k-1})$ if $1 \le k < m$.

- For $\mathbf{z} \in \mathsf{P}_\Lambda^{\mathsf{z}}$ the loop on $\Gamma_\Lambda^\vee$ given in (126)-(127),

$$\ell_\mathbf{z} = e_1{}^{\bullet\circ} \cdot e_2{}^{\circ\bullet} \cdot e_3{}^{\bullet\circ} \cdot \ldots \cdot e_{2m-1}{}^{\bullet\circ} \cdot e_{2m}{}^{\circ\bullet}, \tag{234}$$

becomes on $\Gamma_\Lambda^{\circlearrowleft}$ the closed path which starts and ends at node $\mathbf{b} = b(e_1)$:

$$\ell_\mathbf{z} = e_1{}^{\blacktriangleleft} \cdot e_3{}^{\blacktriangleleft} \cdot \ldots \cdot e_{2m-1}{}^{\blacktriangleleft} \tag{235}$$

with $e_1 = \sigma_1\sigma_0(e_{2m-1})$, $e_{2k+1} = \sigma_1\sigma_0(e_{2k-1})$ if $1 \le k < m$.

$\blacksquare$

Proposition 10 *For every pair* $\mathbf{b}, \mathbf{b}' \in \mathsf{P}_\Lambda^\bullet$ *of nodes of* $\Gamma_\Lambda^{\circlearrowleft}$ *there is an oriented path on* $\Gamma_\Lambda^{\circlearrowleft}$ *which starts at* $\mathbf{b}$ *and ends at* $\mathbf{b}'$.

Proof: Consider the tiling of $\mathbb{R}^2$. Let $\mathbf{b}$ and $\mathbf{b}'$ be two black polygons in the tiling. Take an oriented line segment ℓ which starts in the interior of $\mathbf{b}$, ends in the interior of $\mathbf{b}'$ and does not pass through any vertex of the tiling. Let $e_1, e_2, \ldots, e_{2m-1}e_{2m}$ be the edges of the tiling which ℓ intersects such that (cf. (122))

$$\ell = e_1{}^{\bullet\circ} \cdot e_2{}^{\circ\bullet} \cdot e_3{}^{\bullet\circ} \cdot e_4{}^{\circ\bullet} \cdots e_{2m-1}{}^{\bullet\circ} \cdot e_{2m}{}^{\circ\bullet} \qquad \text{with} \tag{236}$$
$$w(e_k) = w(e_{k+1}) \text{ if } k \text{ odd}, \quad b(e_k) = b(e_{k+1}) \text{ if } k \text{ even}, \ b(e_1) = \mathbf{b}, \ b(e_{2m}) = \mathbf{b}'.$$

A pair $e_{2j-1}{}^{\bullet\circ}e_{2j}{}^{\circ\bullet}$ on ℓ corresponds to a white polygon $\mathbf{w}_j$ which ℓ enters through the edge e_{2j-1} and leaves through the edge e_{2j}. Let $e_{j,1}, \ldots, e_{j,n_j}$ be the edges between e_{2j-1} and e_{2j} on the counter-clockwise oriented boundary of $\mathbf{w}_j$. Then $e_{j,1} = \sigma_0(e_{2j-1})$ and $e_{2j} = \sigma_0(e_{j,n_j})$ and

$$e_{2j-1}{}^{\bullet\circ}e_{2j}{}^{\circ\bullet} = e_{2j-1}{}^{\blacktriangleleft} \cdot e_{j,1}{}^{\blacktriangleleft} \cdots e_{j,n_j}{}^{\blacktriangleleft}. \tag{237}$$

The proof is completed by combining (236) and (237). $\blacksquare$

B.3 Line bundles with connection on $\Gamma_\Lambda^\vee$ and representations of the quiver $\Gamma_\Lambda^{\circlearrowleft}$

A **line bundle with connection** on the graph $\Gamma_\Lambda^\vee$ (cf. [11] §1) consists of a collection of 1-dimensional complex vector spaces $\{V_\mathbf{b}, V_\mathbf{w}\}_{\mathbf{b} \in \mathsf{P}_\Lambda^\bullet, \mathbf{w} \in \mathsf{P}_\Lambda^\circ}$ and a collection of isomorphisms $\left\{ \phi_{e^{\bullet\circ}} : V_{b(e)} \xrightarrow{\sim} V_{w(e)} \right\}_{e \in \mathcal{E}_\Lambda}$.

An **isomorphism** α between two line bundles with connection $\{V_\mathbf{b}, V_\mathbf{w}, \phi_{e^{\bullet\circ}}\}$ and $\{V'_\mathbf{b}, V'_\mathbf{w}, \phi'_{e^{\bullet\circ}}\}$ is a collection of isomorphisms $\alpha_\mathbf{b} : V_\mathbf{b} \xrightarrow{\sim} V'_\mathbf{b}$ for $\mathbf{b} \in \mathsf{P}_\Lambda^\bullet$ and $\alpha_\mathbf{w} : V_\mathbf{w} \xrightarrow{\sim} V'_\mathbf{w}$ for $\mathbf{w} \in \mathsf{P}_\Lambda^\circ$ such that

$$\alpha_{w(e)} \cdot \phi_{e^{\bullet\circ}} \cdot \alpha_{b(e)}^{-1} = \phi'_{e^{\bullet\circ}} \quad \text{for all } e \in \mathcal{E}_\Lambda. \tag{238}$$

Choosing bases for the 1-dimensional vector spaces $\{V_{\mathbf{b}}, V_{\mathbf{w}}\}$ amounts to an isomorphism $\alpha : \{V_{\mathbf{b}}, V_{\mathbf{w}}, \phi_{e\bullet\circ}\} \xrightarrow{\sim} \{V'_{\mathbf{b}}, V'_{\mathbf{w}}, \phi'_{e\bullet\circ}\}$ with $V'_{\mathbf{b}} = V'_{\mathbf{w}} = \mathbb{C}$ for all $\mathbf{b} \in \mathsf{P}^{\bullet}_{\Lambda}$, $\mathbf{w} \in \mathsf{P}^{\circ}_{\Lambda}$ and, hence, all $\phi'_{e\bullet\circ} \in \mathbb{C}^*$.

Two line bundles with connection $\{V'_{\mathbf{b}}, V'_{\mathbf{w}}, \phi'_{e\bullet\circ}\}$ and $\{V''_{\mathbf{b}}, V''_{\mathbf{w}}, \phi''_{e\bullet\circ}\}$ with all $V'_{\mathbf{b}} = V'_{\mathbf{w}} = V''_{\mathbf{b}} = V''_{\mathbf{w}} = \mathbb{C}$ and all $\phi'_{e\bullet\circ}, \phi''_{e\bullet\circ} \in \mathbb{C}^*$ are isomorphic if and only if there are non-zero complex numbers $a_{\mathbf{b}}$ and $a_{\mathbf{w}}$ for $\mathbf{b} \in \mathsf{P}^{\bullet}_{\Lambda}$ and $\mathbf{w} \in \mathsf{P}^{\circ}_{\Lambda}$ such that

$$a_{w(e)} \cdot \phi'_{e\bullet\circ} \cdot a_{b(e)}^{-1} = \phi''_{e\bullet\circ} \quad \text{for all } e \in \mathcal{E}_{\Lambda}. \tag{239}$$

Let $\mathbb{C}^{*\mathcal{E}_{\Lambda}}$ denote the set of tuples $\{\phi'_{e\bullet\circ}\}_{e\in\mathcal{E}_{\Lambda}}$ of non-zero complex numbers. Define an equivalence relation $\sim$ on $\mathbb{C}^{*\mathcal{E}_{\Lambda}}$ by:

$$\{\phi'_{e\bullet\circ}\} \sim \{\phi''_{e\bullet\circ}\} \qquad \Leftrightarrow \qquad \exists a_{\mathbf{b}}, a_{\mathbf{w}} \in \mathbb{C}^* \text{ such that (239) holds.} \tag{240}$$

Recall from (117) that a tuple $\{\phi'_{e\bullet\circ}\} \in \mathbb{C}^{*\mathcal{E}_{\Lambda}}$ induces a homomorphism

$$\mathrm{H}_1(\Gamma^{\vee}_{\Lambda}, \mathbb{Z}) \longrightarrow \mathbb{C}^*, \qquad \theta \mapsto \prod_{e\in\mathcal{E}_{\Lambda}} \phi'_{e\bullet\circ}{}^{\theta(e)}. \tag{241}$$

The fact that $\theta : \mathcal{E}_{\Lambda} \to \mathbb{Z}$ satisfies (116) implies that for $\{\phi'_{e\bullet\circ}\} \sim \{\phi''_{e\bullet\circ}\}$

$$\prod_{e\in\mathcal{E}_{\Lambda}} \phi''_{e\bullet\circ}{}^{\theta(e)} = \prod_{e\in\mathcal{E}_{\Lambda}} \phi'_{e\bullet\circ}{}^{\theta(e)} \times \prod_{\mathbf{w}\in\mathsf{P}^{\circ}_{\Lambda}} \prod_{e:w(e)=\mathbf{w}} a_{\mathbf{w}}^{\theta(e)} \times \prod_{\mathbf{b}\in\mathsf{P}^{\bullet}_{\Lambda}} \prod_{e:b(e)=\mathbf{b}} a_{\mathbf{b}}^{-\theta(e)}$$

$$= \prod_{e\in\mathcal{E}_{\Lambda}} \phi'_{e\bullet\circ}{}^{\theta(e)}. \tag{242}$$

Conclusion: (cf. [11] Formula (1)) *There are bijections between the set of isomorphism classes of line bundles with connection on $\Gamma^{\vee}_{\Lambda}$, the set of $\sim$-equivalence classes in $\mathbb{C}^{*\mathcal{E}_{\Lambda}}$ and the cohomology group $\mathrm{H}^1(\Gamma^{\vee}_{\Lambda}, \mathbb{C}^*)$:*

$$\mathrm{H}^1(\Gamma^{\vee}_{\Lambda}, \mathbb{C}^*) = \mathbb{C}^{*\mathcal{E}_{\Lambda}}/\mathbb{C}^{*\mathsf{P}^{\bullet}_{\Lambda}} = \left\{ \begin{array}{l} \text{isomorphism classes} \\ \text{of line bundles with} \\ \text{connection on } \Gamma^{\vee}_{\Lambda} \end{array} \right\}. \tag{243}$$

$\blacksquare$

Recall that the set of nodes and arrows of the quiver $\Gamma^{\circlearrowleft}_{\Lambda}$ are $\mathsf{P}^{\bullet}_{\Lambda}$ and $\mathcal{E}_{\Lambda}$, respectively, and that the arrow $e^{\blacktriangleleft}$ runs from node $b(e)$ to node $b(\sigma_0(e))$.

A **representation of the quiver** $\Gamma^{\circlearrowleft}_{\Lambda}$ consists of a collection of complex vector spaces $\{V_{\mathbf{b}}\}_{\mathbf{b}\in\mathsf{P}^{\bullet}_{\Lambda}}$ and a collection of linear maps $\{\psi_{e^{\blacktriangleleft}} : V_{b(e)} \to V_{b(\sigma_0(e))}\}_{e\in\mathcal{E}_{\Lambda}}$. The list of dimensions $\{\dim V_{\mathbf{b}}\}_{\mathbf{b}\in\mathsf{P}^{\bullet}_{\Lambda}}$ is called the **dimension vector** of the representation. An **isomorphism** between two representations $\{V_{\mathbf{b}}, \psi_{e^{\blacktriangleleft}}\}$ and $\{V'_{\mathbf{b}}, \psi'_{e^{\blacktriangleleft}}\}$ is a collection of isomorphisms $\alpha_{\mathbf{b}} : V_{\mathbf{b}} \xrightarrow{\sim} V'_{\mathbf{b}}$ for $\mathbf{b} \in \mathsf{P}^{\bullet}_{\Lambda}$ such that

$$\alpha_{b(\sigma_0(e))} \cdot \psi_{e^{\blacktriangleleft}} \cdot \alpha_{b(e)}^{-1} = \psi'_{e^{\blacktriangleleft}} \quad \text{for all } e \in \mathcal{E}_{\Lambda}. \tag{244}$$

Let us now focus on representations with dimension vector $(1, \ldots, 1)$. Choosing bases for the 1-dimensional vector spaces $\{V_{\mathbf{b}}\}$ amounts to an isomorphism $\alpha : \{V_{\mathbf{b}}, \psi_{e\blacktriangleleft}\} \xrightarrow{\sim} \{V'_{\mathbf{b}}, \psi'_{e\blacktriangleleft}\}$ with $V'_{\mathbf{b}} = \mathbb{C}$ for all $\mathbf{b} \in \mathsf{P}_\Lambda^\bullet$ and, hence, all $\psi'_{e\blacktriangleleft} \in \mathbb{C}$.

Two quiver representations $\{V'_{\mathbf{b}}, \psi'_{e\blacktriangleleft}\}$ and $\{V''_{\mathbf{b}}, \psi''_{e\blacktriangleleft}\}$ with all $V'_{\mathbf{b}} = V''_{\mathbf{b}} = \mathbb{C}$ and all $\psi'_{e\blacktriangleleft}, \psi''_{e\blacktriangleleft} \in \mathbb{C}$ are isomorphic if and only if there are non-zero complex numbers $a_{\mathbf{b}}$ for $\mathbf{b} \in \mathsf{P}_\Lambda^\bullet$ such that

$$a_{b(\sigma_0(e))} \cdot \psi'_{e\blacktriangleleft} \cdot a_{b(e)}^{-1} \;=\; \psi''_{e\blacktriangleleft} \quad \text{for all} \;\; e \in \mathcal{E}_\Lambda. \tag{245}$$

Formula (245) defines an equivalence relation $\sim$ on $\mathbb{C}^{\mathcal{E}_\Lambda}$. It also defines an action of the group $\mathbb{C}^{*\mathsf{P}_\Lambda^\bullet}$ on $\mathbb{C}^{\mathcal{E}_\Lambda}$ such that the orbits are precisely the $\sim$-equivalence classes. The subgroup

$$\left\{ \{a_{\mathbf{b}}\} \in \mathbb{C}^{*\mathsf{P}_\Lambda^\bullet} \mid \forall \mathbf{b}, \mathbf{b}' \in \mathsf{P}_\Lambda^\bullet : \; a_{\mathbf{b}} = a_{\mathbf{b}'} \right\} \;\simeq\; \mathbb{C}^* \tag{246}$$

acts trivially.

Conclusion: *There is a bijection between the set of isomorphism classes of representations of the quiver $\Gamma_\Lambda^\circlearrowleft$ with dimension vector $(1, \ldots, 1)$ and the set of orbits of $\mathbb{C}^{*\mathsf{P}_\Lambda^\bullet}/\mathbb{C}^*$ acting on $\mathbb{C}^{\mathcal{E}_\Lambda}$:*

$$\mathbb{C}^{\mathcal{E}_\Lambda} / \left(\mathbb{C}^{*\mathsf{P}_\Lambda^\bullet}/\mathbb{C}^* \right) \;=\; \left\{ \begin{array}{l} \text{isomorphism classes of} \\ \text{representations of } \Gamma_\Lambda^\circlearrowleft \text{ with} \\ \text{dimension vector } (1, \ldots, 1) \end{array} \right\}. \tag{247}$$

$\blacksquare$

Proposition 11 *The map*

$$\mathbb{C}^{*\mathcal{E}_\Lambda} \longrightarrow \mathbb{C}^{\mathcal{E}_\Lambda} , \qquad \{\phi_{e\bullet\circ}\}_{e\in\mathcal{E}_\Lambda} \mapsto \{\psi_{e\blacktriangleleft}\}_{e\in\mathcal{E}_\Lambda} , \quad \psi_{e\blacktriangleleft} = \phi_{e\bullet\circ} \cdot \phi_{\sigma_0(e)\bullet\circ}^{-1} \tag{248}$$

induces an injective map

$$\left\{ \begin{array}{l} \text{isomorphism classes} \\ \text{of line bundles with} \\ \text{connection on } \Gamma_\Lambda^\vee \end{array} \right\} \hookrightarrow \left\{ \begin{array}{l} \text{isomorphism classes of} \\ \text{representations of } \Gamma_\Lambda^\circlearrowleft \text{ with} \\ \text{dimension vector } (1, \ldots, 1) \end{array} \right\} \tag{249}$$

Its image is the set of the classes of those $\{\psi_{e\blacktriangleleft}\} \in \mathbb{C}^{\mathcal{E}_\Lambda}$ which satisfy:

$$\prod_{e\in\mathcal{E}_\Lambda : w(e)=\mathbf{w}} \psi_{e\blacktriangleleft} \;=\; 1 \qquad \text{for all} \quad \mathbf{w} \in \mathsf{P}_\Lambda^\circ. \tag{250}$$

Proof: The map in (248) is compatible with the equivalence relations $\sim$. So, the map in (249) is well defined.

The image of the map (248) is obviously contained in the set of those $\{\psi_{e\blacktriangleleft}\}_{e\in\mathcal{E}_\Lambda}$ which satisfy (250). In order to prove that it is equal to this set we construct for every quiver representation $\{\psi_{e\blacktriangleleft}\}_{e\in\mathcal{E}_\Lambda}$ which satisfies (250) a

line bundle with connection $\{\phi'_{e\bullet\circ}\}_{e\in\mathcal{E}_\Lambda}$ on $\Gamma_\Lambda^\vee$ which by (248) is mapped to $\{\psi_{e\blacktriangleleft}\} \in \mathbb{C}^{\mathcal{E}_\Lambda}$. For the construction we fix a perfect matching m_0 and partition the set $\mathcal{E}_\Lambda$ according to the cycles of the permutation σ_0. Let $(e_1, e_2, \ldots, e_k)$ be such a cycle with indices such that $\sigma_0(e_j) = e_{j+1}$ for $1 \le j \le k-1$, $\sigma_0(e_k) = e_1$ and $\mathsf{m}_0(e_k) = 1$. We then define

$$\phi'_{e_k\bullet\circ} = 1, \qquad \phi'_{e_j\bullet\circ} = \prod_{i=j}^{k-1} \psi_{e_i\blacktriangleleft} \quad \text{for } j = 1, \ldots, k-1. \tag{251}$$

Doing this for all cycles of σ_0 we obtain from $\{\psi_{e\blacktriangleleft}\}_{e\in\mathcal{E}_\Lambda}$ a line bundle with connection $\{\phi'_{e\bullet\circ}\}_{e\in\mathcal{E}_\Lambda}$ on $\Gamma_\Lambda^\vee$. When we subsequently apply Formula (248) to $\{\phi'_{e\bullet\circ}\}_{e\in\mathcal{E}_\Lambda}$ we find the quiver representation $\{\psi'_{e\blacktriangleleft}\}_{e\in\mathcal{E}_\Lambda}$ with

$$\psi'_{e\blacktriangleleft} = \phi'_{e\bullet\circ} \cdot \phi'^{-1}_{\sigma_0(e)\bullet\circ} = \psi_{e\blacktriangleleft} \qquad \text{for all} \quad e \in \mathcal{E}_\Lambda. \tag{252}$$

Conversely, if $\{\psi_{e\blacktriangleleft}\}_{e\in\mathcal{E}_\Lambda}$ is obtained through Formula (248) from a line bundle with connection $\{\phi_{e\bullet\circ}\}_{e\in\mathcal{E}_\Lambda}$, then by substituting (248) into (251) we find

$$\phi'_{e_j\bullet\circ} = \prod_{i=j}^{k-1}\left(\phi_{e_i\bullet\circ} \cdot \phi^{-1}_{\sigma_0(e_i)\bullet\circ}\right) = \prod_{i=j}^{k-1}\left(\phi_{e_i\bullet\circ} \cdot \phi^{-1}_{e_{i+1}\bullet\circ}\right) = \phi_{e_j\bullet\circ} \cdot \phi^{-1}_{e_k\bullet\circ} \tag{253}$$

for $j = 1, \ldots, k$. For $\mathbf{w} \in \mathsf{P}_\Lambda^\circ$ we set $a_\mathbf{w} = \phi^{-1}_{e_\mathbf{w}\bullet\circ}$ where $e_\mathbf{w}$ is the unique element of $\mathcal{E}_\Lambda$ such that $w(e_\mathbf{w}) = \mathbf{w}$ and $\mathsf{m}_0(e_\mathbf{w}) = 1$. Then (253) becomes $\phi'_{e\bullet\circ} = \phi_{e\bullet\circ} \cdot a^{-1}_{w(e)}$ for all $e \in \mathcal{E}_\Lambda$. This shows by (240) that $\{\phi'_{e\bullet\circ}\}_{e\in\mathcal{E}_\Lambda} \sim \{\phi_{e\bullet\circ}\}_{e\in\mathcal{E}_\Lambda}$ and proves the injectivity of the map in (249). $\blacksquare$

Formulas (243), (247), (249) and (250) provide an embedding of the complex torus $\mathrm{H}^1(\Gamma_\Lambda^\vee, \mathbb{C}^*)$ into $\mathbb{C}^{\mathcal{E}_\Lambda}/(\mathbb{C}^{*\mathsf{P}_\Lambda^\bullet}/\mathbb{C}^*)$. One may want to view the closure of the image as a **compactification** of $\mathrm{H}^1(\Gamma_\Lambda^\vee, \mathbb{C}^*)$. The compactification process amounts to allowing tuples $\{\psi_{e\blacktriangleleft}\} \in \mathbb{C}^{\mathcal{E}_\Lambda}$ to have $\psi_{e\blacktriangleleft} = 0$ for some $e \in \mathcal{E}_\Lambda$. From the theory of moduli spaces one expects that the orbit space $\mathbb{C}^{\mathcal{E}_\Lambda}/(\mathbb{C}^{*\mathsf{P}_\Lambda^\bullet}/\mathbb{C}^*)$ has bad singularities which prevent it from being a good moduli space for representations of $\Gamma_\Lambda^\circlearrowright$ with dimension vector $(1, \ldots, 1)$. This raises the questions:

- *Which configurations of zeros must be excluded in order to avoid bad singularities?*

- *How can one resolve the remaining admissible singularities?*

- *Can the path algebra $\mathbb{Z}[\mathsf{Path}(\Gamma_\Lambda^\circlearrowright)]$ be used to construct a **non-commutative resolution of the admissible singularities**?*

86

B.4 The path algebra $\mathbb{Z}[\mathsf{Path}(\Gamma_\Lambda^{\circlearrowleft})]$

B.4.1 Non-commutative resolution of singularities

The last question in §B.3 is motivated by the hope to find an analogue of the beautiful results about the **Jacobi algebra** of the quiver with relations Γ_Λ given by the superpotential $(\mathcal{E}_\Lambda, \sigma_0, \sigma_1)$; see [2] and also [22] Remark 3.8.
The Jacobi algebra is the quotient of the path algebra $\mathbb{Z}[\mathsf{Path}(\Gamma_\Lambda)]$ by an ideal of relations provided by the superpotential $(\mathcal{E}_\Lambda, \sigma_0, \sigma_1)$.

So, the question might ask for an appropriate two-sided ideal $\mathfrak{W}$ in $\mathbb{Z}[\mathsf{Path}(\Gamma_\Lambda^{\circlearrowleft})]$ and to investigate the category of modules over the ring $\mathbb{Z}[\mathsf{Path}(\Gamma_\Lambda^{\circlearrowleft})]/\mathfrak{W}$.

From the above description of $\Gamma_\Lambda^{\circlearrowleft}$ we recognize that this quiver also appears in [19] where it is used in the construction of a type of algebras called **Brauer configuration algebras**. Indeed, in [19] §3 Malič and Schroll construct for permutations σ, α of $\{1, \ldots, n\}$ a quiver $\mathring{Q}$ with vertices corresponding to the cycles of the permutation α and for every $i \in \{1, \ldots, n\}$ an arrow from the cycle of α containing i to the cycle of α containing $\sigma(i)$. Thus, the quiver $\Gamma_\Lambda^{\circlearrowleft}$ is the same as the quiver $\mathring{Q}$ of [19] for $\sigma = \sigma_0$ and $\alpha = \sigma_1$ (but in [19] the cycles of α are white, while for us the cycles of σ_1 are black).

The Brauer configuration algebras in [19] §4 are constructed by taking the path algebra $\mathbb{Z}[\mathsf{Path}(\Gamma_\Lambda^{\circlearrowleft})]$ modulo a two-sided ideal generated by three types of elements. In the notations of the present paper the first type of elements reads

$$e_1{}^{\blacktriangleleft} e_2{}^{\blacktriangleleft} \cdots e_k{}^{\blacktriangleleft} - e_1'{}^{\blacktriangleleft} e_2'{}^{\blacktriangleleft} \cdots e_{k'}'{}^{\blacktriangleleft} \tag{254}$$

with $(e_1, e_2, \ldots, e_k)$ and $(e_1', e_2', \ldots, e_{k'}')$ the cycles of the permutation σ_0 such that $b(e_1) = b(e_1')$. Formula (254) may be a suitable generalization of Equation (250) in the present paper. But *it is not clear if the second and third type of relations in [19] §4 are also relevant in the context of the present paper.*

B.4.2 Toric geometry

We recall from [22] the construction of a compactification of $\mathrm{H}^1(\Gamma_\Lambda^{\vee}, \mathbb{C}^*)$ by means of toric geometry. The Λ-invariant non-negative integer weight functions with the operation $+$ and the degree function (3) form a graded semi-group $\mathcal{W}_\Lambda$ which is generated by the perfect matchings (see [22] Formula (1.3)):

$$\mathcal{W}_\Lambda = \mathbb{Z}_{\geq 0} \mathcal{M}_\Lambda; \tag{255}$$

here $\mathcal{M}_\Lambda$ denotes the set of perfect matchings for $(\mathscr{Z}, \Lambda)$. Standard constructions in algebraic geometry ([15] Chapter II) associate with the graded ring $\mathbb{Z}[\mathcal{W}_\Lambda]$ the *projective scheme* $\mathsf{Proj}(\mathbb{Z}[\mathcal{W}_\Lambda])$ and with the ring $\mathbb{Z}[\mathrm{H}_1(\Gamma_\Lambda^{\vee}, \mathbb{Z})]$ the *affine scheme* $\mathsf{Spec}(\mathbb{Z}[\mathrm{H}_1(\Gamma_\Lambda^{\vee}, \mathbb{Z})])$. The homology group $\mathrm{H}_1(\Gamma_\Lambda^{\vee}, \mathbb{Z})$ is the subgroup of $\mathbb{Z}^{\mathcal{E}_\Lambda}$ generated by the differences $\mathsf{m} - \mathsf{m}'$ of perfect matchings m, m' (see Proposition 4). It follows that $\mathsf{Spec}(\mathbb{Z}[\mathrm{H}_1(\Gamma_\Lambda^{\vee}, \mathbb{Z})])$ is a Zariski dense open

subscheme of $\mathsf{Proj}(\mathbb{Z}[\mathcal{W}_\Lambda])$. Moreover

$$
\begin{aligned}
\mathrm{H}^1(\Gamma_\Lambda^\vee, \mathbb{C}^*) \;&=\; \mathrm{Hom}(\mathrm{H}_1(\Gamma_\Lambda^\vee, \mathbb{Z}), \mathbb{C}^*) \;=\; \mathrm{Hom}_{\mathrm{algs}}(\mathbb{Z}[\mathrm{H}_1(\Gamma_\Lambda^\vee, \mathbb{Z})], \mathbb{C}) \\
&=\; \textit{the set of complex points of}\quad \mathsf{Spec}(\mathbb{Z}[\mathrm{H}_1(\Gamma_\Lambda^\vee, \mathbb{Z})]) \qquad (256) \\
&\subset\; \textit{the set of complex points of}\quad \mathsf{Proj}(\mathbb{Z}[\mathcal{W}_\Lambda]).
\end{aligned}
$$

A perfect matching m_0 gives rise to a sub-semi-group

$$
\mathcal{W}_\Lambda^0[-\mathsf{m}_0] = \left\{\, \nu - \deg(\nu)\mathsf{m}_0 \mid \nu \in \mathcal{W}_\Lambda \,\right\} \tag{257}
$$

in $\mathrm{H}_1(\Gamma_\Lambda^\vee, \mathbb{Z})$ and, hence, an inclusion of semi-group algebras

$$
\mathbb{Z}\big[\mathcal{W}_\Lambda^0[-\mathsf{m}_0]\big] \quad\subset\quad \mathbb{Z}[\mathrm{H}_1(\Gamma_\Lambda^\vee, \mathbb{Z})]. \tag{258}
$$

The union of the affine schemes $\mathsf{Spec}\big(\mathbb{Z}\big[\mathcal{W}_\Lambda^0[-\mathsf{m}_0]\big]\big)$ is an open covering of $\mathsf{Proj}(\mathbb{Z}[\mathcal{W}_\Lambda])$ and their intersection is $\mathsf{Spec}(\mathbb{Z}[\mathrm{H}_1(\Gamma_\Lambda^\vee, \mathbb{Z})])$:

$$
\mathsf{Proj}(\mathbb{Z}[\mathcal{W}_\Lambda]) \;=\; \bigcup_{\mathsf{m}_0 \in \mathcal{M}_\Lambda} \mathsf{Spec}\big(\mathbb{Z}\big[\mathcal{W}_\Lambda^0[-\mathsf{m}_0]\big]\big) , \tag{259}
$$

$$
\mathsf{Spec}(\mathbb{Z}[\mathrm{H}_1(\Gamma_\Lambda^\vee, \mathbb{Z})]) \;=\; \bigcap_{\mathsf{m}_0 \in \mathcal{M}_\Lambda} \mathsf{Spec}\big(\mathbb{Z}\big[\mathcal{W}_\Lambda^0[-\mathsf{m}_0]\big]\big) . \tag{260}
$$

*The above constructions of $\mathsf{Proj}(\mathbb{Z}[\mathcal{W}_\Lambda])$ is in fact standard constructions of the complete toric variety associated with the **matching polytope** (120). The affine covering (259) reflects the fact that the corners of the matching polytope are precisely all perfect matchings.*

The *line bundle* on $\mathsf{Proj}(\mathbb{Z}[\mathcal{W}_\Lambda])$ which corresponds to *"divisor at infinity"*

$$
\mathsf{Proj}(\mathbb{Z}[\mathcal{W}_\Lambda]) \setminus \mathsf{Spec}(\mathbb{Z}[\mathrm{H}_1(\Gamma_\Lambda^\vee, \mathbb{Z})]) \tag{261}
$$

is given by the *Čech cocycle* w.r.t. the affine covering (259)

$$
\big\{ X^{\mathsf{m}_1 - \mathsf{m}_0} \big\}_{\mathsf{m}_0, \mathsf{m}_1 \in \mathcal{M}_\Lambda} . \tag{262}
$$

Here X^{m} is the element of $\mathbb{Z}[\mathcal{W}_\Lambda]$ which corresponds to the perfect matching m.

On the other hand on $\mathsf{Spec}(\mathbb{Z}[\mathrm{H}_1(\Gamma_\Lambda^\vee, \mathbb{Z})])$ there is according to [11] a *Poisson structure*; see Formulas (192)-(193).

B.4.3 Non-commutative geometry of quiver path algebras

For every perfect matching m_0 we define a quiver $\Gamma_{\Lambda;\mathsf{m}_0}^\vee$ with set of nodes $\mathsf{P}_\Lambda^\bullet$ and set of arrows

$$
\text{arrows } \Gamma_{\Lambda;\mathsf{m}_0}^\vee \;=\; \big\{ e_1{}^{\bullet\circ} e_2{}^{\circ\bullet} \mid e_1, e_2 \in \mathcal{E}_\Lambda,\ w(e_1) = w(e_2),\ \mathsf{m}_0(e_2) = 1 \big\}. \tag{263}
$$

The arrow $e_1{}^{\bullet\circ}e_2{}^{\circ\bullet}$ runs from the node $b(e_1)$ to the node $b(e_2)$. For every $e_1 \in \mathcal{E}_\Lambda$ there is exactly one $e_2 \in \mathcal{E}_\Lambda$ such that $w(e_1) = w(e_2)$, $\mathsf{m}_0(e_2) = 1$. So, we can define $\Gamma^\vee_{\Lambda;\mathsf{m}_0}$ also as the quiver with set of nodes $\mathsf{P}^\bullet_\Lambda$ and set of arrows $\mathcal{E}_\Lambda$ and source and target maps

$$
\begin{aligned}
s_{\mathsf{m}_0} &: \mathcal{E}_\Lambda \to \mathsf{P}^\bullet_\Lambda, \quad s_{\mathsf{m}_0}(e) = b(e), \\
t_{\mathsf{m}_0} &: \mathcal{E}_\Lambda \to \mathsf{P}^\bullet_\Lambda, \quad t_{\mathsf{m}_0}(e) = b(e') \quad \text{with} \quad w(e) = w(e'), \mathsf{m}_0(e') = 1.
\end{aligned}
\tag{264}
$$

A path on $\Gamma^\vee_{\Lambda;\mathsf{m}_0}$ is a string

$$
e_1{}^{\bullet\circ} \cdot e_2{}^{\circ\bullet} \cdot e_3{}^{\bullet\circ} \cdot e_4{}^{\circ\bullet} \cdots e_{2m-1}{}^{\bullet\circ} \cdot e_{2m}{}^{\circ\bullet}
\tag{265}
$$

as in (236) satisfying the restriction $\mathsf{m}_0(e_j) = 1$ if j is even. The path (265) runs from node $\mathbf{b} = b(e_1)$ to node $\mathbf{b}' = b(e_{2m})$. As in the proof of Proposition 10 the path (265) can be uniquely expanded to a path from node $\mathbf{b}$ to node $\mathbf{b}'$ on the quiver $\Gamma^\circlearrowleft_\Lambda$. Thus we obtain an inclusion of algebras

$$
\mathbb{Z}\big[\mathsf{Path}(\Gamma^\vee_{\Lambda;\mathsf{m}_0})\big] \quad \subset \quad \mathbb{Z}\big[\mathsf{Path}(\Gamma^\circlearrowleft_\Lambda)\big]
\tag{266}
$$

which we want to view as the *non-commutative analogue* of the inclusion of commutative rings in (258). The question then becomes

$(\star)$ *What are appropriate non-commutative analogues of* (259)-(262)*?*

To get a first idea of what may be involved one can look at how perfect matchings are used.

- The homology group $\mathrm{H}_1(\Gamma^\vee_\Lambda, \mathbb{Z})$ is generated by the differences $\mathsf{m}_1 - \mathsf{m}_0$ of perfect matchings $\mathsf{m}_0, \mathsf{m}_1$. This implies that *the algebra* $\mathbb{Z}[\mathrm{H}_1(\Gamma^\vee_\Lambda, \mathbb{Z})]$ *is generated by the collection of subalgebras* $\mathbb{Z}\big[\mathcal{W}^0_\Lambda[-\mathsf{m}_0]\big]$ *with* $\mathsf{m}_0 \in \mathcal{M}_\Lambda$.

  The algebra $\mathbb{Z}\big[\mathcal{W}^0_\Lambda[-\mathsf{m}_0]\big]$ is generated by the paths $e^\blacktriangleleft$ with $e \in \mathcal{E}_\Lambda$. Recall that $e^\blacktriangleleft = e^{\bullet\circ}\sigma_0(e)^{\circ\bullet}$ and that for every e there is some perfect matching m_0 such that $\mathsf{m}_0(\sigma_0(e)) = 1$. It follows that *the algebra* $\mathbb{Z}[\mathsf{Path}(\Gamma^\circlearrowleft_\Lambda)]$ *is generated by the collection of subalgebras* $\mathbb{Z}\big[\mathsf{Path}(\Gamma^\vee_{\Lambda;\mathsf{m}_0})\big]$ *with* $\mathsf{m}_0 \in \mathcal{M}_\Lambda$.

- In the toric constructions behind (259)-(260) perfect matchings are viewed as maps $\mathsf{m} : \mathcal{E}_\Lambda \to \mathbb{Z}_{\geq 0}$ which satisfy $\sum_{e \text{ edge of } P} \mathsf{m}(e) = 1$ for every polygon P (black as well as white) in the planar tiling; see (3). The difference $\mathsf{m}_1 - \mathsf{m}_0$ of two perfect matchings satisfies the equations (116) and is therefore an element of the homology group $\mathrm{H}_1(\Gamma^\vee_\Lambda, \mathbb{Z})$. As such it is used in the Čech cocycle (262).

  On the other hand, a perfect matching m defines a bijection

$$
\vec{\mathsf{m}} : \mathsf{P}^\circ_\Lambda \to \mathsf{P}^\bullet_\Lambda, \quad \vec{\mathsf{m}}(\mathbf{w}) = \mathbf{b} \Leftrightarrow \exists e \in \mathcal{E}_\Lambda : \mathbf{b} = b(e), \mathbf{w} = w(e), \mathsf{m}(e) = 1.
\tag{267}
$$

Then $\vec{m}_1\vec{m}_0^{-1}$ is a permutation of the set $P_\Lambda^\bullet$ which gives a correspondence between the quivers:

$$\Gamma_{\Lambda\,;m_0}^\vee = \left\{ s_{m_0},\, t_{m_0} : \mathcal{E}_\Lambda \to P_\Lambda^\bullet \right\}, \qquad \Gamma_{\Lambda\,;m_1}^\vee = \left\{ s_{m_1},\, t_{m_1} : \mathcal{E}_\Lambda \to P_\Lambda^\bullet \right\},$$

$$s_{m_1} = s_{m_0}, \qquad t_{m_1} = \vec{m}_1\vec{m}_0^{-1}\, t_{m_0}. \tag{268}$$

The collection of permutations

$$\left\{ \vec{m}_1\vec{m}_0^{-1} \right\}_{m_0, m_1 \in \mathcal{M}_\Lambda}. \tag{269}$$

may be an appropriate analogue of the Čech cocycle (262). The effect on the path algebras, however, looks very complex.

We must leave further investigations on the question $(\star)$ for the future.

C   The textile code

The **textile code** of a link in a thickened torus is defined in [3] Definition 8 using the torus diagram of the link. We are going to analyse this definition for the textiles coming from Zhegalkin Zebra Motives. In that case the crossings in the torus diagram lie at the midpoints of the edges of the planar tiling given by the Zhegalkin Zebra Motive $\mathcal{Z}$. So they correspond to the elements of $\mathcal{E}_\Lambda$ and are labeled $1, \ldots, n$. At the crossing corresponding to $e \in \mathcal{E}_\Lambda$ the situation looks like

if $\eta(e) = -1$: $\quad$ $e^{\circ\bullet}$ $\quad$ $e^{\bullet\circ}$ $\qquad\qquad$ if $\eta(e) = +1$: $\quad$ $e^{\circ\bullet}$ $\quad$ $e^{\bullet\circ}$ $\qquad$ (270)

For every zigzag $\mathbf{z}$ one should list the crossings which involve $\mathbf{z}$ in the order in which they appear on $\mathbf{z}$. This is exactly what we did in (126) and (127). If at crossing e the zigzag $\mathbf{z}$ is undercrossing one should, according to the rules in [3], add a superscript $\pm$ equal to $-\eta(e)$; cf. (65) and (270). So, for this piece of the textile code the rule becomes:

If in the list from (126) for the zigzag $\mathbf{z}$ the crossing e appears
• in odd position and $\eta(e) = -1$ then e gets a superscript $+$ $\qquad$ (271)
• in even position and $\eta(e) = +1$ then e gets a superscript $-$

Note: It follows from (122)-(123) that e appears in odd (resp. even) position in the list (126) for the zigzag $\mathbf{z}$ if $[\ell_\mathbf{z}](e) = -1$ (resp. $[\ell_\mathbf{z}](e) = +1$); here the function $[\ell_\mathbf{z}] : \mathcal{E}_\Lambda \to \{-1, 0, +1\}$ gives the homology class of $\mathbf{z}$ in $H_1(\Gamma_\Lambda^\vee, \mathbb{Z})$.

For the other piece of the textile code we must choose a period parallelogram and determine how the zigzags intersect the sides of the parallelogram. We choose the parallelogram as in §6.1 with the point $\mathbf{p}$ in the interior of a black

$$H_{e^{\bullet\circ}}^{-} \qquad H_{e^{\circ\bullet}}^{-} \qquad H_{e^{\circ\bullet}}^{+} \qquad H_{e^{\bullet\circ}}^{+} \qquad V_{e^{\circ\bullet}}^{+} \qquad V_{e^{\bullet\circ}}^{+} \qquad V_{e^{\circ\bullet}}^{-} \qquad V_{e^{\bullet\circ}}^{-}$$
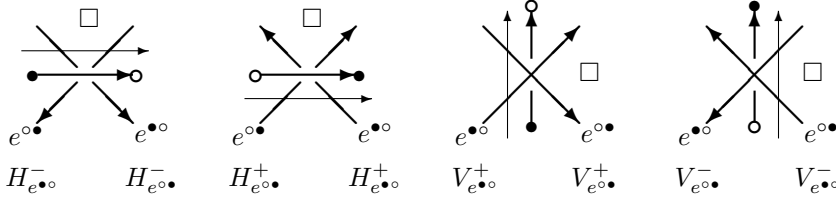
Figure 38: The four types of intersections of zigzags with the sides of the period parallelogram. At each intersection point one side of the parallelogram and two zigzags intersect. The position of the parallelogram is indicated by the □. The two zigzags are indicated by $e^{\circ\bullet}$ and $e^{\bullet\circ}$. The ±-superscripts are the signs attached as in (65) to the crossing of the zigzag with H and V, respectively.

polygon. Then we list (in the format of Formula (122)) the order in which H (resp. V) intersects the edges in the tiling and whether it passes from black to white or from white to black[16].

We write the lists for a zigzag $\mathbf{z}$ and those for H and V in the format of Formula (122) and interpret these as paths in the tiled plane. The path for $\mathbf{z}$ is just $\mathbf{z}$ as curve in the textile structure. The paths for H and V are concatenations of paths between marked points in neighboring black and white polygons passing through the midpoint of the common edge. The points of intersection of zigzag $\mathbf{z}$ with H (resp. V) correspond 1-1 with those $e \in \mathcal{E}_\Lambda$ which appear in both the list for $\mathbf{z}$ and the list for H (resp. V). The four possible situations are shown in Figure 38. Actually, there are two zigzags $\mathbf{z}$ and $\mathbf{z}'$ passing through each such an intersection point e. However, for the construction of the textile code in [3] the above paths representing H and V must be slightly deformed in order to resolve the triple intersections into double intersections. This can be done by moving the horizontal arrows and the vertical arrows as indicated in Figure 38 [17]. Then near e the zigzags $\mathbf{z}$ and $\mathbf{z}'$ cross H or V before crossing each other. The crossings which arise in this way can be denoted as $H_{e^{\circ\bullet}}^{\pm}$, $H_{e^{\bullet\circ}}^{\pm}$, $V_{e^{\circ\bullet}}^{\pm}$, $V_{e^{\bullet\circ}}^{\pm}$ where the superscripts are the signs attached as in (65) to the crossing of the zigzag with H and V, respectively[18]. Figure 38 matches exactly with [3] Figure 7.

Definition 6 *According to [3] Definition 8 the **textile code is obtained** by writing for every zigzag $\mathbf{z}$ the string of symbols for the crossings of $\mathbf{z}$ with the other zigzags (as in (271)) and the symbols for the crossings with the sides of the period parallelogram (as in Figure 38) in the order in which these crossings are encountered as one walks along the zigzag curve $\mathbf{z}$.*

Remark 13 In [3] Definition 8 the authors label the intersections of the side H of the period parallelogram with the zigzags from left to right with symbols

---

[16]Compare this with the construction of the functions $l_1, l_2 : \mathcal{E}_\Lambda \to \{-1, 0, +1\}$ in Formula (115) which give the homology classes of respectively H and V (as in Formula (123)).

[17]With this construction the given period parallelogram has in fact been deformed to another fundamental domain for the translation action of Λ on $\mathbb{R}^2$.

[18]This means that H is always crossing over the zigzag and V is always crossing under the zigzag. So for the torus diagram one actually should take the projection of (203) on the horizontal plane. This fits well with the idea of the "kernel of the fabric".

$h_1, \ldots, h_l$. The labeling in Figure 38 (with subscripts and superscripts) satisfies this requirement if we take the e's in the order specified by Formula (122) for H. Every such an e contributes one intersection point for each of the two zigzags $\mathbf{z}$ and $\mathbf{z}'$ which cross at e. The subscript is $e^{\bullet\circ}$ (resp. $e^{\circ\bullet}$) if e appears in Formula (126) for the zigzag in odd (resp. even) position. By slightly bending the sides of the period parallelogram we have arranged things such that when walking along the zigzag $\mathbf{z}$ or $\mathbf{z}'$ one encounters the intersection with H just before the crossing of $\mathbf{z}$ and $\mathbf{z}'$ at e. Thus we see that in the textile the subscripts of the H terms are completely determined by the superscript of the H term and by the e next to the right of the H term. A similar argument works for the V terms. *So, the subscripts for the H and V terms are redundant and may without loss be omitted. Note that the superscripts of the H's and V's do not depend on the twist function η.* ∎

Remark 14 By deleting the H and V terms from the textile code one obtains the zigzags in the format (126). From this one can subsequently recover the permutations σ_0 and σ_1; see Remark 11. Using (271) one can read the twist function η from the superscripts $\pm$ in the textile code. ∎

Remark 15 Taking the product of the H and V terms along the code line for zigzag $\mathbf{z}$ one obtains a monomial $H^{a_{\mathbf{z}}} V^{b_{\mathbf{z}}}$ with exponents such that $a_{\mathbf{z}}\lambda_1 + b_{\mathbf{z}}\lambda_2$ is the homology class of $\mathbf{z}$ in $\mathrm{H}_1(\mathbb{R}^2/\Lambda, \mathbb{Z}) = \Lambda$. In the kernel of the fabric the integers $a_{\mathbf{z}}$ and $b_{\mathbf{z}}$ are the *linking numbers* of the link component $\mathbf{z}$ with the two external circles. See also [3] Definition 17 and [20] Definition 2.1 and Remark 2.2. In [20] the vector $(a_{\mathbf{z}}, b_{\mathbf{z}})$ is called the **axial type** of the strand $\mathbf{z}$ in the fabric. The definition of vectors $(a_{\mathbf{z}}, b_{\mathbf{z}})$ ($\mathbf{z} \in \mathsf{P}_\Lambda^{\mathbf{z}}$) in [3, 20] works for general doubly periodic textile structures. For textiles coming from a dimer complete Zhegalkin Zebra Motive the vectors $(a_{\mathbf{z}}, b_{\mathbf{z}}) \in \mathbb{Z}^2$ ($\mathbf{z} \in \mathsf{P}_\Lambda^{\mathbf{z}}$) sum to $(0,0)$ and can be ordered such that when put in that order head to tail they form a convex polygon, which (up to an affine transformation) is the **Newton polygon** of $(\mathcal{Z}, \Lambda)$; cf. §5.3. ∎

Definition 7 *From the textile code $\mathcal{T}$ one extracts a quiver $\Gamma_{\mathcal{T}}$ as follows. The set of nodes of $\Gamma_{\mathcal{T}}$ is the set of components of the link $\mathfrak{L}$ and can be identified with the set of zigzags $\mathsf{P}_\Lambda^{\mathbf{z}}$. The set of arrows of $\Gamma_{\mathcal{T}}$ is $\mathcal{E}_\Lambda$. There is an arrow from $\mathbf{z}$ to $\mathbf{z}'$ if there is according to the textile code $\mathcal{T}$ a crossing where the zigzag $\mathbf{z}$ passes under the zigzag $\mathbf{z}'$.*

The quiver $\Gamma_{\mathcal{T}}$ ignores the circles X, Y and the cyclic order in which a zigzag crosses the other zigzags. It only keeps from the textile code $\mathcal{T}$ the information of the over/under crossings.

We denote the textile code for the twist function $\mathbf{1}$ with $\mathbf{1}(e) = 1$ for all $e \in \mathcal{E}_\Lambda$ by $\mathcal{T}^1$. The corresponding textile structure is a *biperiodic alternating link*; cf. Figure 5 and [7].

Remark 16 For the textile code $\mathcal{T}$ with twist function η the quivers $\Gamma_{\mathcal{T}}$ and $\Gamma_{\mathcal{T}^1}$ have the same set of nodes (namely P_Λ^z) and the same set of arrow labels (namely $\mathcal{E}_\Lambda$). The arrows with label e correspond with the oriented curves $\mathcal{I}_e$ and $\overline{\mathcal{J}}_e$, respectively, in Theorem 1 *ii*. ∎

For a textile code $\mathcal{T}$ we define

$$\Gamma_{\mathcal{T}}^+ = \Gamma_{\mathcal{T}} \cap \Gamma_{\mathcal{T}^1} \,. \tag{272}$$

This is a subquiver of both $\Gamma_{\mathcal{T}^1}$ and $\Gamma_{\mathcal{T}}$ with the same set of nodes. If $\mathcal{T}$ is given by the twist function η, then the arrows of $\Gamma_{\mathcal{T}}^+$ are those $e \in \mathcal{E}_\Lambda$ for which $\eta(e) = +1$.

Let $\mathcal{Z}$ be a dimer complete Zhegalkin Zebra Motive and let Λ be a sublattice of $\mathsf{Aut}(\mathcal{Z})$. Let $\mathcal{T}^1$ be the textile code for the twist function $\mathbf{1}$ given by $\mathbf{1}(e) = 1$ for all $e \in \mathcal{E}_\Lambda$ and let $\Gamma_{\mathcal{T}^1}$ be the corresponding quiver. Let m_0 be a perfect matching and let $\mathcal{T}$ be the textile code for the twist function $\eta = (-1)^{\mathsf{m}_0}$. *Assume that there are no oriented closed paths on the quiver $\Gamma_{\mathcal{T}}$.* Then the intersection is a subquiver of $\Gamma_{\mathcal{T}^1}$ with the same set of nodes as $\Gamma_{\mathcal{T}^1}$, but without oriented closed paths. The arrows of $\Gamma_{\mathcal{T}}^+$ are those $e \in \mathcal{E}_\Lambda$ for which $\eta(e) = 1$ (i.e. $\mathsf{m}_0(e) = 0$). In other words $\Gamma_{\mathcal{T}}^+$ is obtained from $\Gamma_{\mathcal{T}^1}$ by removing the arrows e for which $\eta(e) = -1$ (i.e. $\mathsf{m}_0(e) = 1$). For examples see Figure 40.

C.0.1 Example 5.4.3 continued

The link in Figure 33 lies in a thickened 2-torus. Figure 39 shows the corresponding torus diagram, i.e. the projection of the link on the torus with indicated over/under crossings while the torus is represented by the period parallelogram (red) with opposite sides identified. The torus diagram is also the projection of the boundary of the surface $\widetilde{\mathfrak{S}}_{\mathcal{Z},\eta,\nu,\omega}^{\leqslant h}$ on the horizontal plane; see (63). The crossings correspond to the midpoints of the edges in the planar black-white tiling and have been labeled as in Figure 19. Taking into account the orientations of the crossing curves and which one is over-crossing one assigns to the crossings 4, 8, 9, 12 the number $+1$ and the the other crossings the number -1.

The twist function η is given by

$$\eta(e) = -1 \text{ if } e = 4, 8, 9, 12 \,, \qquad \eta(e) = +1 \text{ else.}$$

The curves in the torus diagram correspond to the zigzags given in (131). With the rules from (271) for putting superscripts $\pm$ this leads to the following piece of the textile code

$$
\begin{aligned}
&(3, 4, 6, 8)\,, \quad (5, 11^-, 10, 7^-)\,, \quad (2, 3^-, 11, 12)\,, \\
&(8^+, 1^-, 12^+, 13^-, 9^+, 10^-)\,, \quad (4^+, 14^-, 13, 5^-)\,, \quad (1, 6^-, 7, 9, 14, 2^-)\,.
\end{aligned}
\tag{273}
$$

For the period parallelogram in Figure 19 we have $H = 11^{\bullet\circ}12^{\circ\bullet}2^{\bullet\circ}3^{\circ\bullet}$ and $V = 3^{\bullet\circ}4^{\circ\bullet}6^{\bullet\circ}8^{\circ\bullet}$. Inserting in the lists in (273) the symbols representing the
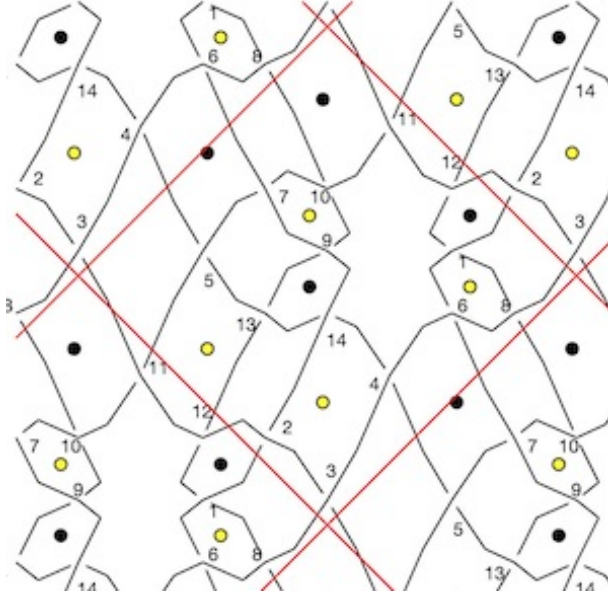
Figure 39: The torus diagram of the link in Figure 33.

crossings of the zigzags with the sides of the parallelogram we arrive at the following textile code:

$$
\begin{array}{ll}
\mathbf{1}: & (H^+, V^+, 3, V^-, 4, V^+, 6, V^-, 8) \\
\mathbf{2}: & (5, H^-, 11^-, 10, 7^-) \\
\mathbf{3}: & (H^-, 2, , H^+, V^+, 3^-, H^-, 11, H^+, 12) \\
\mathbf{4}: & (V^-, 8^+, 1^-, H^+, 12^+, 13^-, 9^+, 10^-) \\
\mathbf{5}: & (V^-, 4^+, 14^-, 13, 5^-) \\
\mathbf{6}: & (1, V^+, 6^-, 7, 9, 14, H^-, 2^-)
\end{array}
\tag{274}
$$

Note that omitting the pairs V^+V^- on the first line and the pairs H^-H^+ on the third line yields exactly the textile code which one can see directly by visual inspection of Figure 39.

The monomials mentioned in Remark 15 are in this example H, H^{-1}, V, HV^{-1}, V^{-1}, $H^{-1}V$ and the exponent vectors $(1,0)$, $(-1,0)$, $(0,1)$, $(1,-1)$, $(0,-1)$, $(-1,1)$ are indeed the sides of the Newton polygon in Figure 27.

The quiver $\Gamma_{\mathcal{T}}$ for the textile code $\mathcal{T}$ in (274) can be determined from the simpler looking data in (273). This quiver is shown on the left in Figure 40. The quiver shown in the middle in Figure 40 is $\Gamma_{\mathcal{T}^1}$ where $\mathcal{T}^1$ is the textile code for the alternating link, i.e. the one with twist function $\mathbf{1}$ given by $\mathbf{1}(e) = 1$ for all $e \in \mathcal{E}_\Lambda$. So, $\Gamma_{\mathcal{T}^1}$ is constructed from the list (see (131) and (271))

$$
\begin{array}{l}
(3, 4^-, 6, 8^-), (5, 11^-, 10, 7^-), (2, 3^-, 11, 12^-), \\
(8, 1^-, 12, 13^-, 9, 10^-), (4, 14^-, 13, 5^-), (1, 6^-, 7, 9^-, 14, 2^-).
\end{array}
\tag{275}
$$

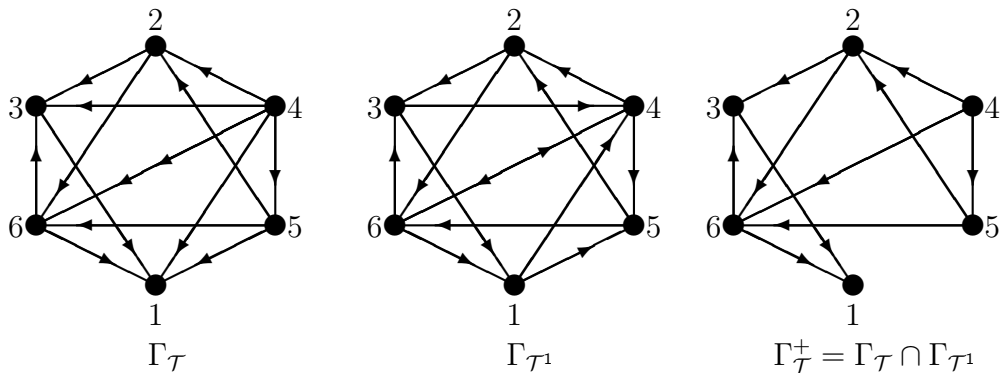The reader is invited to put the labels from $\mathcal{E}_\Lambda = \{1, \ldots, 14\}$ on the arrows of

Figure 40: Quivers for the textile codes $\mathcal{T}$ (273) and $\mathcal{T}^1$ (275).

the quivers $\Gamma_{\mathcal{T}}$ and $\Gamma_{\mathcal{T}^1}$ and to check that $\Gamma_{\mathcal{T}}$ is obtained from $\Gamma_{\mathcal{T}^1}$ by changing the orientation of the arrows with labels $4, 8, 9, 12$.

On the other hand $\Gamma_{\mathcal{T}^1}$ is also the quiver given by the vertices and edges in the tiling on the left in Figure 20. It is also shown (with two obvious misprints) in [13] Figure 17.

The quiver $\Gamma_{\mathcal{T}}^+$ on the right in Figure 40 is obtained from $\Gamma_{\mathcal{T}^1}$ by deleting the arrows with labels $4, 8, 9, 12$ from $\Gamma_{\mathcal{T}^1}$. The quiver $\Gamma_{\mathcal{T}}^+$ is shown in Figure 41. Its nodes are the black circles and its arrows are the black edges oriented such that the grey polygon is on the right of the edge. ∎

Remark 17 The quiver on the left in Figure 40 is connected and contains *no oriented loops*. This implies that the *fabric decomposes in* $|\mathsf{P}_\Lambda^z|$ *separate layers*; see [20] §3.7. The quiver on the right in Figure 40 is a connected subquiver of $\Gamma_{\mathcal{T}^1}$ which contains all nodes of $\Gamma_{\mathcal{T}^1}$ but contains no oriented loops. In the terminology of [12] Definition 5.1.1. and Lemma 5.1.4. it is the **pre-Beilinson quiver** associated with the perfect matching $\{4, 8, 9, 12\}$.

The perfect matching $\{4, 8, 9, 12\}$ is an *internal perfect matching* for the toric diagram of Model 8a in [13] Figure 17, as required by [12]. But for the Newton diagram in Figure 27 of the present paper (which is the toric diagram of model 10c in [13] Figure 26) the perfect matching $\{4, 8, 9, 12\}$ lies over the corner $(0, 0)$; see also (133)-(134).

The eight external perfect matchings for Model 8a are used in [12] §5.2. for the construction of an *exceptional collection of line bundles* on the toric variety associated with the toric diagram of Model 8a. On the other hand the external perfect matchings for Model 8a are the internal perfect matchings for model 10c and these give the eight monomials in the *Hamiltonian* A_0 in (194). ∎

D Connected sums and higher genus

In the present paper we have shown how a Zhegalkin Zebra Motive $\mathcal{Z}$ and a period parallelogram P for a sublatice of $\mathsf{Aut}(\mathcal{Z})$ yield a torus in Euclidean 3-
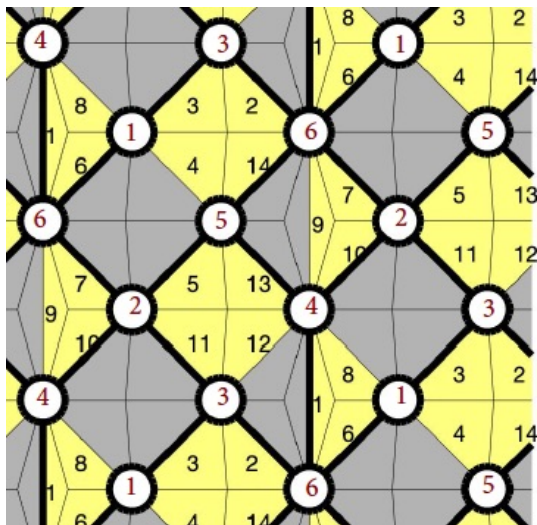
Figure 41: The quiver $\Gamma_{\mathcal{T}}^+$ in Figure 40 as a biperiodic planar quiver.

space equiped with a tiling by black and white polygons and how that leads to a Seifert surface $\mathfrak{S}$ for a link in a thickened torus in $\mathbb{R}^3$ and a ramified covering map $\mathfrak{S} \to \mathbb{D}$ with two ramification points. We now want to demonstrate with an example how one might upgrade this work from the torus to a Riemann surface in $\mathbb{R}^3$ of genus ≥ 2 by taking **connected sums**.

Example.
Consider the Zhegalkin Zebra Motives $\mathcal{Z}_4 = \mathsf{Z}^{21} + \mathsf{Z}^{31} + \mathsf{Z}^{41} + \mathsf{Z}^{61}$ and $\mathcal{Z} = \mathsf{Z}^{21} + \mathsf{Z}^{31} + \mathsf{Z}^{41} + \mathsf{Z}^{62}$ with the period parallelograms shown in Figures 17 and 19. We are going to take the connected sum using the respective vertices of valency 8. Cutting away small open disks around these vertices yields the two octagons in Figure 42. There are two ways for gluing the two tiled tori minus the open disks. The first one identifies the two octagons so that $\bar{1}$ is identified with 3, 5, 6 or 9. The second one identifies $\bar{1}$ with 2, 4, 8 or 10 and interchanges black and white in the $\mathcal{Z}_4$-tiling. The result is in all cases a surface of genus 2 with a tiling with $4 + 4 = 8$ black polygons, 8 white polygons, $12 + 14 + 8 = 34$ edges and $4 + 6 + 8 - 2 = 16$ vertices. As for labeling the edges in the genus 2 tiling: we have $1, \ldots, 12$ coming from $\mathcal{Z}_4$, $\bar{1}, \ldots, \overline{14}$ coming from $\mathcal{Z}$ and $1^+, \ldots, 8^+$ coming from the octagon as indicated in Figure 42. With this labeling of the edges one can easily write down the permutations σ_0, σ_1 for the genus 2 tiling. It is also easy to construct for the genus 2 tiling a positive integer weight function of degree $\deg(\nu) \deg(\nu')$ from positive integer weight functions ν and ν' for $\mathcal{Z}_4$ and $\mathcal{Z}$, respectively. ∎

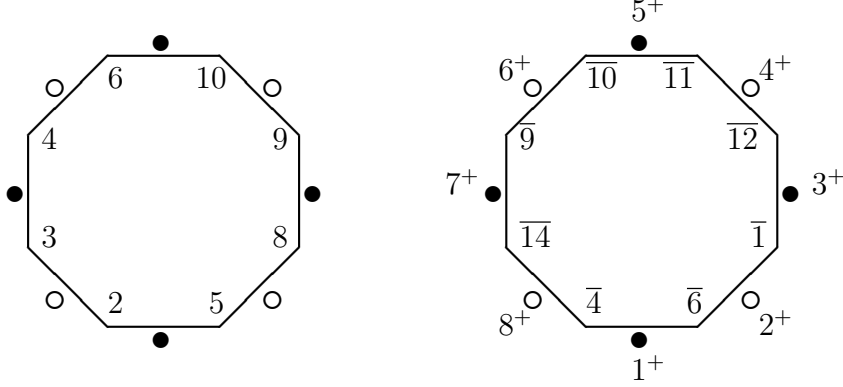*I expect that most constructions and results of the present paper also work for*

Figure 42: Octagons around the 8-valent vertices of $\mathcal{Z}_4$ (left) and $\mathcal{Z}$ (right). The vertices of the octagons are the intersection points of the boundary of the disk with the edges incident with the vertex.

the genus 2 case with some obvious small adaptations.

E A test report on $\mathcal{Z} = \mathsf{Z}^{22} + \mathsf{Z}^{42} + \mathsf{Z}^{61}\mathsf{Z}^{31}\mathsf{Z}^{21}$.

E.1. We consider the Zhegalkin Zebra Motive $\mathcal{Z} = \mathsf{Z}^{22} + \mathsf{Z}^{42} + \mathsf{Z}^{61}\mathsf{Z}^{31}\mathsf{Z}^{21}$ and the lattice $\Lambda = \mathsf{Aut}(\mathcal{Z}) = \mathbb{Z}(4,4) + \mathbb{Z}(4,-4)$. The planar tiling, a period parallelogram and edge labels are shown in Figure 43.[19] In this example

$$|\mathcal{E}_\Lambda| = 30, \ |\mathsf{P}^\bullet_\Lambda| = |\mathsf{P}^\circ_\Lambda| = 8, \ |\mathsf{P}^\star_\Lambda| = 14, \ |\mathsf{P}^\mathsf{z}_\Lambda| = 6.$$

The group $\mathrm{H}_1(\Gamma^\vee_\Lambda, \mathbb{Z})$ has rank 15. According to (11) the Euler characteristic of the surface $\mathbb{X}_{\sigma_0,\sigma_1}$ is $8 + 8 + 6 - 30 = -8$ and, hence, its genus is 5. The group algebra $\mathbb{Z}[\mathrm{H}_1(\Gamma^\vee_\Lambda, \mathbb{Z})]$ is a Laurent polynomial ring in 15 variables. As a basis for $\mathrm{H}_1(\Gamma^\vee_\Lambda, \mathbb{Z})$ we choose the loops $\ell_\mathbf{v}$ given by the 13 vertices $\mathbf{v} \in \mathsf{P}^\star_\Lambda$ with $\mathbf{v} \neq 3$ (this is the centre point of the period parallelogram in Figure 43) together with $\mathfrak{l}_1 = 27^{\bullet\circ}2^{\circ\bullet}3^{\bullet\circ}15^{\circ\bullet}17^{\bullet\circ}22^{\circ\bullet}$ and $\mathfrak{l}_2 = 1^{\bullet\circ}2^{\circ\bullet}4^{\bullet\circ}5^{\circ\bullet}$.

The coordinates of the six zigzag loops w.r.t. this basis are given as the rows in the following matrix

$$\begin{pmatrix} 0 & 0 & 0 & 1 & 0 & 0 & 0 & 0 & 0 & -1 & -1 & -1 & 0 & 1 & 1 \\ 1 & 1 & 1 & 1 & 0 & 1 & 0 & -1 & 0 & 0 & 0 & 0 & -1 & 0 & 2 \\ 0 & 0 & -1 & -1 & 0 & -1 & -1 & -1 & -1 & 0 & -1 & -1 & -1 & -1 & 1 \\ 0 & -1 & 0 & -1 & 0 & -1 & 0 & 0 & 0 & 0 & 0 & 1 & 0 & -1 & -1 \\ 0 & 0 & 0 & 0 & 1 & 1 & 1 & 1 & 1 & 1 & 2 & 1 & 2 & 0 & -2 \\ -1 & 0 & 0 & 0 & -1 & 0 & 0 & 1 & 0 & 0 & 0 & 0 & 0 & 1 & -1 \end{pmatrix} \quad (276)$$

The zigzags corresponding to the rows ending with $(\pm 1, \pm 1)$ can easily be seen in the planar tiling in Figure 43. They are the boundaries of the vertical chain of

---

[19]The planar tiling in Figure 43 has rotational symmetries of order 2. The product of any two of these is a translation from $\Lambda = \mathsf{Aut}(\mathcal{Z})$. So, modulo Λ these rotational symmetries are all equal to the rotation of order 2 about the centre of the period parallelogram in Figure 43. It acts on the more algebraic structures through the following permutation of the edge labels: $(7, 12)(8, 11)(4, 28)(14, 17)(10, 21)(6, 25)(9, 22)(5, 26)(15, 16)(3, 19)(2, 20)(1, 23)(24, 27)(13, 18)(29, 30)$.
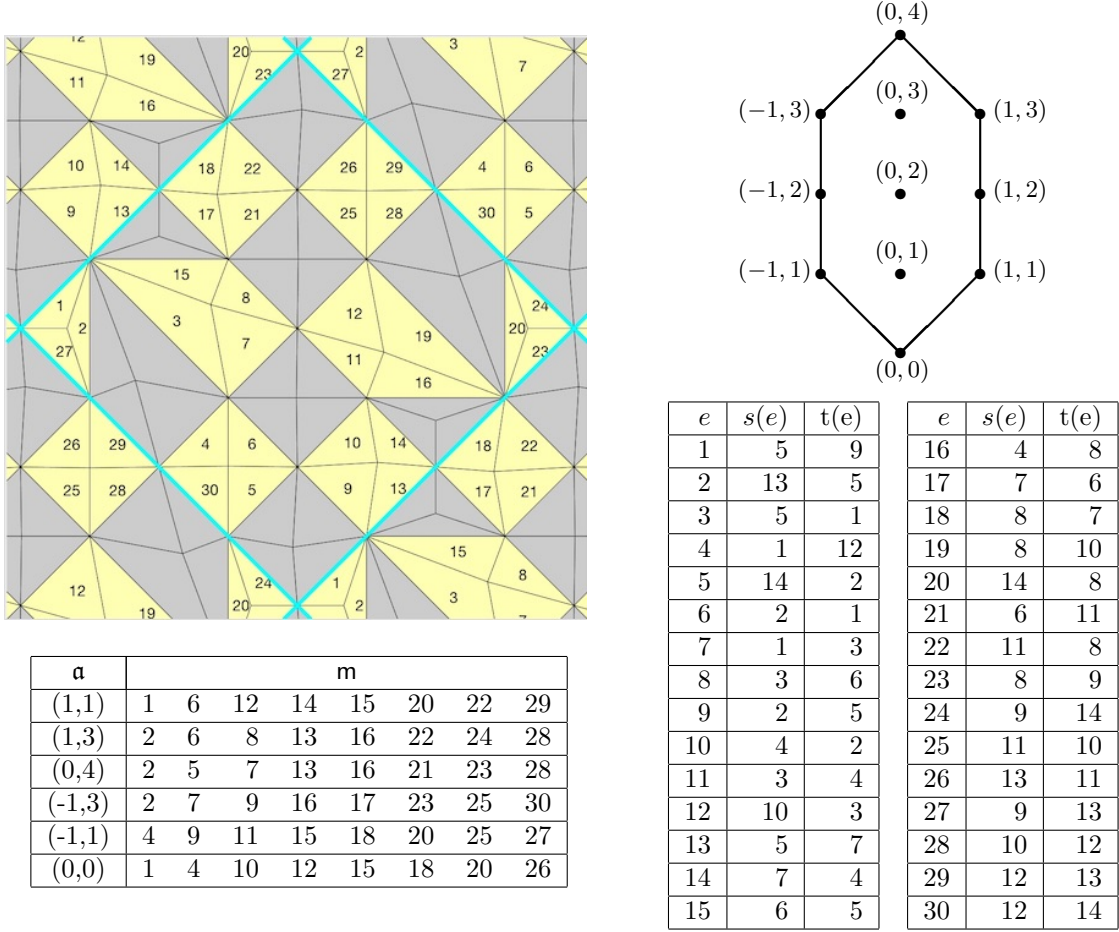
Figure 43: $\mathcal{Z} = \mathsf{Z}^{22} + \mathsf{Z}^{42} + \mathsf{Z}^{61}\mathsf{Z}^{31}\mathsf{Z}^{21}$ and $\Lambda = \mathsf{Aut}(\mathcal{Z}) = \mathbb{Z}(4,4) + \mathbb{Z}(4,-4)$. The planar tiling is shown in Figure 36. Top left and bottom right: period parallelogram, edge labelings and vertex labelings. Top right: the set $\mathcal{N}_{\mathcal{Z},\Lambda,\mathfrak{m}_0,\mathfrak{l}_1,\mathfrak{l}_2}$. Bottom left: perfect matchings at the corners of the Newton polygon.

black squares and the horizontal chain of white squares. The other two zigzags are more complicated. Written in the format (122) they are

$$3^{\bullet\circ}7^{\circ\bullet}11^{\bullet\circ}16^{\circ\bullet}18^{\bullet\circ}17^{\circ\bullet}15^{\bullet\circ}3^{\circ\bullet}4^{\bullet\circ}30^{\circ\bullet}20^{\bullet\circ}23^{\circ\bullet}27^{\bullet\circ}2^{\circ\bullet},$$
$$19^{\bullet\circ}12^{\circ\bullet}8^{\bullet\circ}15^{\circ\bullet}13^{\bullet\circ}14^{\circ\bullet}16^{\bullet\circ}19^{\circ\bullet}28^{\bullet\circ}29^{\circ\bullet}2^{\bullet\circ}1^{\circ\bullet}24^{\bullet\circ}20^{\circ\bullet}.$$
(277)

Since these zigzags have self-intersections the present example is **not minimal** in the sense of [11] Definition 2.1.

Moreover, the lattice generated by the homology classes $[\ell_{\mathbf{v}}]$ ($\mathbf{v} \in \mathsf{P}_\Lambda^\star$) and $[\ell_{\mathbf{z}}]$ ($\mathbf{z} \in \mathsf{P}_\Lambda^{\mathsf{z}}$) is a sublattice of index 2 in $\mathrm{H}_1(\Gamma_\Lambda^\vee, \mathbb{Z})$. To see this one may note that homology class on the first line of (277) is the sum of the homology classes of the loops (see Figure 43)

$$4^{\bullet\circ}30^{\circ\bullet}20^{\bullet\circ}23^{\circ\bullet}27^{\bullet\circ}2^{\circ\bullet}, \qquad 15^{\bullet\circ}7^{\circ\bullet}11^{\bullet\circ}16^{\circ\bullet}18^{\bullet\circ}17^{\circ\bullet},$$
(278)

E.2. There are 152 perfect matchings. The set $\mathcal{N}_{\mathcal{Z},\Lambda,\mathsf{m}_0,\mathfrak{l}_1,\mathfrak{l}_2}$ and the Newton polygon $\mathsf{Newt}_{\mathcal{Z},\Lambda,\mathsf{m}_0,\mathfrak{l}_1,\mathfrak{l}_2}$ for the above $\mathfrak{l}_1$, $\mathfrak{l}_2$ and $\mathsf{m}_0 = \{1,4,10,12,15,18,20,26\}$ are shown in Figure 43. Note that the vectors giving the six sides of the Newton polygon are precisely the last two coordinates in the rows of the matrix (276).

Recall that Formula (192) defines for every $\mathfrak{a} \in \mathcal{N}_{\mathcal{Z},\Lambda,\mathsf{m}_0,\mathfrak{l}_1,\mathfrak{l}_2}$ a polynomial $A_\mathfrak{a}$ in $\mathbb{Z}[\mathrm{H}_1(\Gamma_\Lambda^\vee,\mathbb{Z})]$. One easily checks that $A_{(0,0)} = 1$ and that
  - $A_{(1,1)}$, $A_{(1,3)}$, $A_{(0,4)}$, $A_{(-1,1)}$, $A_{(-1,3)}$ have 1 term.
  - $A_{(1,2)}$ and $A_{(-1,2)}$ have 12 terms
  - $A_{(0,1)}$ and $A_{(0,3)}$ have 22 terms
  - $A_{(0,2)}$ has 78 terms.

Moreover we computed the intersection form on $\mathrm{H}_1(\Gamma_\Lambda^\vee,\mathbb{Z})$ and checked that the following Poisson commutation relations hold:

$$\{A_\mathfrak{a}, X_j\} = 0, \quad \text{for } 1 \le j \le 15\,, \ \mathfrak{a} = (1,1),(1,3),(0,0),(0,4),(-1,1),(-1,3) \quad (279)$$

$$\{A_\mathfrak{a}, A_{\mathfrak{a}'}\} = 0, \quad \text{for } \mathfrak{a},\ \mathfrak{a}' \in \{(1,2),(-1,2),(0,1),(0,2),(0,3)\}. \quad (280)$$

The six perfect matchings m for which $\mathsf{m} - \mathsf{m}_0$ corresponds to a corner of the Newton polygon are listed in Figure 43. The six differences $\mathsf{m} - \mathsf{m}'$ for which m and m' correspond to the endpoints of a side of the Newton polygon are exactly the six zigzags in the format of Formulas (122) and (123). Thus we see that the result in (279) is an immediate consequence of Formula (159) (which holds in general). On the other hand, a simple calculation (by computer) reveals that the elements of the group algebra $\mathbb{Z}[\mathrm{H}_1(\Gamma_\Lambda^\vee,\mathbb{Z})]$ which correspond to the loops in (278) do not Poisson commute with the polynomial $A_\mathfrak{a}$ if $\mathfrak{a}$ is not a corner of the Newton polygon.

We see that for this example even though it is not minimal in the sense of [11] Definition 2.1, Theorem 1.2 of [11] still holds in a slightly adapted formulation:

The functions $A_\mathfrak{a}$ with $\mathfrak{a} \in \mathcal{N}_{\mathcal{Z},\Lambda,\mathsf{m}_0,\mathfrak{l}_1,\mathfrak{l}_2}$ (the set of lattice points in the Newton polygon) Poisson commute. The functions $A_\mathfrak{a}$ with $\mathfrak{a}$ a corner the Newton polygon are Casimirs (i.e. lie in the centre of the Poisson algebra $\mathbb{Z}[\mathrm{H}_1(\Gamma_\Lambda^\vee,\mathbb{Z})]$). The sides of the Newton polygon (i.e. the vectors between two consecutive corners) correspond to the zigzags. There are 11 lattice points in the Newton polygon, of which 6 are corners and 5 are not corners. The dimension of the system (i.e. the rank of $\mathrm{H}_1(\Gamma_\Lambda^\vee,\mathbb{Z})$) is

$$15 = 2 \times 5 + 6 - 1$$

which also agrees with [11] Thm. 1.2.

E.3. I also computed for this example the Seifert matrices $\mathsf{S}_{\eta,\mathfrak{l}_1,\mathfrak{l}_2}$ for $\mathfrak{l}_1$, $\mathfrak{l}_2$ as in §E.1 and all twist functions such that $\eta(e) = 1$ for all e or $\eta = \pm(-1)^\mathsf{m}$ with m a perfect matching. In some cases in which the Seifert matrix is non-degenerate I computed the characteristic polynomial and the minimal polynomial of the monodromy matrix. However, I did not see interesting results to report here.

F   Acknowledgements

References

[1] Adler, M., P. van Moerbeke, P. Vanhaecke. *Algebraic Integrability, Poincaré Geometry and Lie Algebras*, Ergebnisse der Mathematik und ihrer Grenzgebiete 3. Folge Vol. 47, Springer Verlag, Berlin-Heidelberg-New York, 2004

[2] Bocklandt, R., *A Dimer ABC*, Bull. London Math. Soc. 48 (2016) 387-451; see also arXiv:1510.04242

[3] Bright, M., V. Kurlin, *Encoding and Topological Computation on Textile Structures*, arXiv:2007.1487v1

[4] Broomhead, N., *Dimer Models and Calabi-Yau Algebras*, Memoirs of the AMS ♯1011 (January 2012)

[5] Champanerkar, A., I. Kofman, *Determinant density and biperiodic alternating Links*, New York J. Math. 22 (2016) 891-906; see also arXiv:1604.03795v2

[6] Champanerkar, A., I. Kofman, J. Purcell, *Geometrically and diagrammatically maximal knots*, J. London Math. Soc. 94 (2016), no. 3, 883-908; see also arXiv:1411.7915v4

[7] Champanerkar, A., I. Kofman, J. Purcell, *Geometry of biperiodic alternating Links*, J. London Math. Soc. (2) 99 (2019), 807-830; see also arXiv:1802.05343v2

[8] Chiu, K.C.T., T.W. NG, *Hyperbolic Belyi Maps and Shabat-Blaschke Products*, arXiv:1907.10145v1

[9] Feng, B., Y-H. He, K. Kennaway, C. Vafa, *Dimer Models from Mirror Symmetry and Quivering Amoebæ*, arXiv:hep-th/0511287v1

[10] Fulton, W., *Introduction to Toric Varieties*, Annals of Mathematics Studies 131, Princeton University Press (1993)

[11] Goncharov, A., R. Kenyon, *Dimers and cluster integrable systems*, Annales Scientifiques de l' Ec. Norm. Super. tome 46 (2013); also arXiv:1107.5588v2

[12] Hanany, A., C. Herzog, D. Vegh, *Brane Tilings and Exceptional Collections*, arXiv:hep-th/0602041v2

[13] Hanany, A., R-K. Seong, *Brane Tilings and Reflexive Polygons*, Fortschritte der Physik-Progress of Physics, Vol: 60, 695-803; see also arXiv:1201.2614

[14] Hanany, A., R-K. Seong, *Brane Tilings and Specular Duality*, JHEP08 (2012) 107 ; see also arXiv:1206.2386v1

[15] Hartshorne, R., *Algebraic Geometry*, Graduate Texts in Mathematics 52, Springer Verlag (1977)

[16] Kawauchi, A., *A Survey of Knot Theory*, Birkhäuser Verlag (1996)

[17] Lando, S., A. Zvonkin, *Graphs on Surfaces and Their Applications*, Encyclopaedia of Mathematical Sciences vol. 141, subseries Low-Dimensional Topology vol. II, Springer Verlag, Berlin-Heidelberg, 2004

[18] Lickorish, W.B.R., *An Introduction to Knot Theory*, Graduate Texts in Mathematics 175, Springer-Verlag, New York (1997)

[19] Malič, G., S. Schroll, *Dessins d'Enfants and Brauer Configuration Algebras*, arXiv:1908.05509v1

[20] Morton, H., S. Grishanov, *Doubly Periodic Textile Structures*, J. of Knot Theory and Its Ramifications 18 (2009) 1597-1622

[21] Mumford, D., C. Series, D. Wright, *Indra's Pearls, the vision of Felix Klein*, Cambridge University Press (2006), ISBN 978-0-521-35253-6

[22] Stienstra, J. *Zhegalkin Zebra Motives, digital recordings of Mirror Symmetry*, SIGMA 14 (2018), 110; see also: arXiv:1805.09627

JAN STIENSTRA, DEPARTMENT OF MATHEMATICS, UTRECHT UNIVERSITY

e-mail: J.Stienstra@uu.nl